JOHANNES GUTENBERG
UNIVERSITÄT MAINZ

Scaled electrochemical adipic acid derivative production and the regeneration of periodate: Electrifying technical organic synthesis

Dissertation

To attain the academic degree
Doctor rerum naturalium (*Dr. rer. nat.*)
in Chemistry

FB 09 – Faculty of Chemistry,
Pharmaceutical Sciences, Geography and Geosciences
Department of Chemistry

Roland Jan-Reiner Bednarz

Born in Mainz

Mainz, August 2024

PhD Committee

Chair: Prof. Dr. Pol Besenius

First Reviewer: Prof. Dr. Siegfried R. Waldvogel

Second Reviewer: Prof. Dr. Carsten Streb

Day of Graduation: 20.12.2024

“Those, who have the privilege to know, have the duty to act.”

(*Albert Einstein*)

FB09 Fachbereich
Chemie, Pharmazie, Geographie
und Geowissenschaften

Versicherung

für das Gesuch um Zulassung zur Promotion im Fachbereich 09 an der Johannes Gutenberg-Universität Mainz

Hiermit versichere ich Bednarz, Roland Jan-Reiner
Name, Vorname

gemäß § 13 Abs. (3), 3-7 der Promotionsordnung vom 18.10.2021 i.d.F. vom 17.08.2022, dass:

- die eingereichte wissenschaftliche Arbeit noch an keiner anderen deutschen oder ausländischen Hochschule oder vergleichbaren Einrichtung zur Erlangung eines akademischen Grades eingereicht wurde
- ich noch kein Promotions- oder ein vergleichbares Graduierungsverfahren im Promotionsfach erfolglos beendet habe
- ich noch kein Promotions- oder ein vergleichbares Graduierungsverfahren im Fach der Promotion erfolgreich abgeschlossen habe
- die wissenschaftliche Arbeit selbstständig verfasst und ausschließlich die angegebenen Quellen und Hilfsmittel verwendet wurden
- keine entgeltliche Hilfe Dritter, insbesondere Promotionsberatung oder -vermittlung in Anspruch genommen wurde.

22.08.2024
Datum

Unterschrift

Acknowledgments

[redacted]

[redacted]

Table of contents

Abstract

Chemical industrial processes accounted for 6% of all global greenhouse gas emissions in 2020. This account does not consider transport, fugitive emissions, unallocated fuel combustion, or waste emissions. Adipic acid and platform oxidizers like nitric acid are two of the most contributing chemicals, as both productions cause nitrous oxide (N_2O). Achieving a resilient and climate-neutral chemical industry requires rapid and drastic changes. Electrification appears to be one of the most promising approaches for achieving this goal. However, so far only a scant few processes are electrified. The main challenges are constituted by the fragility of the active electrodes, trade-offs between activity and selectivity, and high electricity prices.

In my dissertation, I tackled these challenges with the example of the technical organic syntheses of 3-alkyladipic acid, as well as of the platform oxidizer para-periodate. I demonstrated the adaptable use of modular flow electrolyzers. To significantly increase the space-time yields, I also designed and successfully tested two electrochemical continuously-stirred tank reactors up to 13 L and electrolysis cells with an increased electrode surface.

For the production of 3-alkyladipic acid, we invented a robust anodic foam activation protocol together with industry partners. This includes multifold electrode cleaning and reusing for over 1000 working hours with unaltered performance. For 3-ethyladipic acid, the yield after scale-up was maximized to 59% by a targeted Design of Experiments (DoE) parameter screening. In this instance, the substrates 4-ethylcyclohexanol was chosen because it can be obtained from a massively available regenerative feedstock, namely lignin. Direct use of fluctuating photovoltaic electricity was demonstrated to retain an almost equal 3-propyladipic acid yield. This is realized by the reaction continuing solely during the timeframes when lots of green energy is available. No reactivation of the electrodes was required, despite several pauses of the reaction at nighttime. Such fluctuating usage can contribute to grid stability.

It has already been shown that para-periodate, a powerful platform oxidizer, can be successfully produced by electrooxidation. However, the robustness of the process against impurities, especially with the goal of product recycling, was still an open challenge. We resolved this issue by mineralizing the organic contaminants like active pharmaceutical ingredients, dyes, and iodine compounds. Thus, aqueous solutions, containing several critical organic compounds, can be self-cleaned during this periodate-production.

Overall, the approaches investigated in this study illustrate that a fast structural industrial transition toward the electrification of technical organic synthesis is possible.

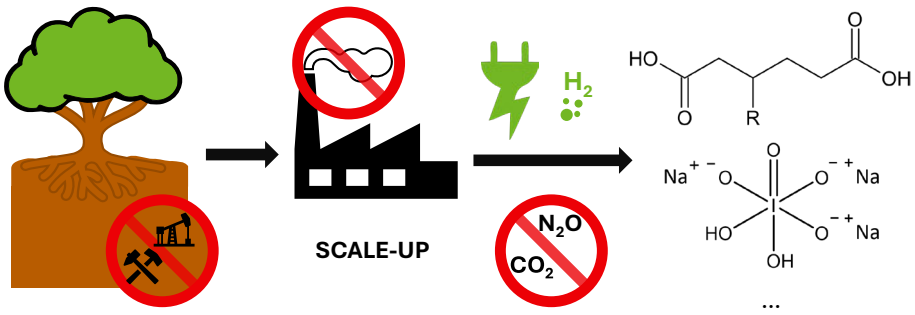

Kurzzusammenfassung

6% aller Treibhausgase waren 2020 auf chemische Industrieprozesse zurückzuführen, exklusive Transport, nicht zugeteilter Brennstoff-Verbrennung, Abfall, sowie flüchtigen Emissionen. Adipinsäure und Plattform-Oxidationsmittel wie Salpetersäure sind zwei der klima-schädlichsten Chemikalien, da während deren Synthese große Mengen Lachgas (N_2O) anfallen. Für eine resiliente, klimaneutrale Wirtschaft sind rasche, drastische Veränderungen auch in der chemischen Industrie nötig. Elektrifizierung scheint dabei einer der vielversprechendsten Wege. Herausforderungen bilden die Stabilität aktiver Elektroden, Kompromisse zwischen Aktivität und Selektivität sowie hohe Industrie-Strompreise.

In meiner Dissertation habe ich diese Herausforderungen anhand der Beispiele der technischen organischen Synthese von 3-Alkyladipinsäure und dem Plattform-Oxidationsmittel para-Periodat in Angriff genommen. Dabei konnte ich den flexiblen Einsatz modularer Fluss-Elektrolyseure zeigen. Um Raum-Zeit-Ausbeuten der Produkte signifikant zu erhöhen, habe ich zusätzlich zwei elektrochemische kontinuierliche Rührkesselreaktoren mit erhöhter Elektrodenfläche mit bis zu 13 L designt und erfolgreich eingesetzt.

Für eine effiziente 3-Alkyladipinsäure-Synthese haben wir gemeinsam mit Industrie-Partnern eine robuste Aktvierungs-Vorschrift für die Nickelschaumanoden entwickelt. Eine wiederholte Elektrodenreinigung ermöglicht den Elektroden-Einsatz für über 1000 Arbeitsstunden bei unveränderten Ergebnissen. Durch ein Design of Experiments (DoE) Parameter-Screening konnte ich die Ausbeute der 3-Ethyladipinsäure auf bis zu 59% steigern. Wir haben das Substrat 4-Ethylcyclohexanol eingesetzt, da es aus Lignin gewonnen werden kann, einer der größten nachwachsenden Rohstoffquellen. Die Ausbeute von 3-Propyladipinsäure blieb beim Einsatz fluktuierenden Stroms aus eine Photovoltaik-Anlage im Vergleich zu konstant angelegtem Strom nahezu unverändert. Diese Kopplung der Synthese an verfügbaren Strom kann das Stromnetz stabilisieren. Trotz mehrfacher Reaktionspausen während der Nächte war eine Neu-Aktivierung der Elektroden nicht erforderlich.

Para-Periodat wurde bereits kürzlich erfolgreich mittels Elektrosynthese dargestellt. Unklar blieb, wir robust der Prozess gegenüber Verunreinigungen ist, was besonders bedeutsam für ein Produkt-Recycling ist. Wir konnten verschiedenste Schadstoffe, wie Wirkstoffe, Farben und Iod-haltige Stoffe, mineralisieren. Selbst wässrige Lösungen, die kritische organische Verbindungen enthalten, können selbstreinigend für die Periodat-Produktion eingesetzt werden.

Insgesamt unterstreichen die Ergebnisse dieser Arbeit, dass eine zügige strukturelle Industrie-wende hin zu einer Elektrifizierung der technischen organischen Synthese möglich ist.

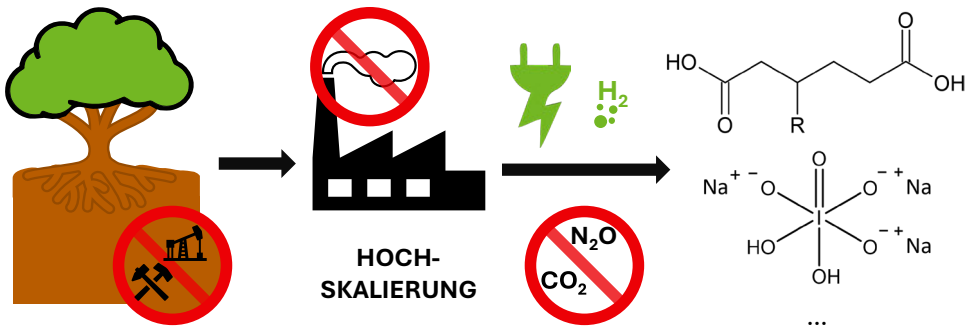

I. Introduction

MOTIVATION: THE NEED TO DIMINISH GREENHOUSE GAS EMISSIONS IN THE CHEMICAL INDUSTRY

"Drastic changes in the global climate system have caused an unprecedented scientific interest - foremost, in the energy sector.[1] Primary energy has to undergo a rapid transition towards 100% renewables.[2] This is a challenging task, not only for the electricity, heating and mobility sectors, but also for the chemical industry.[3] In addition to the energy to run the reactions, also the required raw materials used as substrates, [catalysts,] or for other purposes, need to be reconsidered. Circular economy from cradle-to-cradle, using **biobased feedstocks** up till the end-of-life use of products, is becoming an important benchmark for future processes. Obviously, such large-scale changes in production processes are an extremely complex task and bear high risks. Therefore, they need scaled-up demonstrations of environmentally as well as economically mature concepts to kick-start the process of change.

Electro-organic synthesis fits this need:[4,5] Once organic synthesis meets electrochemistry, a waste-free, safe, green and often more efficient alternative to conventional syntheses is facilitated. A few general remarks regarding electro-organic synthesis: Electricity-driven, a redox reaction occurs simultaneously at two conductive electrodes, which are separated by an electrolyte. […] Industrial relevant electro-organic applications include the Baizer process to adiponitrile [300.000 t/a, e.g. Ascend], fragrance "lily of the valley" (BASF) and maltol flavor (Otsuka).[6,7]

The focus of my project was to achieve a more sustainable synthesis of monomers for polyamides like nylon 6,6. More than **3 Mt of conventional adipic acid** are produced annually;[8] in particular, for the polycondensation to nylon 6,6. Here, the source is crude oil, and the conversion is empowered by nitric acid at elevated temperature. Both need to be replaced for climate as well as environmental reasons. Not only crude oil causes severe CO_2-emissions. Commonly, the oxidation of cyclohexanol and cyclohexanone (KA oil) with nitric acid produces 300 kg nitrous oxide (N_2O) per ton of adipic acid. A global annual production of more than 3 Mt leads to approximately 1 Mt of N_2O being produced – and, still too often, emitted.[9] [Its] climate-polluting effect on a 100-year scale corresponds to 296 CO_2 equivalents;[10] accumulating to annually max. 300 Mt CO_2 equivalents, if exhausted.[11] Nowadays, catalytic N_2O cleavage to N_2 and O_2 at up to 1000 °C is often used, while 10%[8] of the global N_2O emissions[11] still result from the adipic acid synthesis. Noteworthy, the catalytic degradation of N_2O requires significant energy as well. This corresponds to 20–300 Mt of CO_2 equivalents, annually.[10,11] For comparison, Germany emitted about 750 Mt CO_2 equivalents in 2022.[12] [Electrifying] this process would **fully avoid these climate-damaging process**

emissions.[13] While temperatures of close to 100 °C are needed for the conventional process, the electrooxidation can be **performed at room temperature**.

Motivated by replacing the fossil-based feedstock by a regenerative, biobased one, this project shed light on monomeric derivatives carrying an alkyl substituent in their backbone. Lignin resembles the world's largest source of aromatics, especially phenols, which can be hydrogenated to 4-alkylcyclohexanols.[14] Such outstanding potential of biogenic [resources] prompted this research to start from 4-methyl-, 4-ethyl-, and 4-propylcyclohexanols and -nones (Figure 1).

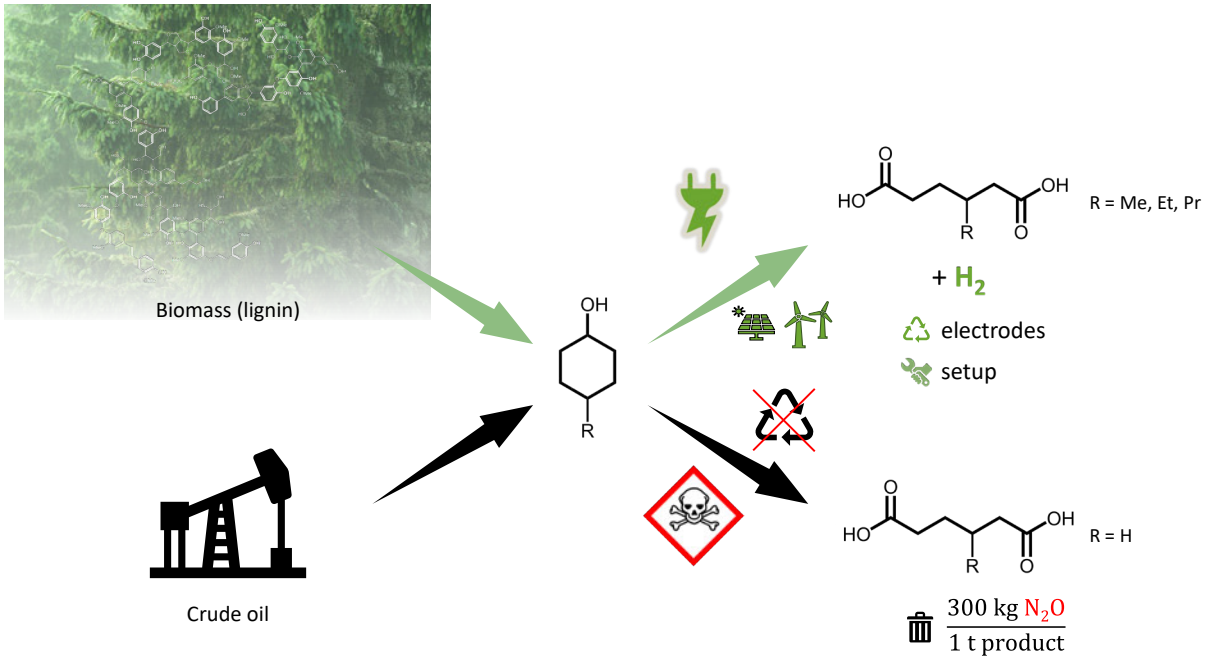

Figure 1. Schematic, summarizing the ideas of this project: The feedstock of cyclohexanol was to be changed from fossil- to biobased. The conversion to adipic acid (derivatives) shall no longer rely on toxic catalysts, nitric acid and the production of climate-polluting nitrous oxide, but on reusable setups, fueled by green electricity in a flexible consumption; contributing to stabilizing the grid in the future.

With these substrates in hand, the Waldvogel group showed good results on a mmol scale.[15] Key to this successful electrooxidation were an aqueous electrolyte and an activated nickel anode. Schäfer et al. published a review in the 80s, highlighting crucial parameters in the electrooxidation of alcohols and ketones in aqueous electrolytes.[16] With this information in hand, my project contained three puzzle parts: Firstly, the middle electrification step in the value chain from lignin [via KA oil and adipic acid derivatives] to polyamides / polyesters was [scaled up and optimized], compared to an earlier study in the Waldvogel group. Additionally, an extension to **renewable energy coupling** of the chemical reactor was performed [demonstrating that the reaction can be slowed or stopped at any time without significantly altering the result].[17] Secondly, the challenges of **reusing the nickel foam anode** for the oxidation of monomeric species were solved.[18] In more detail, an activation and cleaning

procedure was [invented], to almost fully diminish waste generation. Lastly, methods to **efficiently and inexpensively scale-up** this process for technical polycondensations of the isolated products, were a very important milestone.[13]

During my PhD, at first, a procedure to gain active [nickel oxide hydroxides surface at foam anodes] could successfully be optimized, even reusing the foam several times. As a first scaled setup, electrooxidations of alcohols and ketones at these active nickel foams were performed in a large flow electrolyzer (geometrical anode surface area of 108 cm^2) and semi-flow oxidations at an even 12-fold stacked electrode area in an electrochemical continuously stirred tank reactor (e-CSTR). Thereby, **mol-scale electro-conversion** of the 4-alkylcyclohexanone was performed in moderate yields. Remarkably, this process was shown to be working almost as efficiently when purely being supplied by fluctuating solar energy, as with steady current density (26% vs. 27% qNMR yield of 3-propyladipic acid)."

(This text was published as my successful application text for the *EnergieCampus* 2023, organized by the *Stiftung Energie & Klimaschutz* funded by the EnBW *Energie Baden-Württemberg AG*. The German translation was published in the journal *et – Energiewirtschaftliche Tagesfragen* and reused with permission.)

While for the conventional adipic acid synthesis, electrification of the complete process is possible, it might not be so easy adapt to other state-of-the-art oxidation reactions. The replacement of classical oxidizing agents by electrochemically generated ones will support the design of more sustainable and generally applicable processes. In conventional oxidation reactions, powerful **platform oxidizers** with a high oxidation strength usually are utilized. These include potassium chromate, permanganate, or transition-metal catalyzed oxidations, where platform oxidizers keep the transition metal in the highest oxidation state. Other examples of oxidation reactions involve nitric acid, which is used to oxidize alcohols and ketones to carboxylic acids. The commonality of most platform oxidizers is their harsh and toxic synthesis routes or handling, whereby climate-damaging by-products are synthesized. Astonishingly, each ton of produced nitric acid causes between <2 and 10 kg of nitrous oxide (N_2O) as a by-product.[9] According to the authors, the main process is the nitric oxide (NO) decomposition to N_2O and NO_2 at high pressures. In the recent few decades, N_2O abatement strategies have become efficient in destroying 90–99+% of the formed N_2O.[9] Another platform oxidizer is perchlorate. Its extensive use has already become an environmental concern, and will eventually become a concern due to human intake as well, although electrochemical decomposition routes are being investigated.[19] More than 5 Mt per year are still produced of the well-known platform oxidizer hydrogen peroxide, with the production mainly implementing the energy-intensive anthraquinone process via extraction and distillation of the product. Alternatively, electrochemical production procedures of H_2O_2 have lately shown to be suitable. Carbon-based catalyst activity and stability in flow reactors are continuously increasing and their yields are approaching conventional H_2O_2 yields of approximately 20 wt%.[20,21] The main challenges are composed of the catalyst tradeoffs between safety, cost, stability, activity, and selectivity.[20] Another potential "green oxidizer" is electrochemically

generated peroxodicarbonate, which is currently experiencing “a renaissance”.[22] Record concentrations of >0.9 M peroxodicarbonate at a boron-doped diamond (BDD) anode have been realized and the pilot scale process has been validated. As such, its broader application as an electro-oxidized, safe oxidizer is very promising.[22] Its inherent limited lifetime (half-life of a 0.38 M solution under ambient conditions) of <60 min[23] limits its application to on-site synthesis with rapid usage.

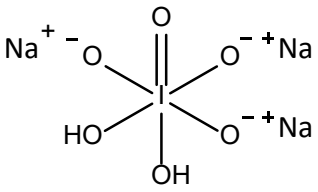

Scheme 1. Structure of sodium *para*-periodate.

One notable alternative to sustainable platform oxidizers is electrochemically generated ***para*-periodate $Na_3H_2IO_6$**, which is mainly used for C,C-bond cleavage.[24] Its synthetic route requires low-valent iodine species, that are dissolved in caustic soda, and a flow electrolyzer with a boron-doped diamond (BDD) anode and stainless-steel cathode.[25] In a galvanostatic approach, the iodine species is oxidized up to **+VII**. As BDD is an incredibly inert, robust, and safe anode material for this transformation[26], long-term stability is a key feature of this synthesis process. With our work, we added another relevant aspect: Once *para*-periodate is depleted in an organic oxidation reaction it does not need to be discarded, but can easily be recycled and reoxidized, maintaining its purity.[27] Organic pollutants are fully mineralized in the re-oxidation and iodine-containing molecules even increase the produced mass of *para*-periodate (Figure 2).

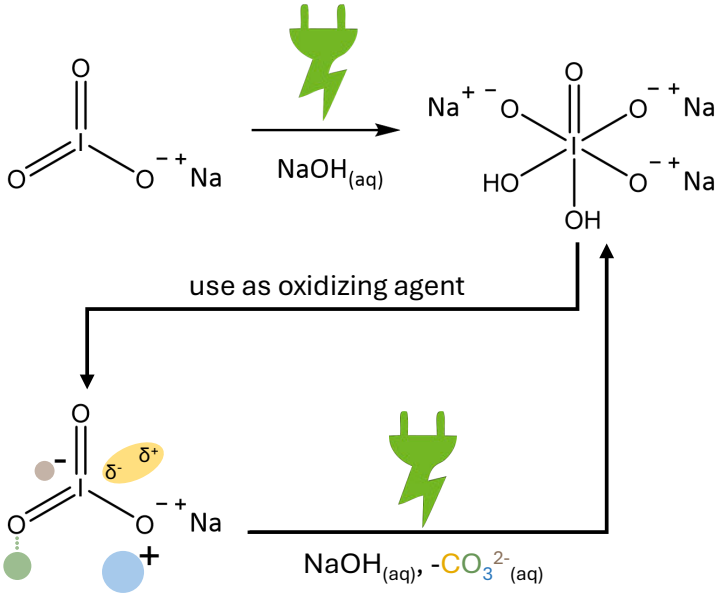

Figure 2. The electrochemical recycling process of *para*-periodate. The robustness of the process regarding impurities is symbolized by the use of colored areas to represent the impurities attached to the iodate after its use as an oxidizing agent. The impurities are mineralized during reoxidation.

ELECTROSYNTHESIS

Electro-organic synthesis is a field of chemistry which focuses on utilizing electricity for chemical redox reactions. This approach is considered **environmentally friendly** because stoichiometric amounts of oxidizing or reducing agents are replaced by electrons, reagent waste is diminished up to waste-free processes, and anodic oxidations can often be conducted in an aqueous electrolyte.[28] The latter typically coincides with a **non-toxic** reaction mixture, depending on the substrate. Once the electricity is stopped, the reaction immediately stops as well, making electro-organic synthesis an **intrinsically safe** technology. The reaction rate can be adapted by tuning the applied current density and voltage.[29] Comparing the absolute primary energy input of electricity compared to fossil fuels in conventional synthesis, no heat losses or energy losses due to side reactions of the energy carrier occur.[30] Thereby, electro-organic synthesis does not only aim for efficiencies close to 1 but makes total processes **economically feasible** – if there is sufficient (steady or fluctuating) electricity supply.[7,31,32] Lastly, electrified processes often even enable shorter reaction pathways. However, for improving the reaction efficiency, many hurdles have to be overcome to fulfill electrochemical requirements like conductivity, stability and activity.[33] Thereby, hazardous, expensive substances may be needed in form of solvents, electrodes, supporting electrolytes or other (set-up related) additives to suppress by-products. The intrinsic nature of heterogeneous reactions may be slower than conventional reactions in homogeneous phase.[29] Thus, not all electrochemical reaction can environmentally surpass its conventional process, yet.[33]

Setting up an electrochemical reaction requires first of all a power supply, which supplies either constant current (**galvanostatic** mode) or constant voltage (**potentiostatic** mode). Via cables, conducting electrodes are attached to the power supply. Electrodes should be chosen to be “inexpensive, non-toxic, stable, manipulatable, resist corrosion and, most importantly, provide high yields and exquisite selectivity.”[34] To achieve high yields, low overpotentials for the desired electrochemical transformation, paired with negligible side reactions (selectivity), are required. In galvanostatic mode, two electrodes (1 working and 1 counter electrode; corresponding to 1 anode and 1 cathode) are sufficient, while a potentiostatic experiment often requires an additional reference electrode. The reason for the latter is a stable voltage, which is typically set versus a reference potential. In a simple case, these electrodes are immersed in or in contact with a conducting fluid – the **electrolyte** (Figure 3). If the intrinsic resistance of the electrolyte is too high, a **supporting electrolyte**, can be added.[35] Typically, this is an organic or inorganic ion pair, acid or base, which is inert in the applied potential window. For kinetic or mass transfer limitation reasons, a mediator may also be added, which mediates the actual reaction by repetitively being reduced or oxidized at the respective electrode itself.[36] It functions as an intermediary reaction between the bulk of the electrolyte and the closer layer at the electrode.

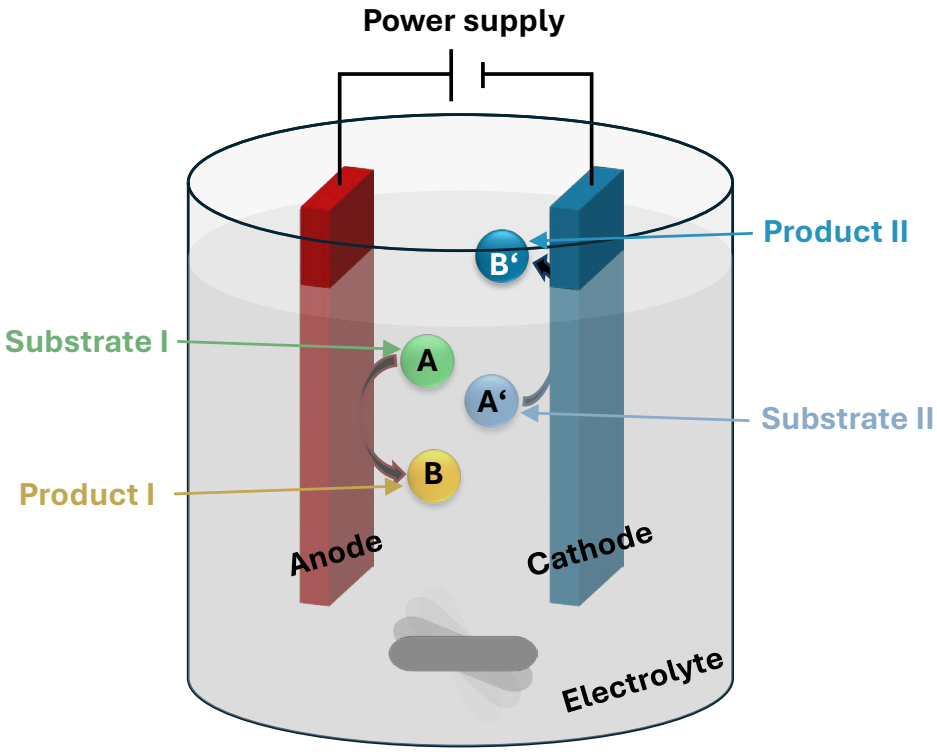

Figure 3. Schematic of an electrochemical setup with two planar electrodes in a beaker-type cell. The electrolyte gets stirred to allow for a homogenous mixture. The reactions take place at the immersed cathode (+) and anode (-). Figure adapted from Heard and Lennox.[34] The spheres depict oxidative/anodic or reductive/cathodic transformations of substrates A or A', e.g. protons (H^+), reduced to B' (hydrogen, H_2) at the cathode, or iodo-containing substrates (A) to *para*-periodate (B), or alkylated KA oil (A) to adipic acid derivatives (B) at the anode.

In the initial planning, the goal of chemists is to find the most efficient approach to convert substrate A to product B. Typically, the oxidation state changes during this transformation. In parallel, a side reaction happens at the other counter electrode, consuming the released electrons. If the product B is formed at the anode, another transformation of a substance A' may be reduced to B' at the cathode, or *vice versa*. If B equals A', but B' is not identical to A, a paired electrolysis occurs.[37] If B and B' are not identical, and B is stable under the applied conditions, an **undivided** cell is applicable. If not, e.g. because B can be reduced back to A or any other unwanted by-product, a separator (often a semi-permeable membrane) is added in between the two electrolyte compartments (**divided** cell).[31] Electrosynthesis often provides high reaction efficiency. If products at one electrode are intentionally further converted at the counter electrode, current efficiencies of above 100% are even typical.[38–40] Furthermore, where a higher current or voltage doesn't lead to more by-products, the space-time-yield proportionally increases.[33] The broadness of potential transformations is demonstrated by the diverse functional group tolerance, typically at ambient conditions, which is a valuable argument for electrosynthesis.[33]

As redox reactions occur within one electrochemical cell simultaneously, a current flows. For better comparison, the current with respect to the geometrical electrode surface is reported:

the **current density** – in mA cm^{-2}. The driving force for an electrochemical reaction is the **voltage** between the working and counter electrode. It depends on various parameters like the electrolyte conductivity, electrode distance, substrate mobility and availability, whether a separator in a divided cell exists, and many more. Typical voltages lie between 1 and 4 V. This voltage can be related with the energy barrier of a conventional reaction, which needs to be overcome for the reaction to occur.

Whether the electrodes are simply immersed in and surrounded by an electrolyte (**batch**-type), or the electrolyte is pumped through the compartments of a **flow** electrolyzer, has several effects on the reaction outcome. Since there is no universal formula to translate specific reaction outcomes from batch cells to flow electrolyzers and *vice versa*, electrosynthetical studies typically test both types of setups. Advantages of the closed-system in a batch-type reactor is the simplicity of the setup and easy gas removal at ambient pressure. Flow electrolyzers enable continuous processes and have several advantages like more efficient heat removal and shorter substrate contact times at the electrode surface, which suppresses slow reactions.

Electrosynthesis eventually originated from Volta's battery (voltaic pile), published in 1800.[41] While back then, electrochemistry purely aimed for current flow, meanwhile researchers investigate how all kinds of organic transformations can be performed, using electricity. In the previous 18 years, complex electrochemical transformations with nearly quantitative yield and very high atom-efficiency have been reported; while conventional approaches perform significantly worse or fail completely: Oxidative C-C cross-coupling of aryls is one of the very successful reactions which were diversly investigated via electrosynthetic routes.[42,43] This is especially interesting for various applications as two aromatic substrates can be directly linked, allowing for unique post-functionalization with functional groups, which likely could not have been combined conventionally. C,N- and N,X-couplings have evolved from this method.[44,45] Hereby, hydrogen gets produced as valuable by-product, instead of waste from stoichiometric oxidants.[33] It should be noted that, on an industrial scale and in the case of pure renewable energy supply, the use of this **green hydrogen** may become an important source of chemical transformations which cannot be easily electrified. Nevertheless, even when using green hydrogen, it is very important to minimize leakage into the atmosphere – not only for economical, but also for environmental reasons. Among others, Sand et al. found that **hydrogen has an indirect global warming potential of GWP20(H_2) = (37.3 ± 15.1)** when being emitted into the atmosphere because of secondary reactions with hydroxyl radicals.[46] Thereby, the lifetime of other greenhouse gases like methane and tropospheric ozone gets extended.

Besides the produced hydrogen, a **value-added product is generated at the anode**, which energetically significantly increases the feasibility of water splitting, since no oxygen gets produced. E.g. in the reactions performed in this thesis, with 3 Mt of adipic acid being produced globally each year, more than 30 kt of green hydrogen would form as a by-product.

Consequently, paired electrosynthetic reactions can enable two concerted reactions to value-added products at two electrodes, if the electrolyte is sufficiently conductive and is stable under electrolysis conditions. Since electrosynthesis is typically claimed to be very sustainable, green chemistry principles necessitate non-toxic elements. Ideally, a non-toxic electrolyte, like water, is chosen. Typically, a supporting electrolyte as salt or base, is needed for sufficient conductivity. Those are typically difficult to recover after the reaction and may interfere with a product isolation via solvent removal. If no water can be present for an electrochemical transformation, some electrolytes contain dry methanol or amines together with carcinogenic, but well hydrogen-donating 1,1,1,3,3,3-hexafluoropropan-2-ol (HFIP).[47–49] Here, typically no additional supporting electrolyte, like a salt, needs to be added, once a base is chosen, which forms an ion pair. HFIP can be recycled via distillation.[48] In terms of "manufacturing", toxic lead, mercury or cadmium electrodes are critical, but used due to their large over-potentials for the hydrogen evolution reaction.[50] Lead leaching, typically via electrode corrosion, is a no-go for pharmaceutical and many other applications.[51] Leaded bronze (CuSn7Pb15) stands out due to its chemical and mechanical stability.[51]

The experiments performed in the present study all used an aqueous electrolyte, because base either stabilized the active nickel surface on the one hand or led to precipitation of the produced oxidizer on the other. In terms of the adipic acid derivative synthesis, the non-toxic, environmentally benign nature of the electrolyte and inexpensive ingredients represented a sustainable electrolyte with the substrate of KA oil mixed in.

MIXTURES

Typically, electrolytes consist of a liquid **homogeneous** phase, conducting electricity via the ions they contain. Typical electrolyte conductivities are above 10 mS cm^{-1}.[52,53] In this case, the electrolyte has low resistance, represented by a relatively low cell voltage. Conversely, some electrolytes may appear naturally **biphasic**, e.g. if an organic substrate is not miscible in the aqueous electrolyte. Here, additives may function as **emulsifiers**. At the electrode, the charge initiates the substrate transformation, often via single-electron transfer. In this way, the total cell voltage may remain relatively low and the substrate concentration in the conducting liquid is as high as it can be. However, working up the reaction mixture may become more complicated due to the complicated separation of the chemical properties of the emulsifier, due to its chemical properties (*tert*-butanol, tensides).

A second option is to not chemically homogenize the two phases but physically aim for an **emulsification**. A chemist may first consider a magnetic stirring bar to seek a sufficiently homogeneous emulsion. For especially nonpolar organic substances, this technique may, however, not suffice, even if a high stirring speed is set. Here, other methods may be utilized. Several options are possible, out of which the two applied in this thesis will be explained hereafter.

A well-known concept for fluid dynamics, resulting in high turbulence, is the **Venturi effect**.[54] If a tube diameter changes, this is linked to the velocity of a perfusing fluid of constant density. It follows the general simplified behavior of incompressible fluids, described by the Bernoulli equation:[55]

$$p_{wide} - p_{narrow} = \frac{1}{2} \rho_{fluid} \left(v^2_{narrow} - v^2_{wide} \right) \qquad (1)$$

As the volume flow has to stay constant in a steady-state case, a narrowed cross-section increases the flow velocity. Therefore, v_{narrow} is always larger than v_{wide} and the right side of equation (1) always positive. In turn, p_{narrow} has to be smaller than p_{wide}. Consequently, we observe a negative pressure at the narrowed cross-section.

An eductor piece makes use of this for sucking in a second fluid (e.g. an immiscible organic substrate like KA oil in caustic soda) at the narrowed cross-section (Figure 4). The high turbulence at the mixing point yields efficient mixing, or, in this case, emulsification: the better the mixing, the smaller the droplets and the longer lasting the stable emulsion, up to hours.[13]

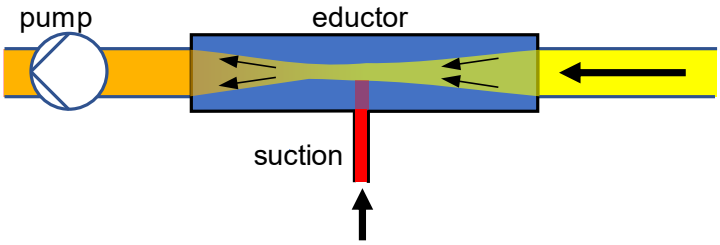

Figure 4. Schematic of the applied Venturi effect within an eductor piece. Due to the narrow cross-section of the main compartment containing the yellow fluid (e.g. water), the red fluid (e.g. oil) gets sucked into the main compartment. High turbulences lead to efficient emulsification of the two fluids (indicated by the orange color).

Another option to increase the stability of the emulsion to several minutes or even hours is to decrease the droplet size of two fluids successively by strong **shear forces**. The shear forces are induced by a very fast rotation of multiple specially designed inner cylinders with notches in a rotor-stator design (one exemplary unit is depicted in Figure 5). The high mass transport and strong shear forces induce nano- to micrometer-sized droplet formation, which causes an emulsion stable for several minutes, if the cylindrical elements are rotated with 12000 rpm. These cylinders have a distance of approximately 1–2 mm. Due to reaction times of hours to days, the mixing process is kept active. Such a disperser machine is in this thesis referred to as an “ultra mixer”.

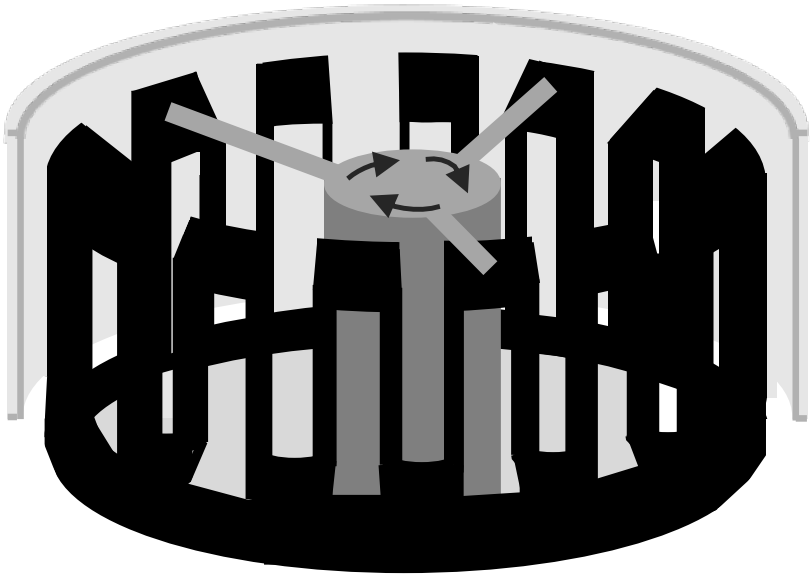

Figure 5. Schematic of an “ultra mixer” with one exemplary outer and inner counter-rotating cylinder which apply large shear forces to emulsify the two liquids.

NICKEL OXIDE HYDROXIDE AS ANODE MATERIAL

Nickel is a ferromagnetic transition metal and is in the same group of the periodic table as palladium and platinum. The main usage is in stainless steel, an alloy of iron, chromium, nickel and molybdenum, which is considered corrosion resistant. Other important usages include Raney-nickel, particularly active, highly disperse, nickel, used in hydrogenation reactions. Furthermore, nickel peroxide (NiOOH) is known to oxidize various alcohols to carboxylic acids in very good yields.[56]

Additionally, **nickel electrodes** for electrolysis have been gaining increasing attention since the 1950s. Using electrodes has the advantage of easier product separation due to heterogeneous catalysis, leading to less waste, as well as being very durable and non-sacrificial compared to NiOOH. Nickel is affordable in relation to other anode materials.[28] The most common electrode materials are carbon-based, followed by platinum.[34] Compared to platinum, Ni even has a thousand-fold lower cradle-to-gate global warming potential, which may become significant on the very large scale.[57] Additionally, Ni electrodes show high chemical inertness in bases and very good mechanical robustness. Increased product yields can be achieved using Ni foams, due to the increased surface area (Figure 6).[15] Ni electrodes can be used in their pristine form,[58–61] or with an active surface layer, commonly **nickel oxide hydroxide** Ni(O)OH.[15,16,62–66] According to Schäfer, “the reactivity of the nickel hydroxide electrode resembles, as far as known, that of the chemical oxidant nickel peroxide.”[16] For the electrooxidation of alcohols and ketones, the urge to use greener alternatives, avoid waste

by-products and use current as the only reagent, led to the replacement of nickel peroxide by nickel anodes with active Ni(O)OH surfaces already in the 1970s.[16]

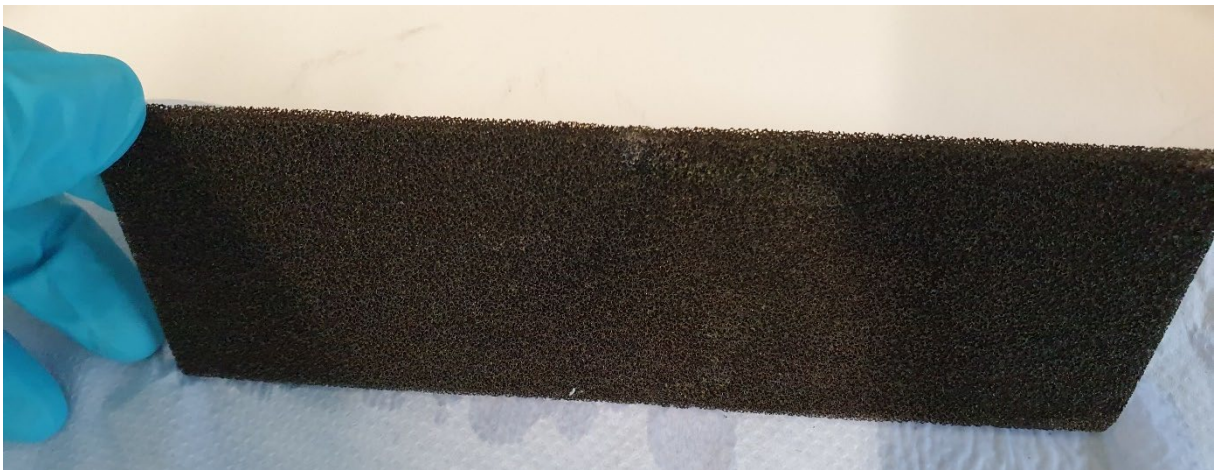

Figure 6. Activated RCM-Ni4753.05 nickel foam with a thickness of 5 mm and an average pore size of 0.4 mm.[67] The black nickel oxide hydroxide has covered the surface homogeneously.

Naturally, metallic nickel forms a passivation layer of nickel oxide in air and water. Obtaining a desired active surface requires specific treatment. The **first observation** of an activated Ni electrode with a Ni(O)OH-type oxidation state was published in 1907 by Foerster, who firstly mentioned the weakly basic $NiSO_{4(aq)}$, $NaOAc_{(aq)}$, $NaOH_{(aq)}$ solution.[68] A more detailed analysis of the surface state and description of the activation was reported by Glemser and Einerhand in 1950.[62,63] The mechanism was first described by Fleischmann et al. (1971) and Vértes et al. (1972) and later extended by Robertson and Schäfer.[69–71,16] They described that the electrode's active surface is in situ formed, starting with the Ni oxidation in contact with an alkaline medium to form α-$Ni(OH)_2$. By aging of α-$Ni(OH)_2$, β-$Ni(OH)_2$ is formed. At 0.63 V vs. NHE in the basic environment, nickel(III) oxide hydroxide (γ-Ni(O)OH) is presented as the active catalyst species.[16,71] Overall, the reaction progresses via a **radical mechanism**, whereby consecutive single electron transfer reactions occur at the electrode surface:[72]

$$Ni(OH)_2 + OH^- \rightleftharpoons Ni(O)OH + H_2O + e^- \qquad (2)$$

Activation procedures did not significantly change in the past century, where polarity changes should stabilize the adsorbed active nickel layer.[15,16,73,74] Hereby, only the nickel electrode which has last been anodic, can be further used, because the final nickel cathode has a reduced, less active, surface layer. Here, we have considered a robust direct current activation approach, including foam electrode reuse after cleaning. The slight electrode darkening (Figure 7) was investigated in this project (Chapter SCALED OXIDATIVE FLOW ELECTROSYNTHESIS OF 3-ALKYLADIPIC ACIDS FROM 4-ALKYLCYCLOHEXANOLS). Further reuse of the nickel foam is possible, until significant damages to the foam or drop in yield would be recognized.

Figure 7. Top: New RCM-Ni4753.05 nickel foam. Bottom: RCM-Ni4753.05 nickel foam after ca. 50 reuses. Dimensions of the nickel foam: 60x180x5 mm^3.

Zirbes et al. successfully investigated the oxidative cleavage of lignin using active nickel oxide hydroxide anodes, observing a positive trend on the yield after several reuses of the nickel foam electrode.[75] Lyalin and Petrosyan oxidized several organic compounds at such nickel oxide hydroxide electrodes.[73]

DESIGN OF EXPERIMENTS (DOE)

Optimizing chemical transformations requires knowledge of various reaction parameters. Either way, qualitative parameters (like the electrode material, the utilized method, or concentrations) should be investigated first. The conventional approach for quantitative (scalable) parameter screening has been to **linearly screen one factor at a time** in defined steps. With the optimum achieved, the next parameter would be tested on top (Figure 8a). While a local optimum for the product yield would be found, it doesn't necessarily correlate with the global optimum. The reason is the possible relevance of an interaction between two tested factors.

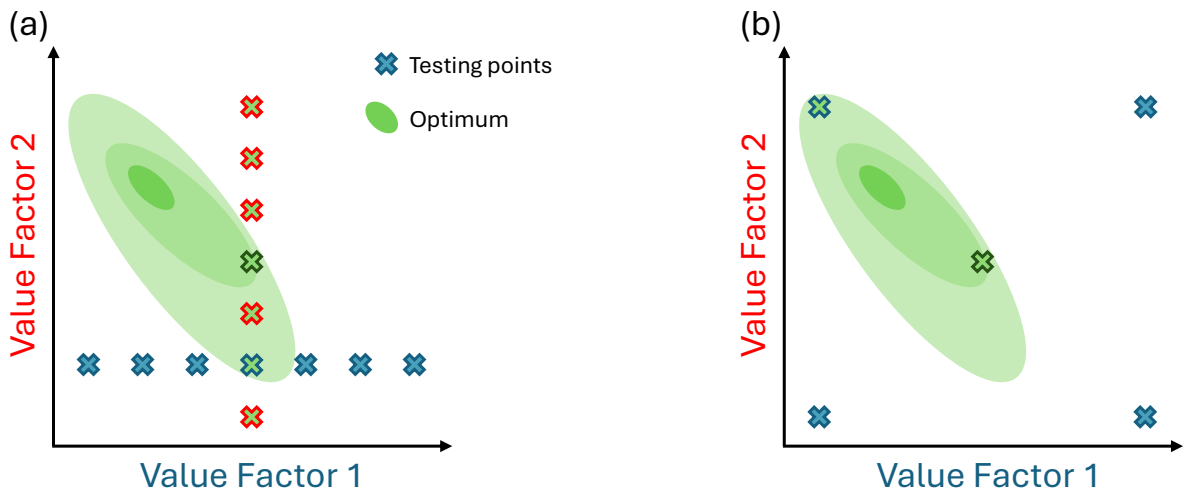

Figure 8. (a) Simplified explanation of classical linear parameter screening, testing one factor at a time. With the local optimum (blue cross with green filling) investigated for factor 1 (blue crosses), the combined local optimum (green cross, green border) of factors 1 (blue crosses) and 2 (red crosses) is investigated further. Deviations between this combined local and global optimum (dark green area) may, however, appear, if significant factor correlations exist. (b) Choice of testing points for the targeted Design of Experiments screening for the same experiment as in (a). Here, the factors to be tested are distributed such that they fill the whole factor space, according to a full-factorial design of a DoE screening. This allows for easier detection of factor correlation effects.

The alternative, utilized in this study, is a targeted parameter screening which considers possible interactions between the factors and at the same time accelerates the process optimization: **Design of Experiments** (DoE). Even though it requires fewer experiments, it retains an equal amount of information, compared to a linear screening (with one factor at a time). The DoE is done in two steps: First, a screening and then an optimization is performed.

For screening, the most accurate option is a full-factorial design. To achieve this, the testing points are chosen from the full *n*-dimensional factor space (Figure 8b). For this, the two boundaries of each factor are chosen, leading to 2^n experimental runs, where *n* is the number of factors. Typically, one more center point experiment with the testing point in the middle of all factorial ranges is measured. In total, this gives a number of 2^n+1 necessary experiments, not considering repetitions for statistical reasons.

If many different factors are considered, this, however, still requires a lot of testing points. In our case, relevant factors include reaction temperature, applied charge, geometrical current density, substrate concentration and flow rate of the electrolyte.

Therefore, a screening with less information, the so-called fractional factorial design, can be utilized. In this case, some of the correlations between several factors are not explicitly investigated. For each of those non-investigated correlations, the number of experiments is halved, saving time and material.

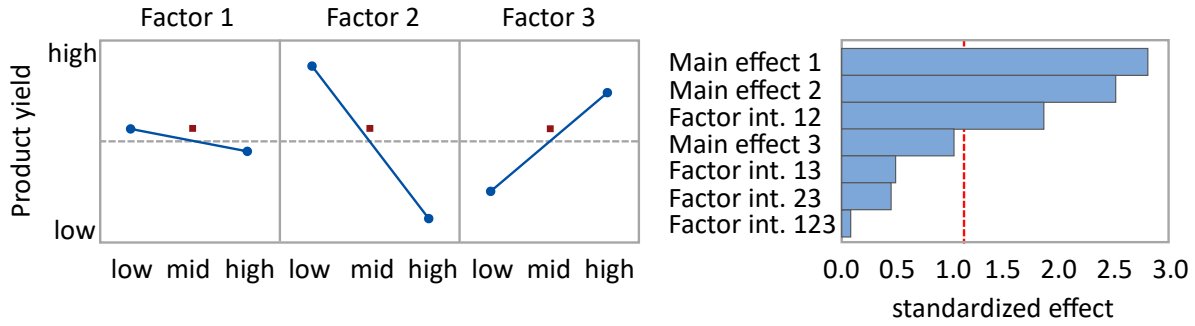

Figure 9. Left: Main effects plot. Right: Pareto chart showing the significance of the main effects and the factor interactions (factor int.). The red line gives the limit of the standardized effect which corresponds to the significance level (typically $\alpha = 0.05$).

After the first DoE screening, the significance of factors and factor interactions is determined from the main effects plot and the Pareto chart (Figure 9). The **main effects plot** displays the average yield obtained for the specific factor value. The two boundary values are connected by a line to show the general trend. The yield corresponding to the center point is plotted additionally. The distance of this center point to the line indicates whether an optimization step is required for this factor. This visualization assumes that the main effects are significantly larger than the correlations.[76]

The **Pareto chart** displays the significance of the main factors and factor interactions. For each factor, its standardized effect is calculated as follows: First, the yield difference between the two boundary values of the analyzed factor is calculated for each set of the other factors, respectively. For the example depicted in Figure 8b, this means that the difference between the two boundary values of factor 1 is calculated for the minimum and maximum of factor 2, respectively. For the resulting yield differences, the average and the standard deviation are calculated. To obtain the standardized effect, the average is divided by the standard deviation. This corresponds to a one-sample t-test, testing the hypothesis of a yield difference of zero.

In the Pareto chart, the main factors and factor interactions are then sorted according to their **standardized effect**. The significance level is typically chosen as $\alpha = 0.05$. All main factors and factor interactions which lie above the significance level are further optimized in the experiment.

Depending on the screening results, the factors can be optimized individually, or in a second DoE step. In the latter case, the testing points are chosen in a star-shaped grid around the local optimum value from the first screening. Thereby, all factors above the significance level are taken into account.

SCALE-UP TECHNOLOGY

After screening and optimization are completed, the process is ready for scale-up. As most electrochemical screening reactions are performed in small (5 mL) cylindrical batch-type screening cells, two general scale-up ideas come to mind: A larger version of the batch reactor or a transfer of the batch-type reaction system into flow, extending throughput volume and process continuation.[77]

Scaling up chemical reactions in batch-type cells is a challenging task due to drastically increasing mass transfer limitations, heat dissipation constraints, and a decrease in electrode-surface-to-volume-ratio.[78] Often, further setup-related challenges arise, such as remaining sufficient mixing or specialized equipment.

In turn, **flow electrolyzers** bear the potential of significantly increased surface-to-volume-ratio in narrow- to zero-electrode-gap cells, efficient heat dissipation via cooling chambers behind both electrode compartments and continuous operation via single-pass flow. While larger flow electrolyzers are commercially available, a series of smaller ones typically have a similar effect. Lastly, simply numbering up the flow electrolyzers is a possibility to enhance productivity linearly. Typically, two disadvantages arise: their relative high costs and, in terms of emulsified electrolytes, the required flow rate to preserve the emulsion may be too high for single-pass flow.

Two concepts of reactor types can theoretically be transferred to electrochemical processing: a **continuously-stirred tank-reactor** (CSTR) or a plug-flow-reactor (PFR). A CSTR optically resembles the batch-type model but has an inflow of fresh substance and an outflow. The vessel is homogeneously mixed. The average retention time of the substrate is sufficient for full conversion. Extending this concept to an electrochemical CSTR, only the electrode system is added to the electrolyte. For a large electrode surface, an electrode stack can be used (Figure 10).[79,80] Such an electrochemical CSTR (**e-CSTR**) is explained in this dissertation (chapter SUSTAINABLY SCALED ELECTROCHEMICAL SYNTHESIS OF 3-PROPYLADIPIC ACID IN LINE WITH FLUCTUATING GRID SUPPLY).

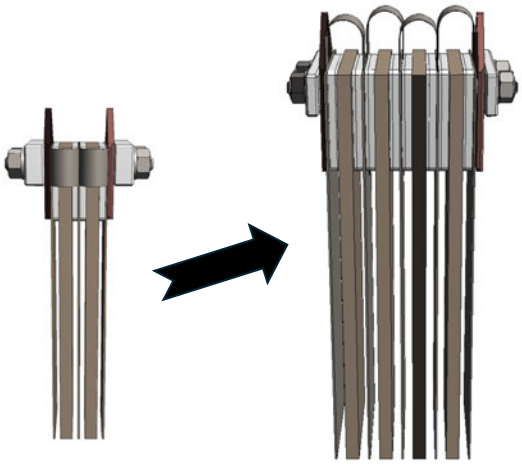

Figure 10. Visualization of a possible stacked electrode scale-up: Extension of an electrode stack with an enlarged geometrical surface area. The stack images, depicting alternating 1 mm thin stainless steel plates (grey) and 5 mm thick nickel foams (brown), were designed by the mechanical workshop of the department of Chemistry at the Johannes Gutenberg-University Mainz.

An alternative to this electrode connection is the bipolar electrode, for which the setup looks similar, but there are no connecting plates between electrodes of equal charge. Instead, the polarity on both sides of each electrode is affected by the outmost electrodes, which are connected to the power supply.[43]

A model for even superior mixing (high Reynolds numbers), heat dissipation and continuous operation is the **plug-flow reactor** (PFR). Conceptually, it is the combination of multiple infinitesimally small CSTRs, set in series. Here, a plug flow within a tube occurs and the reaction progress is occurring in line with the length of the tube. In electrochemical terms, this is more complicated, because a cylindrical electrode setup is required. There are limitations if one of the surface areas is significantly larger than the other. A model with alternating outer anodes and cathodes could be applicable for certain reactions.[81]

Moreover, **scale-up factors**, e.g. electrode distance and surface-to-volume ratio, should be carefully adjusted, compared to the small-scale ones. Maximizing the electrode surface is always advantageous for a high space-time yield. For scaled reactor versions this still, or even especially, holds. In a beaker-type cell, a large dead volume lies behind the electrodes, which increases when the electrode distance is not increased upon scale-up. There, the lack of electric field lines typically hampers the reaction.

One of the most relevant factors is mass transport. Are substrates transported to the electrode surface fast enough? Are the products removed sufficiently fast? Is the mixture homogeneous enough to allow for an unhindered galvanostatic reaction at low voltage? Answers to these questions can be found in the voltage between the electrodes, assuming the high conductivity of the electrolyte. The voltage across the electrolyte is proportional to the charge on the electrodes. A low mass transport can lead to an insufficient removal of electrons from the electrode surface and thereby an increasing voltage. A low voltage is important not

only because it saves energy, but also because it typically increases product selectivity. As voltage determines the height of the energy barriers which can be overcome, high voltages lead to more possible reactions and therefore lower selectivity. This provides a dilemma: Both, for increased reaction speeds as well as when increasing the electrode surface, the charge on the electrodes needs to be increased and therefore also the voltage increases.

A solution to this dilemma may be increased mass transport behavior, e.g. via better agitation or pumping – in the case of flow reactions. Also, a numbering up of reactors, instead of an arbitrary scale-up of a single reactor is an option.

One significant difference between galvanostatic electrochemical reactions and **conventional catalytic approaches** is the reaction behavior at high conversions. For galvanostatic reactions, high conversions necessitate increasing voltages at equal current densities. As mentioned above, high voltages often lower the product selectivity and increase the energy input. In this case, catalytic reactions have the advantage of not being limited to electric field lines. A rough catalytic surface keeps high productivity up to full conversion. To overcome this issue in electrosynthesis, in-situ **product removal and substrate feeding** can stabilize high productivity with good selectivity. Especially this possibility of product removal and substrate feeding, as well as for advanced kinetic control experiments, is a major advantage of scaled reactions compared to small-scale ones, where this is difficult to realize.

Overall, scale-up technologies are crucial tools for applied chemists to transfer knowledge from a scientific to a technical scale. Particular attention needs to be paid to maximizing the electrode surface area and optimizing the surface-to-volume ratio, while keeping a very good mass flow and either a very low voltage or implementing continuous product removal to retain high selectivity.

ADIPIC ACID AND ITS DERIVATIVES

Hexanedioic acid, or adipic acid, is a C_6-dicarboxylic acid synthesized in over 3 Mt annually, following an upward trend.[8] Its common industrial process starts from fossil-based cyclohexanone and cyclohexanol (ketone-alcohol = KA oil). So far, the studied oxidation of cycloalkanols has been conducted using nitric acid at elevated temperatures. The industrial environmentally harmful process of oxidizing cyclohexane to adipic acid is carried out with an overall yield of less than 10%, recycling 90-95% of the substrate, seeking for alternatives.[82,83]

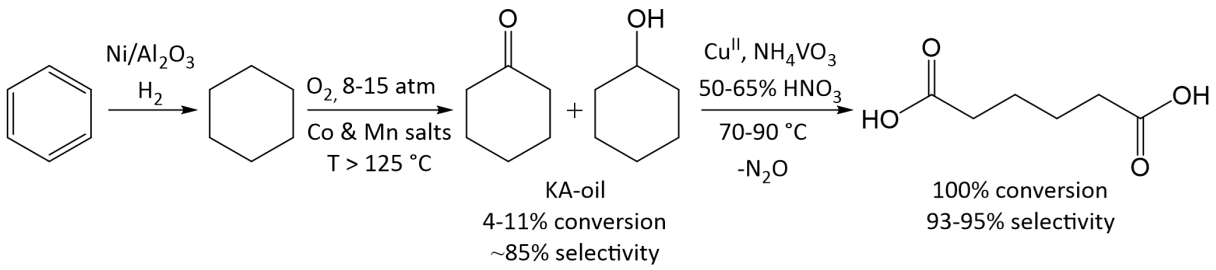

Scheme 2. Simplified reaction sequence of the industrial NO process to get adipic acid.[82,84]

An alternative synthesis route was reported by Hwang et al. in Science.[82] They demonstrated that an ozone oxidation of cyclohexane at 1 atm and room temperature under UV irradiation results in 50% product yield. Adding 8 vol% aqueous 0.5 M HCl to the reaction mixture enhances the yield up to 75%.[82] Despite the high yield, upscaling is difficult because of the required huge area, since UV irradiations does not dissipate far into the bulk.

Further environmentally friendly approaches to adipic acid were published by Rios et al. in their "critical review" in Green Chemistry, highlighting the need for alternatives due to 10% of the global nitrous oxide emissions still originating from the adipic acid production.[8] Moreover, they point out the economical requirement of an alternative adipic acid process which needs to be viable with a selling price of below 1.6 $/kg.

The two reported more sustainable processes which may fulfil the requirements listed above are labeled "butadiene" and "Biotech *cis,cis*-muconic" routes. In the first, petrochemical route, 1,3-butadiene is oxidized in a "carbomethoxylation"[8], using carbon monoxide and methanol at Co salt catalysts, to gain up to 72% adipic acid. Challenges include "catalyst optimization" and substrate recycling.[8] In the second route, *cis,cis*-muconic acid is converted by *E. coli* bacteria from glucose with 30% yield. In a catalytic hydrogenation at "10% Pt/C (34 bar H_2, RT, 2.5 h)"[8] the muconic acid is reduced to adipic acid in 97% conversion. Purification and "catalyst optimization" are named as remaining challenges of this process.[8] One electrochemical approach toward adipic acid was also mentioned: The electroreduction of *cis,trans*-muconic acid in a potentiostatic setup with Pb rod cathode, Ag/AgCl reference electrode and Pt anode.[85] However, under the applied conditions, it was not economically feasible.

There are more electrochemical routes, which were not considered in the "critical review" by Rios et al. Schäfer et al. investigated the galvanostatic electrooxidation of cyclohexanol in caustic soda at an activated Ni(O)OH anode and a stainless steel cathode.[16,86] He utilized a mixture of cyclohexanol in 1 M caustic soda with a geometrical surface area of 16 mA cm^{-2}.

As the rate-determining step of alcohol oxidation to the ketone (and later on to adipic acid), Schäfer highlighted:[16]

$R^1R^2CH\text{-}OH_{adsorbed} + Ni(O)OH \rightarrow R^1R^2C^*\text{-}OH + Ni(OH)_2$

Temperature studies by Schäfer et al. have shown that cyclohexanol gets electrooxidized to cyclohexanone at 25 °C, alcohols with more than six carbon atoms require a reaction temperature of more than 60 °C for good conversion.[16]

Since studies by Rauen et al. have shown that conversion of secondary alcohols toward dicarboxylic acids increases with electrode surface, decent results with nickel foam electrodes compared to flat plate ones have been achieved.[15] Furthermore, electrodeposited $Ni(OH)_2$ on nickel foam electrodes have shown an outstanding specific capacitance[87] and are thus a promising candidate for the oxidation of alcohols to carboxylic acids. Lyalin et al. already

reported a yield of 47% when cyclohexanol is converted to adipic acid at the nickel anode in an aqueous alkali medium.[88]

It is crucial to avoid the presence of additives containing Mg^{2+}, $Fe^{2/3+}$, Cl^- and SiO_3^{2-} which were found to decrease the activity of electrodes.[89,90]

Carboxylic acids are excellent substrates for activating molecules in electrochemical methods. The activation can prevent harsh conditions that are environmentally harmful.[91,92]

From an environmental aspect, the oxidation of cyclohexanol and cyclohexanone to dicarboxylic acids is shown to work with alternative reactions to the conventional NO process. Still, a fossil-based feedstock (Scheme 2) does not diminish the environmental footprint of the product as much as it could. A **regenerative feedstock**, e.g. based on **lignin**, a component of all trees besides cellulose and hemi cellulose, being responsible for the plant's stability, has further advantages. In its phenolic structure, alkylated substituents are inherently present, accessing 4-methyl-, 4-ethyl- and 4-propylcyclohexanol in good yields via a "catalytic reductive fractionation"[14] to the corresponding guaiacols and subsequent hydrogenation at 65 wt % $Ni/SiO_2–Al_2O_3$.[14] Alt has even demonstrated the predominant formation of 4-ethylcyclohexanol when reductively degrading softwood organosolv lignins, using Raney-Ni in *iso*-propanol with 10 V% H_2O in an autoclave with 10 bar H_2 at 240 °C for 96 h.[93] Relatively, 4-methylcyclohexanol formed up to 6-times and 4-propylcyclohexanol even up to 8-times less. He achieved up to 11.0 weight% 4-ethylcyclohexanol, 1.9 weight% 4-methylcyclohexanol and 1.4% 4-propylcyclohexanol.[93] Remarkably, the formation of the alkylated and non-alkylated cyclohexanones was presented as well. Thus, a **KA oil derivative** can also be gained from lignin as a regenerative feedstock.

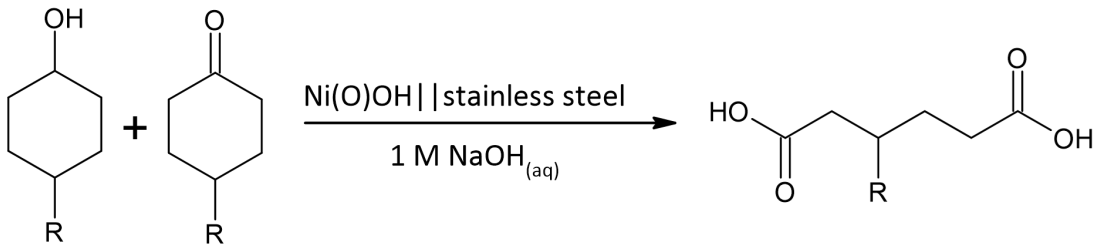

Scheme 3. Reaction equation for the electrooxidation of 4-alkylcyclohexanol and -cyclohexanone to 3-alkyladipic acid in 1 M caustic soda. The substituent R represents methyl, ethyl and propyl.

Rauen et al. investigated the electrooxidation of 4-methylcyclohexanol to 3-methyladipic acid on mmol-scale.[15] In the present work, we study and elaborate on the optimal parameters for the scaled electrooxidation of the other two biogenic alkylated substrates in flow electrolyzers and e-CSTRs.

PLATFORM OXIDIZER PARA-PERIODATE

Additionally to electrifying the reaction itself, like the production of adipic acid derivatives, platform oxidizers will play a crucial role for those processes, which cannot be easily electrified. One very powerful platform oxidizer is *para*-periodate. Periodates are salts of *meta*- or *ortho*-periodic acid. A popular usage is the Malaprade glycol oxidative cleavage, wherein vicinal diols are cleaved to diketones or dialdehydes. In the late 1930s, this option gave access to the content of vicinal and geminal diols in glucose.[94] Later on, the oxidation of alkenes to diols with OsO_4, catalyzed by sodium *meta*-periodate, and its subsequent cleavage was named Malaprade–Lemieux–Johnson oxidation.[95]

The **electrochemical synthesis of periodates at Pb-based anodes** dates to the early 20th century. Müller et al. (1904) reported the potassium meta-iodate oxidation at PbO_2 anode and cathode, first.[96] A diaphragm between the electrochemical compartments is required to prevent perhalogenates from being reduced to their neutral dihalogen species (Br_2, I_2) at the cathode.[97] Further oxidations from iodine via iodic acid or sodium iodate to periodic acid or sodium *meta*-periodate were reported by Willard et al. and Mehltretter et al., respectively.[98,99] Mehltretter observed sodium para-periodate in basic medium.[99] The valence structure of the most common basic periodates is given in Scheme 4.

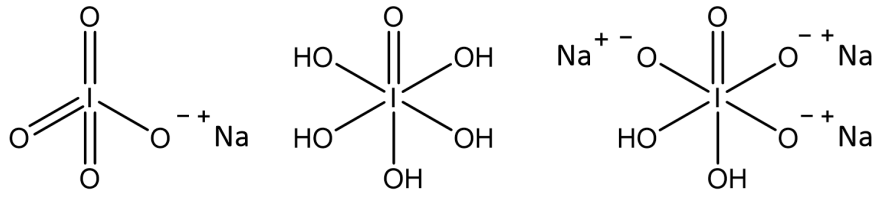

Scheme 4. Structures of the literature known periodates.[26]

In the late 50s, the overpotential of the oxygen evolution potential was investigated in more detail, resulting in a rapid build-up from 1.7 to 2.1 V oxygen overpotential in a diluted sulfuric acid solution at 30 °C within several seconds if a constant current of only 2 mA is applied.[100] With a "normal Nernst potential for the IO_3/HIO_4 redox couple of 1.46 V vs. SCE"[101] and the inherent overpotential for the periodate production, even at lead and boron-doped diamond anodes, causes "a significant current […] at about 2 V versus SCE".[101]

A Japanese research group investigated the electrooxidation of sodium iodate in a divided **flow electrolyzer** in cycling mode in the 1980s, utilizing PbO_2 electrodes.[102] This paved the way for the usage of other flow electrolyzers, foremost at robust and electrochemically very stable boron-doped diamond anodes and stainless steel cathodes.[25,26,101]

Arndt et al. have previously reported an efficient protocol to electro-oxidize sodium iodide or iodate to sodium *para*-periodate in basic medium using a boron-doped diamond anode in a steady state flow electrolyzer.[25,26,103]

Often, degraded oxidizers are considered waste in chemical transformations. Therefore, it is crucial to find ways to recycle them from the waste streams to reduce waste and costs. This can be challenging, especially because of other reaction residues which have to be separated from the degraded oxidizer before the latter can be reactivated. For *para*-periodate, protocols for the activation of the pristine iodine species were previously published,[25] but a demonstration of the recycling of the *para*-periodate from waste streams was lacking so far. In this thesis, we closed this gap by demonstrating the robust reoxidation of used periodate in combination with various chemical impurity compounds, receiving recycled *para*-periodate with high purity.[27]

II. Published Results

OUT OF ITS INFANCY

The text on the following pages reproduces the following article literally, including all figures and tables: Bednarz, Roland J.-R., Brauer, Christopher, Waldvogel, Siegfried R., Out of its infancy – Modular flow cell offers enormous scaling potential for electrosynthesis, *GIT Laboratory Journal* **2021**, online, which has been published in final form at https://analyticalscience.wiley.com/content/article-do/out-its-infancy. This article was used for non-commercial purpose in accordance with Wiley Terms and Conditions for Use of Self-Archived Versions. It is reprinted here with permission of Bednarz, R. J.-R., Brauer, C., Waldvogel, S. R., Out of its infancy – Modular flow cell offers enormous scaling potential for electrosynthesis, *GIT Laboratory Journal* **2021**, online.

Author Contributions (following NISO standard): **R. J.-R. Bednarz**: Conceptualization (lead), formal analysis (lead), investigation (lead), methodology (lead), project administration (lead), visualization (lead), writing – original draft (lead), writing – review & editing (lead); **C. Brauer**: funding acquisition (equal), investigation (supporting), resources (equal), writing – original draft (supporting), writing – review & editing (supporting); **S. R. Waldvogel**: Funding acquisition (lead), conceptualization (lead), resources (lead), formal analysis (equal), methodology (lead), project administration (equal), supervision (lead), validation (lead), writing – original draft (equal), writing – review & editing (lead).

In this publication, significant advances in electrochemical transformation were lately labeled as a renaissance.[1] Decreased reagent waste, increased primary energy efficiency, and high intrinsic safety may be named here. Method-wise, flow electrolyzers even exhibit remarkable features for scale-up: Larger electrode-to-volume-surfaces – compared to pot cells, improved heat dissipation, short contact times of the electrolyte at the electrodes, which suppresses slow reactions, and potentially continuous operation are key points for potential industrial use.

This overview highlights the versatility of a modular flow arrangement with parallel metal plates. Even metal foams, like nickel foam, are utilizable via a contact plate. Their multifold larger surface area and thereby typically higher efficiency as plate electrodes typically justify their use.

As mentioned in the introduction, undivided setups are the easiest and most desirable setup due to less material use and cost, lower voltages in a galvanostatic reaction and less maintenance, e.g. by easier control of flow rates, compared to divided setups.

Despite the desirable properties of undivided flow electrolyzers, divided cells have a key feature: They prevent a formed product from being decomposed at the opposite electrode. Thereby, an oxidation to a fine chemical in the anolyte can potentially be simultaneously

performed in combination with a target molecule reduction in the catholyte. One promising approach could be the combination of two different reactions in the respective compartments which were demonstrated individually by the Waldvogel group: The electro-oxidation of 4-alkylcyclohexanols to get 3-alkyladipic acids[14] and the electro-reduction of cyanamide in acetic acid to get formamidine acetate[16]. In the future, such reactions may potentially be coupled more often, using flow electrolyzers on different scales.

Lastly, the development of a scaled flow electrolyzer with a 108 cm^2 geometrical anodic surface area is presented here. The principal setup follows the 2 x 6 cm^2 model. It additionally includes two tempering chambers, e.g. for a cooling circuit, one behind each electrode. Electrooxidation tests to produce 3-methyladipic acid with this large electrolyzer were successfully performed, using the parameter-set of Rauen et al. on 2 x 6 cm^2 scale.

OUT OF ITS INFANCY

Modular flow cell offers enormous scaling potential for electrosynthesis

Roland J.-R. Bednarz[a], Christopher Brauer[b], Siegfried R. Waldvogel[a,c,d]*

a Department of Chemistry, Johannes Gutenberg University, Duesbergweg 10–14, 55128 Mainz, Germany.

b IKA-Werke GmbH & Co. KG, Janke & Kunkel-Str. 10, 79219 Staufen, Germany.

c Institute of Biological and Chemical Systems – Functional Molecular Systems (IBCS-FMS), Hermann-von-Helmholtz-Platz 1, 76344 Eggenstein-Leopoldshafen, Germany.

d Max-Planck-Institute for Chemical Energy Conversion, Stiftstraße 34–36, 45470 Mülheim an der Ruhr, Germany.

*Email: waldvogel@uni-mainz.de

Overview

Organic electrosynthesis enables the activation of chemical reactions with electricity as a sustainable reagent. It is currently experiencing a significant renaissance.[1–5] Greatly decreased quantities of reagent waste as well as the required scarce raw materials and improved energy conversion in these reactions are just a few of their advantages.[4]

In its early days, electrosynthesis was performed almost exclusively in pot cells, whereas today the focus is increasingly on continuous reaction operation.[6] Above all, the ratio of electrode surface area to reactor volume is considerably larger than in the pot cell, which has a number of advantages. By increasing the electrode area, scalability is possible, which can be achieved, e. g., by parallel operation of operation of several cells. An advantage of flow electrolyzers is the short contact time at the electrodes, compared to pot cells.[7,8] This has the advantage that slow reactions leading to by-products can be cleverly prevented. This is combined with the advantages of flow chemistry, such as continuous and good dissipation of the heat of reaction. Especially in industrial scales, costs and time can be saved both by the continuous operation and by the lowering of by-products.[9–11] Due to the enormous scaling potential compared to pot cells, flow electrolyzers are generally preferred by the industry.

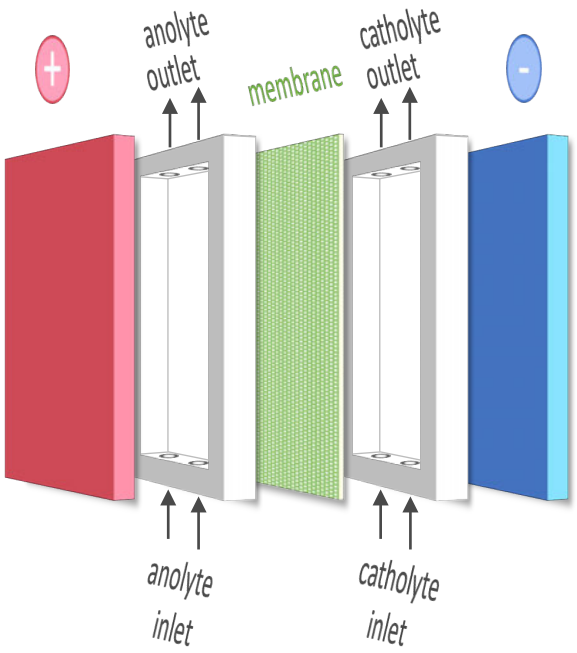

Figure 1. Schematic diagram of a traditional flow electrolyzer with a plate-frame design. The electrodes represent the two outer sides. Parts of the electrodes are covered by the frames in which the electrolyte flows. As an option, an ion-conducting membrane can be inserted between the identical half-cells.

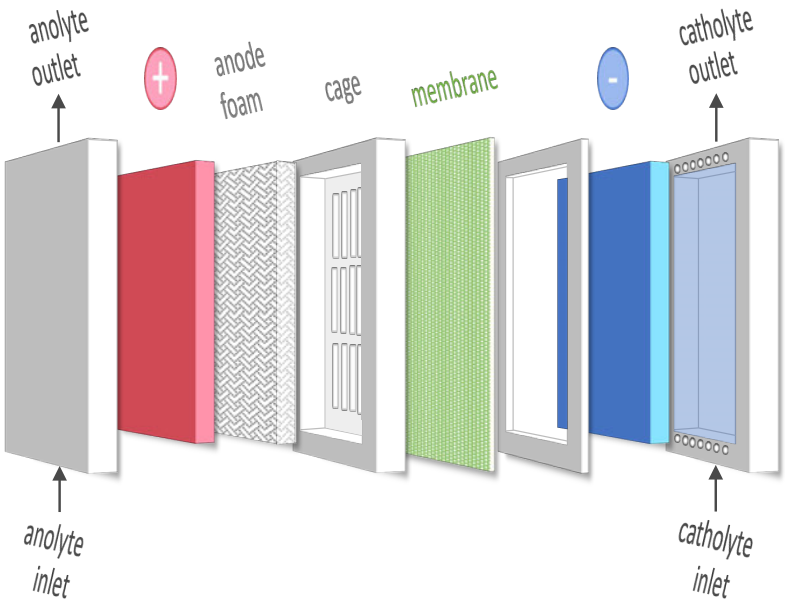

Figure 2. Exploded diagram of the fully modular design of the flow cell with 12 cm^2 geometric anode area with identical half cells. Each of those contains an inlet and outlet for the reaction mixture as well as the respective plate electrode. If required, a cage for a foam electrode can be inserted. This is open on one side for contacting, and the grid acts as a spacer to the counter electrode. For operation as a divided flow cell, an ion-conducting Nafion membrane (green) is used.

When the flow cell was still in its infancy ...

Usually, the two electrodes are arranged coplanar so that the entire surface area can be used equally for the reaction. The first design of a flow cell with such an electrode arrangement is known as the plate-frame model (see Figure 1). Here, the electrolyte was passed between the electrodes via frames and out of the cell at the opposite end. The frames had to be flush with the electrodes on the outside to ensure leak tightness. This concealed valuable electrode area, which subsequently remained unused. In addition, the thickness of the frame limited the electrode spacing. Due to the inlets and outlets these are often several millimeters. Further developments of these classic flow cells have been optimized especially with respect to the electrode area utilization as well as the distance between the electrodes.[12,13] Only by means of a small electrode distance an electric field can be established that is as free of interference as possible. In addition, the small distance ensures low ohmic resistance and paves the way for efficient reactions. In the more advanced model, the classical addition of supporting electrolyte is also eliminated.[13] Also, the problem of parts of the electrode material being obscured by their support in the plate-frame design is solved. These formerly hidden areas are now usable. In addition, the new modular design allows for a variety of applications. This latest generation of flow cells is presented in more detail below.

Figure 3: Photo of a nickel foam electrode in a cage.

The further development of flow cells

In 2017, a small laboratory-scale flux cell was designed with 12 cm^2 of electrode area each, which was developed by the IKA company into the commercial product Electrasyn flow (anode and cathode surfaces each 2 cm x 6 cm) has been further developed.[13] In modular arrangements, this cell offers a wide range of applications for electroorganic reactions.[13–15] The simplest assembly is the undivided cell. It has the advantage that between the electrodes

an unhindered material and charge transport by the electrolyte takes place and the electrodes can theoretically be very close to each other. This is possible because the respective electrodes are embedded into the Teflon frames. The inlets are also located in this frame. Due to the different design, an inter-electrode gap of 0.25 mm up to 5 mm can easily be realized with a simple spacer. However, this design cannot always be applied. When formed products, intermediates or reactants are unstable at the counter electrode, then an ion-conducting membrane, such as Nafion, is used to divide the cell into two half cells. Figure 3 depicts the modular design, which is suitable for both cases. The new generation of flow cells shows its many advantages. In this flow cell, a foam electrode can also be used (cf. Figure 3). Metal foam has a surface area many times larger than a planar electrode of the same dimensions. Since both, contacting and lateral, sealings are much more difficult than in the case of plate electrodes, a cage is provided for this purpose as a holder for the foam electrode (see Figure 2 and Figure 3). It enables contact between the foam electrode and a plate electrode on one side and acts as a defined spacer to the counter electrode. Extensions to the laboratory model can be tempered. Meanwhile, both the electrochemical oxidation of alkylated cyclohexanols to alkylated adipic acids[14] and the electrochemical reduction of cyanamide in acetic acid to formamidine acetate[16] with the 2 x 6 cm^2 flow cell were successfully demonstrated (see Figure 4).

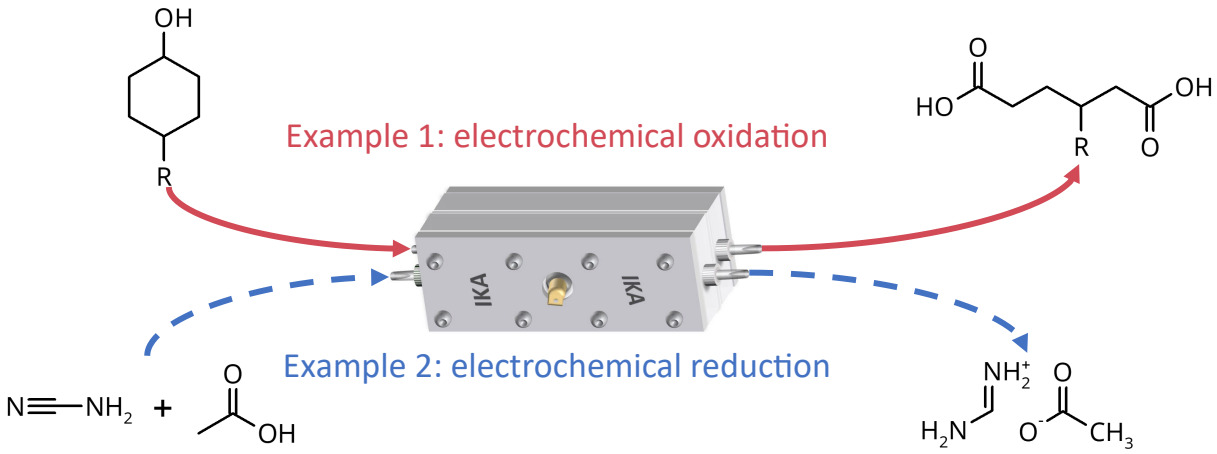

Figure 4. Two typical reactions in the Electrasyn flow electrolyzer with an electrode area of 2 x 6 cm^2 each: The electrochemical oxidation of 4-alkylcyclohexanol to 3-alkyladipic acid in the undivided cell is carried out in good yields.[14] The electrochemical reduction of cyanamide in dilute acetic acid as catholyte with dilute acetic acid as anolyte also proceeds in the cell in splendid yields without noble metals.[16]

After small comes large

In 2020, the established flow cell was used in the context the dehydrogenating cross-coupling of phenols and was scaled up to 4 cm x 12 cm anode area – i. e., by a factor of 4.[15] In addition, the new flow cell included a cooling circuit and thus even achieved a significant productivity and partial yield increase under optimized conditions.[15] The first scaling of the established flow cell for an oxidation reaction was thus successful.[17] Following the scaled flow cell, an

innovative commercial flow cell with nine times the electrode area was established this year, compared to the earlier 2 x 6 model (see Figure 5): the geometric electrode area of the 6 x 18 variant is 108 cm^2. Here, also including a cage, the membrane and spacers can be used in a modular fashion. This cell allows a cooling or heating circuit to be connected for control of the electrolysis temperature. Initial experiments in this reactor proved to be very promising. If several cells are connected in parallel ("numbering-up"), the production rate can be adjusted as required without leaving the optimal working range of the running cell. This new generation of flow cells offers the possibility of efficiently scaling up organic electrosynthesis.

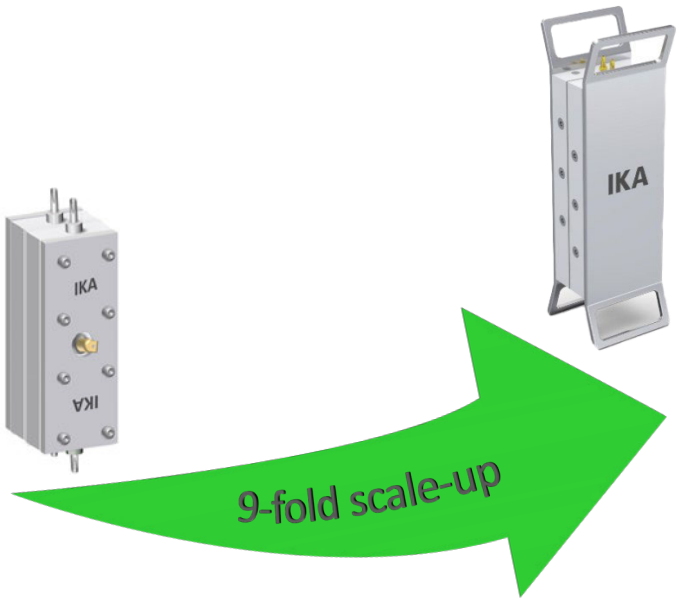

Figure 5. Starting from the laboratory model ElectraSyn flow with electrode areas of resp. 12 cm^2, a flow electrolyzer with a geometric anode area of 108 cm^2 has now been designed. The latter, second generation of the commercial IKA flow cell (electrode surface areas of 6 x 18 cm^2 each) has extended functions compared to the first laboratory model, including the connection of a cooling or heating circuit to the PTFE frame. Technically, flow rates of up to 500 L/h and a maximum current of 50 A can be applied.

References

(1) S. R. Waldvogel, B. Janza, Angew. Chem. Int. Ed. **2014**, 53, 7122–7123.
(2) A. Wiebe, T. Gieshoff, S. Möhle, E. Rodrigo, M. Zirbes, S. R. Waldvogel, Angew. Chem. Int. Ed. **2018**, 57, 5594–5619.
(3) S. Möhle, M. Zirbes, E. Rodrigo, T. Gieshoff, A. Wiebe, S. R. Waldvogel, Angew. Chem. Int. Ed. **2018**, 57, 6018–6041.
(4) D. Pollok, S. R. Waldvogel, Chem. Sci. **2020**, 11, 12386–12400.
(5) M. Yan, Y. Kawamata, P. S. Baran, Chem. Rev. **2017**, 117, 13230–13319.
(6) M. B. Plutschack, B. Pieber, K. Gilmore, P. H. Seeberger, Chem. Rev. **2017**, 117, 11796–11893.
(7) M. M. Hielscher, B. Gleede, W. Siegfried R., Electrochimica Acta **2021**, 368, 137420.
(8) A. A. Folgueiras-Amador, T. Wirth, J. Flow Chem. **2017**, 7, 94–95.
(9) J. L. Röckl, D. Pollok, R. Franke, S. R. Waldvogel, Acc. Chem. Res. **2020**, 53, 45–61.

(10) J. Seidler, J. Strugatchi, T. Gärtner, S. R. Waldvogel, MRS Energy Sustain. **2020**, 7, 42.
(11) S. R. Waldvogel, S. Lips, M. Selt, B. Riehl, C. J. Kampf, Chem. Rev. **2018**, 118, 6706–6765.
(12) B. Endrődi, M. M. Hielscher, C. Janáky, M. Linden, S. R. Waldvogel, in "Electrochemistry in Flow", **2021**, Book chapter in “Flow Chemistry”, in press.
(13) C. Gütz, A. Stenglein, S. R. Waldvogel, Org. Process Res. Dev. **2017**, 21, 771–778.
(14) A. L. Rauen, F. Weinelt, S. R. Waldvogel, Green Chem. **2020**, 22, 5956–5960.
(15) B. Gleede, M. Selt, C. Gütz, A. Stenglein, S. R. Waldvogel, Org. Process Res. Dev. **2020**, 24, 1916–1926.
(16) M. Klein, S. R. Waldvogel, Green Chem. **2021**, 23, 3289–3294.
(17) B. Gleede, M. Selt, R. Franke, S. R. Waldvogel, Chem. – Eur. J. **2021**, 27, 8252–8263.

SCALED OXIDATIVE FLOW ELECTROSYNTHESIS OF 3-ALKYLADIPIC ACIDS FROM 4-ALKYLCYCLOHEXANOLS

This manuscript has been published in the peer-reviewed journal Organic Process Research & Development in 2023. The editors accepted the reuse of this content in the present thesis. It is reprinted here with permission of Bednarz, R. J.-R., Gold A. S., Hammes, J., Rohrmann, D. F., Natalello, S., Mann, M., Weinelt, F., Brauer, C., Waldvogel, S. R., *Org. Process Res. Dev.* **2024**, 28, 5, 1529–1538, https://doi.org/10.1021/acs.oprd.3c00146. The text on the following pages reproduces the following article literally, including all figures and tables.

Author Contributions (following NISO standard): **R. J.-R. Bednarz**: Conceptualization (lead), formal analysis (lead), investigation (lead), methodology (lead), project administration (lead), visualization (lead), writing – original draft (lead), writing – review & editing (lead); **Annika S. Gold**: formal analysis (equal), investigation (equal), writing – original draft (supporting), writing – review & editing (supporting); **J. Hammes**: formal analysis (equal), investigation (equal), writing – review & editing (supporting); **D. F. Rohrmann**: investigation (supporting), writing – review & editing (supporting); **S. Natalello**: investigation (equal), writing – review & editing (supporting); **M. Mann**: visualization (equal), writing – original draft (supporting), writing – review & editing (supporting); **F. Weinelt**: funding acquisition (equal), resources (supporting), writing – original draft (supporting), writing – review & editing (supporting); **C. Brauer**: funding acquisition (equal), investigation (supporting), resources (equal), writing – original draft (supporting), writing – review & editing (supporting); **S. R. Waldvogel**: Funding acquisition (lead), conceptualization (equal), resources (lead), formal analysis (equal), methodology (lead), project administration (equal), supervision (lead), validation (lead), writing – review & editing (lead).

Massive greenhouse gas production, in the order of hundreds of million metric tons of CO_2 equivalents, necessitates alternative routes to synthesize adipic acid.[1–4] Electro-organic synthesis is a powerful candidate to step in.[17–19] With a current global annual demand of approximately 3 million tons of adipic acid electrifying the conventional process will likely require flow processes instead of batch-type ones.[29] This prompted us to investigate the effects of a scaled flow electrolyzer on the electrooxidation of 4-alkylcyclohexanols to 3-alkyladipic acids.

As a starting point, the electrode setup was considered. For aqueous electrooxidations of alcohols, nickel is a literature-known superior anode material,[17–19,36–42] upon which large-surface-area foams have shown especially high yields.[18] On the cathode side, titanium[37–38] can be replaced by the less expensive stainless steel, which did not show any corrosion or different damages via all experiments performed during the present project.[18] Because this

combination led to good results for the electro-oxidation of 4-methylcyclohexanol,[18] we stuck to it for the large-scale investigations of 4-ethylcyclohexanol in this study.

Crucial for a high current efficiency is a robust activation of the nickel foam to nickel oxide hydroxide (Ni(O)OH). Briggs et al.[42] and Schäfer[17] suggested activation procedures using AC current, which have so far been followed by other chemists.[18,34] When aiming to reproduce a homogeneous activation, we encountered major difficulties – in particular for electrodes, which had already been used and cleaned. For this reason, we lowered the complexity of the setup by removing the polarity changer and seeking a DC activation protocol. A crucial pretreatment turned out to be the immersion in caustic soda (1 M) or a thorough rinsing. Right after the aforementioned pretreatment, the electro-oxidation at the nickel surface to Ni(O)OH was shown to be robust, if the activation solution was prepared similarly to the reported ones:[42,45] 0.1 M $NiSO_{4(aq)}$, 0.1 M $NaOAc_{(aq)}$, and 5 mM $NaOH_{(aq)}$. Reusing of the activation solution is possible a few times – depending on the remaining nickel and acetate concentrations.

Notably, scanning electron microscopy images revealed a fiber-like network of electro-generated Ni(O)OH. Thereby the question had risen how far this additional multifold surface increase due to activation dominates the reaction efficiency.[18]

The main focus of the present work was the development and utilization of a novel 9-fold larger flow electrolyzer, compared to earlier laboratory testing, on a semitechnical scale. Thereby, a Design of Experiments screening revealed two significant parameters for the electro-oxidation of 4-ethylcyclohexanol (**1''**) to 3-ethyladipic acid: The substrate concentration *c*(**1''**) of ideally 0.2 M within the tested range between 0.2 and 0.5 M and an optimal flow rate Φ of best 50 mL min^{-1} (range: $10 < \Phi < 50$ mL min^{-1}). On this scale (250 mL), the efficiency of mixing also correlates with the achieved degree of emulsification. The IKA magic LAB / magic PLANT mixing device optimizes this emulsification process significantly. Since in earlier studies smaller reaction volumes were used, these parameters were not known to be important up to now.

Besides the improved understanding of aqueous electrooxidations on a larger scale, more knowledge for a sustainable approach toward adipic acid derivatives was gained. In total, we showed more than 1000 hours of operation with a single electrode set with more than 20 cleaning runs in between multiple reactions. With experimental accuracy, no changes in the yield were observed after these 1000 hours of operation. The foam stays activated as the reaction is running, even over several days. To start a new reaction, the optimized cleaning and activation protocols described here allows for unaltered performance. By reusing the electrode, no electrode waste is produced.

Analysis of the product spectrum showed comparable ratios between main, and by-products compared to earlier studies[18,37–38] and allowed to identify the presence of further carboxylic acids which are, however, yet not clearly characterized.

With kinetic voltage measurements, we analyzed the reaction progress which is characterized by an early phase with a voltage maximum and a trend toward a lower, stabilizing voltage. While first the uncharged and insoluble organic substrate is responsible for the voltage increase, the formed ionic product lowers it again via conductivity decrease. The small fluctuations are likely caused by hydrogen bubble occupancy at the active electrode surface sites.

Lastly, we tested the effect of substrate feeding on the product yield, keeping its concentration stable. We could show up to tripled yields, indicating a general yield improvement when continuously operating this process.

Overall, a robust activation of reusable nickel anodes was presented, and its nano structure was visualized. More than 1000 operating hours with a commercially available 108 cm^2 flow electrolyzer were tested. Furthermore, the relevance of a high flow rate (50 mL min^{-1}) and lower substrate concentration (0.2 M) for the synthesis of 3-ethyladipic acid was demonstrated. The positive effect of substrate feeding on the product yield suggests that continuous operation could be a very useful variant.

SCALED OXIDATIVE FLOW ELECTROSYNTHESIS OF 3-ALKYLADIPIC ACIDS FROM 4-ALKYLCYCLOHEXANOLS

Roland J.-R. Bednarz[a], Annika S. Gold[a], Jasmin Hammes[a], Denis F. Rohrmann[a], Silvio Natalello[a], Moritz Mann[a], Frank Weinelt[b], Christopher Brauer[c], Siegfried R. Waldvogel[a,d,e]*

a Department of Chemistry, Johannes Gutenberg University, Duesbergweg 10–14, 55128 Mainz, Germany.

b Evonik Operations GmbH | Research, Development & Innovation, Paul-Baumann-Straße 1, 45772 Marl, Germany.

c IKA-Werke GmbH & Co. KG, Janke & Kunkel-Str. 10, 79219 Staufen, Germany.

d Institute of Biological and Chemical Systems – Functional Molecular Systems (IBCS-FMS), Hermann-von-Helmholtz-Platz 1, 76344 Eggenstein-Leopoldshafen, Germany.

e Max-Planck-Institute for Chemical Energy Conversion, Stiftstraße 34–36, 45470 Mülheim an der Ruhr, Germany.

*Email: waldvogel@uni-mainz.de

KEYWORDS. scale-up, flow electrolyzer, oxidation, electrosynthesis, 3-ethyladipic acid

ABSTRACT. The rapidly advancing climate change necessitates the development of more sustainable synthetic pathways for critical chemicals, such as adipic acid or its derivatives. Here we present an environmentally benign electrochemical formation of 3-ethyladipic acid using 4-ethylcyclohexanol as the precursor, which can be derived from lignin. The preparation was performed in a scaled and commercially available flow electrolyzer with a geometrical anodic surface area of 108 cm^2, allowing for a production rate of 264 mg h^{-1} for the target compound in a semiflow process. This was an increase in the surface area by a factor of 9 compared to a previously reported electrochemical approach. In this way, 3-ethyladipic acid was obtained in isolated yields of up to 38%, which corresponds to an increase of 15%. The established activation protocol for nickel foams allowed the operation of the foam for more than 1000 h. By monitoring of the reaction progress, substrate feeding was determined to be one crucial parameter to enhance the production rate significantly.

INTRODUCTION

Annually, a million tons of climate-damaging and toxic gases are emitted in the course of producing adipic acid.[1–4] The common production process involves the nitric acid oxidation of a cyclohexanone/cyclohexanol mixture (KA oil) from fossil sources.[5] This results for every synthesized ton of adipic acid in cogeneration of about 300 kg of N_2O, a greenhouse gas exhibiting a 298 times higher global warming potential than CO_2 on a 100-year time scale.[2,5–7] Adipic acid is predominantly used as a monomer in the polycondensation reaction with hexamethylenediamine to form nylon-6.6.[4] With a market volume of over 3 million tons per year,[3,5] with global producers such as Asahi, BASF, Bayer, and DuPont, the reaction is

accompanied by a concomitantly high production of N_2O. Producers agreed to reduce these toxic emissions in 1995.[7] Novel approaches to replace the conventional process, the used feedstock, or even substitute adipic acid are still highly desired. In the recent years, significant to nearly quantitative amounts of the produced N_2O get directly converted on site, e.g., at BASF.[8,9] Twenty-five years ago, Noyori et al. significantly contributed to transforming this reaction into a more climate- and environmentally friendly one.[1] They oxidized cyclohexene in an aqueous hydrogen peroxide solution at 75–90 °C to adipic acid. Therefore, they used Na_2WO_4 and quaternary ammonium bisulfate (1 mol % each) as a phase-transfer catalyst. The epoxide intermediates undergo ring cleavage within the acidic medium. An isolated adipic acid yield of 90% was reported. However, the feedstock for this reaction was not derived from biomass. In particular, the required hydrogen peroxide is energetically rather critical and expensive and requires significant safety precautions. Tungsten and the phase-transfer catalyst may be reused once, including significant losses, and remain as waste afterward. Moreover, chemical research is aiming to transition from fossil-based resources to regenerative ones. One possible avenue is the use of biogenic feedstocks, such as lignin, which is mostly used for energy purposes in the pulping industry.[10–12] It represents the world's largest aromatic feedstock, does not compete with nutrition purposes, and is renewable.[11,13]

Recently, an approach to synthesize adipic acid from lignocellulosic biomass was established via bacterial transformation and subsequent catalytic hydrogenation.[3] Other bacterial pathways to adipic acid from bio-based platform molecules, like 5-hydroxymethylfurfural, glucose, *γ*-valerolactone, and phenolic compounds, have been reviewed by Lang and Li.[5] However, the scalability of such biotechnological processes for industrial purposes is challenging.[5] The combination of biotransformation and subsequent electrosynthesis has demonstrated that sugars can be converted selectively to 3-hexenedioic acid.[14–16] More easily scalable pathways favor the electrochemical oxidation of cyclohexanol in flow reactors.[17–19]

Electrochemistry is a powerful and ecologically and economically sustainable method for organic reactions due to its cost and atom efficiency.[20–24] However, several crucial parameters for electrosynthesis have to be controlled and optimized.[25–27] The versatile nature of electrochemical reactions in undivided setups enables promising scale-up of many transformations.[24,28–30] This especially holds for flow electrolyzers.[19,31,32] Flow electrolyzers have many advantages compared to batch-type electrolysis cells. A narrow interelectrode gap enables lower Ohmic resistivity and better heat dissipation.[30,33] Furthermore, the surface area-to-volume ratio is superior to that of batch-type cells, also leading to a better mass transfer.[34] Larger electrode surfaces additionally enhance these features, if the interelectrode gap does not change. This increased geometrical anode surface area typically enhances the production rate of the target compound linearly. A scaled-flow electrolyzer can also be equipped with cooling features. Generally, this is achieved by channels for the tempering fluid behind the electrodes. A flow electrolyzer setup is usually the prerequisite for a continuous production process, representing an important aspect in translation to a technical scale.[35]

Previous alcohol oxidation protocols have relied on the use of NiOOH electrodes.[18,19,36–38] The enhancing electrooxidation strength of the heterogeneous mediator nickel oxide hydroxide for aliphatic alcohol oxidation was discovered in the 1970s.[36,39,40] The importance of stable, complete, and regular activation of the nickel electrodes was recently emphasized by Cantillo et al.[34]

Here the synthesis of alkylated adipic acids from alkylcyclohexanols is established using multifold larger electrolyzers than previously reported.[18,41] A 9-fold scale-up of the electrochemical flow cell and a robust activation procedure for the nickel anodes were achieved. Based on the robust scale-up, the nickel foam anode could be reused for all reactions reported here. This diminishes the amount of waste generated in the process significantly. Furthermore, a 34% yield improvement in the oxidation of 4-ethylcyclohexanol to 3-ethyladipic acid was established utilizing a Design of Experiments (DoE) approach.[18] Additionally, the byproduct analysis of the electrochemical process was investigated in depth.

RESULTS AND DISCUSSION

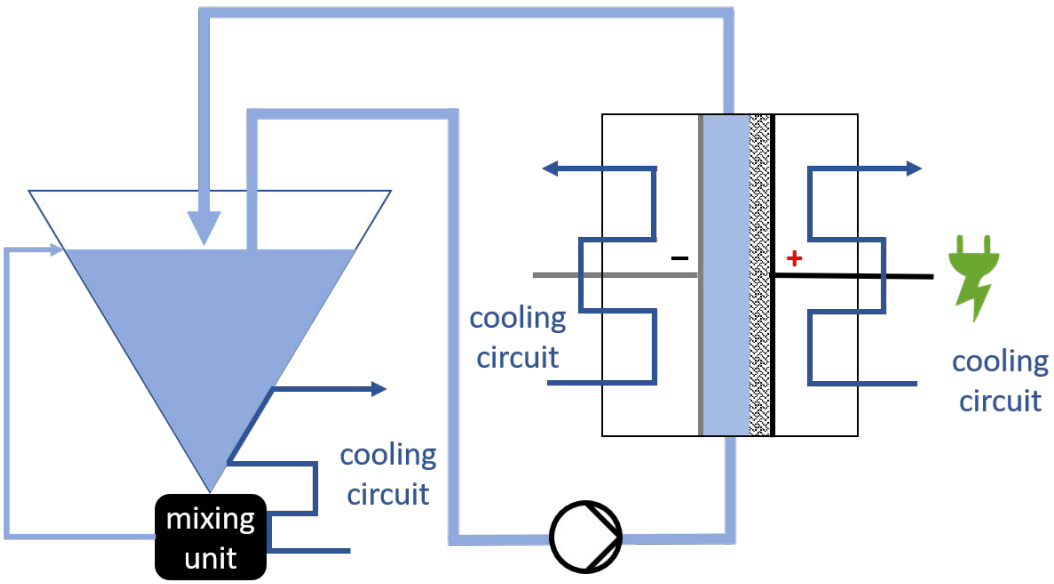

Figure 1. Schematic of the reaction setup in an undivided flow electrolyzer with a stainless steel cathode and a nickel foam anode, contacted by a nickel plate electrode. The electrode spacing is 3 mm. The cooling circuit uses water for tempering between 25 and 50 °C. The reaction mixture is by nature biphasic and therefore emulsified using an IKA magic LAB with a DR mixing element.

A flow electrolyzer cell with a geometrical anodic surface area of 108 cm^2 was designed (Figure 1). The modular cell setup with a self-standing frame and a cage for the foam electrode – all with an active geometrical surface area of 108 cm^2 – make this electrolyzer particularly interesting for scaled electrolysis in flow mode. Moreover, the large heat dissipation is enabled by channels behind the electrodes, providing superior tempering compared to smaller commercial flow electrolyzers wherein only the reservoir could be set to a defined temperature.[18]

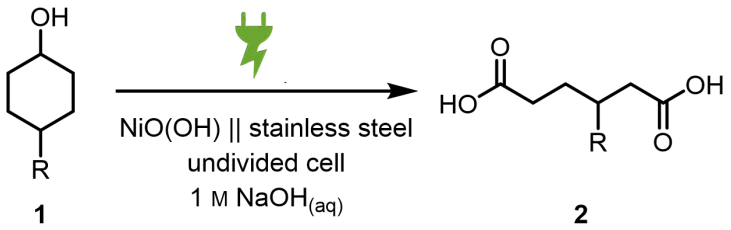

Scheme 1. Reaction Scheme for the Anodic Oxidation of 4-Alkylcyclohexanols (**1**) to 3-Alkyladipic Acids (**2**). **R** Is an *n*-Alkyl Chain Like Methyl or Ethyl.

The efficient electrooxidation of cyclohexanol and its derivatives to their corresponding adipic acids (Scheme 1) requires an active nickel surface.[18,41] To design long-term-stable activated nickel foams, we started from the protocols for the activation of nickel anodes by Briggs et al.[42] and Schäfer.[17] They reported an electrical polarity switch of the electrodes during the activation process, indicating a quicker buildup of the active surface.[42] This anodic-cathodic cycling process results in active Ni(O)OH surfaces with a significantly increased geometrical anodic surface area (Figure 2).

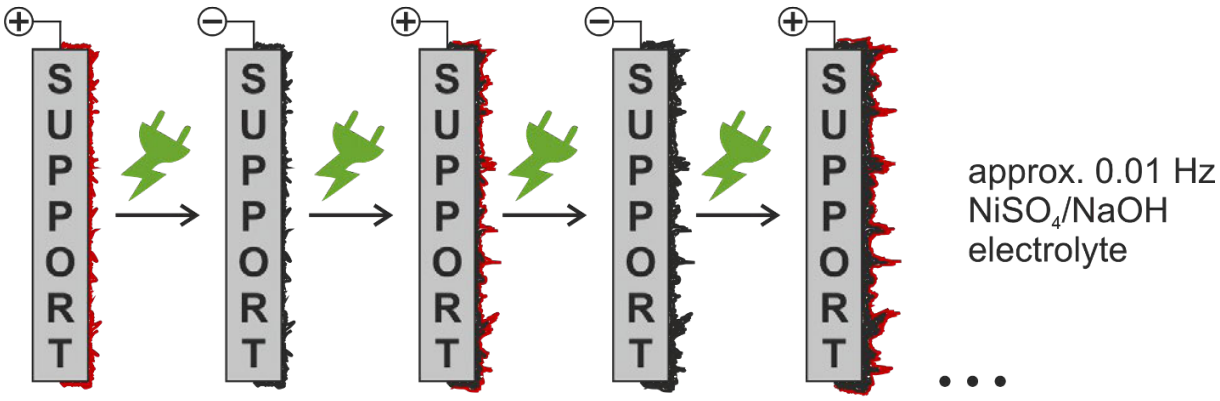

Figure 2. Nickel oxide hydroxide (NiOOH) anodes by AC activation. The NiOOH is reduced to Ni(0), and another layer of NiOOH is grown on top upon the next reversal of polarity. Due to the superior conductivity of Ni, NiOOH is mechanically better attached to the surface. The surface appears optically almost black. The space-time yield of organic oxidations increases significantly if the nickel anodes are activated.[18]

Under those reaction conditions, the reused nickel foam did not reproducibly turn black. Cantillo et al. recently additionally pretreated the nickel electrodes with sandpaper and hydrochloric acid under sonication before the electroactivation for cleaning purposes.[34] Furthermore, they used a 500-fold lower concentration of a base for the activation solution. The nickel electrode, which was last poled as an anode, was further used. They also observed notable deactivation once the nickel plate electrodes were immersed in the alcohol/base mixture without immediately applying current. We modified the protocol, leading to increased stability of the approach. Prior to the activation process, the nickel foam was either thoroughly rinsed with, or briefly immersed in, 1 M caustic soda. Thereby, the basic environment led to a more rapid formation of nickel oxide hydroxide. One reason could be

that a higher concentration of $Ni(OH)_2$ close to the electrode surface is initially achieved, similar to the explanations given by Cantillo et al. for the potential inversion mode.[34]

Once the caustic soda has stopped dripping from the foam, the active anode is assembled in a parallel plate arrangement with stainless steel as a cathode (see Figure 3).

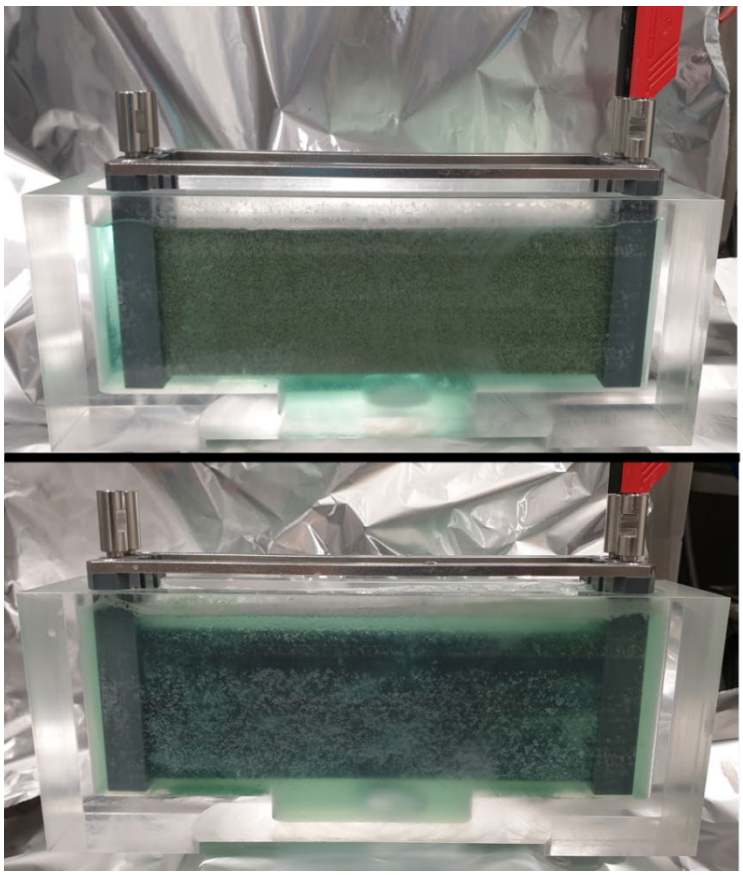

Figure 3. Setup for nickel foam activation, consisting of a poly(methyl methacrylate) case with contacts for cathode and anode. The stainless steel cathode is not visible behind the nickel foam anode in the front. Top: image before activation. Bottom: image after activation.

Here, the polarity was kept constant to ensure a fast and chemically plausible activation procedure. Fleischmann and Pletcher reported that Ni oxidation states of an activated surface range between +II and +IV.[36] A successful oxidation of the nickel species is indicated optically due to a color change from metallic to black.[34] The activated nickel foam electrode was rinsed thoroughly with distilled water.

With this electrolyzer, the reaction of 4-alkylcyclohexanols to give 3-alkyladipic acids was scaled by a factor of 9 compared to previous reports (see electrode comparison in Figure 4).[18]

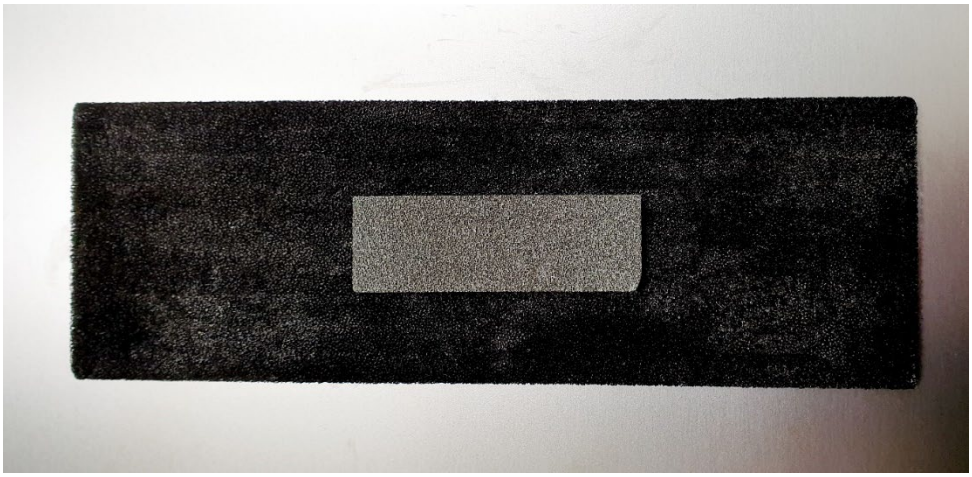

Figure 4. Small nickel anode ($A_{geometric}$ = 12 cm^2) used for earlier flow reactions[18] (silver color) in the middle, on top of the activated nickel foam anode ($A_{geometric}$ = 108 cm^2) (black). Black nickel oxide hydroxide is deposited onto the nickel surface.

A more detailed analysis of the morphology was performed. Remarkably, the activated nickel foam shows a homogeneous network of fibers (Figure 5f). The adsorbates on the nickel foam show a rough morphology, which becomes more distinct with age (Figure 5c,d).

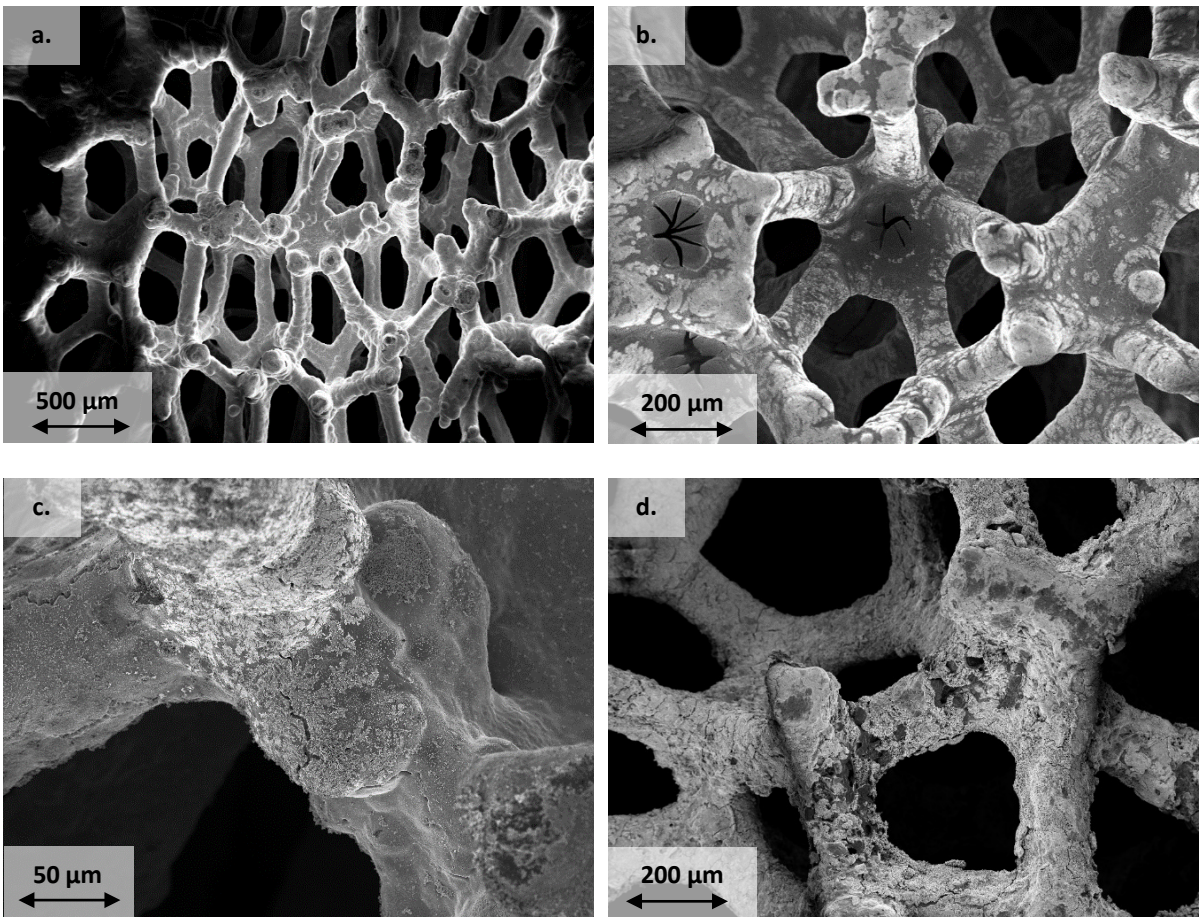

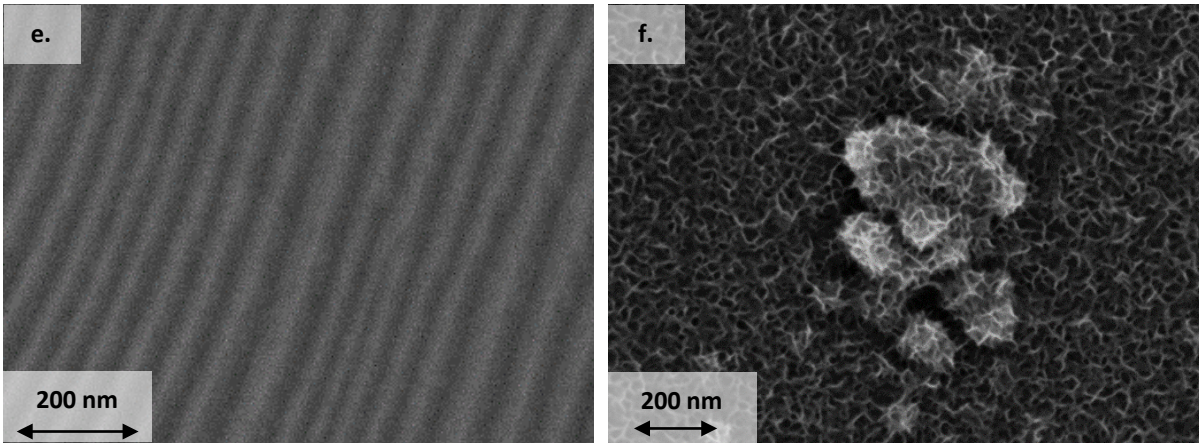

Figure 5. SEM images of nickel foams with different treatments. (a) Unused one as blank. (b) After several cycles, the cleaned foam shows residue. (c) Directly after activation. (d) Three months after being activated. (e) Close-up of blank nickel foam. (f) Close-up of freshly activated nickel foam. The close network of fibers is clearly visible.

The substrates used in this study are 4-alkylcyclohexanols. They can be derived from lignin because lignin contains phenolic motifs which are mostly alkylated in the 4-position.[43] Schutyser et al. reported an equimolar ratio of unsubstituted, 4-methyl-, 4-ethyl-, and 4-*n*-propylcyclohexanol.[43] Small-scale initial studies of the electrochemical oxidation of 4-methylcyclohexanol (**1'**) in batch-type cells and flow electrolyzers were reported previously (Scheme 2).[18]

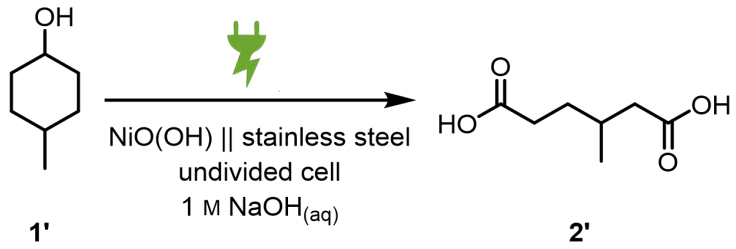

Scheme 2. Anodic Oxidation of 4-Methylcyclohexanol (**1'**) to 3-Methyladipic Acid (**2'**). Reaction conditions: $j_{activation}$ = 5.0 mA cm^{-2} (geometrical current density), $Q_{activation}$ = 9 C cm^{-2}, c(**1'**) = 0.1 M, V_{rct} = 100 mL, flow rate (Φ) = 61 mL min^{-1}, T_{rct} = 50 °C, j_{rct} = 5 mA cm^{-2}, applied charge (Q_{rct}) = 8.0F, v_{mix} = 300 rpm, mixing with magnetic stirring bar.

Nickel foam anodes were superior to sheets for the given reaction to form 3-methyladipic acid (**2'**). A screening of the activation and pore size showed that the activation is essential while the pore size does not have a significant influence. Since a basic medium is relevant for maintaining the self-electro-generating catalytic activity of nickel oxide hydroxide, various bases were tested in different concentrations, with 1 M caustic soda giving the best results. A concentration of 1 M was initially chosen for these heterogeneous electrochemical oxidations at activated nickel oxide hydroxide anodes.[17,39]

Figure 6. Setup of the reaction system: IKA magic LAB and magic PLANT mixing system (left half), moreover functioning as a reservoir; peristaltic pump (right); and the IKA ESF 6x18 flow electrolyzer (behind the pump).

Earlier findings were used as a basis to investigate the efficient scale for the oxidation of lignin-derived alkylated cyclohexanols while implementing the scaled electrolyzer IKA ESF 6x18.[18] A first test showed that **2'** can also successfully be synthesized with the novel flow electrolyzer (see Figure 6 and Scheme 2). Because only an 11% quantitative NMR (qNMR) yield of **2'** was achieved with the previously used parameter set (activation procedure as presented in the Experimental Section with $j_{activation}$ = 5.0 mA cm^{-2}, $Q_{activation}$ = 9 C cm^{-2}, c(**1'**) = 0.1 M, V_{rct} = 100 mL, flow rate (Φ) = 61 mL min^{-1}, T_{rct} = 50 °C, j_{rct} = 5 mA cm^{-2}, applied charge (Q_{rct}) = 8.0F, v_{mix} = 300 rpm, mixing with magnetic stirring bar), appropriate parameters for this novel reaction setup were optimized using a DoE approach. We used 4-ethylcyclohexanol (**1''**) as a substrate and evaluated the efficiency of the formation of 3-ethyladipic acid (**2''**) (Scheme 3) using qNMR. Since the importance of mixing was established on small scale,[18] an efficient physical mixing system with an IKA magic LAB device and integrated DR mixing unit was employed in this study (see Figure 1). In this way, an emulsion of **1''** and 1 M caustic soda as the electrolyte was produced in situ.

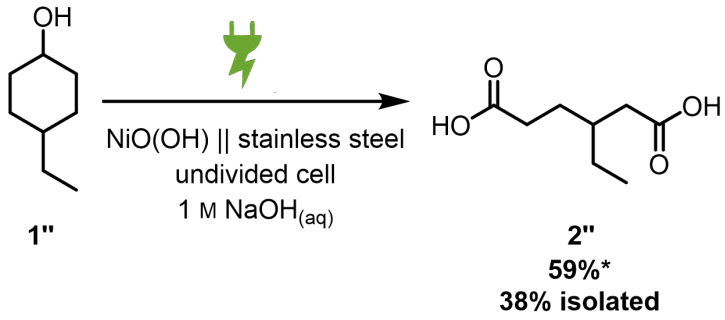

Scheme 3. Anodic Oxidation of 4-Ethylcyclohexanol (**1''**) to 3-Ethyladipic Acid (**2''**). The main product (**2''**) was synthesized in 59% qNMR yield (denoted by *).

For the parameter DoE screening, four parameters were varied: the concentration of the substrate (c), the reaction temperature (T), the flow rate of the reaction medium (Φ), and the current density (j), with the corresponding parameter limits displayed in Table 1. Besides the set parameter limits, central-point experiments were performed. All experiments were repeated once to determine the reproducibility of the experiments, and the reaction sequence of those 18 chemical tests was randomized. The reaction took between 0.9 and 2.3 days. The individual results are shown in Table S1. Quantitative NMR yields up to and including 59% were achieved for the target product (**2''**). Losses during the isolation protocol led to a maximal isolated yield of 38%. The nickel foam anode was reused for all reactions reported here, diminishing the waste stream.

Table 1. Parameter of the DoE screening. The geometrical current density refers to the current in relation to the geometrical anodic surface area of the anodic foam (108 cm^2). Reaction conditions: 1 M $NaOH_{(aq)}$, water, $j_{activation}$ = 7.5 mA cm^{-2} (geometrical current density), $Q_{activation}$ = 10 C cm^{-2}, 9F. The flow rate of the reaction Φ is the cumulative flow rate of both tubes. Each parameter has three data points.

parameter	**lower limit**	**central point**	**upper limit**
temperature of the reaction mixture, T (°C)	25.0	37.5	50.0
concentration of 4-ethylcyclohexanol, c (M)	0.2	0.35	0.5
flow rate of the reaction mixture, Φ (mL min^{-1})	10	30	50
geometrical current density, j (mA cm^{-2})	3	4	5

Figure 7 shows the screening results. The main influences were found to originate from the flow rate and the substrate concentration. Higher flow rates of 30 to 50 mL min^{-1} and lower

substrate concentrations of 0.2 to 0.35 M have a positive effect on 3-ethyladipic acid yield. This is shown by the large differences in product yield in the main effects plot on the left. Additionally, the Pareto chart shows that the interaction of parameters *cΦ* between concentration *c* and flow rate *Φ* possesses an influence below the significance limit. The parameters reaction temperature *T* and current density *j* are below the significance limit.

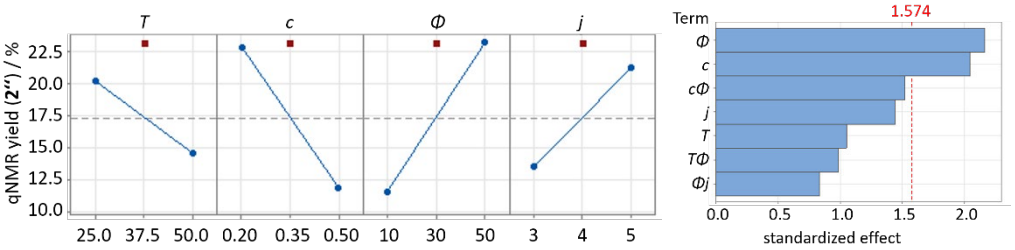

Figure 7. Left: Main effects plot of the four tested parameters, temperature *T* (in °C), substrate concentration *c* (in M), flow rate *Φ* (in mL min^{-1}), and current density *j* (in mA cm^{-2}). The concentration and flow rate were shown to be significant parameters. Blue: measured intervals; red: central points. Right: Pareto chart of the DoE showing the significance of single parameters or parameter interactions concerning the product's qNMR yield. Flow rate and the concentration of **1''** have the greatest influence on the product yield within the tested parameter range. The reliability R^2, which describes how accurately the data set illustrates the reaction behavior, is 34%. Both graphs show strong trends for main effects, which therefore are of high importance for the successful oxidation of **1''** to **2''**.

The analyzed product spectrum is depicted in Scheme 4.

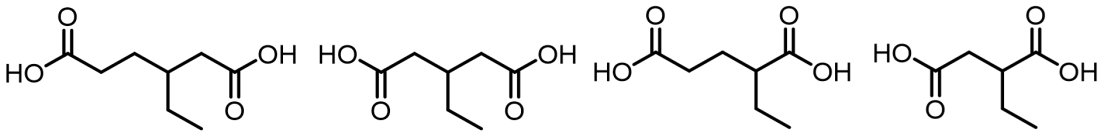

Scheme 4. Structures of 3-ethyladipic acid (**2''**), 3-ethylglutaric acid (**3**), 2-ethylglutaric acid (**4**), and ethylsuccinic acid (**5**).

The following optimized parameter set was identified: T = 25 °C, c(**1''**) = 0.2 M, $j_{reaction}$ = 5 mA cm^{-2}, Φ = 50 mL min^{-1}. Using these parameters, the best quantitative NMR yields were Y_{qNMR}(**2''**) = 59%, Y_{qNMR}(**3**) = 4%, Y_{qNMR}(**4**) = 4%, and Y_{qNMR}(**5**) = 1% (see Table S1, entry 18). Following the workup procedure, **2''** was isolated in a yield of 38%. This is the most efficient isolation of **2''** after an electrochemical synthesis reported to date.

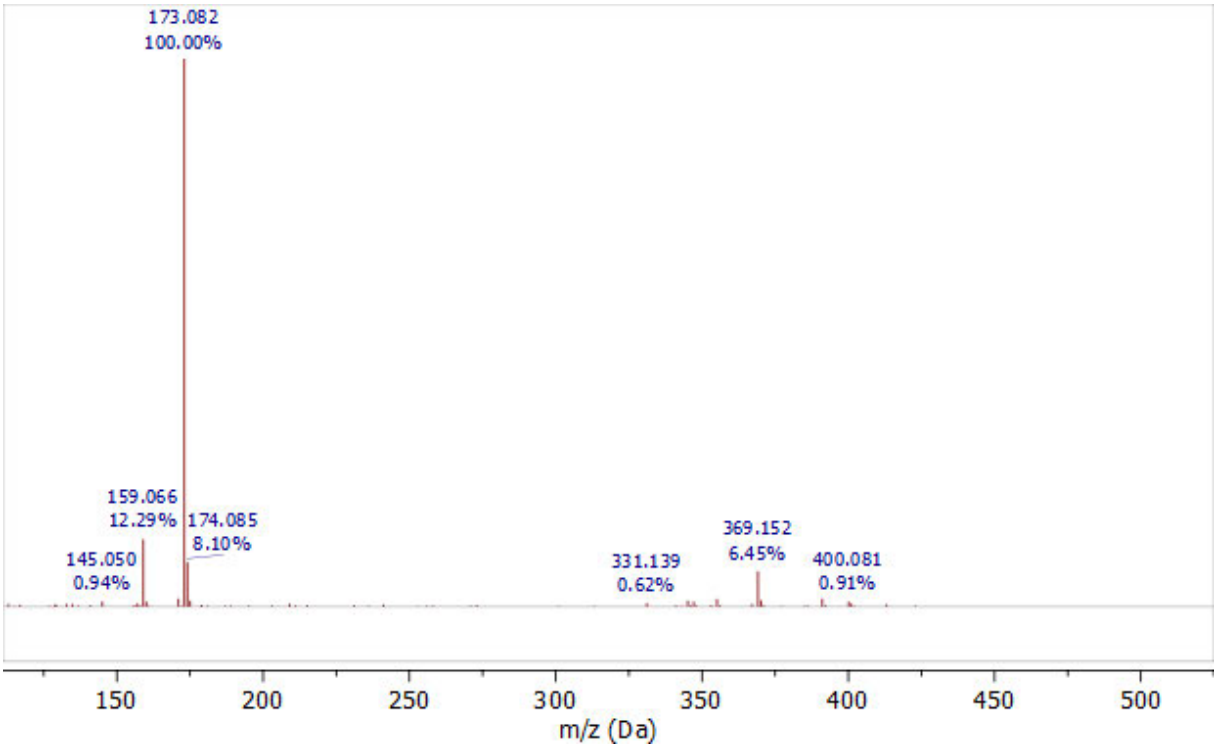

Figure 8. LCMS data of the product mixture with 3-ethyladipic acid (**2''**) as the main product. Higher-molecular-weight fractions are present, which originate from dimers bridged by metals such as sodium. The Q-TOF spectrum was recorded in negative mode.

Analysis of the first extraction fraction indicated that starting compound remained and that intermediates like ketones and further-oxidized species were present, plus colored impurities which could not be fully identified. Furthermore, liquid chromatography coupled to mass spectroscopy (LCMS) measurements of the crude product fraction indicated that higher-molecular-weight fractions of 350 to 400 Da are present in the product mixture (Figure 8). These mostly correspond to dimers bridged by metals such as sodium. The main product could be isolated by vacuum distillation, as presented in the Experimental Section. The isolation was exemplarily shown for the highest crude product yield and applied to a combination of the other DoE product fractions. For a comparison, qNMR yields of the products and byproducts for all DoE experiments were evaluated. The compounds present in this fraction did not correspond to clear sequences of dicarboxylic acid oligomers, and the extensive 2D NMR analysis (COSY, HSQC, HMBC, TOCSY) did not point out the precise structure of those compounds (Figures S12–S15). A MALDI-TOF MS measurement (Figure S10) of the distillation residue revealed that a broad range of oligomers of up to 3000 Da can be found in small concentrations. Although the molecular weight increases in the course of the distillation, there are species with a molecular weight of 1000 Da present after the electrolysis. Due to their very small concentration, those compounds are below the detection concentration in analysis methods like NMR and LCMS. These molecules most likely arise from side reactions and effectively increase the loss fraction observed during these longer screening reactions of up to 2.3 days per reaction (caused by higher substrate concentration). For industrial purposes, the time could be diminished significantly by increasing the number of flow

electrolyzers. Oxidative decarboxylation of the alkylated adipic acid was always observed upon reaction progress, as all product spectra of the screening reactions looked similar. Additionally, the formation of oligomers or polymers of diverse composition might hamper possible higher selectivities. Since their respective stoichiometric amounts are minimal, they were not detectable via NMR analysis.

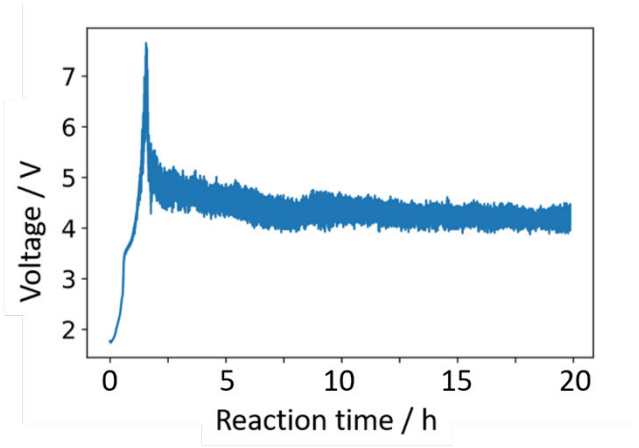

Figure 9. Exemplary voltage curve during the screening of the reaction to form 3-ethyladipic acid (**2''**).

Shedding light on the reaction progress, the voltage was recorded during the screening reactions (see the exemplary voltage curve in Figure 9). In the early reaction stage, the water-insoluble substrate lowers the ionic conductivity. Later on, the ionic product enhances the conductivity, which reduces the cell voltage. In the late reaction stage, this effect on the voltage competes with another one of decreasing substrate concentration: while the same current flows, a continuous production rate can only be compensated with a higher voltage. The fluctuations of up to 1.0 V are expected to be a result of hydrogen formation at the cathode. During the batch activation, gas bubbles of about the same diameter as the electrode spacing (1 mm) formed. The same is expected inside the flow electrolyzer. The intensity of the fluctuations depends on the availability of free active catalyst sites on the anode for the substrate.

The setup was designed to release the formed byproduct hydrogen from the reservoir in the fume hood. Because the outlet tubes were located above the flow cell, no accumulation of hydrogen is possible. Thus, its potential hazard of flammability is taken care of.

A reaction control experiment was performed (Figure 10) to investigate the product formation. Therefore, the reaction volume was further scaled up from 0.25 to 1.0 L. Since the first oxidation product of cyclohexanol is cyclohexanone,[17,37,41] readily available 4-ethylcyclohexanone (**1'''**) was used as the substrate (Scheme 5).

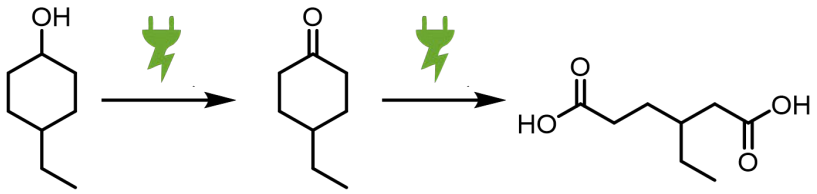

Scheme 5. Anodic oxidation of **1''** to **2''** proceeds via 4-ethylcyclohexanone (**1'''**).[17,37,41]

Every 10 h, 2 mL samples were taken from the reaction mixture, acidified to pH 1 using 4.5 M $H_2SO_{4(aq)}$, extracted with ethyl acetate (4 x 2 mL), and dried over $MgSO_4$, after which the solvent was removed. The samples were analyzed by ^{13}C inverse-gated NMR spectroscopy.

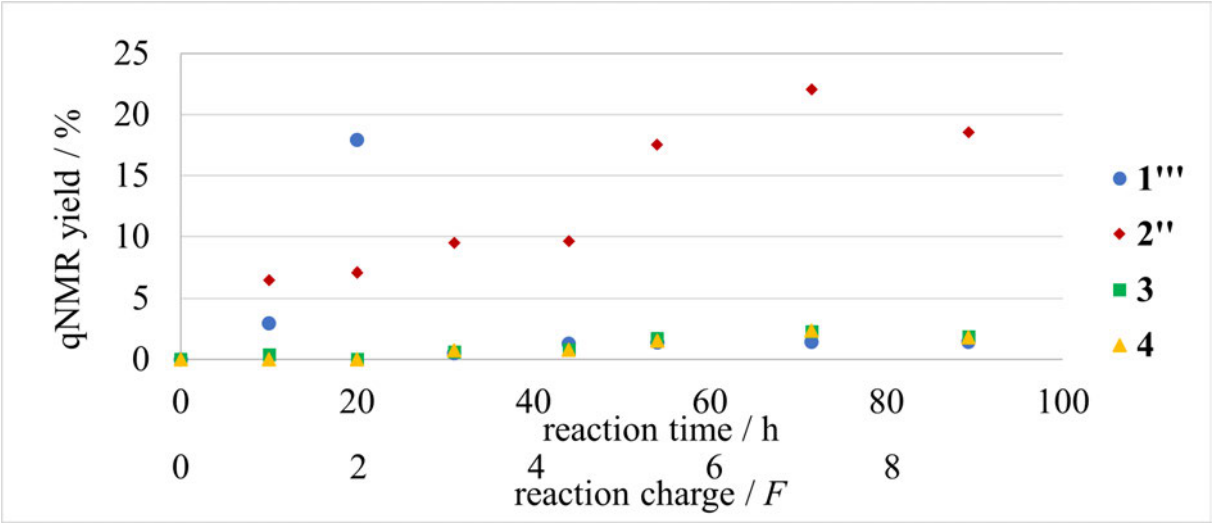

Figure 10. Reaction control experiment of 4-ethylcyclohexanone (**1'''**) to 3-ethyladipic acid (**2''**). Reaction conditions: T = 25 °C, c(**1''**) = 0.2 M, $j_{reaction}$ = 5 mA cm^{-2}, and Φ = 50 mL min^{-1}. Monitoring of the product yields was possible by ^{13}C inverse-gated NMR analyses of the samples. Remaining substrate and qNMR yields of the main product **2''** and side products 2- and 3-ethylglutaric acids (**4** and **3**) are shown. **1'''** shows fluctuations due to losses of the species during the workup. Details are given in Table S2. An applied charge of 9F was accumulated after approximately 90 h.

The main product formation shows small fluctuations, which might depend on the exact amount of reaction mixture drawn: (2.0 ± 0.1 mL). Toward the end of the reaction control experiment, the production rate flattens (Figure 10). A decreasing amount of substrate seems to correlate to decreasing product formation. Feeding the substrate to the reactor continuously was tested to enhance the production rate (Figure 11).

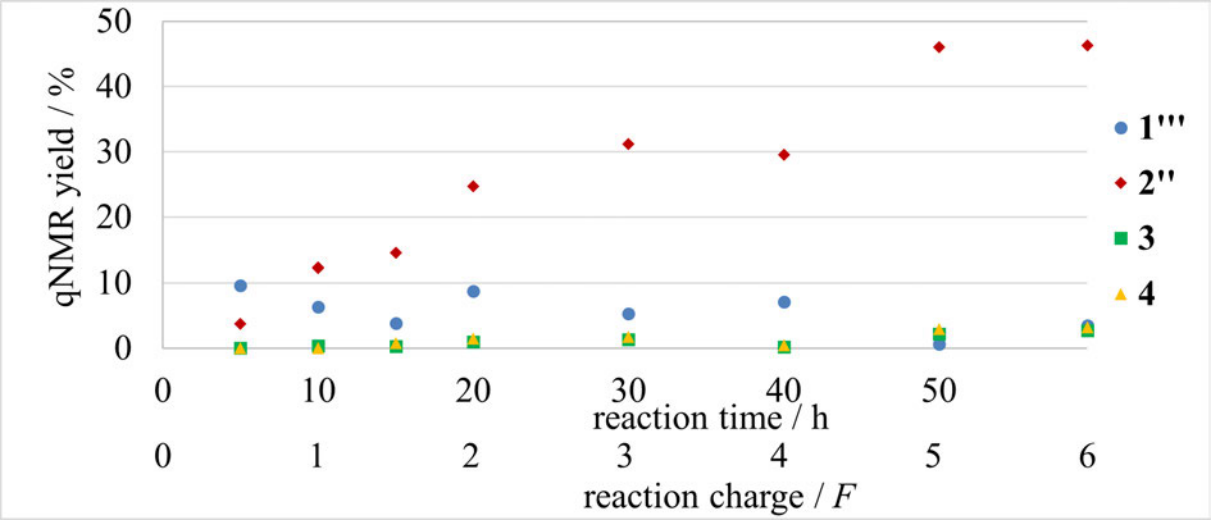

Figure 11. Reaction control experiment of 4-ethylcyclohexanone (**1'''**) to 3-ethyladipic acid (**2''**) including feeding of **1'''** for the theoretical amount of applied charge of 6 *F*. Reaction conditions: *T* = 25 °C, *c*(**1'''**) = 0.2 M = constant (**1'''** was fed continuously, according to the theoretical full consumption within 6 *F*), $j_{reaction}$ = 5 mA cm^{-2}, and Φ = 50 mL min^{-1}. Monitoring of the product yields was possible by ^{13}C inverse-gated NMR analyses of the 2 mL samples with 1,3,5-trimethoxybenzene as the internal standard. Remaining substrate and qNMR yields of the main product **2''** and side products 2- and 3-ethylglutaric acids (**4** and **3**) are shown. Details are given in Table S3. During the workup, **1'''** was partly evaporated, resulting in low relative "yields".

This parameter of substrate feeding was shown to significantly affect the production rate for 3-ethyladipic acid. In the depicted case, the yield nearly tripled after 6 *F*, which is the theoretically required amount of charge. Moreover, the yield was shown to nearly linearly increase with higher applied reaction charge. No generation of oxygen was observed in the early stage of the reaction. With the proportional behavior of product yield, no significant evolution of oxygen is expected. Additionally, the water oxidation at nickel oxide hydroxide has a high overpotential of 0.61 V,[44] resulting in all charge being applied for the main reaction. The observation that the total amount of **1'''** could not be shown to be constant in Figure 11 has to do with its relatively high volatility in combination with the rather harsh conditions during solvent evaporation. This concept is likely applicable to more oxidation reactions in the tested class of transformations.

CONCLUSION

Electrifying the adipic acid synthesis would be a very important step toward a climate-neutral chemical industry. For this reason, we designed and electrochemically optimized a 9-fold-scaled version of a flow electrolyzer for the electro-oxidation of alkylated cyclohexanols. From the Design of Experiments optimization with four tested parameters, quantitative NMR yields of up to 59% for 3-ethyladipic acid were obtained, which is the highest reported yield to date.[18] Moreover, a novel activation process for nickel anodes via contact of the nickel surface with caustic soda prior to the activation resulted in more reliable and robust nickel oxide hydroxide

formation. In this way, the nickel foam electrode can be reused multiple times. Employing this setup for more than 1000 working hours only showed little darkening of the nickel foam and weight loss, as a consequence of the cleaning process. A reaction control experiment revealed lower production rates for decreased substrate concentrations. If the substrate is continuously fed into the system, a significantly increased production rate is determined. Overall, the results brought forward in this study pave the way toward a large-scale clean bio-based adipic acid synthesis in an aqueous solution.

EXPERIMENTAL SECTION

General Considerations. Experimental details, analysis techniques, and additional information are given in the Supporting Information.

Activation of the nickel anode. The activation solution was prepared in accord with the literature:[42,45] 0.1 M $NiSO_{4(aq)}$, 0.1 M $NaOAc_{(aq)}$, and 5 mM $NaOH_{(aq)}$. The activation solution (420 mL) was added to a beaker-type cell (Figure 3) made of PMMA. A stainless steel plate (6 cm x 18 cm) electrode was immersed and connected. Before fully immersing and connecting the nickel foam anode at a 10 mm distance, it was immersed in or thoroughly rinsed with 1 M caustic soda and subsequently dripped off. A current density of 5.0 mA cm^{-2} was applied for 30 min. This correlates with a charge of 9 C cm^{-2}. The activation solution was stirred at 300 rpm. Afterward, the activated dark nickel foam was rinsed with demineralized water. The stainless steel cathode was cleaned by short immersion in diluted sulfuric acid (4 M) and then washed with water and treated with sandpaper (pore size 300) until it was optically homogeneously shiny. Then the cell was rearranged. Although SEM images revealed that the cleaning process does not fully recover the original surface morphology (Figure 5), the above-presented activation procedure can successfully be applied to the cleaned nickel foams as well.

4-Methylcyclohexanol oxidation. 4-Methylcyclohexanol (**1'**) (10 mmol, *c* = 0.1 M,[18] isomeric *cis/trans* mixture, as received) was mixed with caustic soda (1 M) in a beaker (*V* = 100 mL). The cell was tempered to 50 °C by using an external IKA HBC 5 thermostat. The reaction mixture was pumped through the electrolyzer with a flow rate of 61 mL min^{-1}. Here the applied current density was set to 5.0 mA cm^{-2}, and overall, a charge of 8.0*F* was used. After the reaction, the product mixture was collected, *tert*-butyl methyl ether was pumped through the cell, and an acid–base extraction was followed up. For this purpose, the basic reaction medium was extracted three times with *tert*-butyl methyl ether (each 100 mL), acidified with 4.5 M sulfuric acid to pH 1–2, and extracted four times with ethyl acetate (each 100 mL). After drying over $MgSO_4$ and subsequent solvent removal, the product mixture was analyzed using ^{1}H and ^{13}C inverse-gated NMR against 1,3,5-trimethoxybenzene as an internal standard.

Synthesis of 4-ethylcyclohexanol: 4-Ethylphenol (100 g, 0.82 mol) was dissolved in methanol (500 mL). Ruthenium/carbon (10 g, 5% Ru on C) was added to the 1 L autoclave, and a hydrogen atmosphere (10 bar) was applied. The autoclave was tempered to 120 °C. Samples (0.1 mL of reaction medium) were taken once a day to control the yield of 4-ethylcyclohexanol

(**1''**). The product formation was followed by gas chromatography, and the reaction was stopped when no further product formation was observed. 4-Ethylphenol was purchased from Sigma-Aldrich and ruthenium from Heraeus Chemicals. **1''** was synthesized on a 200 g scale in isolated yields of up to 95% after vacuum distillation.

Screening set-up. The setup is depicted in Figure 6. First, Masterflex PharMed™ BPT, L/S 16, tubes were installed for long-term use. For pumping, a Masterflex Ismatec™ peristaltic pump 78018-42 was used. For continuous mixing, an IKA magic LAB/IKA magic PLANT system was used with a DR mixing element. For all experiments, the mixing system worked at 12,000 rpm (≈ 70 L h^{-1} circulation rate) to achieve an optically semistable emulsion for the time during which it was pumped through the flow electrolyzer and back into the mixer. A charge of 9*F* was applied for all reactions.

Workup. After each experiment, the reaction mixture was collected in a vial, and *tert*-butyl methyl ether (50 mL) was pumped through the electrolyzer in cycling mode for 1 min to minimize losses. The same was done with 1 M caustic soda (50 mL). Following up, an acid–base extraction was performed using a perforator according to Ludwig (Figure S2). Hereby, high stirring speeds can be more easily achieved if a small stirring bar is inserted. Additionally, the solvent should be filled up in the main compartment. The yellow basic reaction mixture was extracted with MTBE overnight. Afterward, the two phases were separated, and the aqueous layer was acidified with 4.5 M $H_2SO_{4(aq)}$ to pH 1–2. The extraction of neutralized crude product was then performed in a perforator using ethyl acetate. The two organic fractions were dried over $MgSO_4$, the solvent was removed under lower pressure, and the product was analyzed via ^{13}C inverse-gated NMR with 1,3,5-trimethoxybenzene as an internal standard. The quantitative NMR yields were reported.

Isolation. The carboxylic acid mixture was distilled under a vacuum via a Vigreux column at 10^{-1}–2 mbar. The main product was distilled at a bath temperature of 180–240 °C. Most of the main product was distilled up to 220 °C. A last fraction was distilled between 220 °C and 240 °C without the Vigreux column. The remaining yellow color could be removed by recrystallization from heptane. If ethyl esters of the 3-ethyladipic acid were present, the product mixture was dissolved in caustic soda (3 M), heated to 80 °C, and rigorously stirred for 3 h. Then the mixture was extracted in a separation funnel of adequate size using *tert*-butyl methyl ether (3 x one-third of the aqueous volume), acidified to pH 2–3 with $H_2SO_{4(aq)}$ (4.5 M), and extracted with ethyl acetate. The organic fraction was dried over $MgSO_4$, and after solvent removal, the crystals were recovered. A second recrystallization round optically led to higher purity (Figure S8).

Reaction Control Experiment. 4-Ethylcyclohexanone (>98.0%) was purchased from TCI. For a bigger scale, the IKA magic PLANT 0.5 was replaced by an IKA magic PLANT 1.0. Therein, 4-ethylcyclohexanone (0.2 M, 200 mmol) was mixed with caustic soda (1 M, 970 mL). A current density of 5.0 mA cm^{-2} was applied. A total reaction charge of 8*F* was applied. The first six samples (2.0 ± 0.1 mL) were taken every 10 ± 2 h using a syringe. This volume does not significantly affect the total concentration of substrate or product in the reaction mixture.

They were acidified using 550 µL $H_2SO_{4(aq)}$ (4.5 M) to pH 1 and extracted using ethyl acetate (4 x 2 mL). The organic fraction was dried over $MgSO_4$, and the solvent was evaporated. The analysis was performed using ^{13}C inverse-gated NMR against 1,3,5-trimethoxybenzene as an internal standard.

In case of the feeding reaction control experiment, only the theoretically required amount of charge (6*F*) was applied, and the initial substrate mass of 4-ethylcyclohexanone was additionally fed to the reaction mixture continuously. The same conditions and workup were applied.

ASSOCIATED CONTENT

Supporting Information

The Supporting Information is available free of charge at https://pubs.acs.org/doi/10.1021/acs.oprd.3c00146.

General information on the analysis method, details on the used chemicals, general procedures for flow electrolysis and reaction control experiments, optimizations for the flow electrolysis, the activation process, details on the synthesis of 3-ethyladipic acid, and analytical spectra.

AUTHOR INFORMATION

Corresponding Author

Siegfried R. Waldvogel – *Department of Chemistry, Johannes Gutenberg University, 55128 Mainz, Germany. Institute of Biological and Chemical Systems − Functional Molecular Systems (IBCS-FMS), 76344 Eggenstein-Leopoldshafen, Germany; orcid.org/0000-0002-7949-9638*; Email: waldvogel@uni-mainz.de

Authors

Roland J.-R. Bednarz − *Department of Chemistry, Johannes Gutenberg University, 55128 Mainz, Germany*

Annika S. Gold − *Department of Chemistry, Johannes Gutenberg University, 55128 Mainz, Germany*; orcid.org/0009-0003-7014-5379

Jasmin Hammes − *Department of Chemistry, Johannes Gutenberg University, 55128 Mainz, Germany*

Denis F. Rohrmann − *Department of Chemistry, Johannes Gutenberg University, 55128 Mainz, Germany*

Silvio Natalello − *Department of Chemistry, Johannes Gutenberg University, 55128 Mainz, Germany*

Moritz Mann − *Department of Chemistry, Johannes Gutenberg University, 55128 Mainz, Germany*

Frank Weinelt − *Evonik Operations GmbH, Research, Development & Innovation, 45772 Marl, Germany*

Christopher Brauer − *IKA-Werke GmbH & Co. KG, 79219 Staufen, Germany*

Complete contact information is available at: https://pubs.acs.org/10.1021/acs.oprd.3c00146

Author Contributions

The manuscript was written through the contributions of all authors. All authors approved the final version of the manuscript.

Funding

Financial support by the Bundesministerium für Bildung und Forschung (BMBF) in the frame of APPLE FKZ 031B0663A is gratefully acknowledged.

Notes

The authors declare no competing financial interest.

ACKNOWLEDGMENT

The authors like to thank G. Glasser from the Max Planck Institute for Polymer Research for taking the SEM images, B. Bednarz for performing the XRD measurement, D. Vollmer for stimulating discussions, the university's workshop for designing the beaker-type cell for the nickel foam activation setup, and E. Berger-Nicoletti for measuring the MALDI-ToF MS.

REFERENCES

(1) Sato, K.; Aoki, M.; Noyori, R. A "Green" Route to Adipic Acid: Direct Oxidation of Cyclohexenes with 30% Hydrogen Peroxide. *Science* **1998**, *281* (5383), 1646−1647.

(2) Zhihong, W.; Seidel, S.; Rosland, A.; Tichy, M.; Conneely, D.; Gibbs, M.; Soyka, P.; McFarland, M.; Mainhardt, H.; Reimer, R.; Atkinson, M.; Agyemang-Bonsu, W.; Bakshi, V.; Dolin, E. J.; Gibbs, M. J.; Lawson, K.; Pape, D. *CO-CHAIRS, EDITORS AND EXPERTS*; IPCC, **2018**; p 131.

(3) Vardon, D. R.; Franden, M. A.; Johnson, C. W.; Karp, E. M.; Guarnieri, M. T.; Linger, J. G.; Salm, M. J.; Strathmann, T. J.; Beckham, G. T. Adipic Acid Production from Lignin. *Energy Environ. Sci.* **2015**, *8* (2), 617−628.

(4) Castellan, A.; Bart, J. C. J.; Cavallaro, S. Industrial Production and Use of Adipic Acid. *Catal. Today* **1991**, *9* (3), 237−254.

(5) Lang, M.; Li, H. Sustainable Routes for the Synthesis of Renewable Adipic Acid from Biomass Derivatives. *ChemSusChem* **2022**, *15* (1), e202101531.

(6) Myhre, G.; Shindell, D.; Bréon, F.-M.; Collins, W.; Fuglestvedt, J.; Huang, J.; Koch, D.; Lamarque, J.-F.; Lee, D.; Mendoza, B.; Nakajima, T.; Robock, A.; Stephens, G.; Zhang, H.; Aamaas, B.; Boucher, O.; Dalsøren, S. B.; Daniel, J. S.; Forster, P.; Granier, C.; Haigh, J.; Hodnebrog, Ø.; Kaplan, J. O.; Marston, G.; Nielsen, C. J.; O'Neill, B. C.; Peters, G. P.; Pongratz, J.; Ramaswamy, V.; Roth, R.; Rotstayn, L.; Smith, S. J.; Stevenson, D.; Vernier, J.-P.; Wild, O.; Young, P.; Jacob, D.; Ravishankara, A. R.; Shine, K. Anthropogenic and Natural Radiative Forcing. In *Climate Change 2013: The Physical Science Basis: Contribution of Working Group I to the Fifth Assessment Report*

of the Intergovernmental Panel on Climate Change; Stocker, T. F., Qin, D., Plattner, G.-K., Tignor, M., Allen, S. K., Boschung, J., Nauels, A., Xia, Y., Bex, V., Midgley, P. M., Eds.; Cambridge University Press: Cambridge, U.K., **2013**; pp 659−740.

(7) Reimer, R. A.; Slaten, C. S.; Seapan, M.; Lower, M. W.; Tomlinson, P. E. Abatement of N_2O Emissions Produced in the Adipic Acid Industry. *Environ. Prog.* **1994**, *13* (2), 134−137.

(8) *BASF Report 2021*. BASF, 2022. https://report.basf.com/2021/en/_assets/downloads/entire-basf-ar21.pdf (accessed 2023-05-02).

(9) Ehrenfeld, W. Prozessinnovationen Zur Reduktion von Treibhausgasen: Ein Beispiel Aus Der Chemischen Industrie. *Wirtsch. Im Wandel* **2011**, *17* (5), 179.

(10) Rinaldi, R.; Jastrzebski, R.; Clough, M. T.; Ralph, J.; Kennema, M.; Bruijnincx, P. C. A.; Weckhuysen, B. M. Paving the Way for Lignin Valorisation: Recent Advances in Bioengineering, Biorefining and Catalysis. *Angew. Chem., Int. Ed.* **2016**, *55* (29), 8164−8215.

(11) Breiner, M.; Zirbes, M.; Waldvogel, S. R. Comprehensive Valorisation of Technically Relevant Organosolv Lignins via Anodic Oxidation. *Green Chem.* **2021**, *23* (17), 6449−6455.

(12) Strassberger, Z.; Tanase, S.; Rothenberg, G. The Pros and Cons of Lignin Valorisation in an Integrated Biorefinery. *RSC Adv.* **2014**, *4* (48), 25310−25318.

(13) Kruger, J. S.; Dreiling, R. J.; Wilcox, D. G.; Ringsby, A. J.; Noon, K. L.; Amador, C. K.; Brandner, D. G.; Ramirez, K. J.; Haugen, S. J.; Klein, B. C.; Davis, R.; Hanes, R. J.; Happs, R. M.; Cleveland, N. S.; Christensen, E. D.; Miscall, J.; Beckham, G. T. Lignin Alkaline Oxidation Using Reversibly-Soluble Bases. *Green Chem.* **2022**, *24* (22), 8733−8741.

(14) Matthiesen, J. E.; Carraher, J. M.; Vasiliu, M.; Dixon, D. A.; Tessonnier, J.-P. Electrochemical Conversion of Muconic Acid to Biobased Diacid Monomers. *ACS Sustainable Chem. Eng.* **2016**, *4* (6), 3575−3585.

(15) Dell'Anna, M. N.; Laureano, M.; Bateni, H.; Matthiesen, J. E.; Zaza, L.; Zembrzuski, M. P.; Paskach, T. J.; Tessonnier, J.-P. Electrochemical Hydrogenation of Bioprivileged Cis, Cis -Muconic Acid to trans-3-Hexenedioic Acid: From Lab Synthesis to Bench-Scale Production and Beyond. *Green Chem.* **2021**, *23* (17), 6456−6468.

(16) Suastegui, M.; Matthiesen, J. E.; Carraher, J. M.; Hernandez, N.; Rodriguez Quiroz, N.; Okerlund, A.; Cochran, E. W.; Shao, Z.; Tessonnier, J. Combining Metabolic Engineering and Electrocatalysis: Application to the Production of Polyamides from Sugar. *Angew. Chem., Int. Ed.* **2016**, *55* (7), 2368−2373.

(17) Schäfer, H.-J. Oxidation of Organic Compounds at the Nickel Hydroxide Electrode. *Top. Curr. Chem.* **1987**, *142*, 101−129.

(18) Rauen, A. L.; Weinelt, F.; Waldvogel, S. R. Sustainable Electroorganic Synthesis of Lignin-Derived Dicarboxylic Acids. *Green Chem.* **2020**, *22* (18), 5956−5960.

(19) Bednarz, R. J.-R.; Brauer, C.; Waldvogel, S. R. Out of Its Infancy: Modular Flow Cell Offers Enormous Scaling Potential for Electrosynthesis. *Wiley Analytical Science Magazine*, October 18, 2021. https://analyticalscience.wiley.com/do/10.1002/was.000600208/ (accessed 2023-05-02).

(20) Waldvogel, S. R.; Janza, B. Renaissance elektrochemischer Methoden zum Aufbau komplexer Moleküle. *Angew. Chem.* **2014**, *126* (28), 7248−7249.

(21) Röckl, J. L.; Pollok, D.; Franke, R.; Waldvogel, S. R. A Decade of Electrochemical Dehydrogenative C,C-Coupling of Aryls. *Acc. Chem. Res.* **2020**, *53* (1), 45−61.

(22) Arndt, S.; Weis, D.; Donsbach, K.; Waldvogel, S. R. The "Green" Electrochemical Synthesis of Periodate. *Angew. Chem., Int. Ed.* **2020**, *59* (21), 8036−8041.

(23) Kingston, C.; Palkowitz, M. D.; Takahira, Y.; Vantourout, J. C.; Peters, B. K.; Kawamata, Y.; Baran, P. S. A Survival Guide for the "Electro-Curious". *Acc. Chem. Res.* **2020**, *53* (1), 72−83.

(24) Yan, M.; Kawamata, Y.; Baran, P. S. Synthetic Organic Electrochemical Methods Since 2000: On the Verge of a Renaissance. *Chem. Rev.* **2017**, *117* (21), 13230−13319.

(25) Klein, M.; Waldvogel, S. R. Counter Electrode Reactions – Important Stumbling Blocks on the Way to a Working Electro-organic Synthesis. *Angew. Chem., Int. Ed.* **2022**, *61* (47), e202204140.

(26) Beil, S. B.; Pollok, D.; Waldvogel, S. R. Reproducibility in Electroorganic Synthesis – Myths and Misunderstandings. *Angew. Chem., Int. Ed.* **2021**, *60* (27), 14750−14759.

(27) Dörr, M.; Hielscher, M. M.; Proppe, J.; Waldvogel, S. R. Electrosynthetic Screening and Modern Optimization Strategies for Electrosynthesis of Highly Value-added Products. *ChemElectroChem* **2021**, *8* (14), 2621−2629.
(28) Seidler, J.; Bernhard, R.; Haufe, S.; Neff, C.; Gärtner, T.; Waldvogel, S. R. From Screening to Scale-Up: The DoE-Based Optimization of Electrochemical Reduction of L-Cystine at Metal Cathodes. *Org. Process Res. Dev.* **2021**, *25* (12), 2622−2630.
(29) Pollok, D.; Waldvogel, S. R. Electro-organic Synthesis – A 21st Century Technique. *Chem. Sci.* **2020**, *11* (46), 12386−12400.
(30) Gleede, B.; Selt, M.; Gütz, C.; Stenglein, A.; Waldvogel, S. R. Large, Highly Modular Narrow-Gap Electrolytic Flow Cell and Application in Dehydrogenative Cross-Coupling of Phenols. *Org. Process Res. Dev.* **2020**, *24* (10), 1916−1926.
(31) Atobe, M.; Tateno, H.; Matsumura, Y. Applications of Flow Microreactors in Electrosynthetic Processes. *Chem. Rev.* **2018**, *118* (9), 4541−4572.
(32) Pletcher, D.; Green, R. A.; Brown, R. C. D. Flow Electrolysis Cells for the Synthetic Organic Chemistry Laboratory. *Chem. Rev.* **2018**, *118* (9), 4573−4591.
(33) Gütz, C.; Stenglein, A.; Waldvogel, S. R. Highly Modular Flow Cell for Electroorganic Synthesis. *Org. Process Res. Dev.* **2017**, *21* (5), 771−778.
(34) Jud, W.; Salazar, C. A.; Imbrogno, J.; Verghese, J.; Guinness, S. M.; Desrosiers, J.-N.; Kappe, C. O.; Cantillo, D. Electrochemical Oxidation of Alcohols Using Nickel Oxide Hydroxide as Heterogeneous Electrocatalyst in Batch and Continuous Flow. *Org. Process Res. Dev.* **2022**, *26* (5), 1486−1495.
(35) Selt, M.; Franke, R.; Waldvogel, S. R. Supporting-Electrolyte-Free and Scalable Flow Process for the Electrochemical Synthesis of 3,3′,5,5′-Tetramethyl-2,2′-biphenol. *Org. Process Res. Dev.* **2020**, *24* (10), 2347−2355.
(36) Fleischmann, M.; Korinek, K.; Pletcher, D. The Oxidation of Organic Compounds at a Nickel Anode in Alkaline Solution. *J. Electroanal. Chem. Interfacial Electrochem.* **1971**, *31* (1), 39−49.
(37) Lyalin, B. V.; Petrosyan, V. A. Electrosynthesis of Adipic Acid by Undivided Cell Electrolysis. *Russ. Chem. Bull.* **2004**, *53* (3), 688−692.
(38) Lyalin, B. V.; Petrosyan, V. A. Oxidation of Organic Compounds on NiOOH Electrode. *Russ. J. Electrochem.* **2010**, *46* (11), 1199−1214.
(39) Vértes, G.; Horányi, G.; Nagy, F. A New Method for the Electrochemical Oxidation of Alcohols. *Tetrahedron* **1972**, *28*, 37−42.
(40) Kaulen, J.; Schäfer, H.-J. Oxidation of Primary Alcohols to Carboxylic Acids at the Nickel Hydroxide Electrode. *Synthesis* **1979**, *1979*, 513−516.
(41) Li, Z.; Li, X.; Zhou, H.; Xu, Y.; Xu, S.-M.; Ren, Y.; Yan, Y.; Yang, J.; Ji, K.; Li, L.; Xu, M.; Shao, M.; Kong, X.; Sun, X.; Duan, H. Electrocatalytic Synthesis of Adipic Acid Coupled with H_2 Production Enhanced by a Ligand Modification Strategy. *Nat. Commun.* **2022**, *13* (1), 5009.
(42) Briggs, G. W. D.; Jones, E.; Wynne-Jones, W. F. K. The Nickel Oxide Electrode. *Trans. Faraday Soc.* **1955**, *51*, 1433−1442.
(43) Schutyser, W.; Van den Bossche, G.; Raaffels, A.; Van den Bosch, S.; Koelewijn, S.-F.; Renders, T.; Sels, B. F. Selective Conversion of Lignin-Derivable 4-Alkylguaiacols to 4-Alkylcyclohexanols over Noble and Non-Noble-Metal Catalysts. *ACS Sustainable Chem. Eng.* **2016**, *4* (10), 5336−5346.
(44) Fidelsky, V.; Toroker, M. C. The Secret behind the Success of Doping Nickel Oxyhydroxide with Iron. *Phys. Chem. Chem. Phys.* **2017**, *19* (11), 7491−7497.
(45) Schäfer, H.-J.; Kaulen, J. Oxidation of Alcohols by Electrochemically Regenerated Nickel Oxide Hydroxide. Selective Oxidation of Hydroxysteroids. *Tetrahedron* **1982**, *38* (22), 3299−3308.

ENTRY FOR THE TABLE OF CONTENTS

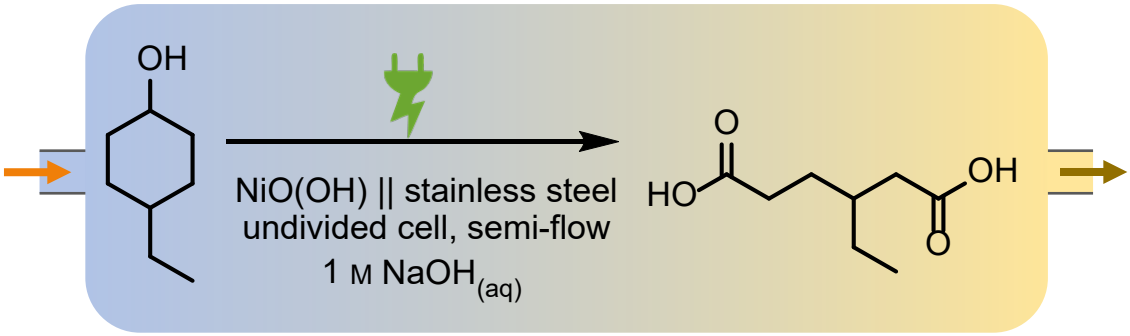

SUSTAINABLY SCALED ELECTROCHEMICAL SYNTHESIS OF 3-PROPYLADIPIC ACID IN LINE WITH FLUCTUATING GRID SUPPLY

This manuscript has been published in the peer-reviewed journal ChemCatChem in 2023. The editors accepted the reuse of this content in this thesis. It is reprinted here with permission of Bednarz, R. J.-R., Jiménez-Meneses, P., Gold, A. S., Monllor-Satoca, D., Stenglein, A., Gómez, R., Waldvogel, S. R., *ChemCatChem* **2023**, *15*, e202300606. The text on the following pages reproduces the following article literally, including all figures and tables.

Author Contributions (following NISO standard): **R. J.-R. Bednarz**: Conceptualization (lead), formal analysis (lead), investigation (lead), methodology (lead), project administration (lead), visualization (lead), writing – original draft (lead), writing – review & editing (lead); **P. Jiménez-Meneses**: conceptualization (equal), formal analysis (supporting), investigation (equal), methodology (lead), project administration (lead), visualization (equal), writing – original draft (lead), writing – review & editing (lead); **A. S. Gold**: formal analysis (equal), investigation (equal), visualization (supporting), writing – original draft (supporting), writing – review & editing (supporting); **D. Monllor-Satoca**: investigation (equal), writing – original draft (supporting), writing – review & editing (supporting); **A. Stenglein**: investigation (supporting), resources (equal), writing – original draft (supporting), writing – review & editing (supporting); **R. Gómez**: funding acquisition (lead), conceptualization (supporting), resources (supporting), formal analysis (supporting), methodology (equal), project administration (supporting), supervision (equal), validation (equal), writing – original draft (equal), writing – review & editing (equal); **S. R. Waldvogel**: Funding acquisition (lead), conceptualization (equal), resources (lead), formal analysis (equal), methodology (lead), project administration (equal), supervision (lead), validation (lead), writing – original draft (equal), writing – review & editing (equal).

Motivated by the aim to implement more sustainable and climate-friendly technologies in the chemical industry, we envisioned an electrochemical process which utilizes a biobased feedstock and produces in an environmentally benign way. Approaching an important adipic acid derivative, originating from lignin,[11] was the foundation of this research: 3-propyladipic acid from 4-propylcyclohexanol. Second, critical steps for an upscaling of its electrochemical conversion, first reported by Rauen et al. in low yields and in mg scale, have been investigated.[15]

Here, we tackled the scale-up to a decaliter scale, in modular electrochemically continuous-stirred-tank-reactors and intended to significantly improve the yields. Investigating the most relevant parameters within two Design of Experiments screening sets, we implemented a mixing technique for the naturally biphasic electrolyte, achieving its emulsification. Hereby, the Venturi effect was used, namely via an eductor piece. Furthermore, the reaction

temperature had a more crucial role for the propyl substituent, compared to our previous study, published in OPRD. Possibly, the higher lipophilicity of the original 4-propylcyclohexanol or -cyclohexanone compared to the ethyl derivative hampers the initial miscibility, which is enhanced with increasing temperature.

With these parameters improved, we modified the reactor and stuck to an electrode stack of nickel foam and stainless steel. Thereby, it was possible to gain kinetic information on the process, e. g. through reaction control experiments. In the resulting analysis, a trend towards a very high selectivity of the main product formation at low applied charges stood out. This motivated us to postulate a formation mechanism for the by-products characterized during the reaction. Here, we based our postulates on published mechanistic steps[13–14,20–21] and pointed out differences to a study by Lyalin et al.[14,18,22]

Precisely tracking the development of the formed intermediates and products on a decaliter scale revealed maximum productivity of 3-propyladipic acid when the maximum concentration of intermediate was present. We then investigated the electro-oxidation of 4-propylcyclohexanone, which was the former intermediate, and fed it into the system continuously. In this way, its concentration should remain constant. We indeed observed a nearly constant productivity of our target product and increased its selectivity.

Overall, we designed and validated a semitechnical electrochemically continuous-stirred tank reactor and a modular electrode stack with a geometrical surface area of 1225 cm^2. The chosen model reaction was the electro-oxidation of potentially bio-based 4-propylcyclohexanol to get 3-propyladipic acid. We showed the relevance of homogenous electrolyte mixing for this electro-oxidation and even suggested a successful emulsification technique. Besides our postulated mechanism, the performed reaction control experiment paved the way to get 48% qNMR yield of 3-propyladipic acid – about 2.5 mol.

SUSTAINABLY SCALED ELECTROCHEMICAL SYNTHESIS OF 3-PROPYLADIPIC ACID IN LINE WITH FLUCTUATING GRID SUPPLY

Roland J.-R. Bednarz[+],[a], Pilar Jiménez-Meneses[+],[b], Annika S. Gold[a], Damián Monllor-Satoca[b], Andreas Stenglein[a], Roberto Gómez[b], Siegfried R. Waldvogel[a,c,d]*

a Department of Chemistry, Johannes Gutenberg University, Duesbergweg 10–14, 55128 Mainz, Germany.

b University Institute of Electrochemistry, University of Alicante, Carretera San Vicente del Raspeig s/n, 03690 San Vincente del Raspeig - Alicante, Spain.

c Institute of Biological and Chemical Systems – Functional Molecular Systems (IBCS-FMS), Hermann-von-Helmholtz-Platz 1, 76344 Eggenstein-Leopoldshafen, Germany.

d Max-Planck-Institute for Chemical Energy Conversion, Stiftstraße 34–36, 45470 Mülheim an der Ruhr, Germany.

* Emails: waldvogel@uni-mainz.de, roberto.gomez@ua.es

[+] These authors contributed equally to this work.

KEYWORDS. carboxylic acids, electrocatalysis, electrochemistry, oxidation, renewable resources

ABSTRACT. Chemical production is a significant contributor to global climate change, which expedites the growing demand for transitioning to more sustainable and climate-friendly methodologies. Ideally this should include high compatibility with the fluctuating electricity supply which results from renewable energy sources in the electrical grid. Here we show an electrochemical path for the 3-propyladipic acid synthesis from 4-propylcyclohexanol implementing a semi-technical electrochemical continuously stirred tank reactor. Following a *Design of Experiments* approach, we found a strong influence of the biphasic electrolyte mixing and the continuous feeding in of the substrate. By switching to an electrolyte recirculation mode and efficient mixing, the isolated product yield could be increased up to 31% for a 10 L total reaction volume, indicating the potential for further scale-up into the technical range. This reaction proceeds while forming several by-products, which have not been fully described yet. A proposal for the formation mechanism is included.

INTRODUCTION. The continuing use of fossil fuels and the net emission of greenhouse gases are among the predominant industrial issues of this century. With a predicted annual world population growth of 0.9% on average until 2035[1] and an exceeding primary energy demand, one-world chemistry has been advocated as an important approach with respect to the global ecological footprint.[2] Organic electrosynthesis appears as a promising approach to make large-scale chemical reactions more environmentally benign while offering precise control over reaction conditions.[3] The prominent feature of this methodology is the use of electrons as green reagent, if renewable electricity is used.[4] Additionally, the direct use of electrons

significantly decreases reaction waste by replacing oxidizers and reductants with reusable electrodes. The electrochemical process becomes inherently safe as the reaction stops once the electrical current flow ends. A further advantage is the adjustable power consumption, via the employed number of cells or the current density, taking into account variances in the grid supply.[5] Moreover, electrochemistry can offer superior or novel synthetic methods[6] and galvanostatic processes enable easy scalability (vide infra).[7]

Some electro-synthetic processes require low current densities to prevent product degradation, which leads to lower space-time-yields. One classic remedy is enlarging the active electrode surface area, which is realizable with foam electrodes or increased electrode size. Besides simply using two larger planar electrodes, electrode stacks with bipolar or monopolar connections are not necessarily limited in number, allowing for increases in electrode size with only minor increases in the cell volume.[8]

Additionally, the use of biomass as a feedstock instead of fossil-fuels is another pathway to increase the sustainability of chemical processes.[9] This change would allow for a decrease in greenhouse gas emissions by more than 60%,[10] compared to traditional synthesis pathways of adipic acid. Previous work by Schutyser et al. illustrated this point, reporting the depolymerization and hydrogenation of lignin to 4-alkylcyclohexanols, such as 4-propylcyclohexanol.[11] Consequently, 4-propylcyclohexanol may become abundantly available when lignin is heavily used as a regenerative feedstock in the future. Therefore, this study focuses on the anodic oxidation of this cyclic alcohol at activated nickel foam electrodes, with a focus on the derived scale-up. Nickel oxyhydroxide anodes regenerate during the electrolysis in alkaline media and have been employed for lignin degradation.[12] The electrochemical oxidation of alcohols has previously been investigated by Schäfer et al., who showed the successful oxidation of alcohols at such nickel oxyhydroxide anodes in caustic soda.[13] Based on these results, Lyalin and Petrosyan electrochemically synthesized adipic acid from cyclohexanol with a yield of 47%.[14] For cyclohexanol, they observed glutaric and succinic acids as by-products, which could also be confirmed by our group for methyl-substituted cyclohexanols.[15] Herein, we present significant improvements in scaling up such electrooxidations, tackling miscibility challenges for biphasic reaction mixtures and enhancing the product yield via substrate feeding. Lastly, we revised the reported reaction mechanism and propose changes how the radical mechanism at a nickel oxyhydroxide anode likely leads to oligomeric species, not described earlier.

RESULTS AND DISCUSSION. We investigated the electrochemical conversion of the alicyclic alcohol **1** into the corresponding adipic acid **2** (Scheme 1).

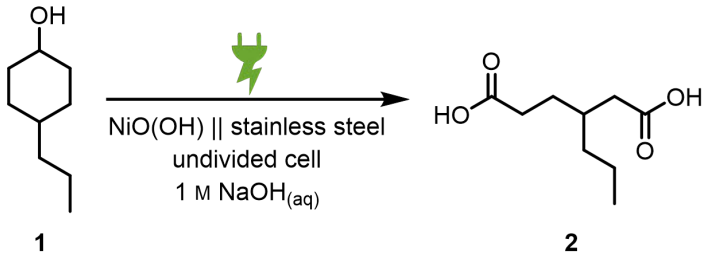

1 **2**

Scheme 1. Anodic oxidation of 4-propylcyclohexanol (**1**) to 3-propyladipic acid (**2**) at nickel oxyhydroxide foam anodes.

An efficient approach to quickly identify significant parameters which affect the product yield is a *Design of Experiments* (*DoE*) parameter screening.[16] Since an active nickel foam anode and a stainless steel cathode are superior electrode materials for this reaction, as previously shown by Rauen et al.,[15] optimization focused on the activation parameters of the nickel foam (current density and applied charge), the current density and applied charge during the reaction, as well as substrate concentration, mixing with the electrolyte, and reaction temperature. All parameters, corresponding to both anode activation and reaction, their corner values, and central points are listed in Table 1 (first row):

Table 1. Parameters of 2^{7-3} DoE screening with a resolution of IV. Seven parameters and their interactions were checked: substrate concentration ($c_{substrate}$), reaction temperature (T), mixing speed with a magnetic stirring bar (v_{mix}), reaction current density (j_{rct}), total applied charge for the reaction (Q_{rct}), current density for activation (j_{act}) and applied charge for the activation (Q_{act}). With two replications and two center point experiments, 34 experiments were performed. Other parameters: 1 M $NaOH_{(aq)}$ as the electrolyte, total reaction volume: V_{tot} = 100 mL, anode geometric surface area A_{anode} = 72 cm^2.

$c_{substrate}$ / M[a]	T / °C[b]	v_{mix} / rpm[c]	j_{rct} / mA cm^{-2}[d]	Q_{rct} / F	j_{act} / mA cm^{-2}[d]	Q_{act} / C cm^{-2}[d]
0.3	40	200	6	6.5	3.5	0.5
0.4	50	350	7	7.0	5.0	5.5
0.5	60	500	8	7.5	6.5	10.5

[a] Initial concentration of 4-propylcyclohexanol. [b] Temperature set in the thermostat. [c] A cylindrical magnetic stirring bar was used. [d] The values refer to the anode geometric surface area.

All experiments were analyzed using ^{13}C Inverse Gated NMR spectroscopy, with 1,3,5-trimethoxybenzene as an internal standard. The individual results are presented in the supporting information (supporting information, Table S1). Hereafter, a summary of the *DoE*

results is shown in a main effects plot, where all the trends for the tested parameters are presented (Figure 1). Thereby, parameter trends that lie below the significance level are highlighted in grey. Thus, their effect on the product yield in the tested range is insignificant for the tested setup.

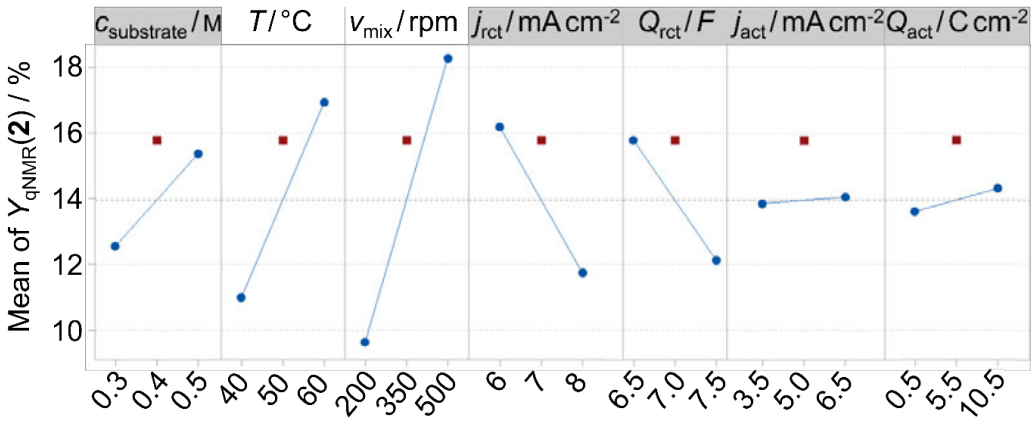

Figure 1. Main effects plot of the Design of Experiments (DoE) screening applying a 2^{7-3}-design with a resolution of IV. The R^2 value for an α-value of 0.05 is 28%. Corner points are represented by blue circles, and center points by red squares. A grey background represents a term not included in the model.

The favorable trends towards higher temperatures (60 °C) and higher stirring speeds (500 rpm) both lead to higher phase exchange rates. The Pareto chart (Figure 2) displays the relative significance of all parameters.

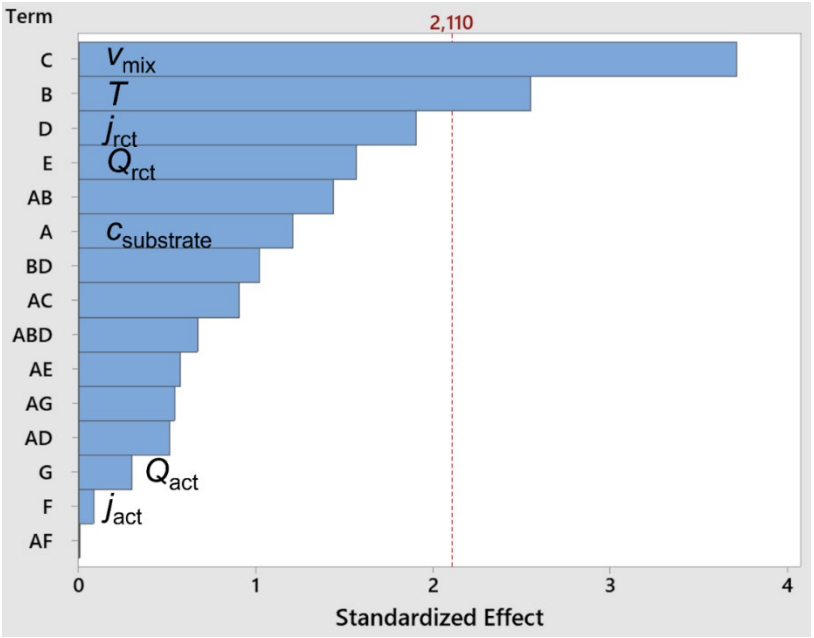

Figure 2. Pareto chart of the first DoE screening results. The most significant effects on the product yield are triggered by the stirring speed (term C) and the reaction temperature (term B). The current density (D), applied charge (E), other parameters, and parameter interactions are below the significance level of α=0.05. The R^2 value is 28%.

These results in particular point out the importance of mixing: at an increased temperature of 60 °C and under vigorous stirring as the yield significantly increases. A previous report revealed that elevated temperatures were unfavorable to achieve higher yields, which is one reason why the temperature was not enhanced further.[15] The screening of higher current densities than those reported previously[15] showed a downward yield trend for this substrate. Likewise, the applied charge value showed a downward trend. The data indicates this trend in a value range beneath the theoretically required 8.0*F*. Therefore, the summarily presented trend may be a sum of fluctuations or it may indicate that side reactions take place which require less charge than the productive pathway. Since this parameter is of lower significance, we focused on the most influential ones instead, namely temperature and stirring speed. This observation has led to the implementation of an eductor, which allows efficient mixing of the alcohol **1** and the aqueous electrolyte, as its solubility is quite low (675.8 mg alcohol/L water, at 20 °C, Figure 3).

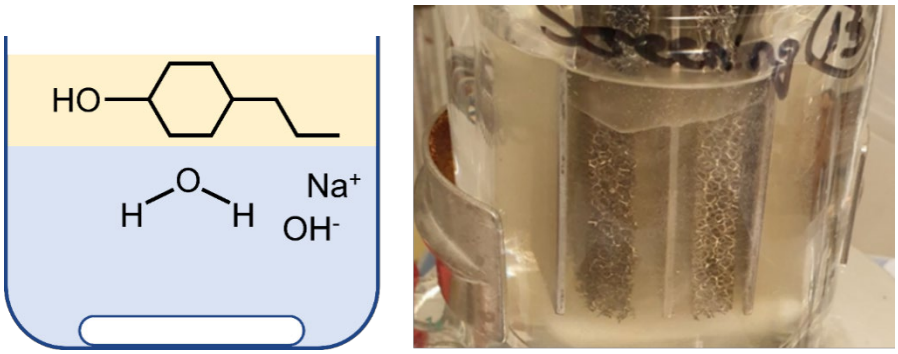

Figure 3. Left: Sketch of the naturally biphasic system of the electrolyte components **1** and caustic soda. Right: Photo taken during an electrolysis during which the biphasic system is visible.

We tested the mixing of two immiscible phases with a commercially available eductor piece (Figure 4), which is a mixing device using the Venturi effect.[17] This biphasic electrolyte system uses the bottom flow of the aqueous layer (1 M $NaOH_{(aq)}$) to suck the above-lying organic phase (4-propylcyclohexanol) in a designed junction. The diameters of the two inflows are intentionally different to induce a pressure drop and a liquid suction (Venturi effect). The resulting turbulence becomes more significant with increasing flow rates. A model system consisting of iodine-colored cyclohexane and water was employed to verify the mixing properties of this setup. The resultant mixture appeared to be homogeneous, confirming the emulsification function. The real electrolyte system also resulted in a homogenous dispersion of the alcohol in the aqueous solution. We could show that flow rates of 250 and 65 L h^{-1} are both sufficient for the generation of an emulsion of the substrate and the aqueous solution for 12 h.

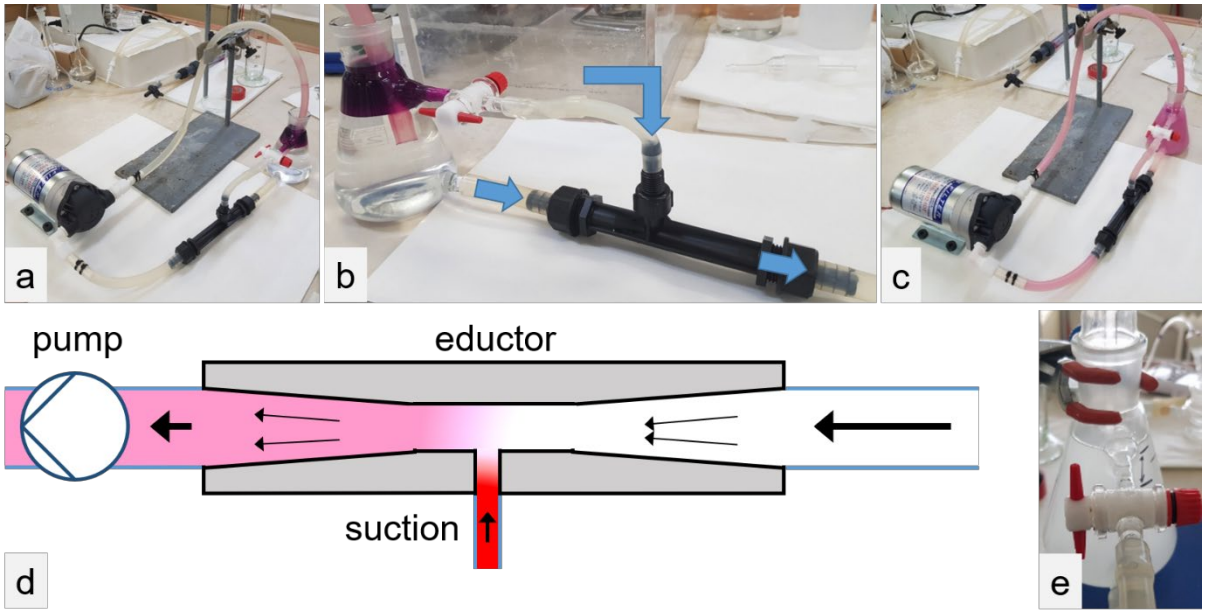

Figure 4. a–c: An emulsification test with an eductor was performed. To facilitate the visualization of emulsification, an iodine-colored organic phase (cyclohexane) and water were used. Whether phases were separating afterward, or a temporarily stable phase mixture was achieved, could thereby be tested. d: Sketch of the working principle of an eductor piece, using the Venturi effect. e: Final emulsified reaction mixture.

Prior to conducting another *DoE* screening with improved mixing properties, the setup was modified to work in a semi-batch mode. Thereby, constant emulsification was ensured, even for experiments that lasted longer than 12 h. With this in hand, the setup was modified to a semi-batch one. Towards this goal, the commercially available 100 mL batch-type cell was modified to include two channels: one enabling the inlet to the reaction volume, and the other for the outflow (Figure 5). From the reservoir (a 100 mL measuring cylinder), two tubes fed the mixing eductor, from where a membrane pump forwarded the mixture to the reactor. The outflow was connected to the reservoir.

Figure 5. The transition from the batch-type cell for the first *DoE* (left) to the semi-flow mode electrolysis cell for the second DoE screening (right).

The tested parameters with the modified setup were substrate concentration and flow rate (Table 2). Hereby, the flow rate was further decreased so that the flow drives both the emulsification and the transport of the reaction mixture (Figure 6).

Table 2. Parameters of 2^2 *DoE* screening with full resolution. One center point and one repetition per experiment were implemented. A set of 10 experiments was performed. Other parameters: 1 M $NaOH_{(aq)}$ as the electrolyte, total reaction volume: V_{tot} = 250 mL, applied current density $j_{reaction}$ = 5 mA cm^{-2}, applied charge $Q_{reaction}$ = 8.5*F*, stirring speed with magnetic stirring bar: v_{mix} = 500 rpm, anode geometric surface area A_{anode} = 128 cm^2, reaction temperature $T_{reaction}$ = 60 °C, nickel foam activation with $j_{act.}$ = 7.5 mA cm^{-2} and $Q_{act.}$ = 5 C cm^{-2}.

$c_{substrate}$ / M[a]	Φ / L h^{-1}[b]
0.4	2*
0.55	16
0.7	30

[a] Initial concentration of 4-propylcyclohexanol. [b] The flow rate was set with a Ritmo R033 membrane pump by Fink Chem+Tec, located between the mixing eductor and the reactor. *For one experiment, a flow of 5 L h^{-1} was set, since with the initially set flow rate, the electrolyte repeatedly stopped flowing after a few minutes of pumping.

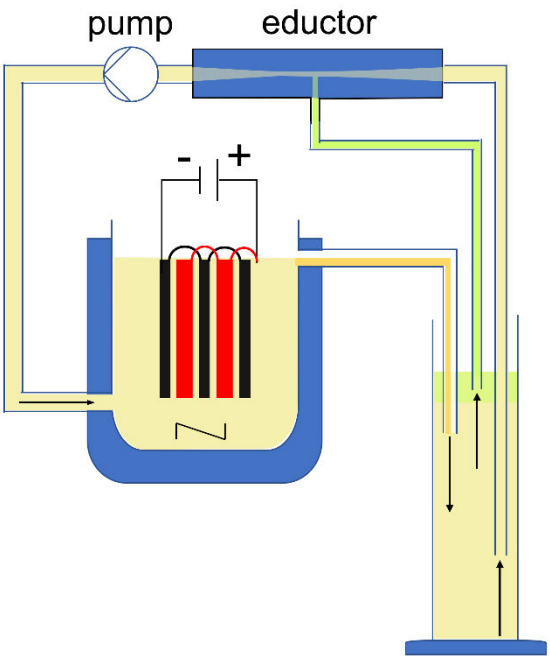

Figure 6. Schematic of the semi-batch setup for the second *DoE* screening. The pump transports the reaction medium and ensures a flow rate for successful emulsification inside the eductor. The eductor has two inlet channels, to continuously mix the two liquid electrolyte phases in the reservoir (100 mL). The product formation takes place in the electrochemical continuous stirred tank reactor (e-CSTR).

The parameter concentration was tested once more, now with an emphasis on higher values. This decision was based on the slightly positive trend towards higher substrate concentrations in the first *DoE* and motivated by a possibly reduced amount of caustic soda per unit of produced **2**.

For these experiments, the ^{13}C Inverse Gated NMR quantification was performed after liquid-liquid extraction using a perforator, as done previously. The detailed results are listed in the supporting information (supporting information, Table S2). These *DoE* screening results display that the stability of the emulsion is still crucial, with high pumping speeds affecting the yield. The optimal result during this screening was a qNMR yield of 35% for **2**. This screening prompted a kinetic investigation of the transpiring reaction (**1** to **2**). The upscaling of the system was also addressed.

For the kinetic study, a larger reaction volume is advantageous, because i) the volume of the withdrawn samples does not significantly affect the total volume and concentration, and ii) kinetic effects may arise as a result of scaling up. For these reasons, the electrode stack was enlarged by a factor of nearly 10 in terms of total geometrical anode surface area ($A_{geom.}$ = 1225 cm^2, equal geometrically active cathodic surface area), in part by increasing the number of individual electrodes (Figure 7). Thus, five anode foams and six stainless-steel sheet electrodes were assembled and respectively connected for one electrode stack. This setup has the additional advantage that both sides of the anodes are electrochemically active. A commercially available 1.5 L glass vessel with a heating jacket by *HWS* was used as a reactor and a custom-made PTFE cap was employed for the installation of the electrode stack. A commercially available 10 L glass reactor with an agitator unit and a heating jacket by *Normag*™ was installed as a reservoir.

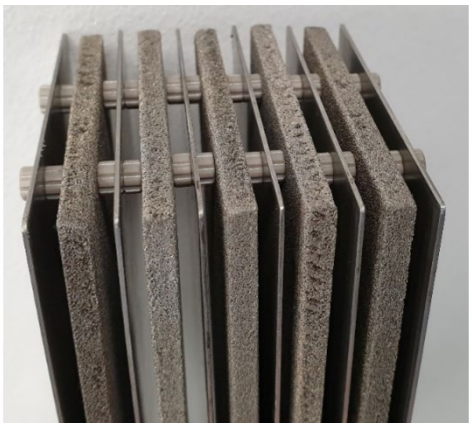

Figure 7. Bottom view of the electrode stack. The nickel foam sides are separated from the stainless-steel cathodes by screws made of polyether ether ketone (PEEK, thickness per side 3 mm). The anode geometric surface area in contact with the electrolyte is 1225 cm^2. The foams have a thickness of 5 mm. The stainless-steel sheets have a thickness of 1 mm.

With this setup, experiments with a total reaction volume of up to 13 L were conducted and samples were taken to observe the product composition or other kinetic effects during the reaction (Figure 8).

Figure 8. Reaction setup of the upscaled e-CSTR. Left: tempered reservoir with agitator. Below: thermostat. Above: eductor piece in black. Right: reactor with electrode stack. Behind: membrane pump. In the background, an Erlenmeyer flask with fresh substrate and a peristaltic pump for substrate feeding are installed. The overall reaction volume is up to 13 L. The yellow color of the reaction mixture in a later reaction stage can be visually perceived.

Figure 9 shows an overview of the results obtained from the product composition analysis in the course of the electrochemical reaction, with the samples taken at different values of applied charge.

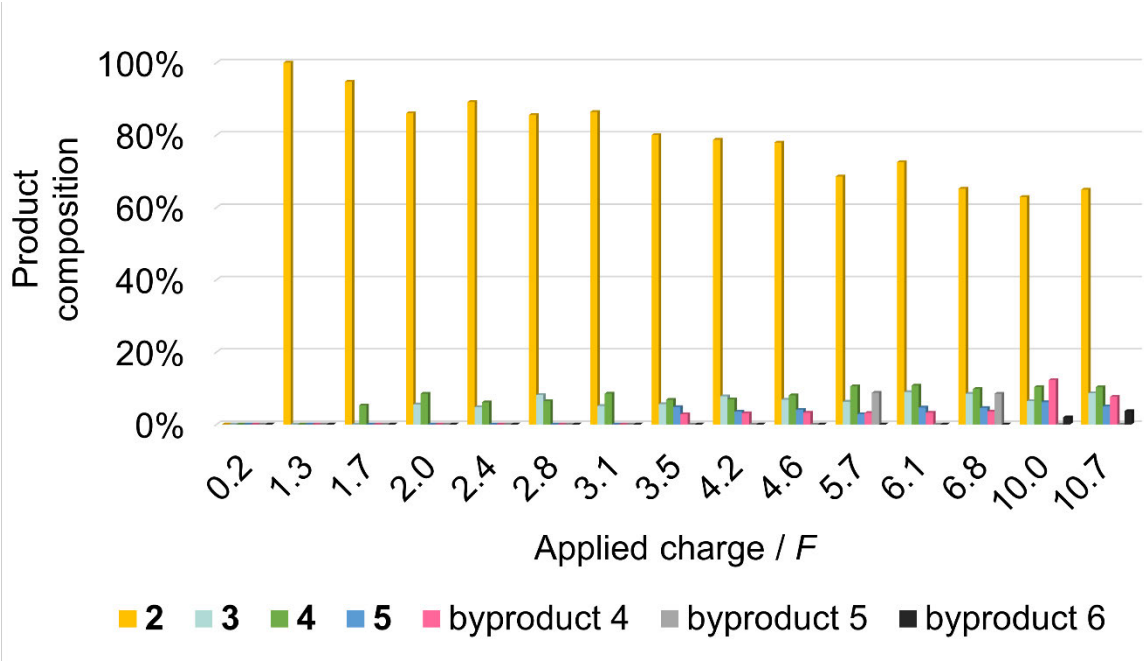

Figure 9. Analysis of the product composition throughout the reaction. Applied parameters: 1 M $NaOH_{(aq)}$ as the electrolyte, substrate concentration c(**1**) = 0.2 M, total reaction volume V_{tot} = 3.1 L, reaction mixture flow rate $\Phi_{reaction}$ = 16 L h^{-1}, applied current density $j_{reaction}$ = 2.5 mA cm^{-2}, applied charge $Q_{reaction}$ = 10.7F, stirring speed with magnetic stirring bar v_{mix} = 300 rpm, anode geometric surface area A_{anode} = 1225 cm^2, reaction temperature $T_{reaction}$ = 50 °C, nickel foam activation with $j_{act.}$ = 6.5 mA cm^{-2} and $Q_{act.}$ = 5 C cm^{-2}. The main product (**2**) as well as further reported alkylated dicarboxylic acid derivatives[15] form in the case of the propyl side chain during the reaction. In a later reaction stage, further dicarboxylic acids arise, which can be observed in the ^{13}C NMR spectrum but not conclusively characterized.

The oxidation from **1** to **2** was previously proposed to take place via the formation of 1,3- and 1,4-cyclohexanediones as intermediates to glutaric and succinic acids.[18] However, with our alkylated substrates, this would result in 4-propyl-4-hydroxycyclohexane-1-one, which is not observed. Also, the tautomeric appearance of the corresponding enol form was not detected. In addition, propylsuccinic acid cannot form via this intermediate. We observed propylsuccinic acid in an NMR yield of up to 6% (Figure 9). Accordingly, a revision to the previous mechanism is unavoidable. We propose a reaction mechanism by subsequent oxidation steps in 1,2-positions. A yellow-colored product solution would fit the supplier information of cyclohexanedione[19] or the bright yellow color of **2**. However, the concentrated product mixture after extraction and solvent removal turned out to be dark orange. Also, an even darker distillation residue remains as a sticky solid. While ^{13}C NMR analyses revealed that the main product **2** seems to be the only compound left, a MALDI ToF MS measurement (supporting information, Figure S7) indicates the formation of high molecular weight compounds. Their end groups should be acidic, according to pH measurements and the fact that they dissolve reversibly in caustic soda. The mechanism we propose here focuses on the interaction with the strongly alkaline electrolyte (Scheme 2). This influence may also be a reason for higher molecular weight by-products being formed.

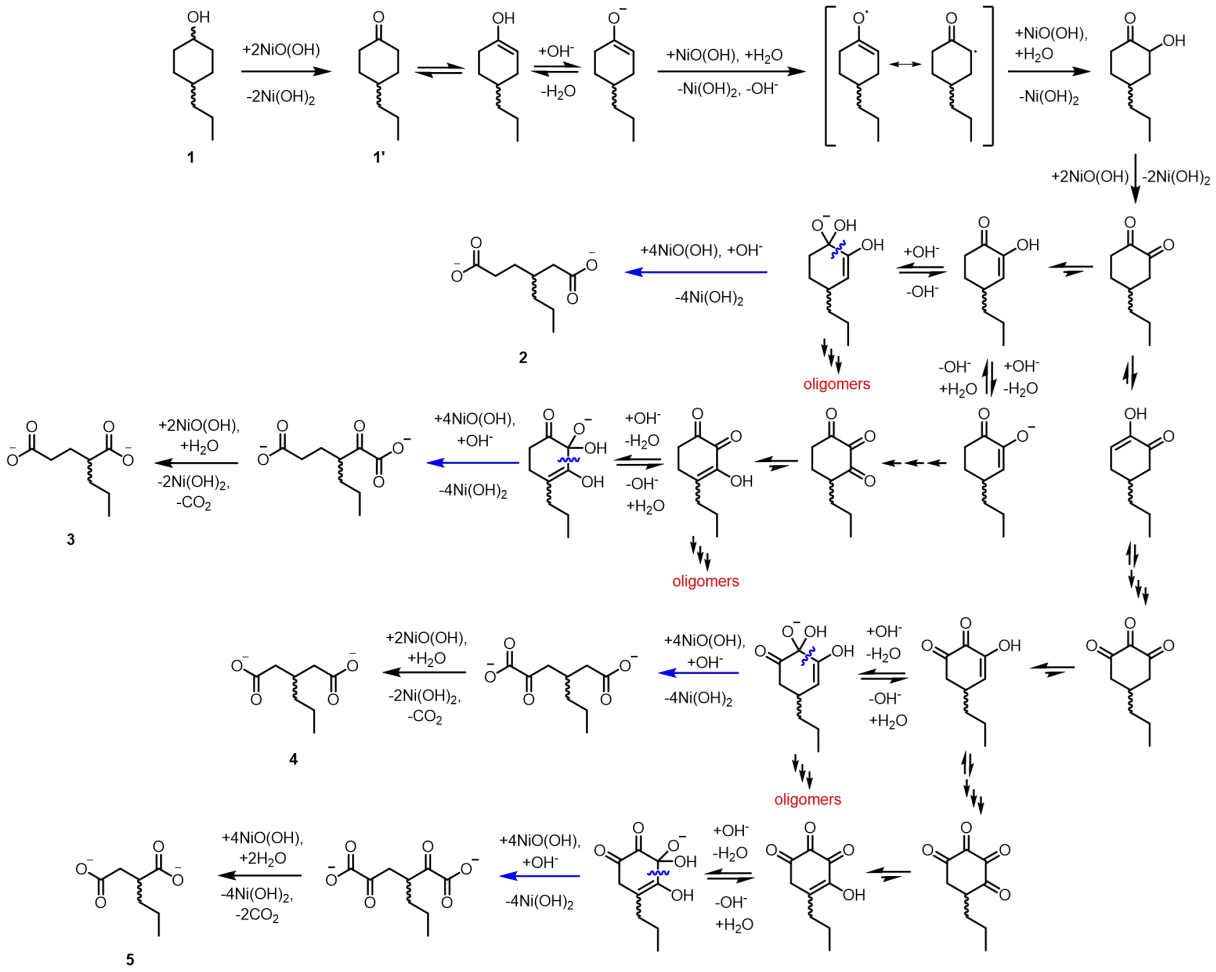

Scheme 2. Reaction mechanism from 4-propylcyclohexanol (**1**) via 4-propylcyclohexanone (**1'**) to 3-propyladipic acid (**2**). Fleischmann et al. reported the oxidation from **1** to **1'**.[20] Its radical nature and mechanism was further investigated by Konaka et al.[21] The keto-enol tautomerization with subsequent deprotonation was reported by Schäfer et al.[13] At the nickel oxyhydroxide surface, the oxidation to the corresponding radical was proposed by Lyalin et al.[14] The next two oxidation steps as well as the water addition were reported by the same group.[22] The tautomerization of **1'** and 4-propylcyclohexane-1,2-dione to their enol forms proceed for the same reason. From an enol form, there is a higher tendency for another oxidation in the 3-position. In contrast, starting from the enol form a nucleophilic attack of hydroxide can also initiate a ring opening. Furthermore, we propose a reaction pathway toward oligomers, since the double bond is electrophilic. The dicarboxylic acids are in their dianion form.

Importantly, the NMR studies (Figure 9) reveal that, initially, the main product **2** is exclusively formed. Only after 1.7*F* was **4** characterized as the first formed by-product. Within another 0.3*F*, **3** was observed in the NMR spectrum. The next by-product was **5**, which was detected after 3.5*F*, and over the course of the reaction, more by-products were seen in the ^{13}C Inverse Gated NMR spectrum and identified as dicarboxylic acids. Quantification was done by integrating the signals in the chemical shift range of the carboxylic acids, whereby equal

integrals for two acid signals were observed in several spectra. Overlapping signals and low quantities of the other by-products have prohibited their identification so far.

A quantitative study was performed next, with samples taken every 3 h, worked up as described in the experimental section. The overview is presented in Figure 10.

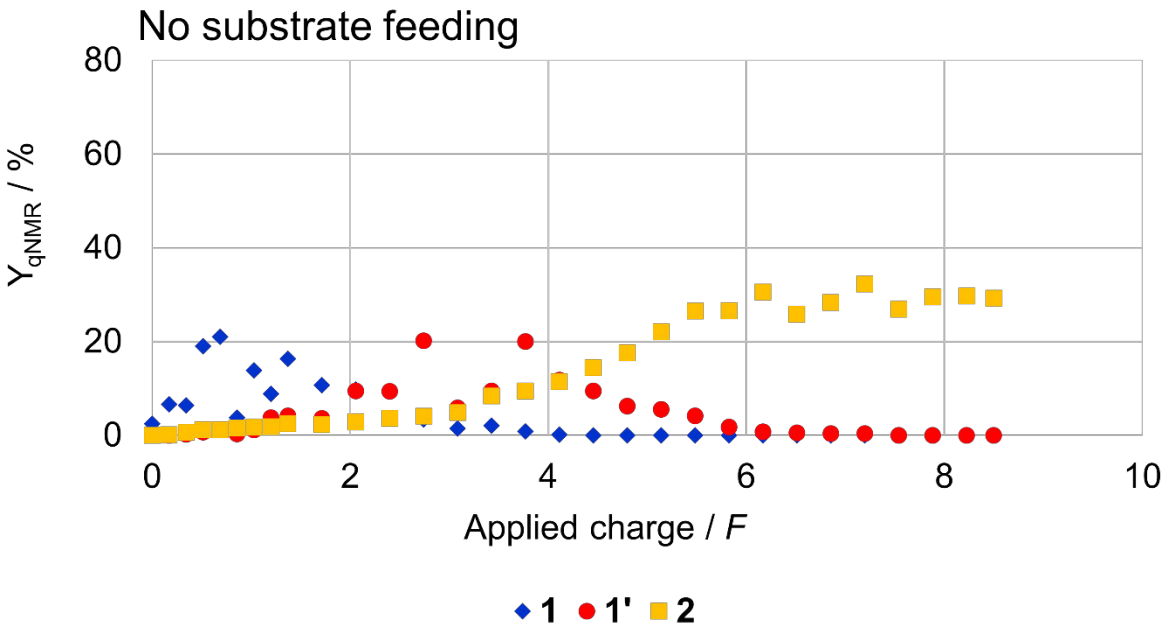

Figure 10. qNMR yields of the reaction control experiment for the oxidation from **1** to **2** via **1'**. The volatilities of **1** and **1'** are the reason for lowered ascertained yields, especially in the early reaction stage. Samples were taken every 3 h and the qNMR yields were evaluated. Reaction parameters: The total reaction volume was V_{tot} = 3.9 L. The amount of substrate was n(**1**) = 2.0 mol, and the nominal reagent concentration was c(**1**) = 0.55 M in 1 M $NaOH_{(aq)}$. A reaction temperature of T = 60 °C and a current density of j_{rct} = 5 mA cm^{-2} were applied. The reaction mixture was pumped from the reservoir through a mixing eductor into the reactor with a flow rate of 16 L h^{-1}. For recirculation, the reaction mixture was flowing back into the reservoir.

As known from the literature[20], **1'** forms as an intermediate at the beginning of the reaction. When most of the starting material is depleted, there is a maximum in the intermediate yield (Figure 10). The production of **2** from **1'** causes a maximum space-time yield of **2** at a later reaction stage, namely where the curvature is zero. Thus, the idea arose to start from **1'** (Scheme 3) for simplicity and availability reasons and to feed **1'** to the system continuously with a flow rate equal to the theoretically maximum oxidation rate. This corresponds to 0.59 mmol min^{-1}, or 9.8 µL min^{-1}.

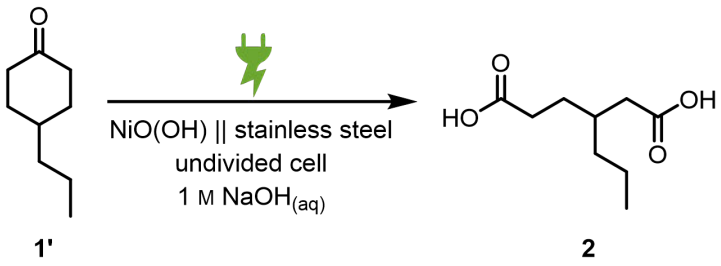

Scheme 3. Anodic oxidation of 4-propylcyclohexanone (**1'**) to 3-propyladipic acid (**2**) at a nickel oxyhydroxide foam anode.

The evaluation of this reaction control experiment is shown in Figure 11.

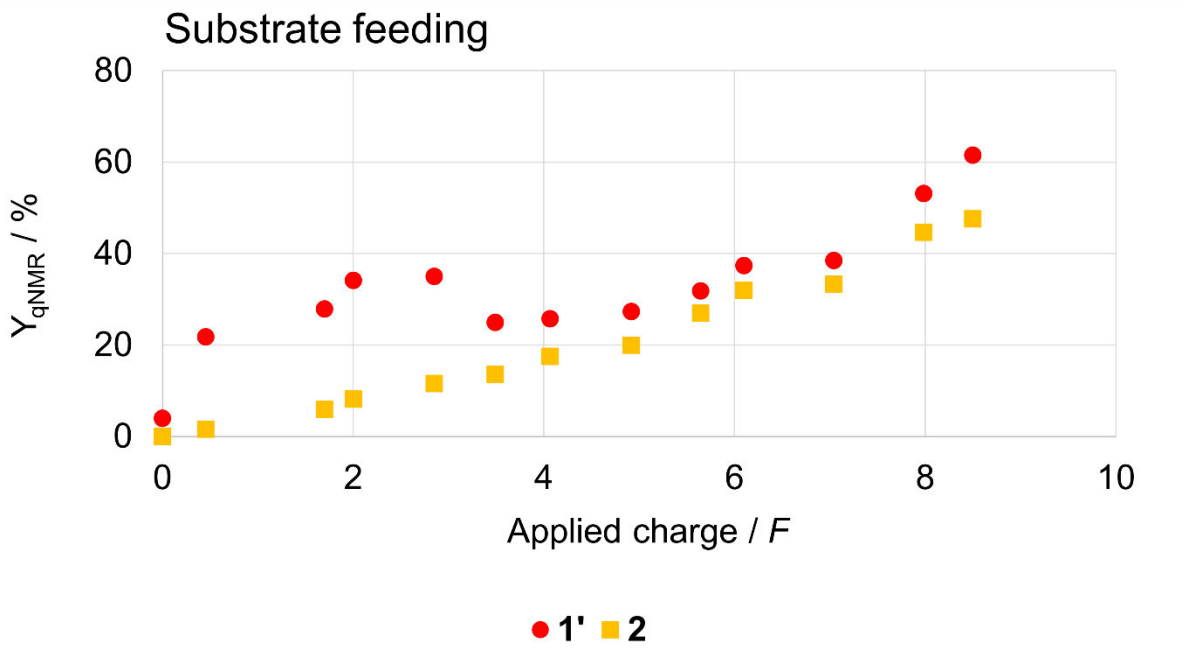

Figure 11. qNMR yields for the reaction control experiment consisting of the anodic oxidation from **1'** to **2** with continuous substrate feeding for a constant concentration. The volatility of **1'** is the reason for a lowered ascertained yield, especially in the early reaction stage. Overall, constant feeding of **1'** should correlate to a stable value of the red data points. Instead, the values fluctuate, because of the compound's volatility during mini workup. Samples were taken regularly and the qNMR yields were evaluated. Reaction parameters: The total reaction volume was V_{tot} = 10.0 L and the initial amount of substrate was n(**1'**) = 5.1 mol. The yields were evaluated against this stoichiometry. Beyond 8*F*, the respective initial amount of substrate was linearly increased according to the theoretical maximal conversion.

Remarkably, the main product **2** shows a nearly proportional increase in yield, when the substrate concentration is kept constant. Additionally, the product yield was shown to significantly increase from about 30% to almost 50% qNMR yield. Thus, substrate feeding can be considered a particularly relevant parameter for increasing the yield of the oxidation of **1'** to **2**. After workup and isolation of **2**, 31% remained. The ^{1}H and ^{13}C NMR spectra of the black, sticky distillation residue exclusively showed signals that are ascribable to **2**. Still, the

remaining **2** could not be successfully removed from the distillation residue. The exact chemical composition of the distillation residue and its behavior is a topic of an ongoing investigation.

CONCLUSIONS. In summary, we showed the successful isolation of 3-propyladipic acid from 4-propylcyclohexanol and 4-propylcyclohexanone with isolated yields of up to 31% on a 10 L scale, corresponding to 48% qNMR yield. In an initial parameter screening, the importance of the biphasic electrolyte mixing emerged. Utilizing a mixing eductor, an emulsion resulted. Upon switching to a recirculation reaction mode, more detailed information was obtained from another *Design of Experiments* screening, pointing to the critical importance of electrolyte emulsification. When the scale-up to a reaction volume of up to 10 L was conducted, reaction control experiments revealed significant yield improvements when continuously feeding the substrate. Optically, the reaction progress was accompanied by the coloring of the electrolyte, which resulted in yellow to red mixtures upon reaction completion. Thereby, the shade deepening correlated with the reaction time. Analyses indicated that the color results from trace compounds of high molecular weight. For their formation, the following mechanistic proposal was presented: The keto-enol tautomerization is favored in cyclohexane 1,2-diones. Due to the mesomeric effect of the carbonyl group, the unsaturated α-carbon is more electrophilic in comparison with a saturated one. Consequently, other nucleophiles can attack this position, initiating a chain reaction. This hypothesis is an interesting starting point for further studies at the nickel oxyhydroxide anode surface. There is significant room for the optimization of the electrocatalyst surface by tailoring the surface structure and composition. This combined with an in-depth knowledge of the prevailing mechanisms should allow for rational progress in organic electrosynthesis.

In a more general vein, these results can contribute to transforming the production of **2** to be more climate friendly. Hence, in the future, it will be relevant to check the effects of renewable energy source fluctuations on the yield. In favorable cases, it may be practical to use electricity from renewable energies immediately upon their conversion.

EXPERIMENTAL SECTION.

General considerations

Experimental details, information about the analyses, and further information is presented in the Supporting information.

Activation of nickel foams

As reported by Briggs et al.[23] and Schäfer et al.[13], an activation solution which is 0.1 M $NiSO_{4(aq)}$, 0.1 M $NaOAc_{(aq)}$ and 5 mM $NaOH_{(aq)}$ was placed in a beaker-type cell, previously cleaned. A simpler reaction setup was used to do the activation in batch mode. The reactor stack was assembled, and the nickel foam anodes were thoroughly rinsed with 1 M caustic soda. Once the caustic soda was not dripping any more, the electrode stack was inserted into the activation solution. Thereby some floccules were observed, which do not hinder the

activation. The activation was performed galvanostatically with a current density of 7.5 mA cm^{-2} until attaining an applied charge of 5 C cm^{-2}, unless stated differently. The activation mixture was stirred at 300 rpm. Then, the electrode stack was disassembled, and the black activated nickel foams were rinsed thoroughly with deionized water. The stainless-steel plates were immersed in diluted $H_2SO_{4(aq)}$ (1–4 M) for a few seconds, washed with water, dried with a tissue, and treated with sandpaper (pore sizes: first 700, then 300). The shiny stainless-steel plates were rinsed with water, acetone and water once more, dried and the cell rearranged.

Setup

For the applied electrode stack, three (or six) stainless steel (alloy type EU norm 1.4571) plates were connected by thin stainless-steel plates, and two (or five) RECEMAT™ nickel foams RCM-Ni4753.05 were also connected by such stainless-steel plates. Since the geometrical surface area of both sides of the anodes was used, one additional cathode was needed. All electrodes were separated by 3 mm thin PTFE spacers, strung on two PTFE cylinders for stability reasons. The stainless-steel sheets were equipped with 3 mm thick polyether ether ketone (PEEK) screws to ensure a homogeneous spacing throughout the large electrode stack.

For the first *DoE* screening, a small electrode stack was combined with a commercially available 100 mL batch-type electrolysis cell. For the second screening, in- and outflow channels were added to the beaker-type electrolysis cell. For the large-scale electrolysis, a commercially available 1.5 L beaker-type electrolysis cell by *HWS* was used. Here, the inflow channel was already a preset and a PTFE lid with an outlet channel and an opening for the electrode stack was tailor-made by the machine workshop at the university of Mainz.

Synthesis of 4-propylcylohexanol

For availability reasons, 4-propylcyclohexanone (**1'**, 1.651 mol) was reduced to the main substrate 4-propylcyclohexanol (**1**) using sodium borohydride (0.826 mol, 2 H^- equivalents) in deionized water (250 mL, Scheme 4). **1'** in methanol (123 mL) was added dropwise (1 drop in 4 sec) to the aqueous solution. The reaction mixture was stirred at 300 rpm. After the completed addition, the reaction was continuously stirred for another 20 h. The reaction progress was observed using TLC (eluent was toluene, coloring agent: vanillin/sulfuric acid, R_f(**1'**)=0.64, R_f(**6**)=0.28). Upon the completed conversion, the turbid reaction mixture was acidified using either hydrochloric acid (10%) or sulfuric acid (4.5 M) to pH 1–2. Subsequently, a 1 M NaOH solution was added until reaching a pH of 12. After threefold extraction using methyl *tert*-butyl ether (MTBE), the combined organic phases were dried over $MgSO_4$ and the solvent was removed at reduced pressure. **1** was synthesized with a yield of 96%.

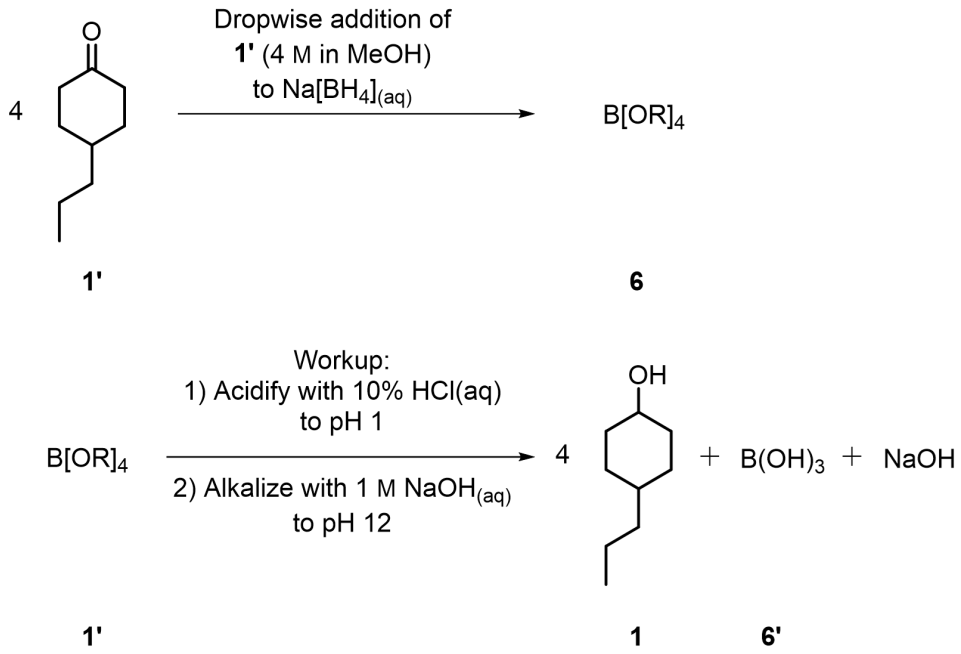

Scheme 4. Reduction of **1'** with sodium borohydride, including the subsequent workup.

Anodic oxidation of 4-propylcyclohexanol

4-Propylcyclohexanol (**1**, isomeric mixture) was mixed with caustic soda (1 M). The activated electrode stack was inserted into the stirred reaction mixture. In the case of a semi-flow reaction, the recirculation of the reaction mixture was established before starting the reaction. After the galvanostatic reaction ended, the product mixture was collected, and the setup and electrode stack were washed and thoroughly rinsed with MTBE (several mL, enough for pumping) and NaOH (1 M), respectively. All phases were combined and worked up.

Reaction control experiments and mini workup

4-Propylcyclohexanone (≥99%) was chosen as the substrate as it could be characterized as the first intermediate in the reaction pathway via NMR spectroscopy and it was readily available. Regarding the further reaction steps, the same parameters were applied as before, unless stated differently. During the reaction, (2.00±0.05) mL of the reaction mixture was retrieved regularly with a syringe, acidified with 4.5 M $H_2SO_{4(aq)}$ to pH 1–2, and extracted with ethyl acetate (4 times, 2 mL each). The organic fractions were combined and dried over $MgSO_4$. Then, the solvent was evaporated at reduced pressure, the residue combined with 1,3,5-trimethoxybenzene as an internal standard, DMSO-d_6 (0.5 mL) was added, and the solution was analyzed using ^{13}C inverse-gated NMR spectroscopy.

General workup

The combined phases in the product mixture were inserted in a sufficiently large perforator according to Ludwig (at least 20% extra spare volume) and a liquid-liquid reaction was performed, first using MTBE until completely discolored. After acidification with diluted $H_2SO_{4(aq)}$ (4.5 M) to pH 1–2, the dicarboxylic acid product mixture was liquid-liquid extracted

with the same perforator using ethyl acetate until completely discolored. The two organic fractions were dried over $MgSO_4$, the solvent was removed at reduced pressure and the product mixture was evaluated using ^{13}C Inverse Gated NMR spectroscopy with 1,3,5-trimethoxybenzene as an internal standard.

For isolation, the acidic mixture was distilled using a Vigreux column at 100–10^{-2} mbar. The products were trapped with liquid nitrogen by using a Schlenk flask. The main product **2** was distilled at about 200 °C. The purity was significantly improved by recrystallization in heptane after first melting the yellow crystals in a heptane phase on a hot plate at about 70 °C, and slowly cooling to room temperature. Then, the crystals were dried.

SUPPORTING INFORMATION.

An additional reference was cited within the Supporting Information.[24]

Acknowledgements

We thank the analytical departments of Johannes Gutenberg University Mainz and the University of Alicante for the measurements and fruitful discussions. Additionally, we are grateful for the support of the glass workshop of the university of Mainz.

This project has received funding from the European Union's Horizon 2020 research and innovation programme under grant agreement no. 820735. This publication reflects the views only of the author, and the European Union cannot be held responsible for any use which may be made of the information contained therein.

The authors declare no competing financial interest. Open Access funding enabled and organized by Projekt DEAL.

Conflict of Interests

The authors declare no conflict of interest.

Data Availability Statement

The data that support the findings of this study are available in the supplementary material of this article.

REFERENCES

(1) F. Birol, L. Cozzi, M. Baroni, T. Morgan, A. Bromhead, M. Argiri, J. Corben, P. Olejarnik, C. Besson, A. Blasi, R. Centurelli, M.-X. Chen, M. D'Ausilio, D. Elis, M. Frank, T. Gould, T. Gül, K. Kumaria, Q. Liu, B. Magné, T. Malyshev, T. Topalgoekceli, D. Wilkinson, A. Yanagisawa, S. Mooney, W*orld Energy Outlook 2010*, Paris, **2010**.

(2) S. A. Matlin, G. Mehta, H. Hopf, A. Krief, *Nat. Chem.* **2016**, *8*, 393–398.

(3) a) S. R. Waldvogel, B. Janza, *Angew. Chem. Int. Ed.* **2014**, *53*, 7122–7123; b) B. Gleede, M. Selt, C. Gütz, A. Stenglein, S. R. Waldvogel, *Org. Process Res. Dev.* **2020**, *24*, 1916–1926; c) D. Hayrapetyan, V. Shkepu, O. T. Seilkhanov, Z. Zhanabil, K. Lam, *Chem. Commun.* **2017**, *53*, 8451–8454; d) T. Noël, Y. Cao, G. Laudadio, *Acc. Chem. Res.* **2019**, *52*, 2858–2869; e) M. Yan, Y. Kawamata, P. S. Baran, *Chem. Rev.* **2017**, *117*, 13230–13319; f) M. C. Leech, K. Lam, *Nat. Rev. Chem.* **2022**, *6*, 275–286; g) M. Zirbes, T. Graßl, R. Neuber, S. R. Waldvogel, *Angew. Chem.*

Int. Ed. **2023**, *62*, e202219217; h) A. Wiebe, T. Gieshoff, S. Möhle, E. Rodrigo, M. Zirbes, S. R. Waldvogel, *Angew. Chem. Int. Ed.* **2018**, *57*, 5594–5619; *Angew. Chem.* **2018**, *130*, 5694–5721; i) S. Möhle, M. Zirbes, E. Rodrigo, T. Gieshoff, A. Wiebe, S. R. Waldvogel, *Angew. Chem. Int. Ed.* **2018**, *57*, 6018–6041; j) S. Möhle, M. Zirbes, E. Rodrigo, T. Gieshoff, A. Wiebe, S. R. Waldvogel, *Angew. Chem.* **2018**, *130*, 6124–6149; k) K. D. Moeller, *Chem. Rev.* **2018**, *118*, 4817–4833; l) R. D. Little, K. D. Moeller, *Chem. Rev.* **2018**, *118*, 4483–4484; m) S. R. Waldvogel, S. Lips, M. Selt, B. Riehl, C. J. Kampf, *Chem. Rev.* **2018**, *118*, 6706–6765.

(4) D. Pollok, S. R. Waldvogel, *Chem. Sci.* **2020**, *11*, 12386–12400.

(5) a) S. B. Beil, D. Pollok, S. R. Waldvogel, *Angew. Chem. Int. Ed.* **2021**, *60*, 14750–14759; b) J. Seidler, J. Strugatchi, T. Gärtner, S. R. Waldvogel, *MRS Energy Sustain.* **2020**, *7*, 42.

(6) a) E. J. Horn, B. R. Rosen, Y. Chen, J. Tang, K. Chen, M. D. Eastgate, P. S. Baran, *Nature* **2016**, *533*, 77–81; b) E. J. Horn, B. R. Rosen, P. S. Baran, *ACS Cent. Sci.* **2016**, *2*, 302–308; c) L. J. Wesenberg, E. Diehl, T. J. B. Zähringer, C. Dörr, D. Schollmeyer, A. Shimizu, J. -i. Yoshida, U. A. Hellmich, S. R. Waldvogel, *Chem. – Eur. J.* **2020**, *26*, 17284–17612; d) M. Linden, S. Hofmann, A. Herman, N. Ehler, R. M. Bär, S. R. Waldvogel, *Angew. Chem. Int. Ed.* **2023**, *62*, e202214820; e) J. Winter, T. Prenzel, T. Wirtanen, D. Schollmeyer, S. R. Waldvogel, *Chem. – Eur. J.* **2023**, *29*, e202203319; f) R. J.-R. Bednarz, C. Brauer, S. R. Waldvogel, *GIT Lab. J.* **2021**, online.

(7) a) J. L. Röckl, D. Schollmeyer, R. Franke, S. R. Waldvogel, *Angew. Chem. Int. Ed.* **2020**, *59*, 315–319; *Angew. Chem.* **2020**, *132*, 323–327; b) S. Arndt, D. Weis, K. Donsbach, S. R. Waldvogel, *Angew. Chem. Int. Ed.* **2020**, *59*, 8036–8041; *Angew. Chem.* **2020**, *132*, 8112–8118.

(8) a) K.-F. Chow, F. Mavré, J. A. Crooks, B.-Y. Chang, R. M. Crooks, *J. Am. Chem. Soc.* **2009**, *131*, 8364–8365; b) S. E. Fosdick, K. N. Knust, K. Scida, R. M. Crooks, *Angew. Chem. Int. Ed.* **2013**, *52*, 10438–10456; c) G. H. M. de Kruijff, T. Goschler, N. Beiser, A. Stenglein, O. M. Türk, S. R. Waldvogel, *Green Chem.* **2019**, *21*, 4815–4823.

(9) L. Gustavsson, B. Johansson, P. Svenningsson, *Energy* **1995**, *20*, 1097–1113.

(10) A. Corona, M. J. Biddy, D. R. Vardon, M. Birkved, M. Hauschild, G. T. Beckham, *Green Chem.* **2016**, *18*, 1839–1854.

(11) W. Schutyser, G. Van den Bossche, A. Raaffels, S. Van den Bosch, S.-F. Koelewijn, T. Renders, B. F. Sels, *ACS Sustain. Chem. Eng.* **2016**, *4*, 5336–5346.

(12) a) M. Zirbes, S. R. Waldvogel, *Curr. Opin. Green Sustain. Chem.* **2018**, *14*, 19–25; b) M. Zirbes, L. L. Quadri, M. Breiner, A. Stenglein, A. Bomm, W. Schade, S. R. Waldvogel, *ACS Sustain. Chem. Eng.* **2020**, *8*, 7300–7307; c) M. Breiner, M. Zirbes, S. R. Waldvogel, *Green Chem.* **2021**, *23*, 6449–6455; d) M. Zirbes, D. Schmitt, N. Beiser, D. Pitton, T. Hoffmann, S. R. Waldvogel, *ChemElectroChem* **2019**, *6*, 155–161.

(13) H.-J. Schäfer, J. Kaulen, *Tetrahedron* **1982**, *38*, 3299–3308.

(14) B. V. Lyalin, V. A. Petrosyan, *Russ. Chem. Bull.* **2004**, *53*, 688–692.

(15) A. L. Rauen, F. Weinelt, S. R. Waldvogel, *Green Chem.* **2020**, *22*, 5956–5960.

(16) a) M. Hielscher, E. K. Oehl, B. Gleede, J. Buchholz, S. R. Waldvogel, *ChemElectroChem* **2021**, *8*, 3904–3910; b) M. Dörr, M. M. Hielscher, J. Proppe, S. R. Waldvogel, *ChemElectroChem* **2021**, *8*, 2621–2629; c) M. Dörr, J. L. Röckl, J. Rein, D. Schollmeyer, S. R. Waldvogel, *Chem. – Eur. J.* **2020**, *26*, 10195–10198; d) M. Santi, J. Seitz, R. Cicala, T. Hardwick, N. Ahmed, T. Wirth, *Chem. – Eur. J.* **2019**, *25*, 16230–16235; e) R. Möckel, J. Hille, E. Winterling, S. Weidemüller, T. M. Faber, G. Hilt, *Angew. Chem. Int. Ed.* **2018**, *57*, 442–445; *Angew. Chem.* **2018**, *130*, 450–454.

(17) a) H. Li, H. Li, X. Huang, Q. Han, Y. Yuan, B. Qi, *Processes* **2020**, *8*, 64; b) M. Georgiou, M. V. Papalexandris, *Int. J. Heat Mass Transf.* **2017**, *115*, 793–809.

(18) B. V. Lyalin, V. A. Petrosyan, *Russ. Chem. Bull.* **2009**, *58*, 2426–2431.

(19) a) C. C. Hach, C. V. Banks, H. Diehl, *Org. Synth.* **1952**, *32*, 35; b) Sigma-Aldrich, SDS 1,2-cyclohexanedione, **2022**.

(20) M. Fleischmann, K. Korinek, D. Pletcher, *J. Electroanal. Chem. Interfacial Electrochem.* **1971**, *31*, 39–49.

(21) R. Konaka, S. Terabe, K. Kuruma, *J. Org. Chem.* **1969**, *34*, 1334–1337.

(22) B. V. Lyalin, V. A. Petrosyan, *Russ. J. Electrochem.* **2010**, *46*, 1199–1214.

(23) G. W. D. Briggs, E. Jones, W. F. K. Wynne-Jones, *Trans. Faraday Soc.* **1955**, *51*, 1433–1442.

(24) W. LF. Armarego, C. L. L. Chai, *Purification of Laboratory Chemicals*, Elsevier, Amsterdam, **2013**.

ENTRY FOR THE TABLE OF CONTENTS

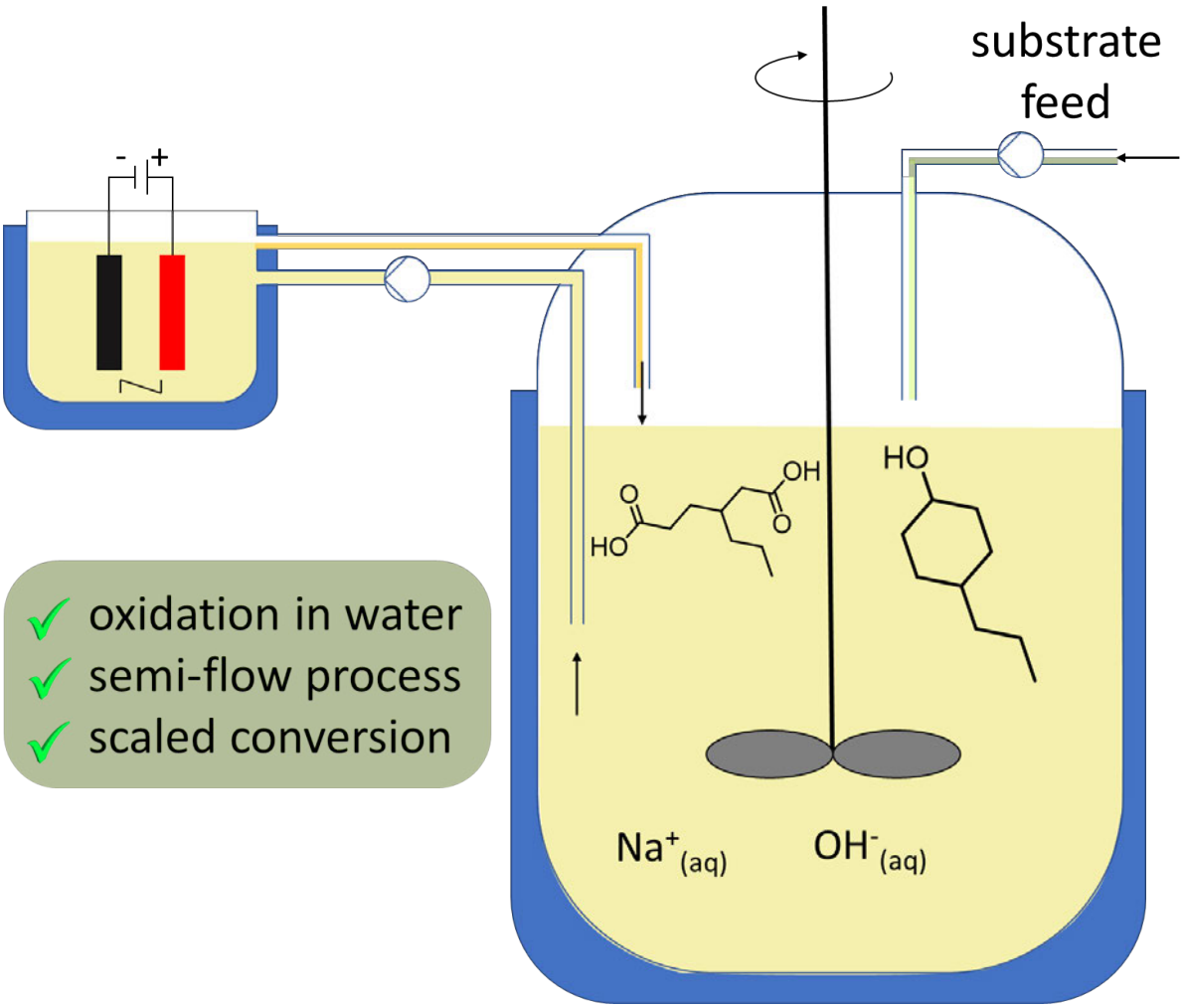

3-Propyladipic acid was successfully electro-synthesized at nickel oxyhydroxide anodes in isolated yields of up to 31% on a scale of 10 L in semi-flow mode. Continuous substrate feeding and mixing with the electrolyte were found to significantly enhance the product yield.

SUN-POWERED ELECTROSYNTHESIS OF 3-PROPYLADIPIC ACID: THE DIRECT COUPLING OF PV PANEL AND ELECTROCHEMICAL REACTOR

This manuscript was submitted to the peer-reviewed journal Renewable Energy in 2024. It is reprinted with permission of Jiménez-Meneses, P., Bednarz, R. J.-R., Montiel, V., Gómez, R., Waldvogel, S. R., if kept under lock for max. 12 months. It reproduces the text of the article literally, including all figures and tables.

Author Contributions (following NISO standard): **P. Jiménez-Meneses:** Conceptualization (lead), data curation (equal), formal analysis (lead), investigation (lead), methodology (lead), validation (lead), visualization (lead), writing – original draft (lead), writing – review & editing (lead); **R. J.-R. Bednarz:** conceptualization (lead), data curation (equal), formal analysis (lead), investigation (equal), methodology (lead), validation (lead), visualization (lead), writing – original draft (lead), writing – review & editing (lead); **Vicente Montiel:** data curation (equal), investigation (supporting), methodology (equal), resources (equal), supervision (equal), validation (equal), writing – original draft (supporting), writing – review & editing (supporting); **S. R. Waldvogel:** conceptualization (equal), funding acquisition (lead), methodology (equal), project administration (equal), resources (supporting), methodology (equal), supervision (equal), writing – original draft (equal), writing – review & editing (equal); **R. Gómez:** conceptualization (lead), funding acquisition (lead), methodology (lead), project administration (equal), resources (lead), supervision (lead), validation (lead), writing – original draft (equal), writing – review & editing (equal).

Renewable energy sources in the electricity grid are increasing steadily because they emit significantly less greenhouse gases into the atmosphere over their lifecycle than fossil-based sources. Furthermore, their state-of-the-art performance, e.g. in cell efficiency,[104] and lifetime of the commercially available modules is typically more than 20 years.[105] Intrinsically, they supply fluctuating electricity, in accordance with the availability of sunlight or wind. As the currently most decentralized renewable energy source, photovoltaic cells show frequent new record efficiencies (Figure 11). Combined with the growing electricity demand while transforming the global primary energy system, the successful incorporation of fluctuating electricity is very advantageous.

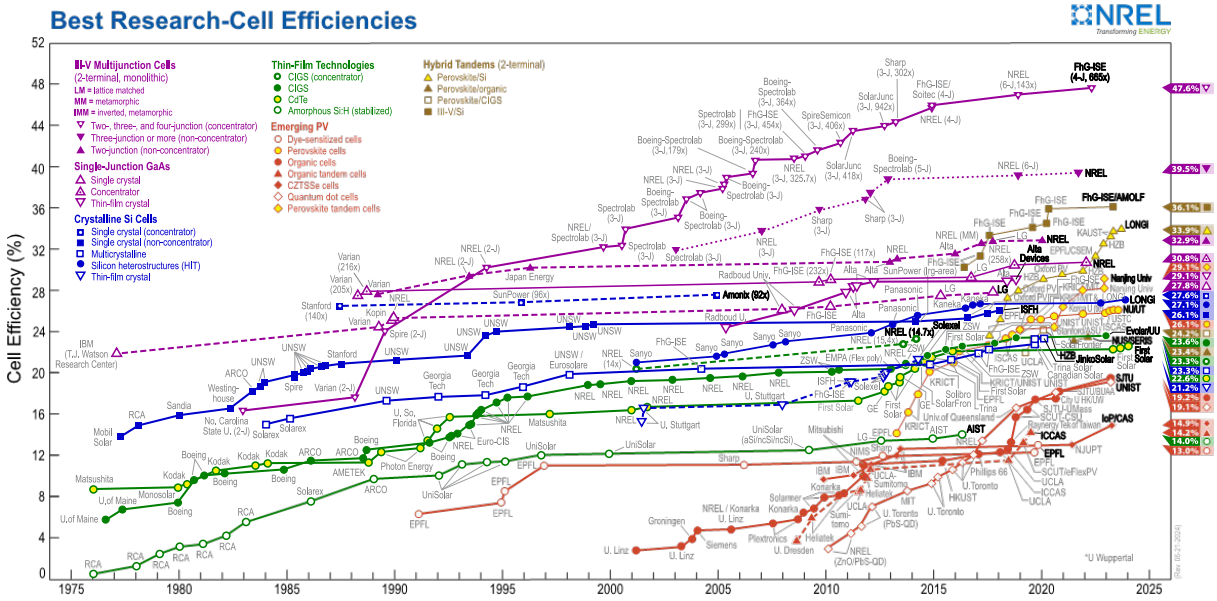

Figure 11. Chart of research photovoltaic cell efficiency records, collected by the National Renewable Energy Laboratory (NREL). The best single crystal silicium cell (non-concentrated) cell efficiency is 26.1%, to date. A four-junction cell with, to date, 47.6% cell efficiency dominates the chart. Data from 21.06.2024.[104] The graphic is reused with permission of NREL.[104]

In this study, we coupled a medium-sized e-CSTR, including a stacked electrode design, containing two anodic foams, with a silicon polycrystalline solar panel. The size of the panel was chosen according to the maximum power for the electrochemical oxidation of 4-propylcyclohexanol (**1**) to 3-propyladipic acid (**2**). A thermostat to temper the reaction to 50 °C, the pumps for cycling mode and the stirring plates for reactor and reservoir were decoupled from the PV panel to more precisely investigate the effect of fluctuations on the electrochemical reaction, only. The experiments were carried out in San Vincente del Raspeig, Spain, because our European project (LIBERATE) partners at the University of Alicante were very experienced in solar coupling and higher solar radiation was expected than in Germany. The weather conditions display cloudy and sunny days and present a realistic scenario for fluctuating renewable energy sources.

Initial experiments were performed to synthesize the product using steady electricity supply up to 8*F*, and an applied charge of Q = 78 kC. Here, 27% yield were achieved, which was in the range of the best screening results with this setup at that time (35%).[49] Next, the first coupling experiment was performed, whereby the other equipment (pumps, heating, stirring) were active via the complete reaction time. In this case, the fading active nickel oxide hydroxide electrode surface during nighttime was not fully recovered the next day. This drawback was expressed in a low yield of only 11%. Additionally, a decay in the active surface at a threshold current density of 1.25 mA cm^{-2} was recognized.

Seeking for the best possible active electrode retention with the present setup, the other equipment was from now on turned off, as soon as the minimum threshold current density

was undercut. Remarkably, the black active surface layer returned recurringly, each morning. Deactivation of active surfaces typically happens, if no electrical current is applied.[74] An automatic surface reactivation with turned on current after multiple hours was rather unexpected. Thereby, a yield of **2** of 26% was achieved, which is nearly identical with the benchmark experiment using steady electricity supply.

Overall, this study indicates the huge potential of coupling electrochemical synthesis to fluctuating electricity. Even with the special case of purely solar coupling and several hours of no electricity supply, we received very similar results compared to classical steady electricity supply.[13]

SUN-POWERED ELECTROSYNTHESIS OF 3-PROPYLADIPIC ACID: THE DIRECT COUPLING OF PV PANEL AND ELECTROCHEMICAL REACTOR

Pilar Jiménez-Meneses[+],a, Roland J.-R. Bednarz[+],b, Vincente Montiel[a], Roberto Gómez[a], Siegfried R. Waldvogel[a,c,d]*

a University Institute of Electrochemistry, University of Alicante, Carretera San Vicente del Raspeig s/n, 03690 San Vincente del Raspeig - Alicante, Spain.

b Department of Chemistry, Johannes Gutenberg University, Duesbergweg 10–14, 55128 Mainz, Germany.

c Institute of Biological and Chemical Systems – Functional Molecular Systems (IBCS-FMS), Hermann-von-Helmholtz-Platz 1, 76344 Eggenstein-Leopoldshafen, Germany.

d Max-Planck-Institute for Chemical Energy Conversion, Stiftstraße 34–36, 45470 Mülheim an der Ruhr, Germany.

* Emails: waldvogel@uni-mainz.de, roberto.gomez@ua.es

[+] These authors contributed equally to this work.

KEYWORDS. renewable energy, photovoltaic panels, grid stabilization, electrooxidation, 3-propyladipic acid

ABSTRACT. Currently, there is an increasing interest in both electrochemical engineering and solar chemistry, which may be satisfied through the development of sun-powered electrochemical processes and reactors. Along these lines, an electrochemical reactor powered by a photovoltaic panel has been demonstrated for the oxidation of 4-propylcyclohexanol to 3-propyladipic acid by using activated NiOOH anodes. The coupling between the photovoltaic panel and the electrochemical reactor is direct and allows to assess the effect of renewable energy source fluctuations (resulting in applied current fluctuations) on the performance of the electrochemical system. The system was controlled to provide a minimum current density of 1.25 mA cm^{-2} to ensure that the anode surface state was maintained throughout the electrolysis. Even in a case in which the anode preservation could limit the power fluctuations that the system may withstand, setting an appropriate control of temperature and hydrodynamics leads to yields of 3-propyladipic acid of up to 26% by using the sun-powered electrolyzer, close to those obtained with a conventional power supply. In a more general vein, this result points to the feasibility of self-standing sun-powered electrosynthesis beyond water splitting.

INTRODUCTION

Concerns about the environmental and climate impact caused by the increasing human population and growing fossil-based industries have been rocketing in the last years. Stricter laws and measures are being negotiated by governments at different levels to reduce the

adverse effect of human activity on climate and nature.[1–3] In addition, the on-going energy crisis has increased the need for new solutions.

With the goal of both drastically limiting the climate crisis caused by emissions of greenhouse gases and finding greener processes in the chemical production, the combination of the valorization of renewable biogenic resources–in particular side-streams, and the use of renewable energy can be a solid route forward.[4] It is worthwhile noting that this would be a truly sustainable route as, not only renewable energy is used, but also a regenerative chemical feedstock (all-round renewable approach).[5] Lignin is the most abundant polymer on Earth after cellulose, comprising between 15 and 30 wt% of the lignocellulosic biomass.[6] Not only lignin plays a key role because of its wide abundance, but it also represents the mayor by-product of the pulping industry,[6] which focuses on the production of cellulose fibers, discarding annually multi-million tons of lignin as a waste stream (black liquor).[7] Such a residual stream is partially separated into lignin, employed as a low-quality fuel, achieving relatively low amounts of energy via burning.[8] However, lignin can be a more profitable resource, as its structure involves a wide range of aromatic units that can be converted into valuable aromatic chemicals.[9] Unfortunately, the complex structure of lignin hinders the development of a universal depolymerization method and limits the generation of specific compounds in high yield. In addition, lignin is prone to condensation and degradation reactions during both the isolation and depolymerization processes.[10–13] Despite this, numerous efforts have been (and are being) made to transform lignin into high-value monomers such as vanillin, acetovanillone or 4-propylcyclohexanol.[6,14–16]

This work focuses on the conversion of 4-propylcyclohexanol as a model compound, as it could be obtained from hardwood lignin by catalytic hydrogenolysis over copper-chromium oxide back in 1938.[17] Later studies further inspected this catalytic hydrogenolysis by using lignins derived from maple or spruce, achieving yields of up to 19.5 wt%.[18–22] The importance of hydrogenating lignin into this alkylated cyclohexanol derives from its possible conversion into 3-propyladipic acid (3PAA), an appropriate precursor for polyamides or polyesters, substituting the well-known and technically relevant adipic acid precursor.[21,23,24] Polymers coming from different precursors may have tailor-made properties. Adipic acid is usually synthesized using nitric acid and copper catalysts, which promotes the production of potent greenhouse gases such as N_2O, being a climate impactful and polluting route.[25] Alternative methods for synthesizing adipic acid involve the oxidation of cyclohexanol utilizing UV light and ozone, providing more environmentally friendly protocols.[26] However, the scale-up of systems based on these processes involves several challenges, e.g., over-irradiation, mass transport, and temperature control.[27,28] Recently, an oxidative electrochemical route from cyclohexanone to adipic acid coupled with H_2 generation has been established. Specifically, a NiOOH anode is modified creating an interlayer with sodium dodecyl sulfate ($Ni(OH)_2$-SDS). The intercalated sodium dodecyl sulfate (SDS) facilitates the enrichment of immiscible cyclohexanone in the local environment of the anode, thereby leading to higher yields of adipic acid.[29]

Here, we have applied an electrochemical route using activated NiOOH electrodes as a more sustainable approach for the conversion of alkylated cyclohexanols into alkylated dicarboxylic acids by oxidation and subsequent ring opening.[21] These electrodes have previously been demonstrated to successfully electrooxidize alcohols to ketones in caustic soda.[30–33] Remarkably, this oxidation is enabled using an electrochemical route, being in line with the principles of green chemistry.[34] The use of electrons as a reagent/product presents higher efficiencies, decreases waste, improves atom economy, and it allows conversions that would not be possible following conventional approaches.[35–37]

On the other hand, electrochemical processes are amenable to be coupled with renewable energy sources (RES), which significantly adds to their sustainable character. In this respect, solar radiation represents a nearly unlimited energy source, having an excellent potential, with a daily average power density of 250 W m^{-2} on a yearly basis.[38] Photovoltaic panels are particularly attractive because of their non-polluting effect during operation, straightforward maintenance, long lifetime, lack of acoustic contamination, possibility of scale-up, minimum impact on the environment and climate, and the possibility of decentralized power generation[38–43] It is worth noting that a simple coupling is possible between electrochemical reactors and photovoltaic panels as both involve the use and generation of direct current. A direct coupling has significant advantages that can be critical in some applications; its simplicity involves lower capital expenditure as it avoids connection to the grid and/or the integration of energy storage systems. In addition, it facilitates self-standing approaches for chemical synthesis or the implementation of containerized solutions. Lastly, the coupling of large-scale electrochemical reactors powered by renewable current can have a significant impact on grid stabilization. Thereby, the applied current may fluctuate over time with renewable generation, within ranges of stable electrochemical production.

In the last 20 years various modalities for coupling photovoltaic panels and electrochemical reactors have been explored on different levels, mainly in the fields of environmental remediation,[44,45] sodium hypochlorite synthesis,[46] and green hydrogen production (water splitting).[47] In contrast with these developments, this approach is still to be demonstrated in organic electrosynthesis, in part because conditions need to be more closely controlled to maintain yield and selectivity. The intrinsic RES fluctuations may affect the performance of the electrosynthesis process more than in other applications. It is thus critical to carry out experimental studies in which the direct coupling is implemented, and the effect of RES fluctuations assessed. In fact, full deployment of this technology requires studying the impact of these fluctuations on electrosynthesis. In this contribution, direct coupling of an electrochemical reactor for 3-propyladipic acid synthesis with a photovoltaic panel is demonstrated and the conditions under which the effect of RES fluctuations can be minimized are identified. One of the main objectives of this contribution is to pave the way for the penetration of solar electrosynthesis.

EXPERIMENTAL SECTION

Chemicals and materials

All commercial chemicals were used without further purification. 1,3,5-Trimethoxybenzene was used as a standard in ^{13}C Inverse Gated NMR analyses, anhydrous sodium sulfate, sulfuric acid, sodium hydroxide, $NiSO_4 \cdot 6H_2O$, $NaOAc \cdot 3H_2O$, and DMSO-d6 were obtained from Sigma Aldrich. 4-Propylcyclohexanol was purchased from CM Fine Chemicals. Methyl *tert*-butyl ether and ethyl acetate were acquired from VWR.

For assembling the electrochemical setup, the following units were employed: As a reservoir, a beaker-type glass cell by HWS (100 mL) was selected. As a tank reactor, a modified glass beaker cell by HWS (100 mL) was utilized. The electrolyzer consisted of an electrode stack (2 Ni foams, 3 stainless steel plates), separated 3 mm from one another by means of PTFE spacers. The stack was connected to a galvanostatic power supply. Nickel anode foams Ni 4753.05 (12 cm x 3 cm x 5 mm) were acquired from RECEMAT. Stainless-steel 1.4571 plates (immersed 12 cm x 3 cm x 1 mm) were used as cathodes. The inter-anode and inter-cathode connections were made of stainless-steel 1.4571 as well. An eductor piece was obtained from Zerodis Store. A LabN6 Peristaltic Pump incl. YZ1515x PPS pump was purchased from Drifton. Fig. 1 displays the electrochemical flow system employed.

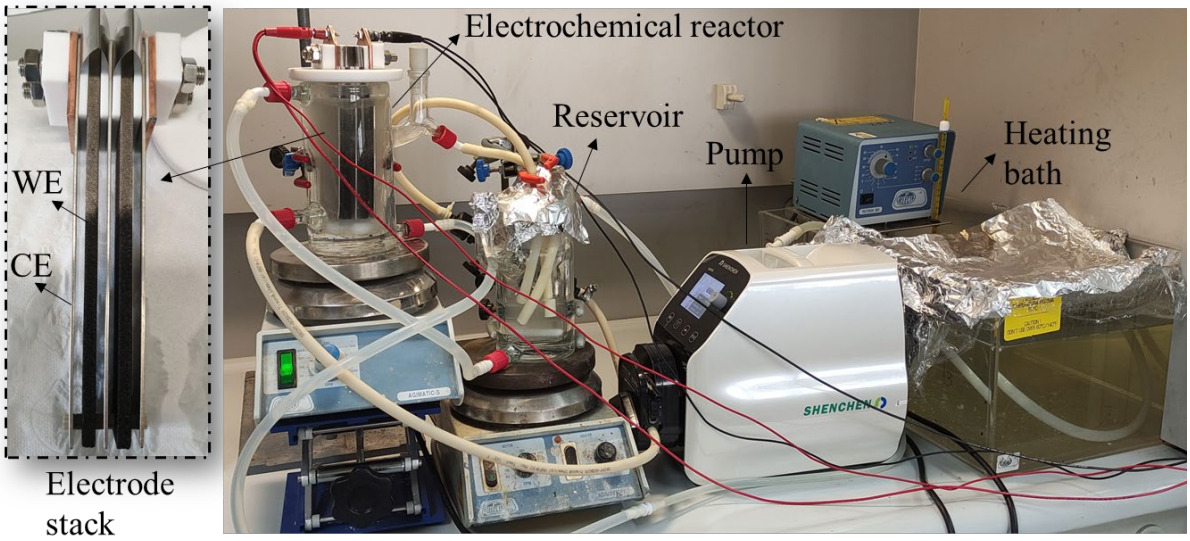

Fig. 1. Electrochemical system employed for the synthesis of 3-propyladipic acid (**2**).

Coupling a photovoltaic panel to the electrochemical reactor

A silicon polycrystalline solar panel was acquired from ATERSA (Solar panel 25W 12V – ESPMC25), assembled onto a home-made support, and directly coupled to the reactor through a programmable DC electronic load. A south orientation with an inclination of 28° was employed for the panel. A pyranometer was assembled on the plane of the panel to measure the sun radiation. Data of solar radiation, voltage in the reactor, applied current density and accumulated charge were recorded to study the effect of these fluctuating parameters in the

performance of the electrosynthesis system. The electricity employed for the oxidation of 4-propylcyclohexanol was produced by the photovoltaic panel. Fig. 2 displays photographs for the photovoltaic panel and for the interface used to collect the data.

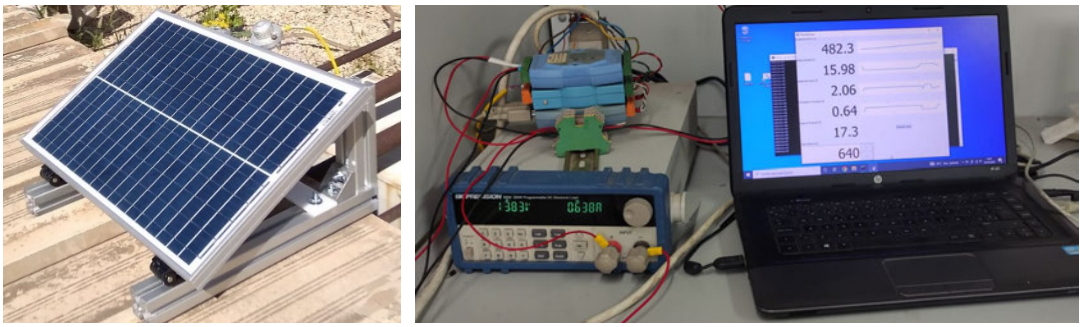

Fig. 2. Left. Assembled photovoltaic panel on the roof of the pilot plant laboratory. Right. Electronic load and modulable interface.

Activation of Ni electrodes

The protocol for the activation of Ni foam anodes was adapted from Schäfer et al, as previously reported by Bednarz et al.[30,48,49] A solution consisting of $NiSO_4 \cdot 6H_2O$ (26.28 g, 0.1 mol, 1 M), $NaOAc \cdot 3H_2O$ (13.51 g, 0.1 mol, 1 M) and NaOH (0.24 g, 5 mmol, 5 mM) dissolved in 1 L deionized water was prepared. The electrode stack was shortly immersed in caustic soda (1 M) prior to activation. Once the caustic soda was not dripping from the electrodes anymore, the system was immersed into the activation solution, which was stirred at 200 rpm. A charge density of 5 C cm^{-2} (geometric area) was applied for activation of the nickel anodes, using a current density of 7.5 mA cm^{-2} for 11.1 min. This protocol, previously optimized,[49] ensured optimal performance. The nickel foams acted as anodes (positive pole), while the stainless-steel sheets operated as cathodes (negative pole). As expected, fluctuating solar radiation led to longer activation times when the current provided by the panel was lower than the optimum as to maintain the activation charge. Surface darkening was visually observed indicating presumably the formation of active nickel(III) surface layers as previously studied by Bednarz et al.[49] The Ni foams were gently rinsed with deionized water. Likely, deposition of Ni(0) occurred at the cathode, necessitating a disassembly of the electrode stack. Subsequent cleaning of the cathodes was performed by immersion of the stainless-steel sheets shortly in 25% $H_2SO_{4(aq)}$ first and, then, in water. The electrode stack was finally reassembled for subsequent use in the electrooxidation of 4-propylcyclohexanol.

Electrosynthesis experiments

A reaction mixture (biphasic) of 4-propylcyclohexanol (0.40 M) in caustic soda (1 M, 250 mL) was recirculated at a temperature of 50 °C, a flow of 16 L h^{-1} and stirred in the electrochemical reactor at 500 rpm. An eductor system was used to improve the mixing of 4-propylcyclohexanol with the aqueous phase. A peristaltic pump was located between eductor and reactor to accomplish recirculation and mixing. An activated electrode stack was immersed into the 4-propylcyclohexanol emulsion, and a constant current density of

3.9 mA cm^{-2} was applied when the electrochemical reactor was powered with a conventional power supply.

In the experimental runs powered with the PV panel, the supplied current fluctuated according to solar radiation, with a maximum current density set at 5 mA cm^{-2}, previously determined as an optimum value.[49] Two modes of operation were tested. In the so-called continuous mode, the PV panel powered the electrochemical reactor continuously (even during nights), which translated into periods in which the current delivered to the electrochemical reactor was close to zero. Heating at 50 °C and solution recirculation/stirring was maintained throughout the test. In contrast, in the non-continuous mode, the electrochemical reactor was not powered if the solar irradiance was below a threshold of 106 W m^{-2} (corresponding to a minimum current density of around 1.25 mA cm^{-2}). In addition, pumping, stirring, and heating were stopped when solar irradiance was below the threshold to minimize mechanical damage of the catalyst.

After passing 8.0*F* (*Q* ~ 78000 C), the reaction was stopped, and the product mixture was collected for isolation of the final product (3-propyladipic acid). The electrolyzer and reservoir were rinsed with caustic soda (1 M) and then, with methyl-*tert*-butyl ether to collect all the product mixture. Electrodes could be reused for further reactions after cleaning. Fig. 3 illustrates a sketch for the direct coupling of the PV panel to the electrochemical reactor.

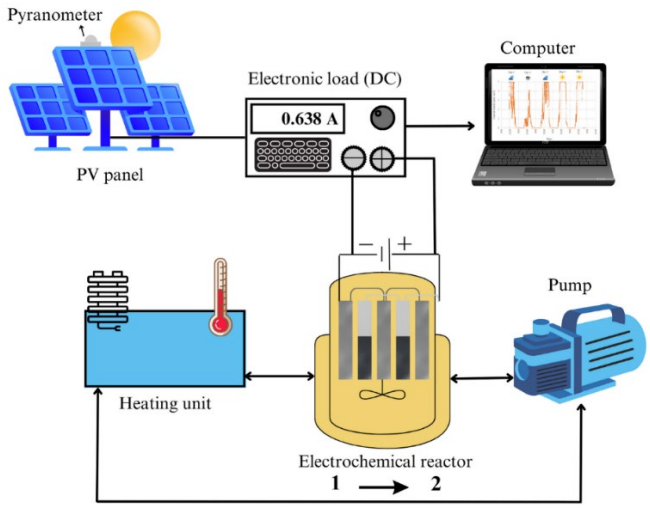

Fig. 3. Sketch for the direct coupling of the PV panel to the electrochemical reactor (including ancillary equipment) for the synthesis of **2** from **1**.

A simple reaction sketch for the synthesis of 3-propyladipic acid (**2**) from 4-propylcyclohexanol (**1**) by using NiOOH-activated anodes and stainless-steel cathodes is shown in Fig. 4.

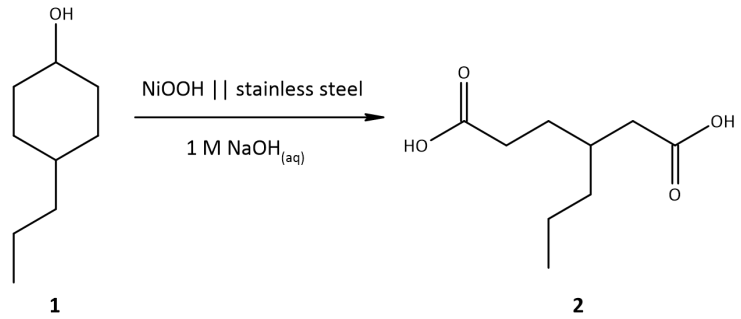

Fig. 4. Anodic oxidation of **1** to **2** at active nickel oxyhydroxide foam anodes. Water reduction takes place at stainless-steel cathodes.

Isolation and characterization of 3-propyladipic acid (2)

The recovered product solutions were treated with methyl-*tert*-butyl ether (3 x 50 mL) by liquid-liquid extraction. Next, the basic aqueous phase (pH>12) was acidified to pH 1–2 using $H_2SO_{4(aq)}$ (25 vol%), causing flocculation within the solution. This mixture was extracted with ethyl acetate (4 x 50 mL). The ethyl acetate fractions were combined, dried over $MgSO_4$, filtered, and the solvent was evaporated under reduced pressure.

Both organic fractions were characterized by ^{13}C Inverse Gated NMR in a 500 MHz BRUKER AVANCE III HD. The quantification was done by integrating the respective signals in the ^{13}C Inverse Gated spectrum against 1,3,5-trimethoxybenzene as internal standard (δ = (55.4±0.02) ppm) as previously established by Bednarz et al.[49] The DMSO-d6 signal was chosen as a reference (δ = 39.52 ppm). MestReNova software was employed for the analysis of the respective signals. Although ^{13}C NMR is not commonly employed for quantification, the ^{13}C Inverse Gated mode has facilitated a reliable approximation for quantification. ^{13}C Inverse Gated NMR (150 MHz, DMSO-d6, + Standard, δ): 174.84 (C-6), 174.37 (C-1), 161.43 (C-1'), 92.96 (C 2'), 55.28 (C-3'), 38.57 (C-2), 35.60 (C-3), 33.85 (C-7), 31.24 (C-5), 28.71 (C-4), 19.32 (C-8), 14.36 (C 9).

RESULTS AND DISCUSSIONS

Experiments powered by a conventional power supply

Before performing the experiments using PV panels, blank experiments using a conventional power supply were carried out in the first place to check the reproducibility of the system and for the sake of comparison. Tests using a conventional power supply gave qNMR yields for **2** of 27%. This value aligns with previous results obtained in under laboratory conditions with non-fluctuating current densities using the optimum parameters obtained during the extensive Design of Experiments (*DoE*) screening conducted by Bednarz et al.[49] This yield was subsequently utilized as a benchmark for comparing with the outcomes of subsequent experiments using the PV-powered modes.

Cell voltage was monitored to assess the system behavior, with its maximum value being below 2 V. As shown in Fig. 5, the cell voltage gradually increased over time, starting at

approximately 1.70 V and reaching around 1.86 V at the end of the electrolysis. This is a common trend in electrosynthesis reactions, and it may be attributed to reagent consumption and surface deactivation caused by either electrocatalyst evolution/etching or fouling.

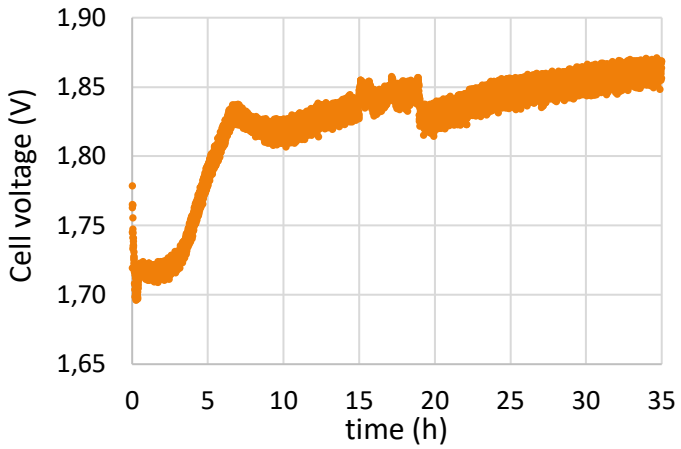

Fig. 5. Cell voltage vs time recorded during the electrosynthesis of **2** using a conventional power supply. Electrolysis conditions: 0.40 M 4-propylcyclohexanol in caustic soda (1 M, 250 mL), temperature of 50 °C, recirculating flow of 16 L h^{-1}, stirring at 500 rpm, anode geometric surface area of 128 cm^2, constant current density of 3.9 mA cm^{-2} and a total applied charge of 8*F*.

Coupling photovoltaic panel and electrochemical reactor

As mentioned above, direct coupling may be advantageous because of its simplicity and versatility, avoiding the need for energy storage systems. In our case, a direct connection of the photovoltaic panel to the electrochemical reactor through a DC electronic charge allowed us to evaluate the effect on the electrosynthesis of fluctuations in the applied current density due to typical changes in solar irradiation. It is critical to demonstrate that these fluctuations do not affect in a substantial way the electro-synthesized product yields. Otherwise, the applicability of the approach would be seriously compromised. Specifically, the validity of this approach was studied for the synthesis of **2**. It is worth noting that, in the electro-synthetic process, the RES fluctuations should not only be withstood by the electrosynthesis process itself, but they also should not be deleterious for maintaining a proper activation of the electrodes, specifically the anode. Thus, the case under scope should be considered as challenging as it may require stringent experimental conditions for the appropriate functioning of the coupling.

Once the electrochemical reactor was properly connected to the photovoltaic panel (including the monitoring of relevant parameters), two limiting cases were studied. The rationale for this testing modes derives from the hypothesis that low current densities can provoke low yields of the desired product. First, the system was studied under the so-called continuous mode and then under the non-continuous mode. In the first case, the electrochemical reactor was continuously powered by the solar panel under different insolation conditions, including the night periods. The only limitation was the maximum current density (5 mA cm^{-2}) delivered to

the electrochemical reactor. In the second case, apart from the maximum current density setpoint, a minimum solar radiation threshold was established, under which no power was delivered to the electrochemical reactor to avoid undesired reactions. The heating, recirculation, and stirring of the solution/emulsion were also interrupted under this threshold, as these parameters are known to induce the deactivation of the anodes.

Solar-powered activation of the Ni electrodes

Analogous protocols were applied for the activation of the nickel anodes regardless of the operation mode. In this case, the maximum current density to be supplied by the photovoltaic panel was set at 7.5 mA cm^{-2}. Small fluctuations (current densities between 6.2–7.5 mA cm^{-2}) were observed not to cause noticeable negative effects on the anode surface activation, which was characterized by the darkening of the nickel foams.

Solar-powered electrooxidation of 4-propylcyclohexanol (1). Continuous mode

The effect of fluctuations, including the application of low or zero current densities with continuous stirring was analyzed with a focus on the yields of **2** and the inspection of the anodes (to assess the resilience of the activation layer).

Fig. 6 depicts the solar irradiance as measured by a pyranometer (A), the corresponding current density delivered to the electrochemical reactor (B), which was stopped once the desired charge (8*F*) had been circulated, and the cell voltage (C) versus time for the whole duration of the experimental run. As observed, the test spanned five days with different meteorological conditions (2 sunny days, 2 partly cloudy days, and one cloudy/rainy day). Such a weather variability led to wide fluctuations in the sub-hour scale, together with the day and night cycles. A solution 0.40 M 4-propylcyclohexanol in caustic soda (1 M, 250 mL) was employed as an electrolyte, which was thermostated at 50 °C and both recirculated at 16 L h^{-1} and stirred at 500 rpm. The maximum current density was set at 5 mA cm^{-2} (anode geometric surface area of 128 cm^2) and the total applied charge was of 8*F*.

The qNMR yield of the product was 11%, less than half that reached in conventional (galvanostatic) experiments. An important observation is that while sub-hour fluctuations did not lead to apparent changes in the nickel foam anodes, inspection of the anodes revealed an important loss of the Ni-based activation layer (loss of the black coloration) when low current densities were applied. These results reveal the negative impact of applying low-to-zero current densities to the electro-synthetic system while maintaining solution/dispersion heating, recirculation, and mixing. Although reactivation of the electrodes was possible subsequently (for current densities above 1.25 mA cm^{-2} approximately) according to the aspect of the anode, its performance did not fully recover, resulting in a rather low product yield, presumably by the appearance of side reactions.

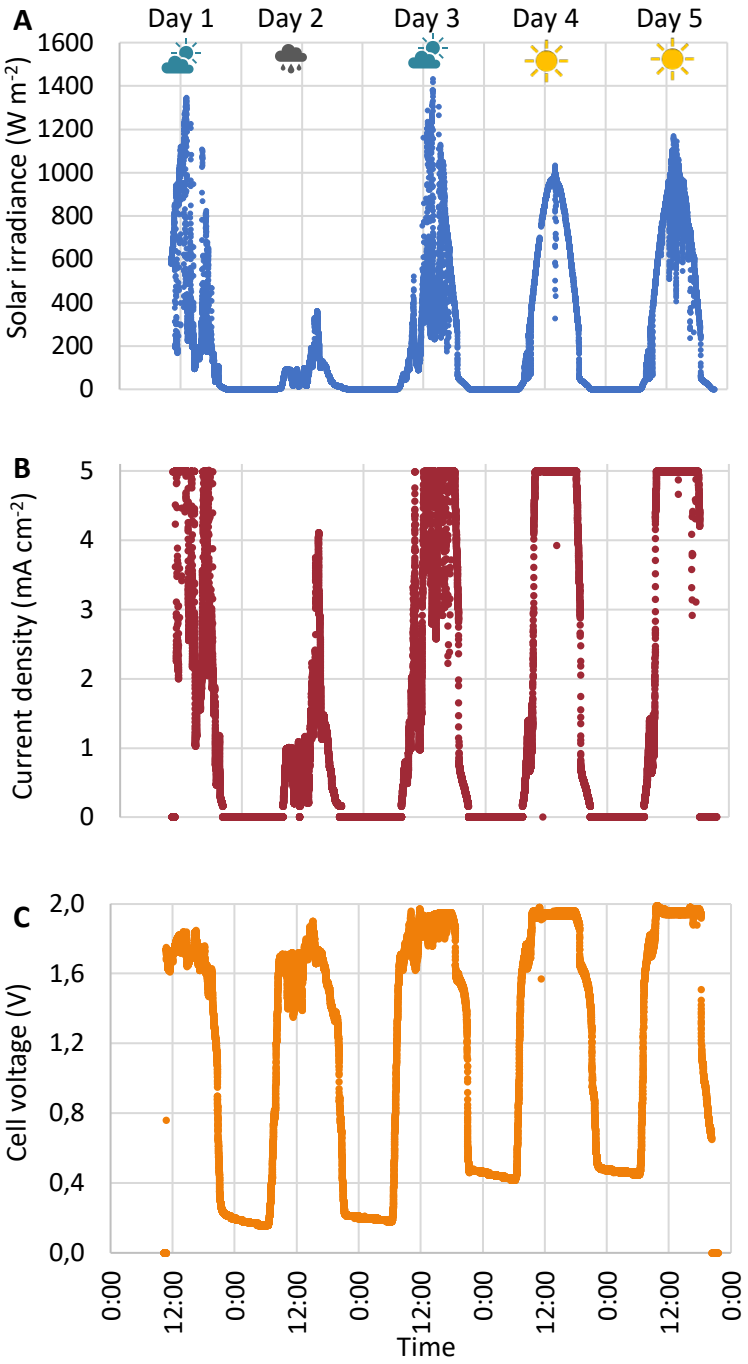

Fig. 6. Data recorded during the solar electrosynthesis of **2** using the direct coupling of a PV panel and an electrochemical reactor (continuous mode). **A**. Solar irradiance vs time. **B**. Current density vs time. **C**. Cell voltage vs time. The total applied charge was 8*F*. The experiments were carried out in May 2022 at the San Vicente campus of the University of Alicante (San Vicente del Raspeig, Alicante, Spain).

As previously emphasized, maintaining anode polarization is of paramount importance in achieving favorable outcomes. Valuable insights into anode stability can also be derived from the rest potentials observed in panel C. The low cell voltage values observed when no current is applied to the system, often referred to as the open-circuit voltage, serve as an indicator of anode depolarization within the system under investigation. Conversely, higher values of this

rest potential would imply enhanced surface stability, suggesting that the oxy-hydroxide film would be preserved, at least partially. Notably, during days 3 and 4, when the system was subjected to a higher load, the initial rest voltage was high (approximately 0.45 V) as compared to days 1 and 2 (around 0.20 V), pointing to higher stability of the anode surface during subsequent nighttime periods. It is also worth noting that, as expected, the open circuit potential decreased in all cases during nighttime due to a partial loss of the oxy-hydroxide film.

Solar-powered electrooxidation of 4-propylcyclohexanol (1). Non-continuous mode

Based on previous results, it is apparent that the enhancement of the process should be based on diminishing electrode deactivation and, thus, secondary reactions. This led to the definition of the non-continuous mode. A minimum incident solar irradiance (106 W m^{-2}) was chosen as a threshold below which no power was delivered to the electrochemical reactor. In addition, to help maintaining the integrity and polarization of the anode, heating, stirring, and pumping were interrupted in the periods in which the electrochemical reactor was off. This was intended to preserve the active layer on the Ni-based anode as it minimizes both depolarizing reactions leading to the reduction of Ni(III) and mechanical damage. To mitigate low current densities and minimize needless system interruptions, a 15-minute time delay was applied before implementing system activation or deactivation. Therefore, a transient deviation in solar radiation levels either above or below the predefined threshold of 106 W m^{-2} did not trigger an immediate system startup or shutdown.

Fig. 7 depicts solar irradiance (A), the corresponding current density delivered to the electrochemical reactor (B), which was stopped once the desired charge (8*F*) was applied, and the cell voltage (C) versus time for the whole duration of the experimental run. As in the previous case, the experiment lasted for 5 days, 3 of which were sunny and 2 of them partly cloudy. Under these reaction conditions, a final yield of **2** was 26%, which is in the range of the standard experiments. The electrolysis conditions were the same as for the continuous mode.

It is important to mention that in this case, inspection of the anode foams while the system was receiving energy did not reveal an apparent loss of the NiOOH activation layer (dark coloration). This is believed to explain the much higher product yield obtained here with respect to the continuous mode test. One important finding is that fluctuations in the sub-hour scale do not seem to significantly affect the efficiency of the coupled system as the final product yield is virtually the same as that obtained in the absence of fluctuations (electrochemical reactor connected to a conventional power supply).

The application of a higher load to the system, the deliberate avoidance of low current densities, and the interruption of stirring at low-to-zero current densities collectively contribute to an enhanced anode surface stability. This improvement is evident from the increased rest voltage values, typically hovering around 0.6 V, being significantly higher than in the continuous mode operation.

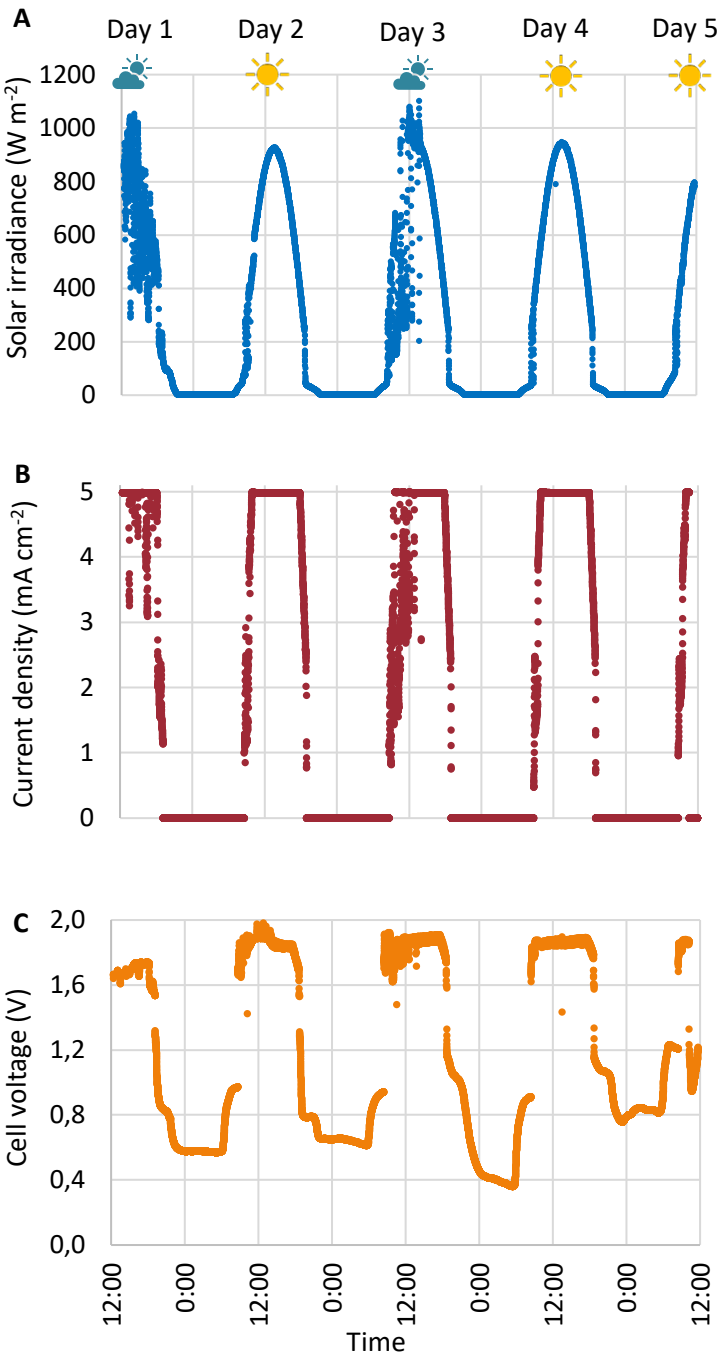

Fig. 7. Data recorded during the solar electrosynthesis of **2** using the direct coupling of a PV panel and the electrochemical reactor (non-continuous mode). **A**. Solar irradiance vs time. **B**. Current density vs time. **C**. Cell voltage vs time. The total applied charge was 8*F*. The experiments were carried out in June 2022 at the San Vicente campus of the University of Alicante (San Vicente del Raspeig, Alicante, Spain).

It is important to emphasize that, in both operating modes, the anodes experienced deactivation during nighttime periods. A crucial element contributing to the success of the non-continuous mode was the meticulous management of energy supply during these periods. In the continuous mode, the system received energy at low-to-zero current densities, leading to undesired reactions because of anode deactivation. Conversely, in the non-

continuous mode, the system was deliberately shut down under low and zero current densities to prevent the aforementioned undesired reactions and to promote a more efficient overall reaction.

Fig. 8 summarizes the results obtained for both the continuous and non-continuous modes using PV panels as power source together with standard experiments using a conventional power supply. These data were obtained in subsequent experiments carried out with the same set-up.

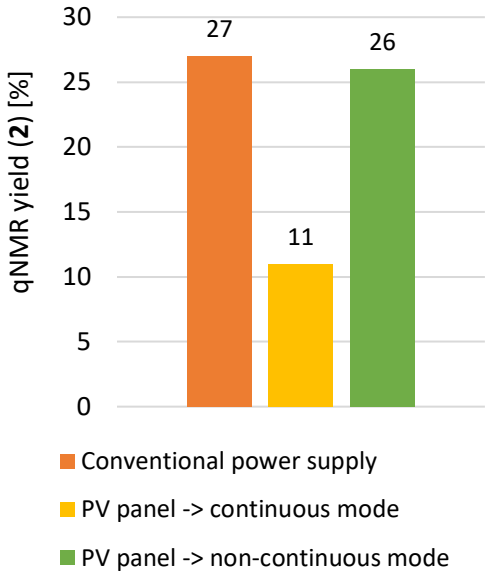

Fig. 8. Yields of **2** under standard conditions and under both continuous and non-continuous mode using PV panels as a power source.

These promising results are in our opinion a proof of concept that demonstrates the feasibility of coupling an electrosynthesis reactor to PV panels in a direct way, while maintaining performance. They also demonstrate that the mode the set-up is operated affects, in a dramatic way, the performance of the system. In this case, the generation of the desired product occurs at the anode, whose activation layer needs to be preserved, which requires avoiding depolarization. Continuous heating, stirring, and recirculation favor depolarization of the anode and loss of the activation layer, while it was protected by shutting down power, heating, recirculation, and stirring when the solar radiation delivered by the panel did not attain a threshold value. The importance of preserving the active system by interrupting the reaction when the solar instensity is too low must be pointed out as it is crucial for this system. More importantly, the results presented here illustrate how the direct connection of PV panels to electrosynthesis reactor temperature and hydrodynamic conditions, among others, are controlled according to the specific characteristics of the process being developed.

CONCLUSIONS

The electro-oxidative conversion of the lignin-derived 4-propylcyclohexanol to 3-propyladipic acid powered by solar energy has been demonstrated. The anodes are nickel foams that need

to be activated with the formation of an NiOOH layer. A direct coupling of a PV panel and the electrochemical reactor was carried out and the test extended for five consecutive days under two different operational modes, continuous and non-continuous. In the continuous mode, power was delivered to the electrochemical reactor continuously, although it was very low during nights and solution/emulsion heating, stirring, and recirculation were maintained during the whole test duration. In contrast, in the non-continuous mode, when the solar intensity on the panel was below a threshold, power was not delivered to the reactor and heating, stirring, and recirculation were shut down.

The continuous mode led to yields of 3-propyladipic acid of 11%, much lower than those obtained applying purely galvanostatic conditions with a conventional power supply. The low-to-zero values of current applied to the system at nights, together with permanent heating, stirring, and pumping likely caused deactivation of the anodes. Working with inactivated electrodes favored parallel undesired reactions. In contrast, the non-continuous operational mode was in this case much more efficient. A minimum solar irradiance of 106 W m^{-2} (corresponding to an approximated current density value of 1.25 mA cm^{-2}) was established to minimize the undesired impacts of low-to-zero current densities. In fact, similar yields (26%) to those obtained with a conventional power supply (27%) were achieved, overcoming the drawbacks appreciated in the continuous mode. It should be noted that the need for maintaining the anode activation makes this system particularly sensitive to power fluctuations, as current does not only trigger electrochemical oxidation, but it also helps to maintain anode activation. In any case, the system has been shown to withstand wide RES fluctuations with an appropriate management of the hydrodynamic conditions and temperature.

In a more general vein, this work paves the way for the development of solar electrosynthesis with the deployment of decentralized production or even containerized solutions.

ABBREVIATIONS

3PAA: 3-propyladipic acid,

RES: renewable energy sources

ACKNOWLEDGMENTS

The authors also thank Dr. Eduardo Expósito and Francisco Gallud for support in the technical work developed at the pilot plant of the University of Alicante.

Funding: This project has received funding from the European Union's Horizon 2020 research and innovation program under grant agreement no. 820735 (LIBERATE). This publication reflects the views only of the authors, and the European Union cannot be held responsible for any use which may be made of the information contained therein.

REFERENCES

(1) European Commission, The European Emissions Trading System (2005).

(2) United Nations Framework Convention on Climate Change, Paris Agreement (2015).

(3) D. Vollmer, R. J.-R. Bednarz, S. Seiffert, B. Bednarz, The benefits of Nobel Prizes, Nature Physics 18 (2022), 1383–1384. https://doi.org/10.1038/s41567-022-01830-6.

(4) M. Garedew, F. Lin, B. Song, T.M. Dewinter, J.E. Jackson, C.M. Saffron, C.H. Lam, P.T. Anastas, Greener Routes to Biomass Waste Valorization: Lignin Transformation Through Electrocatalysis for Renewable Chemicals and Fuels Production, ChemSusChem 13 (2020) 4214–4237. https://doi.org/10.1002/cssc.202000987.

(5) D. Pollok, S.R. Waldvogel, Electro-organic synthesis – a 21st century technique, Chem. Sci. 11 (2020) 12386–12400. https://doi.org/10.1039/D0SC01848A.

(6) R. Rinaldi, R. Jastrzebski, M.T. Clough, J. Ralph, M. Kennema, P.C.A. Bruijnincx, B.M. Weckhuysen, Paving the Way for Lignin Valorisation: Recent Advances in Bioengineering, Biorefining and Catalysis, Angew. Chem. Int. Ed. 55 (2016) 8164–8215. https://doi.org/10.1002/anie.201510351.

(7) A.J. Ragauskas, G.T. Beckham, M.J. Biddy, R. Chandra, F. Chen, M.F. Davis, B.H. Davison, R.A. Dixon, P. Gilna, M. Keller, P. Langan, A.K. Naskar, J.N. Saddler, T.J. Tschaplinski, G.A. Tuskan, C.E. Wyman, 2014. Lignin Valorization: Improving Lignin Processing in the Biorefinery. Science. 344, 1246843. https://doi.org/10.1126/science.1246843.

(8) J.G. Linger, D.R. Vardon, M.T. Guarnieri, E.M. Karp, G.B. Hunsinger, M.A. Franden, C.W. Johnson, G. Chupka, T.J. Strathmann, P.T. Pienkos, G.T. Beckham, Lignin valorization through integrated biological funneling and chemical catalysis, PNAS 111 (2014) 12013–12018. https://doi.org/10.1073/pnas.1410657111.

(9) M. Zirbes, S.R. Waldvogel, Electro-conversion as sustainable method for the fine chemical production from the biopolymer lignin, Curr. Opin. Green Sustain. Chem. 14 (2018) 19–25. https://doi.org/10.1016/j.cogsc.2018.05.001.

sdf

(10) W. Schutyser, G. Van den Bossche, A. Raaffels, S. Van den Bosch, S. Koelewijn, T. Renders, B.F. Sels, Selective Conversion of Lignin-Derivable 4-Alkylguaiacols to 4-Alkylcyclohexanols over Noble and Non-Noble-Metal Catalysts, ACS Sustain. Chem. Eng. 4 (2016) 5336–5346. https://doi.org/10.1021/acssuschemeng.6b01580.

(11) C. Li, X. Zhao, A. Wang, G.W. Huber, T. Zhang, Catalytic Transformation of Lignin for the Production of Chemicals and Fuels, Chem. Rev. 115 (2015) 11559–11624. https://doi.org/10.1021/acs.chemrev.5b00155.

(12) F.S. Chakar, A.J. Ragauskas, Review of current and future softwood kraft lignin process chemistry, Ind. Crops. Prod. 20 (2004) 131–141. https://doi.org/10.1016/j.indcrop.2004.04.016.

(13) P. Sannigrahi, A.J. Ragauskas, Aqueous Pretreatment of Plant Biomass for Biological and Chemical Conversion to Fuels and Chemicals, John Wiley & Sons, NJ, 2013.

(14) J. Zakzeski, P.C.A. Bruijnincx, A.L. Jongerius, B.M. Weckhuysen, The Catalytic Valorization of Lignin for the Production of Renewable Chemicals, Chem. Rew. 110 (2010) 3552–3599. https://doi.org/10.1021/cr900354u.

(15) M. Breiner, M. Zirbes, S.R. Waldvogel, Comprehensive valorisation of technically relevant organosolv lignins via anodic oxidation, Green Chem. 23 (2021) 6449–6455. https://doi.org/10.1039/D1GC01995C.

(16) M. Zirbes, T. Graßl, R. Neuber, S.R. Waldvogel, 2023. Peroxodicarbonate as a Green Oxidizer for the Selective Degradation of Kraft Lignin into Vanillin. Angew. Chem. Int. Ed. 62, e202219217. https://doi.org/10.1002/anie.202219217.

(17) E. E. Harris, J. D'Ianni, H. Adkins, Reaction of Hardwood Lignin with Hydrogen, J. Am. Chem. Soc. 60 (1938) 1467–1470. https://doi.org/10.1021/ja01273a056.

(18) H.P. Godard, J.L. McCarthy, H. Hibbert, Hydrogenation of Wood, J. Am. Chem. Soc. 62 (1940) 988–988. https://doi.org/10.1021/ja01861a508.

(19) J.R. Bower, J.L. Mccarthy, H. Hibbert, Studies on Lignin and Related Compounds. LXIII. Hydrogenation of Wood (Part 2), J. Am. Chem. Soc. 63 (1941) 3066–3068. https://doi.org/10.1021/ja01856a056.

(20) J. R. Bower, Jr., L. M. Cooke, H. Hibbert, Studies on Lignin and Related Compounds. LXX. Hydrogenolysis and Hydrogenation of Maple Wood, J. Am. Chem. Soc. 65 (1943) 1192–1195. https://doi.org/10.1021/ja01246a049.
(21) A.L. Rauen, F. Weinelt, S.R. Waldvogel, Sustainable electroorganic synthesis of lignin-derived dicarboxylic acids, Green Chem. 22 (2020) 5956–5960. https://doi.org/10.1039/d0gc02210a.
(22) H. P. Godard, J. L. McCarthy, H. Hibbert, Studies on Lignin and Related Compounds. LXII. High Pressure Hydrogenation of Wood Using Copper Chromite Catalyst (Part 1), J. Am. Chem. Soc. 63 (1941) 3061–3066. https://doi.org/10.1021/ja01856a055.
(23) J. Kühlborn, A. Danner, H. Frey, R. Iyer, A.J. Arduengo, T. Opatz, Examples of xylochemistry: colorants and polymers, Green Chem. 19 (2017) 3780–3786. https://doi.org/10.1039/C7GC01244F.
(24) R. Hu, M. Li, T. Shen, X. Wang, Z. Sun, X. Bao, K. Chen, K. Guo, L. Ji, H. Ying, P. Ouyang, C. Zhu, A sustainable process to 100% bio-based nylons integrated chemical and biological conversion of lignocellulose, Green Energy Environ. (2022). https://doi.org/10.1016/j.gee.2022.11.004.
(25) K. Weissermel, H. Arpe, Industrial organic chemistry, 4, completely rev. ed. Wiley-VCH, Weinheim, 2003.
(26) K.C. Hwang, A. Sagadevan, One-pot room-temperature conversion of cyclohexane to adipic acid by ozone and UV light, Science 346 (2014) 1495–1498. https://doi.org/10.1126/science.1259684.
(27) E. Kayahan, M. Jacobs, L. Braeken, L.C.J. Thomassen, S. Kuhn, T. van Gerven, M.E. Leblebici, Dawn of a new era in industrial photochemistry: the scale-up of micro- and mesostructured photoreactors, Beilstein J. Org. Chem. 16 (2020) 2484–2504. https://doi.org/10.3762/bjoc.16.202.
(28) J. Nikl, K. Hofman, S. Mossazghi, I.C. Möller, D. Mondeshki, F. Weinelt, F. Baumann, S.R. Waldvogel, 2023. Electrochemical oxo-functionalization of cyclic alkanes and alkenes using nitrate and oxygen. Nature Communications. 14, 4565. https://doi.org/10.1038/s41467-023-40259-0.
(29) Z. Li, X. Li, H. Zhou, Y. Xu, S. Xu, Y. Ren, Y. Yan, J. Yang, K. Ji, L. Li, M. Xu, M. Shao, X. Kong, X. Sun, H. Duan, 2022. Electrocatalytic synthesis of adipic acid coupled with H2 production enhanced by a ligand modification strategy, Nat. Commun. 13, 5009. https://doi.org/10.1038/s41467-022-32769-0.
(30) J. Kaulen, N.J. Schäfer, Oxidation of alcohols by electrochemically regenerated nickel oxide hydroxide. Selective oxidation of hydroxysteroids, Tetrahedron 38 (1982) 3299–3308. https://doi.org/10.1016/0040-4020(82)80110-5.
(31) M. Fleischmann, K. Korinek, D. Pletcher, The oxidation of organic compounds at a nickel anode in alkaline solution, J. Electroanal. Chem. Interf. Electrochem. 31 (1971) 39–49. https://doi.org/10.1016/s0022-0728(71)80040-2.
(32) B.V. Lyalin, V.A. Petrosyan, Electrosynthesis of Adipic Acid by Undivided Cell Electrolysis, Russ. Chem. Bull. 35 (2004) 688–692. https://doi.org/10.1002/chin.200452055.
(33) B.V. Lyalin, V.A. Petrosyan, Oxidation of organic compounds on NiOOH electrode, Russ J Electrochem 46 (2010) 1199–1214. https://doi.org/10.1134/S102319351011001.
(34) P. Anastas, N. Eghbali, Green Chemistry: Principles and Practice, Chem. Soc. Rev. 39 (2010) 301–312. https://doi.org/10.1039/b918763b.
(35) B. A. Frontana-Uribe, R. Daniel Little, J. G. Ibanez, A. Palma, R. Vasquez-Medrano, Organic electrosynthesis: a promising green methodology in organic chemistry, Green Chem. 12 (2010) 2099–2119. https://doi.org/10.1039/c0gc00382d.
(36) S. Möhle, M. Zirbes, E. Rodrigo, T. Gieshoff, A. Wiebe, S.R. Waldvogel, Modern Electrochemical Aspects for the Synthesis of Value-Added Organic Products, Angew. Chem. Int. Ed. 57 (2018) 6018–6041. https://doi.org/10.1002/anie.201712732.
(37) A. Wiebe, T. Gieshoff, S. Möhle, E. Rodrigo, M. Zirbes, S.R. Waldvogel, Electrifying Organic Synthesis, Angew. Chem. Int. Ed. 57 (2018) 5594–5619. https://doi.org/10.1002/anie.201711060.
(38) A.J. Bard, M.A. Fox, Artificial Photosynthesis: Solar Splitting of Water to Hydrogen and Oxygen, Acc. Chem. Res. 28 (1995) 141–145. https://doi.org/10.1021/ar00051a007.
(39) E. Zacchei, A. Colacicco, 2022. Direct Method to Design Solar Photovoltaics to Reduce Energy Consumption of Aeration Tanks in Wastewater Treatment Plants. Infrastructures. 7, 7060079. https://doi.org/10.3390/infrastructures7060079.

(40) D. Valero, J.M. Ortiz, E. Expósito, V. Montiel, A. Aldaz, Electrochemical Wastewater Treatment Directly Powered by Photovoltaic Panels: Electrooxidation of a Dye-Containing Wastewater, Environ. Sci. Technol. 44 (2010) 5182–5187. https://doi.org/10.1021/es100555z.
(41) M. Millán, V.M. García-Orozco, J. Lobato, C.M. Fernández-Marchante, G. Roa-Morales, I. Linares-Hernández, R. Natividad, M.A. Rodrigo, 2021. Toward more sustainable photovoltaic solar electrochemical oxidation treatments: Influence of hydraulic and electrical distribution. J. Environ. Manage. 285, 112064. https://doi.org/10.1016/j.jenvman.2021.112064.
(42) F. Hussin, G. Issabayeva, M.K. Aroua, Solar photovoltaic applications: opportunities and challenges, Rev. Chem. Eng. 34 (2018) 503–528. https://doi.org/10.1515/revce-2016-0058.
(43) P.G.V. Sampaio, M.O.A. González, Photovoltaic solar energy: Conceptual framework, Renew. Sust. Energ. Rev. 74 (2017) 590–601. https://doi.org/10.1016/j.rser.2017.02.081.
(44) D. Valero, J.M. Ortiz, E. Expósito, V. Montiel, A. Aldaz, Electrocoagulation of a synthetic textile effluent powered by photovoltaic energy without batteries: Direct connection behaviour, Solar Energy Mater. Solar Cells 92 (2008) 291–297. https://doi.org/10.1016/j.solmat.2007.09.006.
(45) D. Valero, V. García-García, E. Expósito, A. Aldaz, V. Montiel, Electrochemical treatment of wastewater from almond industry using DSA-type anodes: Direct connection to a PV generator, Sep. Purif. Technol. 123 (2014) 15–22. https://doi.org/10.1016/j.seppur.2013.12.023.
(46) E. Chinello, H.H. Mohammad S., D. Psaltis, C. Moser, Solar-Electrochemical Platforms for Sodium Hypochlorite Generation in Developing Countries, J. Electrochem. Soc. 166 (2019) E336–E346. https://doi.org/10.1149/2.0491912jes.
(47) M. Lee, S. Haas, V. Smirnov, T. Merdzhanova, U. Rau, 2022. Scalable Photovoltaic-Electrochemical Cells for Hydrogen Production from Water - Recent Advances. ChemElectroChem. 9, e202200838. https://doi.org/10.1002/celc.202200838.
(48) R. J.-R. Bednarz, A.S. Gold, J. Hammes, D.F. Rohrmann, S. Natalello, M. Mann, F. Weinelt, C. Brauer, S.R. Waldvogel, Scaled Oxidative Flow Electrosynthesis of 3-Alkyladipic Acids from 4-Alkylcyclohexanols, Org. Process Res. Dev. 28 (2024) 1529–1538. https://doi.org/10.1021/acs.oprd.3c00146.
(49) R. J.-R. Bednarz, P. Jiménez-Meneses, A.S. Gold, D. Monllor-Satoca, A. Stenglein, R. Gómez, S.R. Waldvogel, 2023. Sustainably scaled electrochemical synthesis of 3-propyladipic acid in line with fluctuating grid supply. ChemCatChem. 15, e202300606. https://doi.org/10.1002/cctc.202300606.

ROBUST AND SELF-CLEANING ELECTROCHEMICAL PRODUCTION OF PERIODATE

This manuscript has been published by the peer-reviewed journal ChemSusChem in 2022. The editors accepted the reuse of this content in the present thesis. It is reprinted with permission of Kisukuri, C. M., Bednarz, R. J.-R., Kampf, C., Arndt, S., Waldvogel, S. R., *ChemSusChem* **2022**, *15* (16), e202200874.

Author Contributions (following NISO standard): **C. M. Kisukuri**: Conceptualization (lead), formal analysis (lead), investigation (lead), methodology (lead), project administration (lead), visualization (lead), writing – original draft (lead), writing – review & editing (lead); **R. J.-R. Bednarz**: Conceptualization (lead), formal analysis (lead), investigation (lead), methodology (lead), project administration (lead), visualization (lead), writing – original draft (lead), writing review & editing (lead); **C. Kampf**: formal analysis (equal), investigation (equal), writing – original draft (supporting), writing – review & editing (supporting); **S. Arndt**: methodology (supporting), writing – original draft (supporting), writing – review & editing (supporting); **S. R. Waldvogel**: Funding acquisition (lead), conceptualization (equal), resources (lead), formal analysis (equal), methodology (lead), project administration (equal), supervision (lead), validation (lead), writing – original draft (equal), writing – review & editing (equal).

Fascinating research by Arndt et al. to electro-generate the platform oxidizer *para*-periodate, utilizing a flow electrolyzer, motivated this work.[55] The goal of this study was to investigate the robustness of a recycling process to regain *para*-periodate from a contaminated iodine source of lower oxidation strength. This was imitated by adding organic impurities and iodo-containing compounds, like contrast media.

By testing dyes, the optical decomposition of the species was best visible and could be followed via UV/*Vis* spectroscopy. For pharmaceutical active ingredients (APIs), their degradation could be kinetically followed via liquid-chromatography with coupled mass spectrometry and ^{1}H nuclear magnetic resonance spectroscopy. The degradation of iodine-containing compounds, which can themselves be fed to the periodate-recycle, was tracked via LC-MS and gas chromatography-MS. Remarkably, all tested substances were degraded or even fully mineralized at the boron-doped diamond electrode, tested by Arndt et al.,[55] when being subjected to the *para*-periodate synthesis. The cathode reaction is the production of hydrogen, which mainly originates from water reduction. Changes in the required applied charge originated from the ionic nature of the compounds' structure. Electron-rich compounds are degraded faster than electron-deficient ones. 5-iodoisophthalate and 2,4,6-triiodophenol were >99% degraded within only 82 and 112 equivalents of produced *para*-periodate, respectively.

The following dyes were subjected to degradation in the *para*-periodate synthesis: Fluorescein, sudan I, naphthol green, brilliant black, diamine green, methylene blue, rose bengal and PTCDA. The order reflects the relative amount of required degradation charge, expressed in the paper with 3–52 kiloequivalents of *para*-periodate. The last two formed intermediates, which showed higher UV/*Vis* intensities prior to being fully mineralized.

In terms of APIs, the degradation charge of iohexol, fluorouracil, diodrast and diatrizoate was investigated. These compounds are listed in their degradation effort from immediately, when coming in contact with the anolyte solution up to nearly 1 kiloequivalent of *para*-periodate.

The range of direct degradation to the formation of more stable intermediates was investigated for the following iodine-containing molecules: diiodomethane, dimethyl 5-iodoisophthalate, 2,4,6-triiodophenol, 2-iodobenzoic acid, 2-iodoaniline, 3-iodobenzoic acid and methyl-4-iodobenzoate. Up to 430 equivalents *para*-periodate were necessary to 99% degrade the products. The last ester remained in the state of the stabilized carboxylic acid, which can be attributed to a particular high stability via the electron-deficient substitution pattern.

The anodic oxidation of iodine species is mediated by hydroxyl radicals,[55,67] which prompted us to propose reaction steps for the formation of para-periodate, starting from iodide.

When comparing the purity of the recycled para-periodate, from contaminated iodo-streams, with its original oxidation in pure water, the same purity was determined by LC. This emphasizes the powerful self-cleaning behavior of the electrochemical *para*-periodate process.

ROBUST AND SELF-CLEANING ELECTROCHEMICAL PRODUCTION OF PERIODATE

*Camila M. Kisukuri[+],[a], Roland J.-R. Bednarz[+],[a], Christopher Kampf[a], Sebastian Arndt[a], Siegfried R. Waldvogel[a]**

a Department of Chemistry, Johannes Gutenberg University, Duesbergweg 10–14, 55128 Mainz, Germany.

* Emails: waldvogel@uni-mainz.de, roberto.gomez@ua.es

[+] These authors contributed equally to this work.

KEYWORDS. degradation, electrochemistry, organic dyes, periodate, self-cleaning

ABSTRACT. Periodate, a platform oxidizer, can be electrochemically recycled in a self-cleaning process. Electrosynthesis of periodate is well established at boron-doped diamond (BDD) anodes. However, recovered iodate and other iodo species for recycling can contain traces of organic impurities from previous applications. For the first time, it was shown that the organic impurities do not hamper the electrochemical re-oxidation of used periodate. In a hydroxyl-mediated environment, the organic compounds form CO_2 and H_2O during the degradation process. This process is often referred to as "cold combustion" and provides orthogonal conditions to periodate synthesis. To demonstrate the strategy, different dyes, pharmaceutically active ingredients, and iodine compounds were added as model contaminations into the process of electrochemical periodate production. UV/Vis spectroscopy, NMR spectroscopy, and mass spectrometry (MS) were used to monitor the degradation of organic molecules, and liquid chromatography-MS was used to control the purity of periodate. As a representative example, dimethyl 5-iodoisophthalate (2 mM), was degraded in 90, 95 and 99% while generating 0.042, 0.054, and 0.082 kilo equiv. of periodate, respectively. In addition, various organic iodo compounds could be fed into the periodate generation for upcycling such iodo-containing waste, for example, contrast media.

INTRODUCTION

The EU aims for Europe being climate neutral by 2050. This ambitious goal requires electrification of many industrial processes. Electro-organic synthesis may contribute to this goal substantially because it provides sustainable access to a growing number of compounds while allowing for controlled degradation of others (i.e., pollutants and waste products).[1–9] Electro-organic reactions provide numerous advantages compared to conventional synthetic approaches.[5,10–15] For example, hazardous and stoichiometric chemical redox reagents can be substituted directly by electricity derived from regenerative energy sources. This increases atom economy and lowers waste production for the desired reaction.[5,10,11,16,17] Further advantages are the improvement of safety and milder reaction conditions. In total, this sustainable approach can pay off.[18]

Batch-type electrolysis cells, typically used in research laboratories, limit the scale-up of electrochemical reactions to a technical scale due to low space-time yields. One potential

approach to practically and economically overcome this scalability issue is the operation of the electrolysis reactions under continuous-flow conditions.[19,20] Advantages of this approach are the higher energy efficiency due to smaller interelectrode distance (narrow gap) and the improved selectivity due to higher electrode surface-to-volume ratio in a flow electrolyzer.[21-26] Therefore, efficiencies of mass, energy, and electron transfer can be enhanced significantly.[27–30]

Periodate represents a strongly oxidizing hypervalent iodine species, able to facilitate a large scope of oxidative transformations in organic synthesis.[31,32] Prominent examples include cleavage of carbon-carbon bonds of a variety of 1,2-difunctionalized alkanes,[33] iodinations of alkenes and arenes,[34,35] oxidation of polysaccharides, as well as Malprade and Lemieux-Johnson oxidations.[36,37] Periodate is thus widely used in the synthesis of active pharmaceutical ingredients (APIs) (Figure 1).[38–40]

Commonly, periodate can be produced from $NaIO_3$, which can be synthesized from iodine and excess $NaClO_3$.[41] However, due to the high costs related to purification after the synthetic process or protocols with low efficiencies, traditional methods are reported as expensive.[42,43] Additionally, they involve dangerous and toxic reagents and show poor atom efficiency.[44,45]

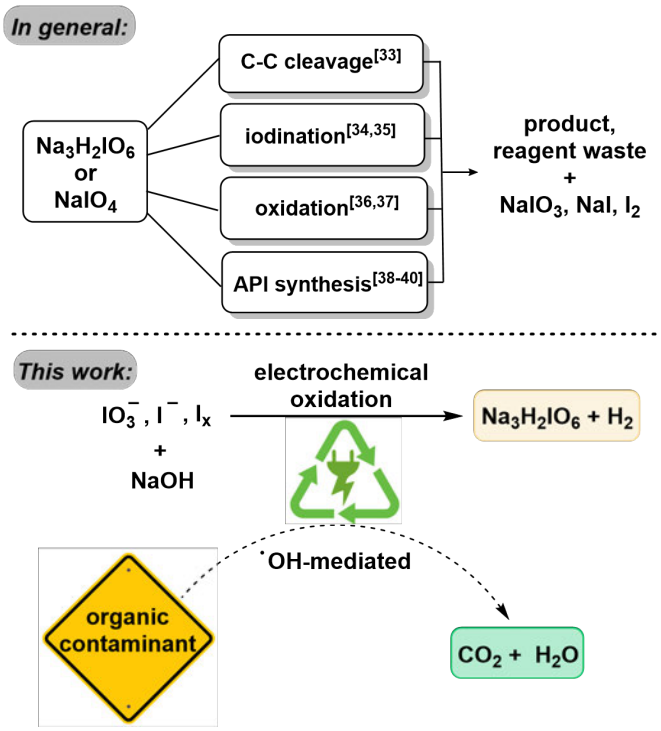

Figure 1. Examples of reported use of periodate in comparison to the use of periodate as platform oxidizers and elimination of organic impurities (this work).

An electrochemical approach is generally preferred over a chemical method.[46] Among the large variety of electrosynthesis pathways, oxidative reactions can be carried out at lead dioxide (PbO_2) or boron-doped diamond (BDD) anodes.[44] Among these two, PbO_2 has often been used preferentially as the anode material, due to electro-catalytic effects and its high overpotential for oxygen evolution in aqueous media.[47] Nevertheless, at high positive

potentials PbO_2 electrodes can form “mud”, increasing energy consumption and product contamination.[48,49]

In the last decades, the research for innovative electrode materials has focused on BDD anodes. Favorable properties of BDD electrodes include: (i) wide range of acceptable solvents; (ii) low background currents; (iii) reduced fouling; (iv) no corrosion at high temperatures; and (v) biocompatibility.[50–54]

Janssen and Blijlevens reported the use of BDD anodes for the production of periodate, mostly based on expensive lithium salts.[48] Recently, we established the sodium periodate production using electro-organic synthesis in a flow electrolyzer.[55] In this protocol, alkali iodides were used as the least expensive commercial source of iodine and caustic conditions were chosen to achieve a high current efficiency of 84%, while avoiding the precipitation of iodine. Highly toxic anti-reducing agents could be omitted using a divided cell setup employing a Nafion membrane. The electrochemically produced *para*-periodate has been successfully demonstrated to efficiently degrade lignin,[56] and to achieve the final oxidative step in the synthesis of levetiracetam and sulfoximines.[57,58]

Here, we demonstrate that electrolyses to the periodate platform oxidizer are highly robust against the presence of several organic contaminants (i.e., dyes, APIs, and other iodine compounds). Mineralization of these impurities is not harming the oxidative recycling of periodate. As shown previously, the formation of periodate occurs via hydroxyl radicals, which can also degrade and mineralize the organic impurities.[59–61] In this study, 8 different organic dyes, 3 contrast media, and 8 different iodine compounds were tested as impurities and shown to degrade during periodate recycling, as verified by UV/*Vis* spectroscopy and mass spectrometry (MS). Iodo compounds (e.g., from industrial processes) could even enhance the periodate yield by upcycling. Degradation of the compounds was measured in the scale of kilo equivalents of *para*-periodate in a co-production process. Dimethyl 5-iodoisophthalate was degraded with 90, 95, and 99% efficiency, while generating 0.042, 0.054, and 0.082 kilo equiv. of para-periodate, respectively. Commonly, all investigated examples were degraded to 99%, while consuming 0.082–52.4 kilo equiv. of periodate.

RESULTS AND DISCUSSION

General flow electrolyzer for periodate production

At first, the platform developed for the synthesis of sodium periodate was set in operation. The parameters were adjusted to the best reaction conditions. This includes the use of a divided flow electrolysis cell composed of a stainless-steel cathode (4 x 12 cm^2) and a BDD anode (4 x 12 cm^2). A Nafion membrane was used to separate the compartments. The electrochemical reaction parameters were adjusted to a galvanostatic reaction using a constant current density of 312 mA cm^{-2} (I = 15 A). The aqueous anolyte (4 M NaOH; 0.21 M $Na_3H_2IO_6$) and aqueous catholyte (4 M NaOH) solutions were pumped through the electrolyzer with a flow rate of 7.5 L h^{-1}. A complementary pump was used to keep the volume of catholyte

and anolyte constant. Here, a rate of 0.3 mL min^{-1} was used. Also, a cryostatic bath circulator, for controlling the temperature of the electrolyzer was employed. To test the degradation of the organic contaminants, selected compounds were added into the anodic compartment. Figure 2 schematically illustrates the set-up to re-oxidize periodate and degrade organic molecules. A detailed set of pictures of the system is displayed in the Supporting Information (Figures S1 and S2).

In general, the established flow system proved to be robust, not showing leaks or clogging after the re-oxidation and degradation experiments.

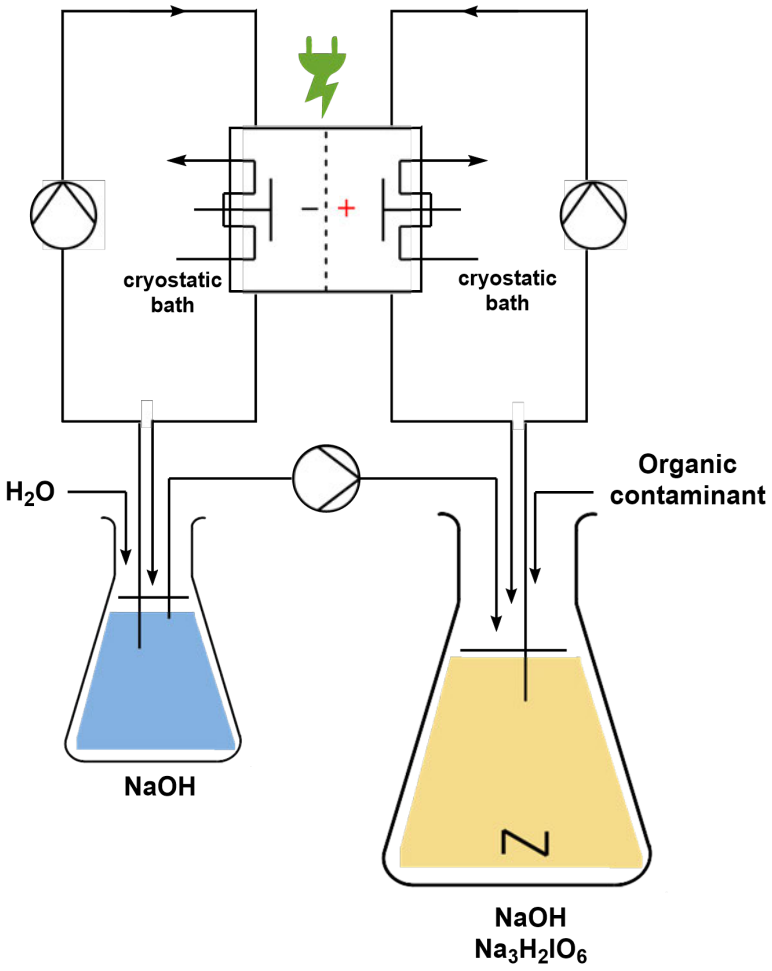

Figure 2. General scheme for the periodate platform oxidizer: self-cleaning electrochemical re-oxidation to periodate following the degradation of organic compounds; cooling cryostat pump.

Re-oxidation to *para*-periodate using dye-containing solutions

The UV/*Vis* measurements were used to easily follow the degradation (Figures S3–S18) of different dyes present in the anodic compartment. For these experiments, a dye concentration of $1x10^{-4}$ M was used. This concentration proved to be ideal to direct measurements of UV/*Vis* without any type of dilution steps and with good sensitivity. To clarify that not only the fluorophore was degraded but a total degradation happened, high-

resolution (HR)MS analyses were performed. Examples are displayed in the Supporting Information (section 14). The experiments were performed using the parameters displayed in Table 1.

Table 1. Electrochemical degradation of dyes in *para*-periodate platform oxidizer process.[a]

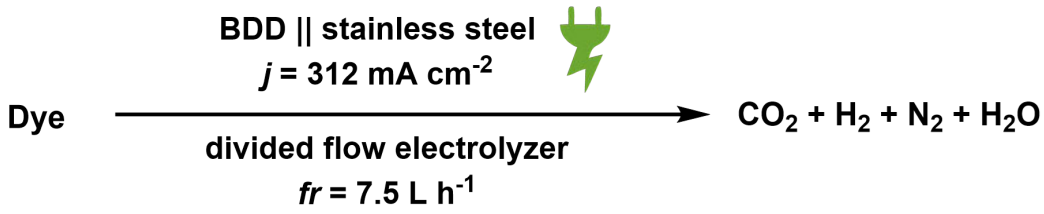

Dye (0.1 mM)	Degradation [kilo equiv. of $Na_3H_2IO_6$]		
	>90%	>95%	>99%
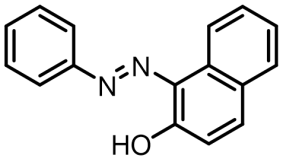 Sudan I **(1)**	2.4	3.2	5.0
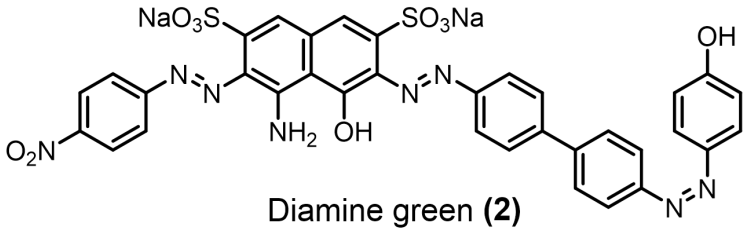 Diamine green **(2)**	3.7	4.8	7.4
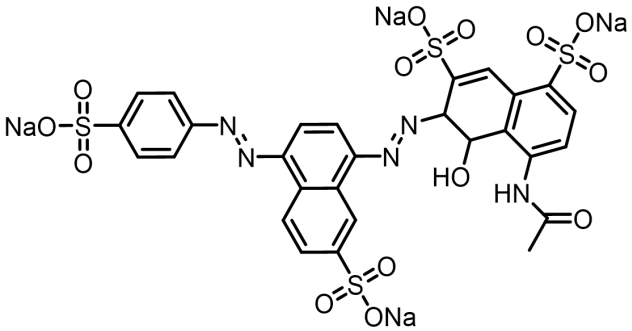 Brilliant black **(3)**	3.0	4.0	6.2
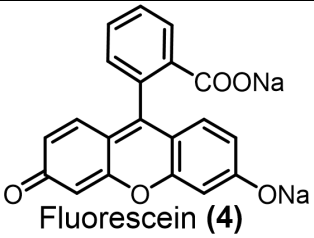 Fluorescein **(4)**	1.6	2.0	3.1
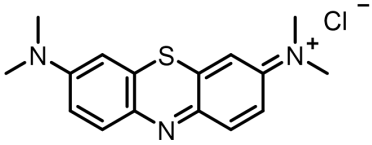 Methylene blue **(5)**	26.2	34.1	52.4

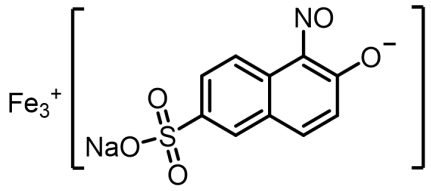 Naphthol green **(6)**	2.9	3.7	5.8
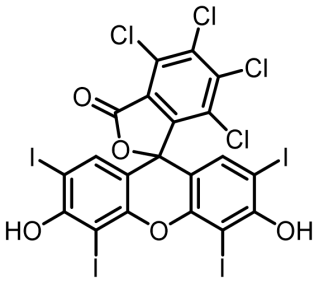 Rose bengal (**7**)	*the data was not fit by the exponential equation; formation of intermediate species (see Supporting Information)*		
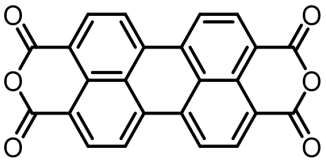 PTCDA (**8**)	*the data was not fit by the exponential equation; formation of intermediate species (see Supporting Information)*		

[a] reaction conditions: Flow electrolyzer (BDD|Nafion membrane|stainless steel, 4 x 12 cm^2 = 48 cm^2); dye (0.1 mM), NaOH (4 M), $Na_3H_2IO_6$ (0.21 M), H_2O (200 mL), j = 312 mA cm^{-2}, Q = 6–149F, RT. Degradation determined by UV/*Vis* analysis. All the kilo equiv. of periodate were calculated as showed in the section 11 (Supporting Information).

Initially, aza dyes as sudan I (**1**), diamine green (**2**), and brilliant black (**3**) were added into the periodate platform oxidizer process. Figure 3 depicts the variation of aza dye concentrations by normalized absorbance as a function of time and the periodate equivalents generated during the process. For a complete sodium *para*-periodate synthesis, 10F (8-electron oxidation of NaI and 2F for side reactions) are required for 1 equivalent.[55]

The equivalents of periodate production for 90% degradation of aza dyes decreases in the following order: **1** < **3** < **2**. Compound **1** degrades faster than compounds **2** and **3**, requiring 2.4 kilo equiv. of *para*-periodate being co-produced. Diamine green (**2**) and brilliant black (**3**) took 3.7 and 3.0 kilo equiv. of *para*-periodate to degrade until 90%, respectively. To further demonstrate the versatility of periodate's self-cleaning process, different dye structures were tested next: fluorescein (**4**), methylene blue (**5**), naphthol green (**6**), rose bengal (**7**), and perylenetetracarboxylic dianhydride (PTCDA) (**8**). Figure 4 displays the variation of ionic dyes' concentrations **4**–**8** by normalized absorbance as a function of time and *para*-periodate equivalents.

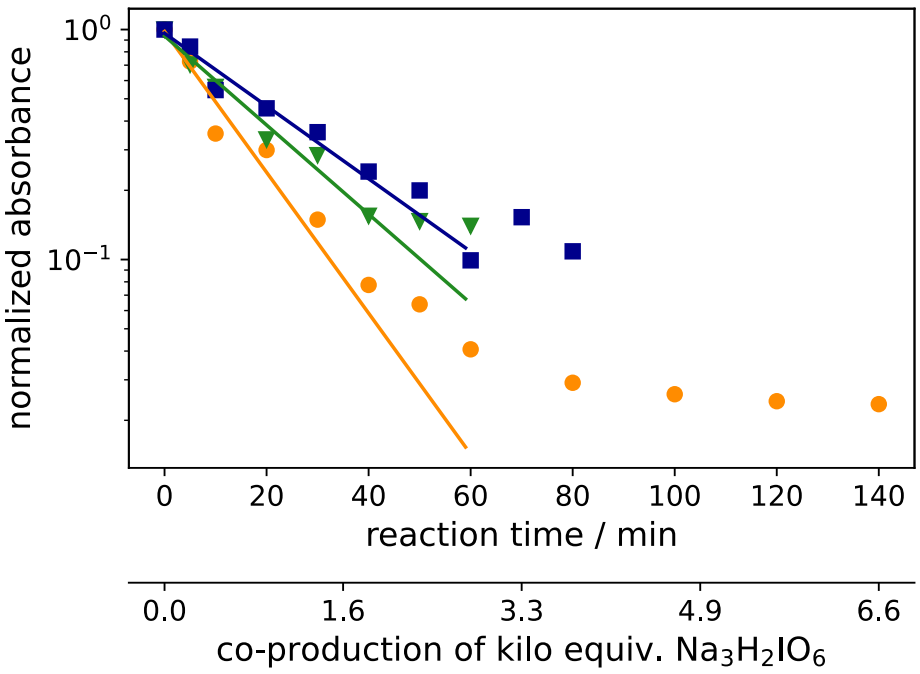

Figure 3. The degradation rate of the aza dyes brilliant black (blue ■), diamine green (green ▼) and sudan I (orange ●) during the electrochemical re-oxidation of *para*-periodate, j = 312 mA cm^{-2}, the flow rate was 7.5 L h^{-1}, in a divided flow electrolyzer. All UV-*Vis* spectra were recorded in caustic soda (0.21 M $Na_3H_2IO_6$, 4 M NaOH, 0.1 mM dye).

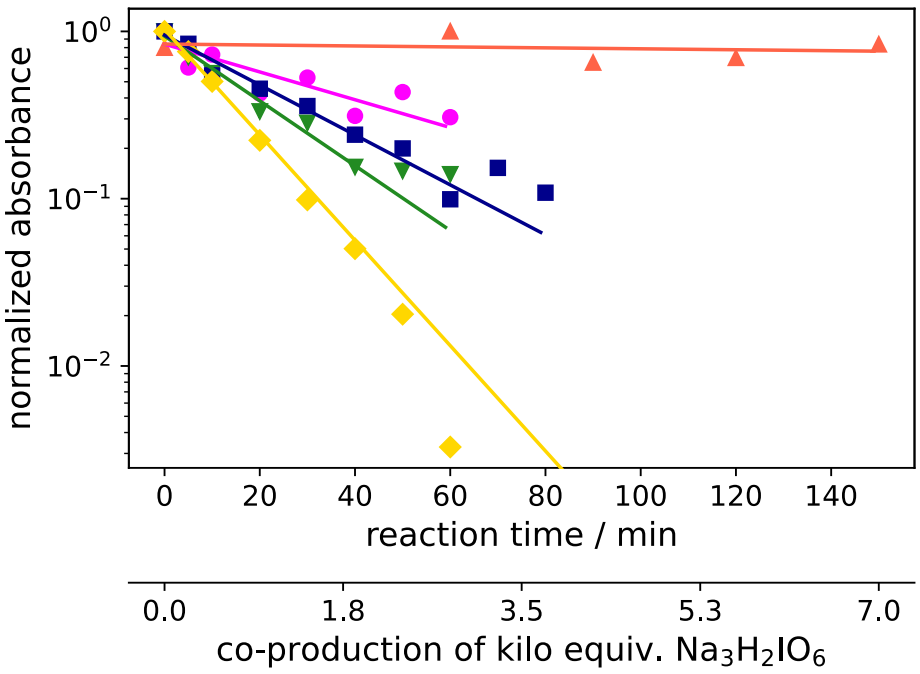

Figure 4. Kinetic degradation rate of the tested ionic dyes methylene blue (orange ▲), naphthol green (pink ●), brilliant black (blue ■), diamine green (green ▼) and fluorescein (yellow ♦) during electrochemical re-oxidation of *para*-periodate using UV/*Vis* data at a current density of 312 mA cm^{-2}, the flow rate of 7.5 L h^{-1}, in a divided flow electrolyzer. All UV-*Vis* spectra were recorded in caustic soda (0.21 M $Na_3H_2IO_6$, 4 M NaOH, 0.1 mM dye).

A 90% degradation of **4** corresponds to 1.6 kilo equiv. of *para*-periodate production. Ionic dyes like **5** and **6** were 90% decomposed within 26.2 and 2.9 kilo equiv. of *para*-periodate, respectively. The experiments with **7** and **8** took 8.2 and 18.8 kilo equiv. of *para*-periodate to be 90% degraded, respectively. Additionally, during the experiments with **7** and **8** we observed color variations in the degradation process, which could correspond to intermediate structures, formed during the re-oxidation process. This behavior made it difficult to fit such curves and follow the degradation by exponential fit equations. An image of the degradation process can be seen in the Supporting Information (Figures S16–S18). Considering the structure of the dyes in relation to the decomposition, a correlation between 90% degradation time and the compounds' structural nature could be confirmed. In general, more electron rich compounds are more easily degraded than less electron rich ones.

As illustrated in Table 1, we also compared the percentage of dye degradation in >95 and >99% with the equivalents of co-generated *para*-periodate. The results were derived from the respective exponential fit equations (Supporting Information, section 11). The equivalents of *para*-periodate follow the rationale mentioned above and depend on the electronic nature of each dye. More electron-rich dyes need less equiv. of *para*-periodate being co-generated, whereas electron-deficient ones need significantly more for the parallel occurring mineralization process. As an example, we can note the difference in equivalents necessary for the degradation of **1** (>95 and >99% using 3.2, and 5.0 kilo equiv. of *para*-periodate) compared with **5** (>95 and >99% using 34.1 and 52.4 kilo equiv.). In this case, compound **5**, a more electron-deficient dye, needs 10 times more equiv. of *para*-periodate to be >99% degraded.

Re-oxidation to *para*-periodate using iodo, contrast, and chemotherapy agent-containing solutions

The degradation of iodine and chemotherapy agents was monitored using different analytical methods.[62] Methods with clear monitoring of degradation were used, according to each compound. Therefore, the concentration of each pharmaceutical had to vary to maintain a good sensibility of the respective detection. Regarding the experiments with diodrast (**9**), diatrizoate (**10**), and iohexol (**11**), liquid chromatography (LC)-MS was applied as analytic method and an initial concentration of 0.8 mM was used for these compounds. Details of the LC-MS analyses are provided in the Supporting Information (section 7). For fluorouracil (**12**), ^{1}H and ^{19}F (Figure S33a, b) nuclear magnetic resonance (NMR) spectroscopy and a concentration of 3 mM were used to identify the degradation.

Table 2 displays the results to contrast and chemotherapy agent degradation comparing with the equiv. of *para*-periodate. For >90, >95 and >99% degradation of **9**, 0.208, 0.241 and 0.319 kilo equiv. of $Na_3H_2IO_6$ production were necessary. On the other hand, **10** was >90, >95 and >99% degraded using 0.507, 0.644 and 0.962 kilo equiv. of *para*-periodate production. When **11** was subjected to the degradation process, the signal corresponding to this compound, observed by LC-MS, disappeared only in contact with the anolyte solution. In this

case, immediate glycol cleavage occurs by the contact of basic/*para*-periodate solution, thus modifying the initial structure.

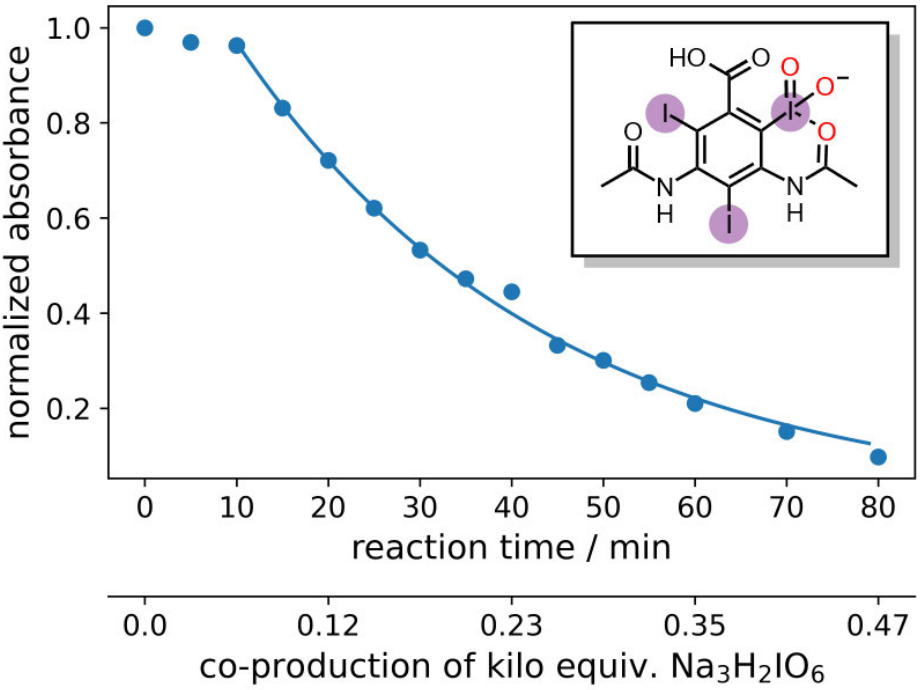

Figure 5. UV//*Vis* analysis and proposed complex for the degradation of diatrizoate. The analysis was recorded in caustic soda (0.21 M $Na_3H_2IO_6$, 4 M NaOH, 0.8 mM diatrizoate).

Table 2. Electrochemical degradation of APIs in *para*-periodate platform oxidizer process.[a]

pharmaceutically active ingredients (API) → **BDD || Stainless steel**, ***j* = 312 mA cm^{-2}**, **divided flow cell**, ***fr* = 7.5 L h^{-1}** → **$CO_2 + H_2 + N_2 + H_2O + HF$**			
API (0.8–3 mM)	**Degradation [kilo equiv. of $Na_3H_2IO_6$]**		
	>90%	**>95%**	**>99%**
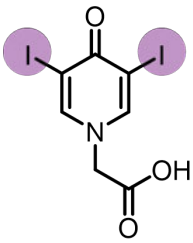 Diodrast **(9)**[b,c]	0.208	0.241	0.319

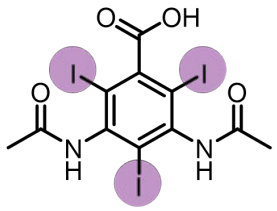 Diatrizoate **(10)**[b,c]	0.507	0.644	0.962
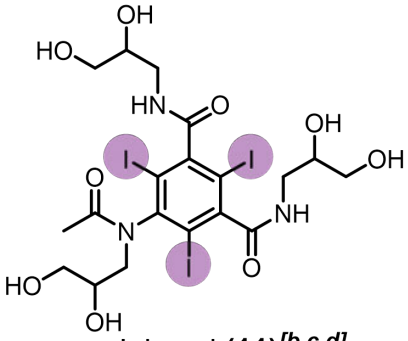 Iohexol **(11)**[b,c,d]	*direct complete glycol cleavage in contact with anolyte solution*		
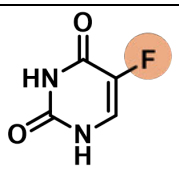 Fluorouracil **(12)**[e,f]	0.056	0.072	0.110

[a] Reaction conditions: Flow electrolyzer (BDD|Nafion membrane|stainless steel, 4x12 cm^2 = 48 cm^2); dye (0.8–3 mM), NaOH (4 M), $Na_3H_2IO_6$ (0.21 M), H_2O (200 mL), 312 mA cm^{-2}, Q = 9–12*F*, RT. All kilo equiv. of periodate were calculated as showed in section 11 (Supporting Information). [b] Concentration of 0.8 mM. [c] Degradation determined by LC-MS. [d] Degradation without electricity. [e] Concentration of the 3 mM. [f] Degradation determined by ^{1}H NMR spectroscopy.

The LC-MS analyses were illustrated in the Supporting Information (Figures S60–S63). A further ^{1}H and ^{13}C NMR spectroscopic investigation indicated that the degradation process occurs in the alkyl chains, carbonyl, as well in the aromatic parts of the molecule. Probably, in the degradation process of the pharmaceuticals, halogen species are replaced by oxidative radicals formed at the anode. This is a comparably slow process. Thus, the more halogen atoms are present in the molecule, the more equiv. of *para*-periodate are necessary.[63,64] The first oxidation potentials of the APIs were measured using cyclic voltammetry, which support this hypothesis (Supporting Information, section 15).

Another factor that can cause a delay in the degradation process and increases the amount of necessary production of *para*-periodate is the possible formation of some interaction of *para*-periodate with the organic compounds. Thus, *para*-periodate can form intermediate complexes, which first need to cleave before the actual degradation can start.

As an example, the data analysis of **10** degradation is depicted (Figure 5). Here, we observed that the degradation of this compound starts with a delay, showing an exponential decay only after 10 min. This behavior can indicate a formation of some species as shown in the inset of

Figure 5. Furthermore, the initial delay could be observed in other compounds as **9** and **12**. The degradation analyses of all the other investigated compounds can be found in the Supporting Information (Figures S40–S55).

Re-oxidation to *para*-periodate using iodo compound-containing solutions

Given the broad generality and operational simplicity of this degradation protocol triggered by *para*-periodate as platform oxidizer, we intended to explore the application of the methodology to late-stage diversification of versatile iodine compounds (see Table 3). Once again, different analytical methods as gas chromatography (GC), GC-MS and ^{1}H NMR spectroscopy were used to follow the degradation.

When diiodomethane (**13**) was employed to the re-oxidation within the *para*-periodate process, once being in contact with the anolyte solution the replacement of an iodine atom for a hydroxyl group can be observed, forming iodomethanol (**13b**). Over time, iodomethanol can form hydrate in equilibrium with formaldehyde, which can easily oxidize further under the given conditions.[65] But, when methyl 4-iodobenzoate (**14**) was employed to the re-oxidation *para*-periodate process, we did not observe the degradation process. Instead, we observed the formation of 4-iodobenzoic acid (**14b**). Next, we investigated *ortho*- and *meta*-substituted iodobenzoic acids (**15** and **16**). For those compounds, >99% degradation was achieved using 0.271 and 0.430 kilo equiv. of *para*-periodate, respectively. The 2-iodoaniline (**17**) was tested and could be >90, >95 and >99% degraded using 0.171, 0.222 and 0.341 kilo equiv. of *para*-periodate. Nevertheless, dimethyl 5-iodoisophthalate (**18**) and 2,4,6-triiodophenol (**19**) were >99% degraded in surprisingly small amounts of *para*-periodate: 0.082 and 0.112 kilo equiv., respectively.

As shown in the previous and in this section, organic iodo compounds can be fed into the *para*-periodate generation for upcycling such iodo-containing waste into the platform oxidizer.

Purity of *para*-periodate formed and influence of the pollutants

To clarify that after the re-oxidation process, we have *para*-periodate in high grade, LC-MS analysis was carried out after the degradation process. The results (Supporting Information, section 12) showed that after the process, the *para*-periodate has the same purity as before adding the organic contaminant into the anolyte compartment.

Table 3. Electrochemical degradation of iodine compounds in *para*-periodate platform oxidizer process.[a]

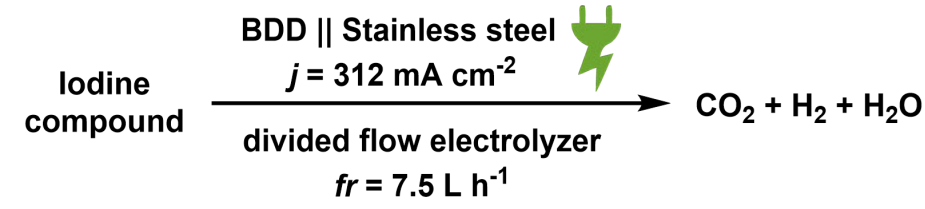

Iodine compound (0.4–2 mM)	Degradation [kilo equiv. of $Na_3H_2IO_6$]		
	>90%	>95%	>99%
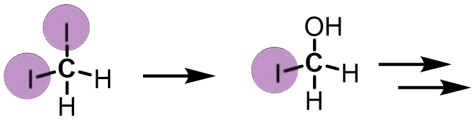 Diiodomethane **(13a)**[b,c,d] Iodomethanol **(13b)**[f]	*direct degradation*		0.25
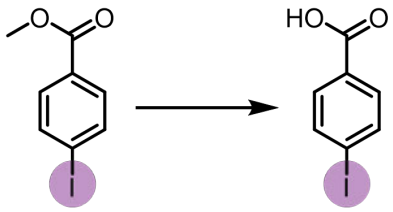 Methyl 4-iodobenzoate **(14a)**[b,c,d] 4-Iodobenzoic acid **(14b)**[d]	*no further degradation of the carboxylic acid.*		
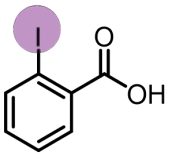 2-Iodobenzoic acid **(15)**[f,g]	0.136	0.176	0.271
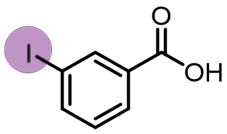 3-Iodobenzoic acid **(16)**[f,d]	0.216	0.281	0.430
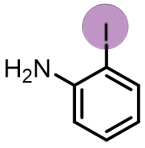 2-Iodoaniline **(17)**[f,h]	0.171	0.222	0.341
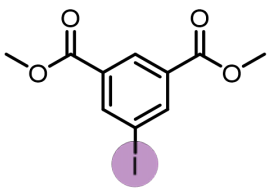 Dimethyl 5-iodoisophthalate **(18)**[f,g]	0.042	0.054	0.082

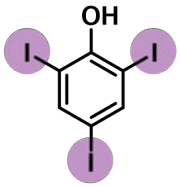 2,4,6-Triiodophenol **(19)**[f,h]	0.065	0.079	0.112

[a] Reaction conditions: Flow electrolyzer (BDD|Nafion membrane|stainless steel, 4x12 cm^2 = 48 cm^2); dye (0.4–2 mM), NaOH (4 M), $Na_3H_2IO_6$ (0.21 M), H_2O (200 mL), 312 mA cm^{-2}, *Q* = 0.5–23*F*, RT. All kilo equiv. of periodate were calculated as showed in section 11 (Supporting Information). [b] Concentration of the 0.4 mM. [c] Degradation without electricity. [d] Determined by ^1H NMR spectroscopy. [f] Concentration of the 2 mM. [g] Determined by GC. [h] Determined by GC-MS.

Thereafter, we could verify that we can electrochemically produce high-grade *para*-periodate using solutions containing organic molecules inside: We performed the following experiments, showed in Scheme 1.

In these cases, LC-MS analyses (Supporting Information) showed that formed $Na_3H_2IO_6$ exhibits the same purity grade than the *para*-periodate formed using Millipore water. The current efficiency (CE) for this experiment was 82% compared with 84% when the reaction was performed using Millipore water.

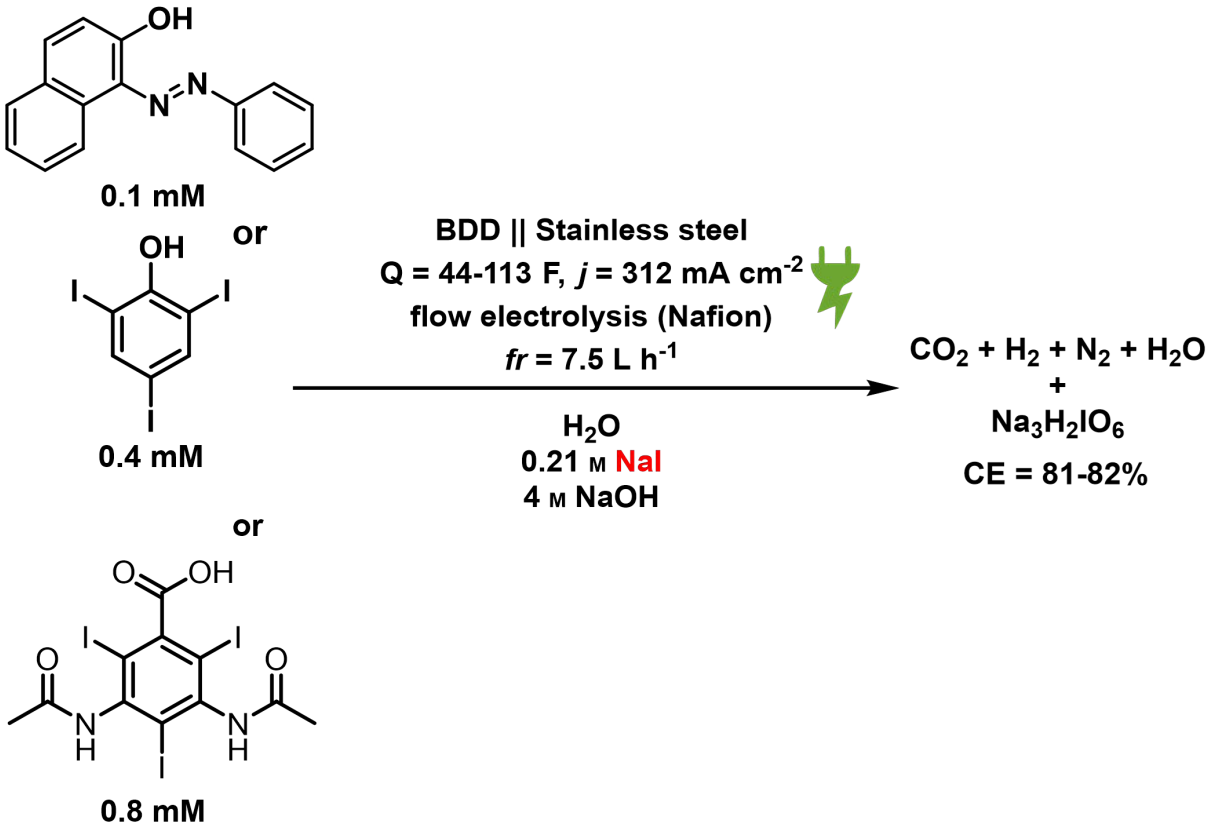

Scheme 1. Synthesis of *para*-periodate using solutions containing sudan I, 2,4,6-triiodophenol and diatrizoate.

Role of hydroxyl radicals in the re-oxidation to *para*-periodate

In the periodate platform oxidizer process, dissolved unconverted iodine species are recycled within the anolyte, while *para*-periodate crystallizes during the process.[66–70] This means having a constant cycle of *para*-periodate production using unconverted iodine species.

Regarding the theorical process analysis, 4 molecules of H_2O and 8 equiv. of hydroxide are consumed for the oxidation of 1 equiv. of iodine. 3 equiv. of H_2O and 6 equiv. of hydroxide are required for the oxidation of iodonium (I^+), which is generated by disproportion of I_2 requiring two additional equiv. of hydroxide for the formation of IO^-. One molecule of H_2O and 2 equiv. of hydroxide are required for the oxidation of iodate to periodate. In all cases, the same number of hydroxide equiv. is generated at the cathode. To form *para*-periodate from *meta*-periodate, only 2 equiv. of hydroxide are consumed. Among the electrochemical methods, anodic oxidation is driven by generated hydroxyl radicals.[55,67]

Equations (1)–(5) illustrate the process of formation and recycling of the *para*-periodate at the anode:

$$I^- + 8OH^- \rightarrow IO_4^- + 4H_2O + 8e^- \quad (1)$$

$$IO^- + 6OH^- \rightarrow IO_4^- + 3H_2O + 6e^- \quad (2)$$

$$IO_3^- + 2OH^- \rightarrow IO_4^- + H_2O + 2e^- \quad (3)$$

$$2H_2O \rightarrow 4H^+ + O_2 + 4e^- \quad (4)$$

$$IO_4^- + 2OH^- \rightarrow H_2IO_6^{3-} \quad (5)$$

CONCLUSION

We studied the influence of organic contaminations onto the regeneration of the electrochemical platform oxidizer *para*-periodate. It turned out that this re-oxidation to *para*-periodate results in a self-cleaning process due to the degradation of these organic compounds. Since the oxidation process at the anode is mediated by hydroxyl radicals, a concurrent mineralization of the organic entities occurs. The robustness of this platform process was demonstrated by contaminants consisting of dyes, active pharmaceutical ingredients, and organo-iodine compounds.

In the concurrent degradation within the periodate process, we could observe a correlation between the electronic nature of the contaminant and the oxidation efficiency: Electron-rich contaminants are degraded first and need fewer equivalents of *para*-periodate being co-produced than less electron-rich compounds. Also, this strategy could degrade iodine compounds. Lastly, the iodo species can be recycled in the system for advanced *para*-periodate production.

To the best of our knowledge, this is the first example re-oxidizing *para*-periodate using contaminated water with organic molecules. This is the prerequisite for using periodate as a

versatile platform oxidizer for sensitive applications, wherein the different streams for recycling may contain various contaminants. These are efficiently mineralized during the anodic process.

EXPERIMENTAL SECTION

The anodic compartment consists of the organic compound (0.1 mM for dyes, else 0.2–3 mM) and iodine sources, $NaIO_3$ or NaI (0.21 M) in caustic soda (32 g NaOH in 200 mL deionized water, 4 M). The cathodic compartment only contains caustic soda (4 M). The BDD anode and stainless-steel cathode, separated with a Nafion membrane, were connected to a galvanostat and both electrolytes were pumped (flow rate = 7.5 L h^{-1}) in cycling mode. A constant feed loop of catholyte to the anodic compartment was installed (flow rate = 0.3 mL min^{-1}). This was necessary to keep the volume of both compartments constant. The co-production of *para*-periodate (j = 313 mA cm^{-2}, Q as stated) was carried out at room temperature and the heat dissipated via a cryostatic bath circulator. Both compartments were stirred (300 rpm). The terminal voltage was (9.5±0.5) V. For a reaction control, samples (2 mL) were taken in regular time steps, filtered over a glass frit to remove the access of *para*-periodate, and the permeate neutralized using $NaHSO_{4(aq)}$ (2 M). Then, the solution was measured using the adequate analysis technique.

ACKNOWLEDGEMENTS

Support by Forschungsinitiative Rheinland-Pfalz in the frame of SusInnoScience is highly appreciated. The financial support by Deutsche Forschungsgemeinschaft in frame of UNODE FOR 2982 (Wa 1276/23-1). Open Access funding enabled and organized by Project DEAL.

CONFLICT OF INTEREST

The authors declare no conflict of interest.

DATA AVAILABILITY STATEMENT

The data that supports the findings of this study are available in the supplementary material of this article.

REFERENCES

(1) G. G. Botte, *Electrochem. Soc. Interface* **2014**, *23*, 49–55.
(2) F. B. Mainier, L. P. C. Monteiro, A. C. M. Rocha, R. J. Mainier, *Am. J. Eng. Res. 2013*, *10*, 24–30.
(3) K. Scott, *Dev. Chem. Eng. Mineral Process.* **2008**, *1*, 71–117.
(4) D. Pollok, S. R. Waldvogel, *Chem. Sci.* **2020**, *11*, 12386–12400.
(5) A. Wiebe, T. Gieshoff, S. Möhle, E. Rodrigo, M. Zirbes, S. R. Waldvogel, *Angew. Chem. Int. Ed.* **2018**, *57*, 5594–5619; *Angew. Chem.* **2018**, *130*, 5694–5721.
(6) S. Möhle, M. Zirbes, E. Rodrigo, T. Gieshoff, A. Wiebe, S. R. Waldvogel, *Angew. Chem. Int. Ed.* **2018**, *57*, 6018–6041; *Angew. Chem.* **2018**, *130*, 6124–6149.
(7) X. Dong, J. L. Roeckl, S. R. Waldvogel, B. Morandi, *Science* **2021**, *371*, 507–514.
(1) G. G. Botte, *Electrochem. Soc. Interface* **2014**, *23*, 49–55.
(2) F. B. Mainier, L. P. C. Monteiro, A. C. M. Rocha, R. J. Mainier, *Am. J. Eng. Res.* **2013**, *10*, 24–30.
(3) K. Scott, *Dev. Chem. Eng. Mineral Process.* **2008**, *1*, 71–117.
(4) D. Pollok, S. R. Waldvogel, *Chem. Sci.* **2020**, *11*, 12386–12400.
(5) A. Wiebe, T. Gieshoff, S. Möhle, E. Rodrigo, M. Zirbes, S. R. Waldvogel, *Angew. Chem. Int. Ed.* **2018**, *57*, 5594–5619; *Angew. Chem.* **2018**, *130*, 5694–5721.
(6) S. Möhle, M. Zirbes, E. Rodrigo, T. Gieshoff, A. Wiebe, S. R. Waldvogel, *Angew. Chem. Int. Ed.* **2018**, *57*, 6018–6041; *Angew. Chem.* **2018**, *130*, 6124–6149.
(7) X. Dong, J. L. Roeckl, S. R. Waldvogel, B. Morandi, *Science* **2021**, *371*, 507–514.
(8) S. P. Blum, T. Karakaya, D. Schollmeyer, A. Klapars, S. R. Waldvogel, *Angew. Chem. Int. Ed.* **2021**, *60*, 5056–5062; *Angew. Chem.* **2021**,*133*, 5114–5120.
(9) S. P. Blum, L. Schäffer, D. Schollmeyer, S. R. Waldvogel, *Chem. Commun.* **2021**, *57*, 4775–4778.
(10) M. Yan, Y. Kawamata, P. S. Baran, *Chem. Rev.* **2017**, *117*, 13230–13319.
(11) M. Dörr, M. M. Hielscher, J. Proppe, S. R. Waldvogel, *ChemElectroChem* **2021**, *8*, 2621–2629.

(12) T. Wirtanen, T. Prenzel, J.-P. Tessonnier, S. R. Waldvogel, *Chem. Rev.* **2021**, *121*, 10241–10270.
(13) J. L. Röckl, D. Pollok, R. Franke, S. R. Waldvogel, *Acc. Chem. Res.* **2020**, *53*, 45–61.
(14) L. Schulz, S. R. Waldvogel, *Synlett* **2019**, *30*, 275–286.
(15) S. R. Waldvogel, S. Lips, M. Selt, B. Riehl, C. J. Kampf, *Chem. Rev.* **2018**, *118*, 6706–6765.
(16) T. H. Meyer, I. Choi, C. Tian, L. Ackermann, *Chem* **2020**, *6*, 2484–2496.
(17) C. M. Kisukuri, V. A. Fernandes, J. A. C. Delgado, A. P. Häring, M. W. Paixão, S. R. Waldvogel, *Chem. Rec.* **2021**, *21*, 2502–2525.
(18) J. Seidler, J. Strugatchi, T. Gärtner, S. R. Waldvogel, *MRS Energy Sustain.* **2020**, DOI:10.1557/mre.2020.42.
(19) D. Pletcher, R. A. Green, R. C. D. Brown, *Chem. Rev.* **2018**, *118*, 4573–4591.
(20) M. B. Plutschack, B. Pieber, K. Gilmore, P. H. Seeberger, *Chem. Rev.* **2017**, *117*, 11796–11893.
(21) S. B. Beil, D. Pollok, S. R. Waldvogel, *Angew. Chem. Int. Ed.* **2021**, *60*, 14750–14759; *Angew. Chem.* **2021**, *133*, 14874–14883.
(22) A. Lipp, M. Selt, D. Ferenc, D. Schollmeyer, S. R. Waldvogel, T. Opatz, *Org. Lett.* **2019**, *21*, 1828–1831.
(23) B. Gleede, M. Selt, R. Franke, S. R. Waldvogel, *Chem. Eur. J.* **2021**, *27*, 8252–8263.
(24) C. Gütz, V. Grimaudo, M. Holtkamp, M. Hartmer, J. Werra, L. Frensemeier, A. Kehl, U. Karst, P. Broekmann, S. R. Waldvogel, *ChemElectroChem* **2018**, *5*, 247–252.
(25) C. Gütz, A. Stenglein, S. R. Waldvogel, *Org. Process Res. Dev.* **2017**, *21*, 771–778.
(26) B. Gleede, M. Selt, C. Gütz, A. Stenglein, S. R. Waldvogel, *Org. Process Res. Dev.* **2020**, 24, 1916–1926.
(27) N. Tanbouza, T. Ollevier, K. Lam, *iScience* **2020**, DOI: 10.1016/j.isci.2020.101720.
(28) T. Noël, Y. Cao, G. Laudadio, *Acc. Chem. Res.* **2019**, *52*, 2858–2869.
(29) R. J.-R. Bednarz, C. Brauer, S. R. Waldvogel, *GIT Lab. J.* **2021**, *10*, 50–52.
(30) H. Li, C. P. Breen, H. Seo, T. F. Jamison, Y.-Q. Fang, M. M. Bio, *Org. Lett.* **2018**, *20*, 1338–1341.
(31) S. A. Snyder, Angew. Chem. Int. Ed. 2017, 56, 8045–8045; *Angew. Chem.* **2017**, *129*, 8157–8157.
(32) A. Sudalai, A. Khenkin, R. Neumann, *Org. Biomol. Chem.* **2015**, *13*, 4374–4394.
(33) P. Liu, B. Pang, S. Dechert, X. C. Zhang, L. B. Andreas, S. Fischer, F. Meyer, K. Zhang, *Angew. Chem. Int. Ed.* **2020**, *59*, 3218–3225; *Angew. Chem.* **2020**, *132*, 3244–3251.
(34) P. V. Chouthaiwale, P. U. Karabal, G. Suryavanshi, A. Sudalai, *Synthesis* **2010**, *22*, 3879–3882.
(35) L. Kraszkiewicz, M. Sosnowski, L. Skulski, *Tetrahedron* **2004**, *60*, 9113–9119.
(36) M. Zhou, R. H. Crabtree, *Chem. Soc. Rev.* **2011**, *40*, 1875–1884.
(37) B. Plietker, *Synthesis* **2005**, *15*, 2453–2472.
(38) K. Satyanarayana, K. Srinivas, V. Himabindu, G. M. Reddy, *Org. Process Res. Dev.* **2007**, *11*, 842–845.
(39) X. Wang, Y. Zeng, L. Sheng, P. Larson, X. Liu, X. Zou, S. Wang, K. Guo, C. Ma, G. Zhang, H. Cui, D. M. Ferguson, Y. Li, J. Zhang, C. C. Aldrich, *J. Med. Chem.* **2019**, *62*, 2305–2332.

(40) X. Gao, S. K. Woo, M. J. Krische, *J. Am. Chem. Soc.* **2013**, *135*, 4223–4226.
(41) G. Brauer, ed. *Handbook of preparative inorganic chemistry*, V2., Vol. 2. Elsevier, Amsterdam, **2012**.
(42) P. Galletti, G. Martelli, G. Prandini, C. Colucci, D. Giacomini, *RSC Adv.* **2018**, *8*, 9723–9730.
(43) H. Liimatainen, J. Sirviö, H. Pajari, O. Hormi, J. Niinimäki, *J. Wood Chem. Technol.* **2013**, *33*, 258–266.
(44) D. Kong, P. Wan, Y. Chen, Z. U. H. Khan, Y. Tang, *Int. J. Electrochem. Sci.* **2015**, *10*, 6422–6432.
(45) B. N. Grgur, M. M. Gvozdenović, J. S. Stevanović, B. Z. Jugović, Lj. T. Trišović, *Chem. Eng. J.* **2006**, *124*, 47–54.
(46) S. R. Waldvogel, B. Janza, *Angew. Chem. Int. Ed.* **2014**, *53*, 7122–7123; *Angew. Chem.* **2014**, *126*, 7248–7249.
(47) Y. Xia, Q. Dai, J. Chen, *J. Electroanal. Chem.* **2015**, *744*, 117–125.
(48) L. J. J. Janssen, M. H. A. Blijlevens, *Electrochim. Acta* **2003**, *48*, 3959–3964.
(49) Y. Aiya, S. Fujii, K. Sugino, K. Shirai, *J. Electrochem. Soc.* **1962**, *109*, 419–424.
(50) J. V. Macpherson, *Phys. Chem. Chem. Phys.* **2015**, *17*, 2935–2949.
(51) N. Yang, S. Yu, J. V. Macpherson, Y. Einaga, H. Zhao, G. Zhao, G. M. Swain, X. Jiang, *Chem. Soc. Rev.* **2019**, *48*, 157–204.
(52) S. R. Waldvogel, S. Mentizi, A. Kirste, *Boron-Doped Diamond Electrodes for Electroorganic Chemistry. In: Heinrich, M., Gansäuer, A. (Eds) Radicals in Synthesis III*., Springer, Heidelberg, **2011**.
(53) S. Lips, S. R. Waldvogel, *ChemElectroChem* **2019**, *6*, 1649–1660.
(54) S. O.Ganiyu, E. V. Santos, C. A.Martínez-Huitle, S. R. Waldvogel, *Curr. Opin. Electrochem.* **2022**, DOI: 10.1016/j.coelec.2021.100903.
(55) S. Arndt, D. Weis, K. Donsbach, S. R. Waldvogel, *Angew. Chem. Int. Ed.* **2020**, *59*, 8036–8041; *Angew. Chem.* **2020**, *132*, 8112–8118.
(56) J. Klein, K. Alt, S. R. Waldvogel, *Adv. Sustain. Syst.* **2022**, DOI: 10.1002/adsu.202270010.
(57) S. Arndt, B. Grill, H. Schwab, G. Steinkellner, U. Pogorevčnik, D. Weis, A. M. Nauth, K. Gruber, T. Opatz, K. Donsbach, S. R. Waldvogel, M. Winkler, *Green Chem.* **2021**, *23*, 388–395.
(58) M. Klein, S. R. Waldvogel, *Angew. Chem. Int. Ed.* **2021**, *60*, 23197–23201; *Angew. Chem.* **2021**, *133*, 23382–23387.
(59) Z. Wang, A. Berbille, Y. Feng, S. Li, L. Zhu, W. Tang, Z. L. Wang, *Nat. Commun.* **2022**, DOI: 10.1038/s41467-021-27789-1.
(60) A. S. Mramba, P. P. Ndibewu, L. L. Sibali, K. Makgopa, *Electroanalysis* **2020**, *32*, 2615–2634.
(61) Y. Jiang, H. Zhao, J. Liang, L. Yue, T. Li, Y. Luo, Q. Liu, S. Lu, A. M. Asiri, Z. Gong, X. Sun, *Electrochem. commun.* **2021**, *123*, 106912–106932.
(62) A. Nowak, G. Pacek, A. Mrozik, *Rev Environ. Sci. Biotechnol.* **2020**, *19*, 337–354.
(63) G. Korshin, M. Yan, *Environ. Eng. Res.* **2018**, *23*, 345–353.
(64) E. Hapeshi, A. Lambrianides, P. Koutsoftas, E. Kastanos, C. Michael, D. Fatta-Kassinos, *Environ. Sci. Pollut. Res.* **2013**, *20*, 3592–3606.

(65) J. Clayden, N. Greeves, S. G. Warren, *Organic Chemistry*, Oxford Universiy Press, Oxford, **2012**.
(66) Y.-C. Lee, M.-J. Chen, C.-P. Huang, J. Kuo, S.-L. Lo, *Ultrason. Sonochem.* **2016**, *31*, 499–505.
(67) L.-H. Chia, X. Tang, L. K. Weavers, *Environ. Sci. Technol.* **2004**, *38*, 6875–6880.
(68) M. P. Shah, ed. *Removal of Refractory Pollutants from Wastewater Treatment Plants*, CRC Press, Boca Raton, **2021**.
(69) X. Li, X. Liu, C. Lin, C. Qi, H. Zhang, J. Ma, *Chemosphere* **2017**, *181*, 609–618.
(70) X. Yu, M. Zhou, Y. Hu, K. G. Serrano, F. Yu, *Environ. Sci. Pollut. Res.* **2014**, *21*, 8417–8431.

ENTRY FOR THE TABLE OF CONTENTS

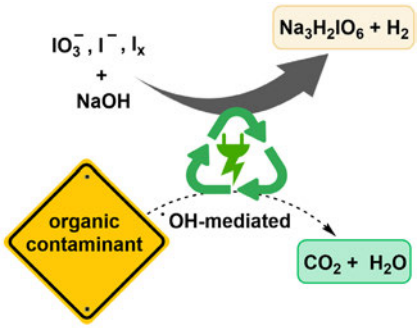

The platform oxidizer periodate can be electrochemically recycled in a self-cleaning process. To demonstrate the versatile nature of the strategy, different dyes, pharmaceutically active ingredients, and iodine compounds were added to the process. The *para*-periodate could be recovered with a high purity compared to classically synthesized *para*-periodate. The organic impurities do not hamper the reoxidation to the *para*-periodate. Moreover, they can be totally mineralized during the process, creating the basis for a robust platform process.

III. Synopsis

Overall, in this dissertation two important electrochemical processes were investigated and optimized: the **production of biogenic adipic acid derivatives** and the **recycling of degraded *para*-periodate**. For the production of adipic acid derivatives, the focus has been on green electrification of the chemical synthesis, including the significant reduction of greenhouse gases and waste production compared to the conventional NO process, as well as choosing substrates which can originate from biomass, like lignin. With these prerequisites, the electro-organic oxidations of two adipic acid derivatives were investigated: from 4-ethylcyclohexanol to 3-ethyladipic acid and from 4-propylcyclohexanol to 3-propyladipic acid. Such adipic acid derivatives can be utilized to tailor the properties of the resulting polyamides or polyesters containing these monomers.

As a first step, the electrooxidation of 4-ethylcyclohexanol to **3-ethyladipic acid** was optimized and scaled up. The newly designed 108 cm^2 flow electrolyzer was validated hereby and is now commercially available. To maximize the yield, the two main approaches were an improved nickel foam activation, which is fundamental for the electrooxidation, and a *DoE* screening, to find the other most important parameters. The invented cleaning and **activation protocol for the nickel foam** allows for more than 1000 hours of operation by repeated reactivation of a single set of electrodes. No significant damage of the foam or relevant drop in yield was observed thereby. The novel activation protocol was filed as a patent in cooperation with industry partners. For the further yield maximization, the *DoE* screening revealed that the flow rate and the substrate concentration were the two most important parameters. The optimized parameter set gained a **qNMR yield of 59%** (38% isolated).

For the further scale-up of the reaction a stacked electrode reactor was required. The applicable current densities for the synthesis of dicarboxylic acids are limited to circumvent Kolbe electrolysis or Hofer-Moest oxidation. Therefore, the only possibility to significantly increase the space-time yields is a significant increase in the electrode surface area. Thus, we designed a modular electrode stack, utilizing a decalitre **electrochemical continuously-stirred tank reactor** (e-CSTR). With an anodic geometric surface area in contact with the electrolyte of 1225 cm^2, mol-scale transformations (**productivity: >35 mmol/h**) to hectogram product recovery were possible. The activation reactions with the used electrode stack showed optically high homogeneity over the complete immersed surface area and the cathodes showed well-distributed generation of hydrogen bubble formation. Both indicate that larger electrode stacks seem chemically not limited.

In this reactor, the electrooxidation of 4-propylcyclohexanol to **3-propyladipic acid** was optimized. Again, a *DoE* parameter screening was performed, demonstrating the importance of mixing up to an emulsification of the naturally biphasic system. A follow-up reaction control experiment demonstrated that the substrate concentration declined over time, leading to a diminished productivity. This was resolved by introducing a **feeding of the substrate**, which increased the yield significantly to a **qNMR yield of 48%** (31% isolated) on a 10 L scale. The

analysis was performed using either ^{13}C inverse-gated NMR spectroscopy or ion chromatography with a Metrosep Organic Acids column. The kinetic studies and the observed product and by-product selectivites allowed for developing a mechanistic proposal for the formation of by-products.

Isolation of the products was best performed via fractionated vacuum distillation. This is necessary, because by-products of the adipic acid derivate synthesis may be disadvantageous for polycondensation reactions. Foremost glutaric and succinic acids, carrying a C-5 or C-4 backbone, respectively, tend to cyclize under imidization.[106] This leads to low molecular weights of resulting polyamides.

Direct coupling experiments between the e-CSTR and photovoltaic panels allowed the investigation of the impact of in-time current density fluctuations. Remarkably, the reaction with fluctuating current from the photovoltaic panels **yielded very similar results** for the 3-propyladipic acid production compared to steady-state electricity supply. 1.25 mA/cm^2 should be supplied as a minimum current density to preserve the active anode surface and keep the reaction progressive. For lower current density supplies, all mixing and pumping actions are stopped, whereby the active surface fades. Once enough electricity for the minimum supply is available again, the reaction is resumed. Remarkably, when resuming the reaction, the active anode surface is quickly regained without manual reactivation. Such extreme fluctuations tested here only using photovoltaic supply indicate that typical, more modest, renewable energy fluctuations in a future electricity grid seem easily applicable to electro-oxidations from various alcohols via ketones or aldehydes up to carboxylic acids. On a technical scale, such direct couplings between fluctuating renewable energy sources and electro-synthetic processes could significantly stabilize the grid.

For the electrochemical synthesis of ***para*-periodate**, the goal was to regain *para*-periodate from aqueous waste streams with a mixture of degraded *para*-periodate and contaminants. This was achieved for varies organic contaminants, like dyes or API residues, as well as iodine-containing organic compounds. Such **contaminants are mineralized** in the process of reoxidation. Thereby, electron-rich compounds degrade faster than electron-deficient ones. Exemplarily, sudan I was **>99% mineralized using 5.0 kilo equiv. of *para*-periodate**. In waste streams with iodine-containing organic compounds, this iodine can be oxidized to periodate while decomposing the, often toxic or environmentally harmful, residue.

With the electrification results for the semi-technical oxidation of secondary alcohols and ketones as well as the demonstration of a robust recycle process for *para*-periodate, obtained and advanced in this thesis, another big step is done towards replacing fossil-based and very emissive conventional production with such electrochemical processes.

IV. Outlook

As the chemical industry was responsible for 6% of the total global greenhouse gas emissions in 2020,[107] and still is a predominant power consumer in the primary energy sector, transformation to climate neutrality is key in the next years. In particular the adipic acid synthesis still causes approximately 300 Mt of CO_2 equivalents to be produced, annually. Green electrification of this process would fully diminish this greenhouse gas production during operation. For the annually produced 3 Mt of adipic acid, a full replacement of the conventional process by electrosynthesis, assuming the productivity obtained in this work (35 mmol/h at 1225 cm^2 Ni foam surface), would require a total geometrical nickel surface area of 8.2 km^2. The required surface area can be greatly diminished if electrode stacks are used. For an electrode thickness of 5 mm, approximately 9 kt Ni foam are necessary for the annual production. Compared to the required amount of nitric acid as conventional oxidizer, the nickel mass is a factor 300 less.[108]

The **amount of nickel**, required for producing the global demand, should still be diminished in the future. Two promising pathways are **further yield increase** (>58%) and setup alteration with **thinner electrodes**, whereby an optimum with respect to the total foam electrode surface is to be found. Tackling yield improvement with process optimization is particularly promising using modular cell designs of flow electrolyzers and electrochemical continuously-stirred tank reactors because they provide the possibility of in-situ **product adsorption at anion exchange resins** in continuous reaction mode, even on semi-technical scales. Our ChemCatChem publication points out particularly high selectivity at an early reaction state, which suggests that an in-situ product separation would be worth investigating. A possible process flow sheet is depicted in Figure 12.

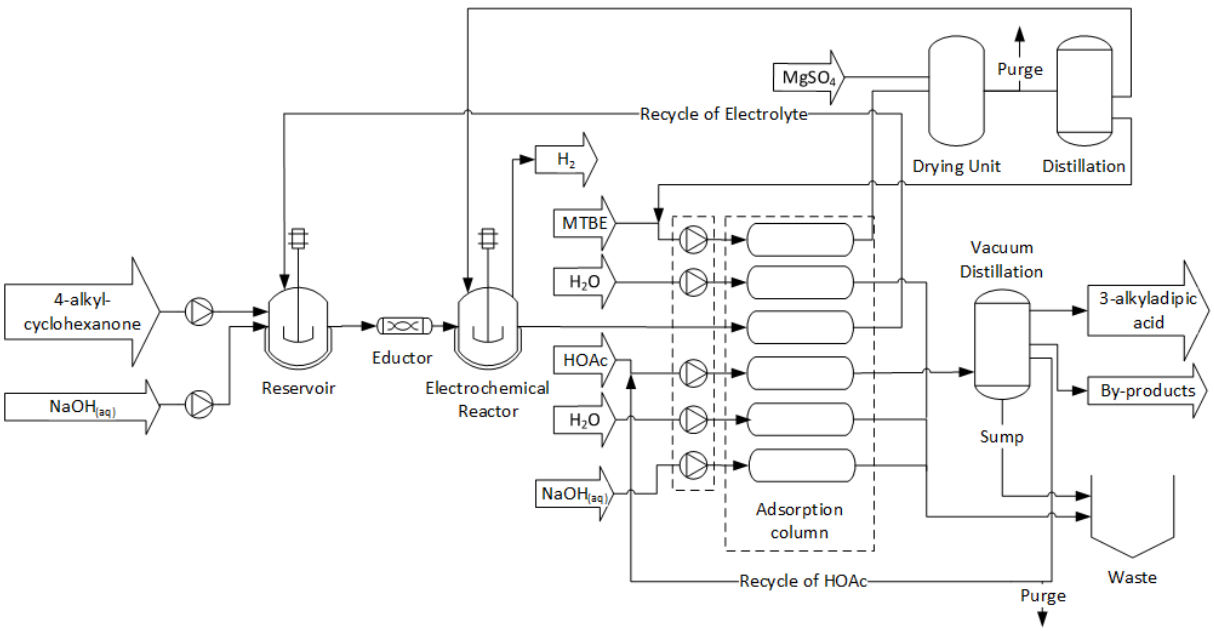

Figure 12. Process flow sheet for an energetically feasible electrosynthesis of 4-alkylcyclohexanone or -cyclohexanol with subsequent adsorption-desorption of the

product. The flow sheet was designed in the software Visio by Microsoft in collaboration with Theresa Rücker.

This proposal for yield optimization bases on two adsorption columns for replacement and follow a desorption of the dicarboxylic acids as follows: Via MTBE purging, the remaining **substrate** which has wettened column wall and resin particles is separated first and can be **recycled** via solvent distillation. Next, the basic pH is neutralized, flushing with water. With glacial acetic acid the system is acidified, desorbing the product. Afterward, the system is first neutralized with water to prevent acetic acid to adsorb to the resin. For final regeneration, less than one batch volume suffices to re-establish the reaction mixtures' pH.

Automation of this process would also be very promising, as it mainly requires the basic functions like pumps, different liquids and multi-way valves, which have already been in use by Hielscher et al.[109] (Vacuum) distillation columns can be included, as well as an eductor piece inserted.

The process described above may also be tested for **all kinds of alcohols, ketones and aldehydes** which can be oxidized under electrochemical, undivided conditions.

In terms of **thinner electrodes**, an electrode stack inside a **flow electrolyzer** would be promising. Since the electrode edges would experience less shear forces within a flow electrolyzer, as no powerful agitator is present and the edges would be stabilized by the case, thinner electrodes may not hinder a long lifetime.

What would also be worth testing in more detail is the **electrode spacing**. 3 mm seem promising, but if the spacers are modified to 2 mm or 4 mm, this may affect the yield as well. Thereby, the effect of the **size of formed hydrogen bubbles** at the cathode surface can be investigated as a function of the product yield.

Another relevant aspect to possibly increase the yield is to adapt the active electrode surface layer. Li et al. modified the **Ni hydroxide surface layer** using sodium dodecyl sulfonate, reporting an adipic acid yield of 84% and about 0.15 V lower voltage for the electrooxidation.[110] They reported major challenges with solubility. Since we tackled this issue, a **combination of our emulsion with an electrode modification** like the one suggested by Li et al. could increase the yield of adipic acid and its derivatives, carrying additional carbon atoms. However, also the mechanical robustness for long-term use needs to be investigated further.

With respect to active anodes, only nickel as a **metal oxide hydroxide** was tested for the 3-alkyladipic acid synthesis, here. Possible metal combinations including **nickel, iron or cobalt**, since they are chemically similar, may improve the yield even further.[75]

Especially modified adipic acid backbones are of high interest for **polyamides**, since they can lead to **elevated glass-transition temperatures** compared to Nylon-6,6 or

polycaprolactame.[111,112] Those are highly desirable for various applications, where light-weight polymers instead of metal alloys are desired.

For *para*-periodate as a powerful platform oxidizer, a very important next step would be to **separate the reacted periodate** from the product solution as iodate or lower valent iodine species. Then, in a single electro-oxidation step, *para*-periodate could be recovered with the process demonstrated in this thesis. Additionally, a **freshly produced *para*-periodate** may have similar features than a freshly produced peroxodicarbonate. Its enhanced oxidative strength may be strong enough to merge several oxidation steps in a one-pot-reaction. This would be worth to investigate further – for example for the **oxidation of biogenic terpenes to the corresponding dicarboxylic acids**. In contrast to the electrooxidation described in this work which started from lignin-derived alkylated cyclohexanols, a double bond is the starting point in **terpenes** and no oxygen-containing substrate is required. If a milder oxidation of the terpenes is chosen in the first place, a direct electrochemical oxidation of the corresponding terpene-derived secondary alcohol or ketone can be performed.

The **purity of hydrogen** produced in all reactions may be investigated in the future, as the global production would be on kt scale.

To check which other factors are the most central ones which need to be optimized, a **lifecycle assessment** should be performed. It determines the costs of a product over its whole lifecycle, which reveals the most important weak points of the process. For the continuous electrified production process of 3-alkyladipic acid or *para*-periodate such a lifecycle assessment would be a very important next step to establish the production in the chemical industry.

Furthermore, it should be noted that green electrification of the chemical industry requires huge amounts of inexpensive renewable energy. Since trends for the CAPEX costs for renewable energies – foremost solar power – are remarkably descending, keeping insignificantly low OPEX costs, 100% renewable energies are approachable. Here, **larger scale coupling experiments** with solar or wind electricity supply are desirable. Modelling their electricity production and using this as the input for the coupling experiments is a feasible and adaptable approach on lab scale.

When considering that in the future, most likely, predominantly fluctuating renewable energies will be in the grid, many more open research questions **on enhanced grid stability** will become important. The chemical industry shows huge potentials to contribute to grid stability by **coupling electrochemical reactions to the momentary electricity supply**. Foremost, attention should be paid to those electrochemical reactions for which very high yields are achieved for a wide range of current densities. Depending on the oxidation process, the limits for electricity fluctuations may have to be individually determined. I consider it to be very likely that financial compensation will soon be paid for such impactful large-scale grid stability processes. This would enhance the attractiveness of an electrification of technical organic productions. Therefore, a large new research field in chemistry may have just begun.

V. Publications and supervised students

PUBLICATIONS

1. Roland J.-R. Bednarz, *Groß angelegte elektrochemische Produktion von Adipinsäure-Derivaten: Elektrifizierung der technischen organischen Synthese*, *et – Energiewirtschaftliche Tagesfragen* **2024**, *4*, 71–73.
2. Roland J. R. Bednarz, Christopher Brauer, Siegfried R. Waldvogel, *Out of its infancy – Modular flow cell offers enormous scaling potential for electrosynthesis*, *GIT Laboratory Journal* **2021**, online.
3. Roland J.-R. Bednarz, Annika S. Gold, Jasmin Hammes, Denis F. Rohrmann, Silvio Natalello, Moritz Mann, Frank Weinelt, Christopher Brauer, Siegfried R. Waldvogel, *Scaled oxidative flow electrosynthesis of 3-alkyladipic acids from 4-alkylcyclohexanols*, *Org. Process Res. Dev.* **2024**, *28*, 5, 1529–1538.
4. Roland J.-R. Bednarz,[‡] Pilar Jiménez-Meneses,[‡] Annika S. Gold, Damián Monllor-Satoca, Andreas Stenglein, Roberto Gómez, Siegfried R. Waldvogel, *Sustainably scaled electrochemical synthesis of 3-propyladipic acid in line with fluctuating grid supply*, *ChemCatChem* **2023**, *15*, e202300606.
5. Pilar Jiménez-Meneses,[‡] Roland J.-R. Bednarz,[‡] Vincente Montiel, Roberto Gómez, Siegfried R. Waldvogel, *Sun-powered electrosynthesis of 3-propyladipic acid: the direct coupling of PV panel and electrochemical reactor*, *Renew. Energy* **2024**, submitted.
6. Camila M. Kisukuri,[‡] Roland J.-R. Bednarz,[‡] Christopher Kampf, Sebastian Arndt, Siegfried R. Waldvogel, *Robust and self-cleaning electrochemical production of periodate*, *ChemSusChem* **2022**, *15* (16), e202200874.
7. Siegfried R. Waldvogel, Roland J.-R. Bednarz, Frank Weinelt, Ernst Roemer, *Herstellung einer stabilen aktivierten Nickeloxidhydroxid-Schaum-Elektrode*, **2023**, invention report, EP 23171120.1.
8. Roland J.-R. Bednarz, Siegfried R. Waldvogel, Ernst Roemer, Frank Weinelt, *Elektrochemisches Hochdurchsatz-Oxidationsverfahren*, **2023**, invention report, EP 23171123.5.
9. Siegfried R. Waldvogel, Silja Hofmann, Roland J.-R. Bednarz, Adina T. Muff, Frank Weinelt, Franz-Erich Baumann, *Dicarbonsäuren aus Terpenen*, **2023**, 2023E00237 DE.

[‡] These authors contributed equally to this work.

SUPERVISED STUDENTS

1. [redacted], Optimierung der anodischen 4-Propylcyclohexanol-Oxidation und effiziente Extraktion von 3-Propyladipinsäure, Bachelor Thesis (October 2021 – January 2022), scientific assistant (January 2022 – April 2022, April 2022 – July 2022)

2. [redacted], Nebenprodukt-Charakterisierung der elektrochemischen, Lignin-abgeleiteten 4-Alkylcyclohexanol-Oxidation sowie Optimierung der Produktfällung, Bachelor Thesis (June 2022 – September 2022)

3. [redacted], scientific assistant (May 2022 – August 2022)

List of abbreviations

A	geometrical electrode area (typically anodic surface area)
AC	alternating current
API	active pharmaceutical ingredient
BDD	boron-doped diamond
c	concentration [mol L^{-1}] (mol L^{-1} = M)
C	electric capacity [*F*] (1*F* = 1 C V^{-1} = 1 As V^{-1})
CSTR	continuously-stirred tank reactor
DC	direct current
DMSO-d_6	hexadeuterodimethyl sulfoxide
DoE	*Design of Experiments*
e-CSTR	electrochemical continuously-stirred tank reactor
F	Faraday constant: 96485.332 C mol^{-1}
HER	hydrogen evolution reaction
HFIP	1,1,1,3,3,3-hexafluoropropan-2-ol
I	electric current [A]
j	geometrical current density [mA cm^{-2}]
KA oil	ketone alcohol oil (referring to cyclohexanone and cyclohexanol)
n	amount of substance [mol]
Ni(O)OH	nickel oxide hydroxide
NMR	nuclear magnetic resonance spectroscopy
m	mass [g]
OER	oxygen evolution reaction
PFR	plug flow reactor
PV	photovoltaic
Q	applied charge [C] (*Q* = *n* * *z* * *F*)
Φ	flow rate [mL min^{-1}]
Q	applied charge [*F*]
SCE	saturated calomel electrode
T	temperature [°C]
U	voltage [V]
V	total reaction volume
vol%	volume %
wt%	weight %
z	electrons transferred per unit reaction

References

(1) Seidler, J.; Strugatchi, J.; Gärtner, T.; Waldvogel, S. R. Does Electrifying Organic Synthesis Pay off? The Energy Efficiency of Electro-Organic Conversions. *MRS Energy & Sustainability* **2020**, *7* (1), 42. https://doi.org/10.1557/mre.2020.42.

(2) Vollmer, D.; Bednarz, R. J.-R.; Seiffert, S.; Bednarz, B. The Benefits of Nobel Prizes. *Nat. Phys.* **2022**, *18* (12), 1383–1384. https://doi.org/10.1038/s41567-022-01830-6.

(3) Biber, A.; Felder, M.; Wieland, C.; Spliethoff, H. Negative Price Spiral Caused by Renewables? Electricity Price Prediction on the German Market for 2030. *The Electricity Journal* **2022**, *35* (8), 107188. https://doi.org/10.1016/j.tej.2022.107188.

(4) Biddinger, E. J.; Modestino, M. A. Electro-Organic Syntheses for Green Chemical Manufacturing. *Electrochem. Soc. Interface* **2020**, *29* (3), 43–47. https://doi.org/10.1149/2.F06203IF.

(5) Bednarz, R. J.-R.; Brauer, C.; Waldvogel, S. R. Out of Its Infancy – Modular Flow Cell Offers Enormous Scaling Potential for Electrosynthesis. *GIT Laboratory Journal* **2021**, online.

(6) Pletcher, D.; Walsh, F. C. *Industrial Electrochemistry*, 2nd ed.; Springer Science & Business Media, 2012.

(7) Pollok, D.; Waldvogel, S. R. Electro-Organic Synthesis – a 21st Century Technique. *Chem. Sci.* **2020**, *11* (46), 12386–12400. https://doi.org/10.1039/D0SC01848A.

(8) Rios, J.; Lebeau, J.; Yang, T.; Li, S.; Lynch, M. D. A Critical Review on the Progress and Challenges to a More Sustainable, Cost Competitive Synthesis of Adipic Acid. *Green Chem.* **2021**, *23* (9), 3172–3190. https://doi.org/10.1039/D1GC00638J.

(9) Mainhardt, H.; Kurger, D. N_2O Emissions from Adipic Acid and Nitric Acid Production. *IPCC Good Practice Guidance and Uncertainty Management in National Greenhouse Gas Inventories* **2001**, 183–195.

(10) Ehhalt, D.; Prather, M.; Dentener, F.; Derwent, R.; Dlugokencky, E.; Holland, E.; Isaksen, I.; Katima, J.; Kirchhoff, V.; Matson, P.; Midgley, P.; Wang, M.; Berntsen, T.; Bey, I.; Brasseur, G.; Buja, L.; Collins, W. J.; Daniel, J.; DeMore, W. B.; Derek, N.; Dickerson, R.; Etheridge, D.; Feichter, J.; Fraser, P.; Friedl, R.; Fuglestvedt, J.; Gauss, M.; Grenfell, L.; Grübler, A.; Harris, N.; Hauglustaine, D.; Horowitz, L.; Jackman, C.; Jacob, D.; Jaeglé, L.; Jain, A.; Kanakidou, M.; Karlsdottir, S.; Ko, M.; Kurylo, M.; Lawrence, M.; Logan, J. A.; Manning, M.; Mauzerall, D.; McConnell, J.; Mickley, L.; Montzka, S.; Müller, J. F.; Olivier, J.; Pickering, K.; Pitari, G.; Roelofs, G. J.; Rogers, H.; Rognerud, B.; Smith, S.; Solomon, S.; Staehelin, J.; Steele, P.; Stevenson, D.; Sundet, J.; Thompson, A.; van Weele, M.; Joos, F.; McFarland, M. Atmospheric Chemistry and Greenhouse Gases. *IPCC* **2001**, 241–287.

(11) Shimizu, A.; Tanaka, K.; Fujimori, M. Abatement Technologies for N2O Emissions in the Adipic Acid Industry. *Chemosphere - Global Change Science* **2000**, *2* (3–4), 425–434. https://doi.org/10.1016/S1465-9972(00)00024-6.

(12) Umweltbundesamt. Emission der von der UN-Klimarahmenkonvention abgedeckten Treibhausgase, 2023. https://www.umweltbundesamt.de/daten/umweltindikatoren/indikator-emission-von-treibhausgasen.

(13) Bednarz, R. J.-R.; Jiménez-Meneses, P.; Gold, A. S.; Monllor-Satoca, D.; Stenglein, A.; Gómez, R.; Waldvogel, S. R. Sustainably Scaled Electrochemical Synthesis of 3-Propyladipic Acid in Line with Fluctuating Grid Supply. *ChemCatChem* **2023**, *15* (17), e202300606. https://doi.org/10.1002/cctc.202300606.

(14) Schutyser, W.; Van den Bossche, G.; Raaffels, A.; Van den Bosch, S.; Koelewijn, S.-F.; Renders, T.; Sels, B. F. Selective Conversion of Lignin-Derivable 4-Alkylguaiacols to 4-Alkylcyclohexanols over Noble and Non-Noble-Metal Catalysts. *ACS Sustainable Chem. Eng.* **2016**, *4* (10), 5336–5346. https://doi.org/10.1021/acssuschemeng.6b01580.

(15) Rauen, A. L.; Weinelt, F.; Waldvogel, S. R. Sustainable Electroorganic Synthesis of Lignin-Derived Dicarboxylic Acids. *Green Chem.* **2020**, *22* (18), 5956–5960. https://doi.org/10.1039/D0GC02210A.

(16) Schäfer, H.-J. Oxidation of Organic Compounds at the Nickel Hydroxide Electrode. *Top. Curr. Chem.* **1987**, *142*, 101–129. https://doi.org/10.1007/3-540-17871-6_13.

(17) Jiménez-Meneses, P.; Bednarz, R. J.-R.; Montiel, V.; Waldvogel, S. R.; Gómez, R. Sun-Powered Electrosynthesis of 3-Propyladipic Acid: The Direct Coupling of PV Panel and Electrochemical Reactor. *Renewable Energy (in submission)*.

(18) Bednarz, R. J.-R.; Gold, A. S.; Hammes, J.; Rohrmann, D. F.; Natalello, S.; Mann, M.; Weinelt, F.; Brauer, C.; Waldvogel, S. R. Scaled Oxidative Flow Electrosynthesis of 3-Alkyladipic Acids from 4-Alkylcyclohexanols. *Org. Process Res. Dev.* **2024**, *28* (5), 1529–1538. https://doi.org/10.1021/acs.oprd.3c00146.

(19) Kumar, K. S.; Kavitha, S.; Parameswari, K.; Sakunthala, A.; Sathishkumar, P. Environmental Occurrence, Toxicity and Remediation of Perchlorate – A Review. *Chemosphere* **2023**, *311*, 137017. https://doi.org/10.1016/j.chemosphere.2022.137017.

(20) Siahrostami, S.; Villegas, S. J.; Bagherzadeh Mostaghimi, A. H.; Back, S.; Farimani, A. B.; Wang, H.; Persson, K. A.; Montoya, J. A Review on Challenges and Successes in Atomic-Scale Design of Catalysts for Electrochemical Synthesis of Hydrogen Peroxide. *ACS Catal.* **2020**, *10* (14), 7495–7511. https://doi.org/10.1021/acscatal.0c01641.
(21) Wen, Y.; Zhang, T.; Wang, J.; Pan, Z.; Wang, T.; Yamashita, H.; Qian, X.; Zhao, Y. Electrochemical Reactors for Continuous Decentralized H_2O_2 Production. *Angewandte Chemie* **2022**, *134* (35), e202205972. https://doi.org/10.1002/ange.202205972.
(22) Rücker, T.; Schupp, N.; Sprang, F.; Horsten, T.; Wittgens, B.; Waldvogel, S. R. Peroxodicarbonate – a Renaissance of an Electrochemically Generated Green Oxidizer. *Chem. Commun.* **2024**, 10.1039.D4CC02501F. https://doi.org/10.1039/D4CC02501F.
(23) Ziogas, A.; Belda, J.; Kost, H.-J.; Magomajew, J.; Sperling, R. A.; Wernig, P. Peroxodicarbonate: Electrosynthesis and First Directions to Green Industrial Applications. *Current Research in Green and Sustainable Chemistry* **2022**, *5*, 100341. https://doi.org/10.1016/j.crgsc.2022.100341.
(24) Sklarz, B. Organic Chemistry of Periodates. *Quarterly Reviews, Chemical Society* **1967**, *21* (1), 3–28.
(25) Arndt, S.; Weis, D.; Donsbach, K.; Waldvogel, S. R. The "Green" Electrochemical Synthesis of Periodate. *Angew. Chem. Int. Ed.* **2020**, *59* (21), 8036–8041. https://doi.org/10.1002/anie.202002717. Arndt, S.; Weis, D.; Donsbach, K.; Waldvogel, S. R. Die "grüne" elektrochemische Synthese von Periodat. *Angew. Chem.* **2020**, *132* (21), 8112–8118. https://doi.org/10.1002/ange.202002717.
(26) Arndt, S.; Rücker, R.; Stenglein, A.; Waldvogel, S. R. Reactor Design for the Direct Electrosynthesis of Periodate. *Org. Process Res. Dev.* **2022**, *26* (8), 2447–2455. https://doi.org/10.1021/acs.oprd.2c00116.
(27) Kisukuri, C. M.; Bednarz, R. J.; Kampf, C.; Arndt, S.; Waldvogel, S. R. Robust and Self-Cleaning Electrochemical Production of Periodate. *ChemSusChem* **2022**, *15* (16). https://doi.org/10.1002/cssc.202200874.
(28) Leech, M. C.; Lam, K. A Practical Guide to Electrosynthesis. *Nat Rev Chem* **2022**, *6* (4), 275–286. https://doi.org/10.1038/s41570-022-00372-y.
(29) Frontana-Uribe, B. A.; Little, R. D.; Ibanez, J. G.; Palma, A.; Vasquez-Medrano, R. Organic Electrosynthesis: A Promising Green Methodology in Organic Chemistry. *Green Chem.* **2010**, *12* (12), 2099. https://doi.org/10.1039/c0gc00382d.
(30) Cembellín, S.; Batanero, B. Organic Electrosynthesis Towards Sustainability: Fundamentals and Greener Methodologies. *The Chemical Record* **2021**, *21* (9), 2453–2471. https://doi.org/10.1002/tcr.202100128.
(31) Schäfer, H. J. Contributions of Organic Electrosynthesis to Green Chemistry. *Comptes Rendus. Chimie* **2011**, *14* (7–8), 745–765. https://doi.org/10.1016/j.crci.2011.01.002.
(32) Pletcher, D.; Walsh, F. C. *Industrial Electrochemistry*; Springer Netherlands: Dordrecht, 1993. https://doi.org/10.1007/978-94-011-2154-5.
(33) Yuan, Y.; Lei, A. Is Electrosynthesis Always Green and Advantageous Compared to Traditional Methods? *Nat Commun* **2020**, *11* (1), 802. https://doi.org/10.1038/s41467-020-14322-z.
(34) Heard, D. M.; Lennox, A. J. J. Electrode Materials in Modern Organic Electrochemistry. *Angew Chem Int Ed* **2020**, *59* (43), 18866–18884. https://doi.org/10.1002/anie.202005745.
(35) Gombos, L. G.; Nikl, J.; Waldvogel, S. R. Dual Roles of Supporting Electrolytes in Organic Electrosynthesis. *ChemElectroChem* **2024**, *11* (8), e202300730. https://doi.org/10.1002/celc.202300730.
(36) Haupt, J. D.; Berger, M.; Waldvogel, S. R. Electrochemical Fluorocyclization of *N* -Allylcarboxamides to 2-Oxazolines by Hypervalent Iodine Mediator. *Org. Lett.* **2019**, *21* (1), 242–245. https://doi.org/10.1021/acs.orglett.8b03682.
(37) Hilt, G. Recent Advances in Paired Electrolysis and Their Application in Organic Electrosynthesis. *Current Opinion in Electrochemistry* **2024**, *43*, 101425. https://doi.org/10.1016/j.coelec.2023.101425.
(38) Hartmer, M. F.; Waldvogel, S. R. Electroorganic Synthesis of Nitriles via a Halogen-Free Domino Oxidation–Reduction Sequence. *Chem. Commun.* **2015**, *51* (91), 16346–16348. https://doi.org/10.1039/C5CC06437F.
(39) Dong, X.; Roeckl, J. L.; Waldvogel, S. R.; Morandi, B. Merging Shuttle Reactions and Paired Electrolysis for Reversible Vicinal Dihalogenations. *Science* **2021**, *371* (6528), 507–514. https://doi.org/10.1126/science.abf2974.
(40) Strehl, J.; Abraham, M. L.; Hilt, G. Linear Paired Electrolysis—Realising 200 % Current Efficiency for Stoichiometric Transformations—The Electrochemical Bromination of Alkenes. *Angew Chem Int Ed* **2021**, *60* (18), 9996–10000. https://doi.org/10.1002/anie.202016413. Strehl, J.; Abraham, M. L.; Hilt, G. Lineare gepaarte Elektrolyse – Realisierung von 200 % Stromausbeute in stöchiometrischen Umsetzungen – die elektrochemische Bromierung von Alkenen. *Angewandte Chemie* **2021**, *133* (18), 10084–10088. https://doi.org/10.1002/ange.202016413.
(41) Volta, A. On the electricity excited by the mere contact of conducting substances of different kinds. In a letter from Mr. Alexander Volta, FRS Professor of Natural Philosophy in the University of Pavia, to the Rt.

Hon. Sir Joseph Banks, Bart. KBPR S. *Philosophical transactions of the Royal Society of London* **1800**, *90*, 403–431. https://doi.org/10.1098/rstl.1800.0018.
(42) Röckl, J. L.; Pollok, D.; Franke, R.; Waldvogel, S. R. A Decade of Electrochemical Dehydrogenative C,C-Coupling of Aryls. *Acc. Chem. Res.* **2020**, *53* (1), 45–61. https://doi.org/10.1021/acs.accounts.9b00511.
(43) Waldvogel, S. R.; Lips, S.; Selt, M.; Riehl, B.; Kampf, C. J. Electrochemical Arylation Reaction. *Chem. Rev.* **2018**, *118* (14), 6706–6765. https://doi.org/10.1021/acs.chemrev.8b00233.
(44) Gieshoff, T.; Kehl, A.; Schollmeyer, D.; Moeller, K. D.; Waldvogel, S. R. Insights into the Mechanism of Anodic N–N Bond Formation by Dehydrogenative Coupling. *J. Am. Chem. Soc.* **2017**, *139* (35), 12317–12324. https://doi.org/10.1021/jacs.7b07488.
(45) Bieniek, J. C.; Mashtakov, B.; Schollmeyer, D.; Waldvogel, S. R. Dehydrogenative Electrochemical Synthesis of N-Aryl-3,4-Dihydroquinolin-2-Ones by Iodine(III)-Mediated Coupling Reaction. *Chem. Eur. J.* **2023**, *30* (7), e202303388. https://doi.org/10.1002/chem.202303388.
(46) Sand, M.; Skeie, R. B.; Sandstad, M.; Krishnan, S.; Myhre, G.; Bryant, H.; Derwent, R.; Hauglustaine, D.; Paulot, F.; Prather, M.; Stevenson, D. A Multi-Model Assessment of the Global Warming Potential of Hydrogen. *Commun Earth Environ* **2023**, *4* (1), 203. https://doi.org/10.1038/s43247-023-00857-8.
(47) Elsler, B.; Wiebe, A.; Schollmeyer, D.; Dyballa, K. M.; Franke, R.; Waldvogel, S. R. Source of Selectivity in Oxidative Cross-Coupling of Aryls by Solvent Effect of 1,1,1,3,3,3-Hexafluoropropan-2-Ol. *Chem. Eur. J* **2015**, *21* (35), 12321–12325. https://doi.org/10.1002/chem.201501604.
(48) Röckl, J. L.; Dörr, M.; Waldvogel, S. R. Electrosynthesis 2.0 in 1,1,1,3,3,3-Hexafluoroisopropanol/Amine Mixtures. *ChemElectroChem* **2020**, *7* (18), 3686–3694. https://doi.org/doi.org/10.1002/celc.202000761.
(49) Tajima, T.; Kurihara, H.; Shimizu, S.; Tateno, H. Anodic Alkoxylation of Lactams Followed by Reactions with Carbon Nucleophiles in a One-Pot Manner Using HFIP as a Solvent. *Electrochemistry* **2013**, *81* (5), 353–355. https://doi.org/10.5796/electrochemistry.81.353.
(50) Gütz, C.; Grimaudo, V.; Holtkamp, M.; Hartmer, M.; Werra, J.; Frensemeier, L.; Kehl, A.; Karst, U.; Broekmann, P.; Waldvogel, S. R. Leaded Bronze: An Innovative Lead Substitute for Cathodic Electrosynthesis. *ChemElectroChem* **2018**, *5* (2), 247–252. https://doi.org/10.1002/celc.201701061.
(51) Gütz, C.; Selt, M.; Bänziger, M.; Bucher, C.; Römelt, C.; Hecken, N.; Gallou, F.; Galvão, T. R.; Waldvogel, S. R. A Novel Cathode Material for Cathodic Dehalogenation of 1,1-Dibromo Cyclopropane Derivatives. *Chem. Eur. J.* **2015**, *21* (40), 13878–13882. https://doi.org/10.1002/chem.201502064.
(52) Schille, B.; Giltzau, N. O.; Francke, R. On the Use of Polyelectrolytes and Polymediators in Organic Electrosynthesis. *Angew Chem Int Ed* **2018**, *57* (2), 422–426. https://doi.org/10.1002/anie.201710659. Schille, B.; Giltzau, N. O.; Francke, R. Zur Nutzung von Polyelektrolyten und Polymediatoren in der organischen Elektrosynthese. *Angewandte Chemie* **2018**, *130* (2), 429–433. https://doi.org/10.1002/ange.201710659.
(53) Zhang, W.; Chen, X.; Wang, Y.; Wu, L.; Hu, Y. Experimental and Modeling of Conductivity for Electrolyte Solution Systems. *ACS Omega* **2020**, *5* (35), 22465–22474. https://doi.org/10.1021/acsomega.0c03013.
(54) Venturi, G. B.; translated by Nicholson, W. Experimental Researches Concerning the Principle of the Lateral Communication of Motion in Fluids, Applied to the Explanation of Various Hydraulic Phenomena. *Journal of Natural Philosophy, Chemistry and the Arts* **1799**, *2*, 172-179,273-276,422-494,v3p13-22,v3p59-61.
(55) Tipler, P. A.; Mosca, G. *Physik: für Studierende der Naturwissenschaften und Technik*; Kersten, P., Wagner, J., Eds.; Springer Berlin Heidelberg: Berlin, Heidelberg, 2019. https://doi.org/10.1007/978-3-662-58281-7.
(56) Nakagawa, K.; Konaka, R.; Nakata, T. Oxidation with Nickel Peroxide. I. Oxidation of Alcohols. *J. Org. Chem.* **1962**, *27* (5), 1597–1601. https://doi.org/10.1021/jo01052a026.
(57) Nuss, P.; Eckelman, M. J. Life Cycle Assessment of Metals: A Scientific Synthesis. *PLoS ONE* **2014**, *9* (7), e101298. https://doi.org/10.1371/journal.pone.0101298.
(58) Gao, Y.; Hill, D. E.; Hao, W.; McNicholas, B. J.; Vantourout, J. C.; Hadt, R. G.; Reisman, S. E.; Blackmond, D. G.; Baran, P. S. Electrochemical Nozaki–Hiyama–Kishi Coupling: Scope, Applications, and Mechanism. *J. Am. Chem. Soc.* **2021**, *143* (25), 9478–9488. https://doi.org/10.1021/jacs.1c03007.
(59) Sheng, H.; Meng, X.-H.; Xiao, D.-D.; Fan, M.; Chen, W.-P.; Wan, J.; Tang, J.; Zou, Y.-G.; Wang, F.; Wen, R.; Shi, J.-L.; Guo, Y.-G. An Air-Stable High-Nickel Cathode with Reinforced Electrochemical Performance Enabled by Convertible Amorphous Li2CO3 Modification. *Advanced Materials* **2022**, *34* (12), 2108947. https://doi.org/10.1002/adma.202108947.
(60) Li, Z.; Sun, W.; Wang, X.; Li, L.; Zhang, Y.; Li, C. Electrochemically Enabled, Nickel-Catalyzed Dehydroxylative Cross-Coupling of Alcohols with Aryl Halides. *J. Am. Chem. Soc.* **2021**, *143* (9), 3536–3543. https://doi.org/10.1021/jacs.0c13093.
(61) Tortajada Palmero, P. J.; Kärnman, T.; Martínez-Pardo, P.; Nilsson, C.; Holmquist, H.; Johansson, M. J.; Martín-Matute, B. Electrochemical Reduction of Alkenes over a Nickel Foam Guided by Life Cycle, Safety and Toxicological Assessments. November 24, 2023. https://doi.org/10.26434/chemrxiv-2023-p4q71.

(62) Glemser, O.; Einerhand, J. Über höhere Nickelhydroxyde. *Z. Anorg. Chem.* **1950**, *261* (1–2), 26–42. https://doi.org/10.1002/zaac.19502610103.
(63) Glemser, O.; Einerhand, J. Die Struktur höherer Nickelhydroxyde. *Z. Anorg. Chem.* **1950**, *261* (1–2), 43–51. https://doi.org/10.1002/zaac.19502610104.
(64) Briggs, G. W. D.; Jones, E.; Wynne-Jones, W. F. K. THE NICKEL OXIDE ELECTRODE. *Trans. Faraday Soc.* **1955**, *51*, 1433–1442. https://doi.org/10.1039/TF9555101433.
(65) Beil, S. B.; Breiner, M.; Schulz, L.; Schüll, A.; Müller, T.; Schollmeyer, D.; Bomm, A.; Holtkamp, M.; Karst, U.; Schade, W.; Waldvogel, S. R. About the Selectivity and Reactivity of Active Nickel Electrodes in C–C Coupling Reactions. *RSC Adv.* **2020**, *10* (24), 14249–14253. https://doi.org/10.1039/D0RA02673E.
(66) Klein, J.; Waldvogel, S. R. Selective Electrochemical Degradation of Lignosulfonate to Bio-Based Aldehydes. *ChemSusChem* **2023**, *16*, e202202300. https://doi.org/doi.org/10.1002/cssc.202202300.
(67) Recemat BV. *Datasheet Nickel Foam*; Datasheet; Recemat BV: Dodewaard, the Netherlands, 2018; p 1. https://www.recemat.nl/nickel-nickelchromium/ (accessed 2024-07-10).
(68) Foerster, F. Die Vorgänge im Eisen-Nickelsuperoxydsammler. I. Über Nickelsuperoxydelektroden. *Z. Elektrochem.* **1907**, *13* (28), 414–434. https://doi.org/10.1002/bbpc.19070132804.
(69) Fleischmann, M.; Korinek, K.; Pletcher, D. The Oxidation of Organic Compounds at a Nickel Anode in Alkaline Solution. *J. Electroanal. Chem.* **1971**, *31* (1), 39–49. https://doi.org/10.1016/S0022-0728(71)80040-2.
(70) Vértes, G.; Horányi, G.; Nagy, F. A NEW METHOD FOR THE ELECTROCHEMICAL OXIDATION OF ALCOHOLS. *Tetrahedron* **1972**, *28*, 37–42. https://doi.org/10.1016/0040-4020(72)80052-8.
(71) Robertson, P. M. On the Oxidation of Alcohols and Amines at Nickel Oxide Electrodes: Mechanistic Aspects. *J. Electroanal Chem.,* **1980**, *111*, 97–104.
(72) Schäfer, H. J.; Schneider, R. Oxidation of Partially Protected Carbohydrates at the Nickel Hydroxide Electrode. *Tetrahedron* **1991**, *47* (4–5), 715–724. https://doi.org/10.1016/S0040-4020(01)87061-7.
(73) Lyalin, B. V.; Petrosyan, V. A. Oxidation of Organic Compounds on NiOOH Electrode. *Russ J Electrochem* **2010**, *46* (11), 1199–1214. https://doi.org/10.1134/S1023193510110017.
(74) Jud, W.; Salazar, C. A.; Imbrogno, J.; Verghese, J.; Guinness, S. M.; Desrosiers, J.-N.; Kappe, C. O.; Cantillo, D. Electrochemical Oxidation of Alcohols Using Nickel Oxide Hydroxide as Heterogeneous Electrocatalyst in Batch and Continuous Flow. *Org. Process Res. Dev.* **2022**, *26* (5), 1486–1495. https://doi.org/10.1021/acs.oprd.2c00064.
(75) Zirbes, M.; Schmitt, D.; Beiser, N.; Pitton, D.; Hoffmann, T.; Waldvogel, S. R. Anodic Degradation of Lignin at Active Transition Metal-Based Alloys and Performance-Enhanced Anodes. *ChemElectroChem* **2019**, *6* (1), 155–161. https://doi.org/10.1002/celc.201801218.
(76) Montgomery, D. C. *Design and Analysis of Experiments*, 9th ed.; John Wiley & Sons, Inc.: Hoboken, NJ, 2022.
(77) Lehnherr, D.; Chen, L. Overview of Recent Scale-Ups in Organic Electrosynthesis (2000–2023). *Org. Process Res. Dev.* **2024**, *28* (2), 338–366. https://doi.org/10.1021/acs.oprd.3c00340.
(78) Toulouse, C.; Cezerac, J.; Cabassud, M.; Le Lann, M. V.; Casamatta, G. Optimisation and Scale-up of Batch Chemical Reactors: Impact of Safety Constraints. *Chemical Engineering Science* **1996**, *51* (10), 2243–2252. https://doi.org/10.1016/0009-2509(96)00081-4.
(79) De Kruijff, G. H. M.; Goschler, T.; Derwich, L.; Beiser, N.; Türk, O. M.; Waldvogel, S. R. Biobased Epoxy Resin by Electrochemical Modification of Tall Oil Fatty Acids. *ACS Sustainable Chem. Eng.* **2019**, *7* (12), 10855–10864. https://doi.org/10.1021/acssuschemeng.9b01714.
(80) de Kruijff, G. H. M.; Goschler, T.; Beiser, N.; Stenglein, A.; Türk, O. M.; Waldvogel, S. R. Sustainable Access to Biobased Biphenol Epoxy Resins by Electrochemical Dehydrogenative Dimerization of Eugenol. *Green Chem.* **2019**, *21* (17), 4815–4823. https://doi.org/10.1039/C9GC02068C.
(81) Jud, W.; Kappe, C. O.; Cantillo, D. A Continuous Flow Cell for High-Temperature/High Pressure Electroorganic Synthesis. *ChemElectroChem* **2020**, *7*, 2777–2783. https://doi.org/doi.org/10.1002/celc.202000696.
(82) Hwang, K. C.; Sagadevan, A. One-Pot Room-Temperature Conversion of Cyclohexane to Adipic Acid by Ozone and UV Light. *Science* **2014**, *346* (6216), 1495–1498. https://doi.org/10.1126/science.1259684.
(83) Guo, X.; Xu, M.; She, M.; Zhu, Y.; Shi, T.; Chen, Z.; Peng, L.; Guo, X.; Lin, M.; Ding, W. Morphology-Reserved Synthesis of Discrete Nanosheets of CuO@SAPO-34 and Pore Mouth Catalysis for One-Pot Oxidation of Cyclohexane. *Angew. Chem.* **2020**, *132*, 2628–2633. https://doi.org/10.1002/anie.201911749.
(84) Van De Vyver, S.; Román-Leshkov, Y. Emerging Catalytic Processes for the Production of Adipic Acid. *Catal. Sci. Technol.* **2013**, *3* (6), 1465–1479. https://doi.org/10.1039/C3CY20728E.

(85) Matthiesen, J. E.; Carraher, J. M.; Vasiliu, M.; Dixon, D. A.; Tessonnier, J.-P. Electrochemical Conversion of Muconic Acid to Biobased Diacid Monomers. *ACS Sustainable Chem. Eng.* **2016**, *4* (6), 3575–3585. https://doi.org/10.1021/acssuschemeng.6b00679.
(86) Kaulen, J.; Schäfer, H.-J. Oxidation of Primary Alcohols to Carboxylic Acids at the Nickel Hydroxide Electrode. *Synthesis* **1979**, 513–516. https://doi.org/10.1055/S-1979-28735.
(87) Li, H. B.; Yu, M. H.; Wang, F. X.; Liu, P.; Liang, Y.; Xiao, J.; Wang, C. X.; Tong, Y. X.; Yang, G. W. Amorphous Nickel Hydroxide Nanospheres with Ultrahigh Capacitance and Energy Density as Electrochemical Pseudocapacitor Materials. *Nat Commun* **2013**, *4* (1), 1894. https://doi.org/10.1038/ncomms2932.
(88) Lyalin, B. V.; Petrosyan, V. A. Electrosynthesis of Adipic Acid by Undivided Cell Electrolysis. *Russ Chem Bull* **2004**, *53* (3), 688–692. https://doi.org/10.1023/B:RUCB.0000035658.50123.07.
(89) Fioshin, M. Y.; Avrutskaya, I. A. Electrochemical Oxidation of Organic Compounds on Anodes Consisting of Certain Transition Metal Oxides. *Russ. Chem. Rev.* **1975**, *44* (11), 986–992. https://doi.org/10.1070/RC1975v044n11ABEH002405.
(90) Avrutskaya, I. A.; Fioshin, M. Ya.; Mulina, T. E.; Arkhinova, T. A. Behavior of a Nickel Hydroxide Electrode in Electrosynthetic Processes. *Elektrokhimiya* **1975**, *11* (8), 1176–1179.
(91) Kolbe, H. Beobachtungen über die oxydirende Wirkung des Sauerstoffs, wenn derselbe mit Hülfe einer elektrischen Säule entwickelt wird. *J. Prakt. Chem.* **1847**, *41* (1), 137–139. https://doi.org/10.1002/prac.18470410118.
(92) Leech, M. C.; Lam, K. Electrosynthesis Using Carboxylic Acid Derivatives: New Tricks for Old Reactions. *Acc. Chem. Res.* **2020**, *53* (1), 121–134. https://doi.org/10.1021/acs.accounts.9b00586.
(93) Alt, K. Katalytische Zugänge zu 4-Propylcyclohexanol, Johannes Gutenberg-University, Mainz.
(94) Jackson, E. L.; Hudson, C. S. The Structure of the Products of the Periodic Acid Oxidation of Starch and Cellulose. *J. Am. Chem. Soc.* **1938**, *60* (5), 989–991. https://doi.org/10.1021/ja01272a001.
(95) Pappo, R.; Allen, Jr., D.; Lemieux, R.; Johnson, W. Notes - Osmium Tetroxide-Catalyzed Periodate Oxidation of Olefinic Bonds. *J. Org. Chem.* **1956**, *21* (4), 478–479. https://doi.org/10.1021/jo01110a606.
(96) Müller, E. Die elektrolytische Bildung der Überjodsäure und ihrer Salze. Ein Beitrag zur Kenntnis elektrolytischer Oxydationsprozesse). *Z. Elektrotech. Elektrochem.* **1904**, *10* (4), 49–68. https://doi.org/10.1002/bbpc.19040100402.
(97) Müller, R. *Allgemeine und technische Elektrochemie nichtmetallischer Stoffe*; Springer Berlin Heidelberg: Berlin, Heidelberg, 1937. https://doi.org/10.1007/978-3-662-43079-8.
(98) Willard, H. H.; Ralston, R. R. The Electrolytic Oxidation of Iodine and of Iodic Acid. *Trans. Electrochem. Soc.* **1932**, *62* (1), 239. https://doi.org/10.1149/1.3493783.
(99) Mehltretter, C. L. Electrolytic Process for Making Periodic Acid Solutions. US2830941 (A), 1958. https://patents.google.com/patent/US2830941A/en.
(100) Rüetschi, P.; Angstadt, R. T.; Cahan, B. D. Oxygen Overvoltage and Electrode Potentials of Alpha - and Beta - PbO2. *Journal of the Electrochemical Society* **1959**, *106* (7), 547–551. https://doi.org/10.1149/1.2427435.
(101) Janssen, L. J. J.; Blijlevens, M. H. A. Electrochemical Oxidation of Iodate to Periodate. *Electrochimica Acta* **2003**, *48* (25–26), 3959–3964. https://doi.org/10.1016/S0013-4686(03)00535-8.
(102) Hirakata, K.; Mochizuki, M.; Kanai, H.; Itai, R. Electrolytic Cell for Producing Periodates. US4687565, August 18, 1987. https://www.freepatentsonline.com/4687565.pdf.
(103) Waldvogel, S. R.; Arndt, S.; Groß, R. Method for Preparing Periodates via Anodic Oxidation in a Steady State Reactor. WO2023194432A1, October 12, 2023. https://patents.google.com/patent/WO2023194432A1/en.
(104) National Renewable Energy Laboratory. Best Research-Cell Efficiency Chart, 2024. https://www.nrel.gov/pv/cell-efficiency.html (accessed 2024-07-13).
(105) Dunlop, E. D.; Halton, D.; Ossenbrink, H. A. 20 Years of Life and More: Where Is the End of Life of a PV Module? In *Conference Record of the Thirty-first IEEE Photovoltaic Specialists Conference, 2005.*; IEEE: Lake buena Vista, FL, USA, 2005; pp 1593–1596. https://doi.org/10.1109/PVSC.2005.1488449.
(106) Legay, R.; Roussel, J.; Boutevin, B. Synthesis of Polyglutarimides from p(Methyl Methacrylate) and Cyclohexylamine. I. Influence of Working Conditions on Imidization Reaction. *J. Appl. Polym. Sci.* **2000**, *76* (13), 1876–1888. https://doi.org/10.1002/(SICI)1097-4628(20000624)76:13<1876::AID-APP5>3.0.CO;2-A.
(107) Ritchie, H. Sector by Sector: Where Do Global Greenhouse Gas Emissions Come from? [Online Resource], 2020. https://ourworldindata.org/ghg-emissions-by-sector (accessed 2024-05-01).
(108) Castellan, A.; Bart, J. C. J.; Cavallaro, S. Industrial Production and Use of Adipic Acid. *Catal. Today* **1991**, *9* (3), 237–254. https://doi.org/10.1016/0920-5861(91)80049-F.
(109) Hielscher, M. M.; Dörr, M.; Schneider, J.; Waldvogel, S. R. LABS: Laboratory Automation and Batch Scheduling – A Modular Open Source Python Program for the Control of Automated Electrochemical

Synthesis with a Web Interface. *Chemistry An Asian Journal* **2023**, *18* (14), e202300380. https://doi.org/10.1002/asia.202300380.
(110) Li, Z.; Li, X.; Zhou, H.; Xu, Y.; Xu, S.-M.; Ren, Y.; Yan, Y.; Yang, J.; Ji, K.; Li, L.; Xu, M.; Shao, M.; Kong, X.; Sun, X.; Duan, H. Electrocatalytic Synthesis of Adipic Acid Coupled with H2 Production Enhanced by a Ligand Modification Strategy. *Nat Commun* **2022**, *13* (1), 5009, 1–12. https://doi.org/10.1038/s41467-022-32769-0.
(111) Parodi, E.; Govaert, L. E.; Peters, G. W. M. Glass Transition Temperature versus Structure of Polyamide 6: A Flash-DSC Study. *Thermochimica Acta* **2017**, *657*, 110–122. https://doi.org/10.1016/j.tca.2017.09.021.
(112) Temin, S. C. Effect of Structure on the Glass Temperature of Polyamides. *J of Applied Polymer Sci* **1965**, *9* (2), 471–481. https://doi.org/10.1002/app.1965.070090209.

Appendix

SUPPORTING INFORMATION

In the following, the supporting information of all papers listed in this dissertation are presented in the following order:

- Scaled oxidative flow electrosynthesis of 3-alkyladipic acids from 4-alkylcyclohexanols
- Sustainably scaled electrochemical synthesis of 3-propyladipic acid in line with fluctuating grid supply
- Sun-powered electrosynthesis of 3-propyladipic acid: the direct coupling of PV panel and electrochemical reactor
- Robust and self-cleaning electrochemical production of periodate

Scaled oxidative flow electrosynthesis of 3-alkyl-adipic acids from 4-alkylcyclohexanols

Roland J.-R. Bednarz[a], Annika S. Gold[a], Jasmin Hammes[a], Denis F. Rohrmann[a], Silvio Natallelo[a], Moritz Mann[a], Frank Weinelt[b], Christopher Brauer[c], Siegfried R. Waldvogel[a,d*]

a Roland J.-R. Bednarz, Annika S. Gold, Jasmin Hammes, Denis F. Rohrmann, Silvio Natallelo, Dr. Moritz Mann, and Prof. Dr. Siegfried R. Waldvogel
Department of Chemistry
Johannes Gutenberg University Mainz
Duesbergweg 10-14, 55128 Mainz (Germany)
*Email: waldvogel@uni-mainz.de

b Dr. Frank Weinelt
Evonik Operations GmbH | Research, Development & Innovation
Paul-Baumann-Straße 1, 45772 Marl (Germany)

c Christopher Brauer
IKA-Werke GmbH & Co. KG
Janke & Kunkel-Str. 10, 79219 Staufen (Germany)

d Prof. Dr. Siegfried R. Waldvogel
Institute of Biological and Chemical Systems – Functional Molecular Systems (IBCS-FMS)
Hermann-von-Helmholtz-Platz 1, 76344 Eggenstein-Leopoldshafen (Germany)

Table of Contents

1. General Information

The used reagents were utilized in analytical or sufficiently pure grades. Solvents were purified by standard methods like distillation or demineralization.[1] As reaction conditions, ambient pressure and temperature were applied, unless stated else. The electrodes which were applied for the reactions were commercially available and contain small channels on the inlet and outlet side: stainless steel (1.4571) and Recemat™ RCM-Ni4753.05 (average specific surface: 5400 m^2 m^{-3}) nickel foam. They fit the setup of the IKA ElectraSyn flow 6-18. For the activation, a separate stainless steel (1.4571) sheet electrode (6x18 cm^2) was cut by the university workshop. Geometrical current densities of the foams are reported here for two reasons: First, to the best of our knowledge it is not sufficient to consider the foam as an ideal plate with the reaction taking place at the outer surface. Since the foam is porous, the surface area inside the foam has to be considered as well. However, the field inside the foam is not constant – it is largest at the side towards the counter electrode. Since the drift velocity is proportional to the electric field, the current density is also not constant inside the foam. Therefore, using the total activated catalyst's surface area does not give the effective foam volume which determines the actual current density.
Second, precise measurements of the surface would need to be done after activation since the nickel oxyhydroxide adsorbs and builds up at the nickel substrate, changing the total area (see Figure 5 e vs. f). This especially holds, since the active layer forms even smaller fiber networks.
Overall, determining the precise active catalyst's surface area would be very difficult and is not expected to be easily correlated to the exact current density. Therefore, we suggest working with the geometrical current density and giving the porosity of nickel foam, as the most straightforward option, when working with activated nickel foams.
As galvanostat, a TDK Lambda Genesys 750 W/1500 W power supply was used. The reaction mixture was pumped using a reglo digital Masterflex™ hose pump (model no. 78018-42) by Ismatec through Ismapren tubings (size 16). A heating circuit was installed and connected to an IKA refrigerated and heating circulator WICO CBC 5 C (model RN41).

Melting point: The melting point of 3-ethyladipic acid (**2''**) was measured using a type M-565 device (Büchi, Essen, Germany). Uncorrected values are presented. The heating rate was 1 °C per minute.

NMR Spectroscopy: A Bruker Avance III 600 (Bruker, probe head: 5 mm TCI-CryoProbe head with *z* gradient and ATM) NMR spectrometer was used to record ^{1}H (600 MHz) and ^{13}C (151 MHz) Inverse Gated spectra at 25 °C. Chemical shifts (δ) are reported in parts per million (ppm). The quantification was done by integrating the respective signals in the ^{13}C Inverse

Gated spectrum against 1,3,5-trimethoxybenzene as internal standard (δ = (55.4±0.02) ppm). The DMSO-d6 signal was chosen as a reference (δ = 39.52 ppm).

Liquid chromatography: photodiode array analysis was performed by using a DUGA-20A3 device from Shimadzu, which was equipped with a C18 column from Knauer (Eurospher II, 100-5 C18, 150x4 mm). The column was conditioned to 25 °C and the flow rate was set to 1 mL/min. The aqueous eluent was buffered with formic acid (0.8 mL/2.5 L) and stabilized with Acetone (5 vol%). To prepare the samples, the carboxylic acid product mixture was extracted from the reaction mixture by acid-base extraction with ethyl acetate, dried over $MgSO_4$ and the solvent evaporated. The product was filtrated (VWR 13 mm syringe filters w/ 0.45 µm PTFE membrane), dissolved and diluted in acetonitrile (MS grade). This organic solution was analyzed by liquid chromatography.

High resolution mass spectra: were obtained using a G6545A Q-ToF (Agilent GmbH, Waldbronn, Germany) with dual AJS electrospray ion source (Dual AJS ESI). MS parameters were as follows: Mass rage: 80 – 3200 m/z, Scan rate: 1 spectrum s^{-1}, Nebulizer pressure: 25 psig, Capillary Voltage: 3500 V, Fragmentor: 50 V, Skimmer: 45 V, Dry gas temperature: 275 °C, Dry gas flow: 10 L min^{-1}, Sheath gas temperature: 350 °C, Sheath gas flow: 10 L min^{-1}. Mass calibration was performed on the day of measurement using an external standard. The mass accuracy of the measurement results is better than 5 ppm. Chromatographic separation was carried out on a 1260 Infinity II HPLC system (Agilent GmbH, Waldbronn, Germany) with G7111B 1260 Quaternary Pump, G7129A 1260 Vialsampler, and G7116A 1260 Multicolumn Thermostat equipped with an Agilent EclipsePlus C18 RRHP (2.1 x 50 mm, 2.1 µm particle size) analytical column. Eluents were 98% H_2O with 2% ACN and 0.05% formic acid (Eluent A) and 2% H_2O with 98% ACN and 0.05% formic acid (Eluent B). The following gradient elution was applied for separation at flow rate of 200 µL min^{-1}: Starting at 10% B for 1 min, followed by a linear increase to 95% B at 10 min, maintaining 95% B until 30 min, before going back to 10% B at 33 min. The column was equilibrated at 10% B for 15 min before the next measurement. Injection volume was 2 µL. Data was recorded using Agilent MassHunter Workstation LC/MS software version 11.0 and data analysis was performed using Agilent MassHunter Workstation Qualitative Analysis software version 10.0.

MALDI TOF MS: The Autoflex MALDI TOF mass spectrometer by Bruker Daltonik GmbH (Fahrenheitstraße 4, 28359 Bremen, Germany) with a smartbeam ™II Nd:YAG laser (355 nm) was utilized. The image was measured in linear mode. 2-[(2E)-3-(4-*tert*-Butylphenyl)-2-methylprop-2-enylidene]malononitrile (DCTB) was used as a matrix.

2. Used Chemicals

4-Ethylphenol [123-07-9] Aldrich®, 99%

Methanol [67-56-1] ROTISOLV®, ≥99%

Sulfuric acid [7664-93-9] Fisher Chemical, ≥95%

Nickel(II)sulfate heptahydrate [10101-98-1] Sigma-Aldrich, ≥99%

Sodium acetate [127-09-3] Acros Organics, >99%

Sodium hydroxide [1310-73-2] VWR, 98.8%

4-Methylcyclohexanol (cis- and trans- mixture) [589-91-3] TCI, >98%

4-Ethylcyclohexanone [5441-51-0] TCI, >98%

Magnesium sulfate [7487-88-9] Thermo Fisher Scientific, 97%

3. General Procedures

3.1. Procedure for flow electrolysis:

The commercially available modular IKA *ESF* 6-18 flow electrolyzer was undivided with a nickel foam (Recemat™ RCM-Ni4753.05) anode, connected by a nickel sheet, and a stainless steel (1.4404) cathode, each having dimensions of 6 x 18 cm^2. A PTFE spacer (0.5 mm) was used. A general schematic is depicted in Figure S1.

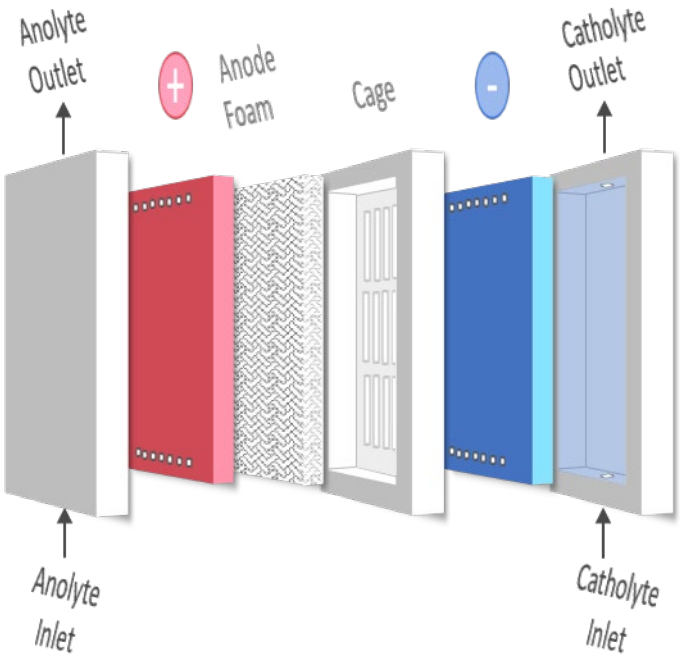

Figure S1. Explosion sketch of a modular flow electrolyzer with two in- and outlets for the electrolyte. The active anode is a nickel foam, which is connected via a nickel sheet electrode and located in a half-open cage. The electrode spacing can be modified. A cooling circuit can be connected for the IKA *ESF* 6-18, which is not indicated here. Modified from [2], copyright 2021 Wiley Analytical Science.

The commercially available mixing unit IKA magic LAB® was connected to the agitated reservoir IKA magic PLANT®. Therein, the electrolyte, consisting of $NaOH_{(aq)}$ (1 M) and the substrate 4-alkylcyclohexanol (**1**), was emulsified. This mixing unit has a powerful DR mixing element and pumps the fluid in cycles into the reservoir from where it returns. This flow rate is 12,000 rpm (representing approximately 70 L h^{-1}). From there, a peristaltic pump feeds the upright standing flow cell from the bottom. Tubes on the outlet side are connected with the reservoir, enabling safe removal of the formed hydrogen. A given charge amount as well as current density were applied and monitored, using a python software control and the galvanostat TDK Lambda Genesys. After the electrolysis stopped, the reaction mixture was pumped out of the electrolyzer in reversed flow direction. Then, methyl *tert*-butyl ether (MTBE, 80 mL) and 1 M caustic soda (80 mL) were used to clean the cell, successively. All fractions were combined and worked up using liquid-liquid extraction in a 2 L perforator (Figure S2).

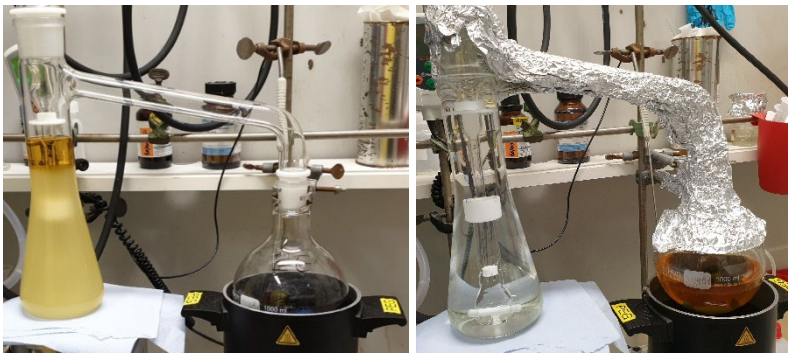

Figure S2. Left: liquid-liquid extraction of acidified reaction medium using ethyl acetate, using a perforator according to Ludwig. Right: A quantitative extraction can optically be determined by discoloration.

Thereby, non-acidic components were extracted first from the basic aqueous reaction mixture using MTBE. After acidification to pH 1–2, the acids were extracted using ethyl acetate. The organic fractions were dried over $MgSO_4$, and the solvents removed. The remaining acid fraction was weighed, and the products quantitatively analyzed by ^{13}C Inverse Gated NMR spectroscopy. 1,3,5-Trimethoxybenzene (0.1 mmol) was used as an internal standard.

3.2. Procedure of reaction control experiments:

Following the reaction protocol mentioned above, in steps of 10 hours (approximately 1 *F*), samples of (2.00±0.10) mL reaction mixture were taken from the reservoir with a 3 mL syringe (Figure S3).

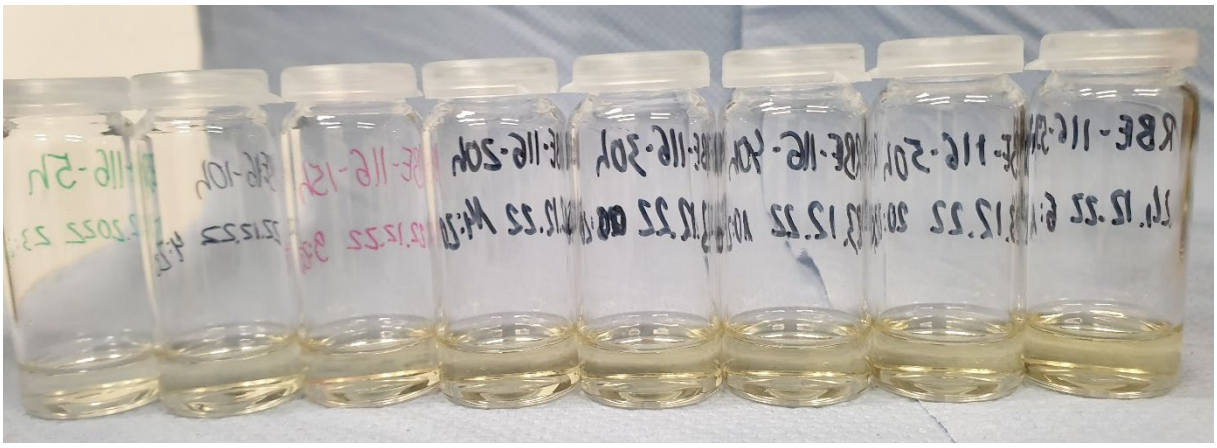

Figure S3. Samples taken after 5 h, 10 h, 15 h, 20 h, 30 h, 40 h, 50 h and 59.6 h. An optical transition from colorless to pale yellow can be seen, corresponding to side products in very low quantity.

Then, the collected samples were acidified to pH 1–2 using 550 µL $H_2SO_{4(konz.)}$ each. After adding 2 mL ethyl acetate and a 10 mm stirring bar, the biphasic mixture was rigorously stirred at 300 rpm. Then, the organic phase was dried over $MgSO_4$ (Figure S4). This extraction was

performed four times. The solvent was removed, and the product mixture analyzed by ^{13}C Inverse Gated NMR spectroscopy. 1,3,5-Trimethoxybenzene (0.1 mmol) was used as an internal standard.

Figure S4. Workup of four samples, in the front row. The mini columns in the back contain $MgSO_4$ as drying agent.

4. Optimizations for Flow Electrolysis (6 x 18 cm^2 electrodes)

The screening results are included in Table S1. While most reproductive experiments show very similar yields, the fluctuations for the highest yields are more compelling (35% and 59%). Those reaction conditions still lead to the best reported electrochemical results of **2''**, achieved so far. Change of typical electrolysis parameters like flow rate had no clear influence onto the by-product distribution.

Table S1. Screening results of flow experiments from 4-ethylcyclohexanol (**1''**) to 3-ethyladipic acid (**2''**). Parameters are displayed and qNMR yields of **2''**, 2-ethylglutaric acid (**4**), 3-ethylglutaric acid (**3**) and ethylsuccinic acid (**5**). * Quantitative NMR yields, analysed with ^{13}C Inverse Gated NMR spectroscopy. Integration versus the internal standard 1,3,5-trimethoxy-benzene.

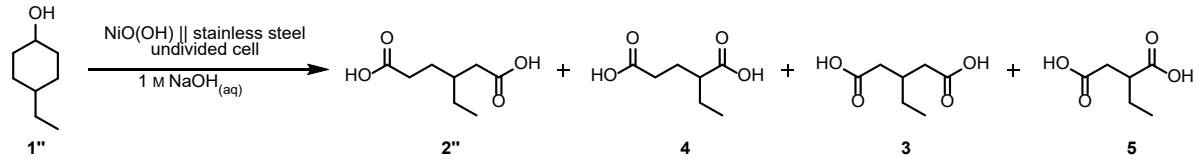

Screening no.	*T* / °C	*c*(4ECHol) / M	*Φ* / mL min^{-1}	*j* / mA cm^{-2}	*Y*(2'')* / %	*Y*(4)* / %	*Y*(3)* / %	*Y*(5)* / %
1	50	0.5	50	5	24	2	2	0.3
2	37.5	0.35	30	4	15	2	1.3	1.1
3	50	0.2	10	3	6	0.6	0.5	0.2
4	50	0.5	10	5	11	0.9	0.5	0
5	50	0.2	10	3	6	0.8	0.7	0.3
6	37.5	0.35	30	4	15	2	1.3	1.1
7	50	0.5	10	5	11	0.9	0.5	0
8	50	0.2	50	3	12	1.2	1.3	0.5
9	50	0.2	50	3	14	2	2	2
10	50	0.5	50	5	20	3	2	1.4
11	25	0.5	10	3	28	3	2	1.0
12	25	0.2	10	5	8	0.9	0.7	0.4
13	25	0.5	50	3	12	0.8	0.8	0.3
14	25	0.2	10	5	8	0.9	0.7	0.4
15	25	0.5	50	3	30	3	2	1.0
16	25	0.2	50	5	35	3	3	1.2
17	25	0.5	10	3	12	0.8	0.6	0.2
18	25	0.2	50	5	59	4	4	1.2

Hereafter, the data is graphically reported, while the experiments are ordered by yield of **2''** (Figure S5).

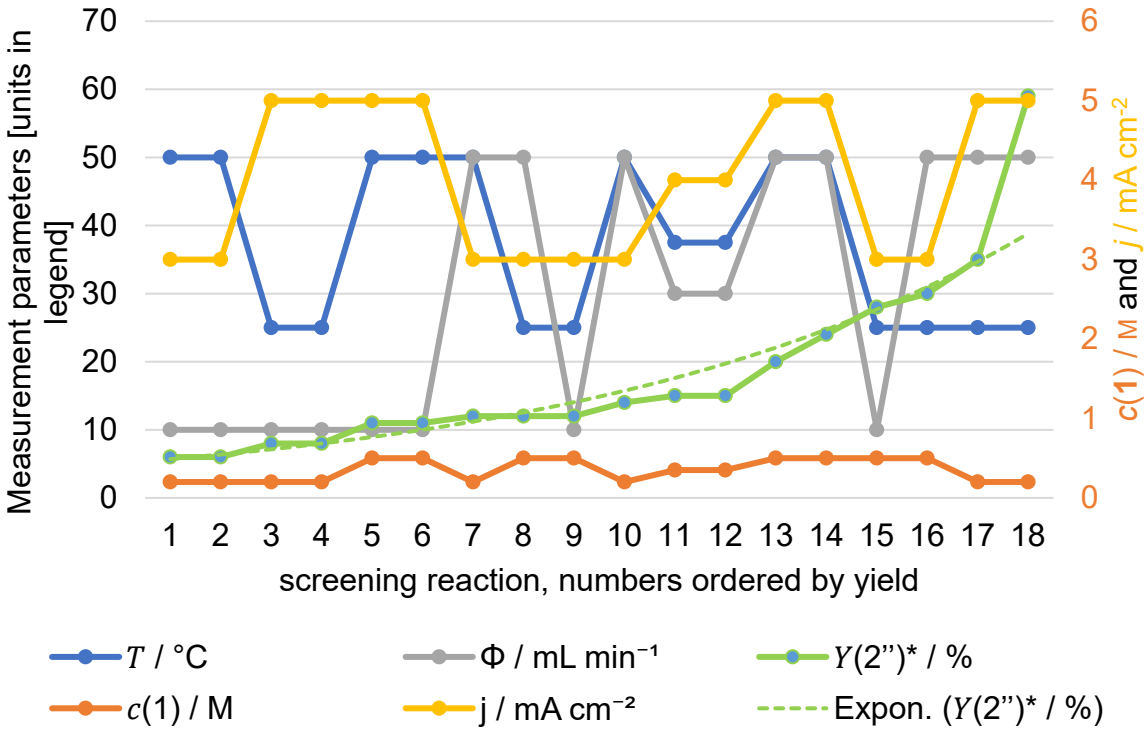

Figure S5. Graphical analysis of parameters in order with increasing qNMR yields of **2''** (*). The results follow an exponential fit with the exception of the couple of best results.

The results can be fitted to an exponential curve, showing a trend in less and more important parameter combinations. The *DoE* results that a high stirring speed combined with a low substrate concentration enhance the yield, if also the current density is high, has also graphical evidence. Since the best results show a more significant fluctuation, this parameter set was repeated: The follow-up experiment had a 3-ethyladipic acid qNMR yield of 38%.

For the reaction control experiments (see Figures 10 and 11) without substrate feeding (Table S2) and with substrate feeding (Table S3), the qNMR results are reported below.

Table S2. Results of the reaction control experiment from 4-ethylcyclohexanone (**1'''**) to 3-ethyladipic acid (**2''**). The applied charge is shown for each data point as well as the corresponding qNMR yields of **1'''**, **2''**, **4** and **3**. * Quantitative NMR yields, analysed with ^{13}C Inverse Gated NMR spectroscopy. Integration versus the internal standard 1,3,5-trimethoxy-benzene.

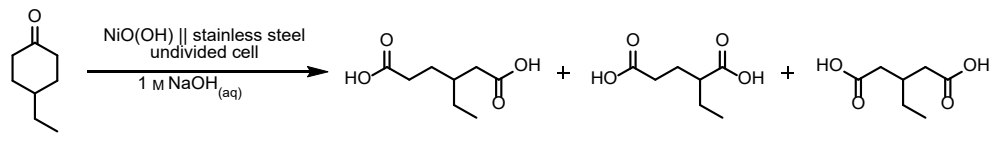

Sample no.	*Q* / *F*	*Y*(1''')* / %	*Y*(2')* / %	*Y*(4)* / %	*Y*(3)* / %
1	0.0	0.0	0.0	0.0	0.0
2	1.0	3	7	0.0	0.4
3	2.0	18	7	0.0	0.0
4	3.1	0.5	10	0.7	0.6
5	4.4	1.3	10	0.8	0.8
6	5.4	1.4	18	1.5	2
7	7.1	1.4	22	2	2
8	8.9	1.4	19	2	2

Table S3. Results of the reaction control experiment from 4-ethylcyclohexanone (**1’’’**) to 3-ethyladipic acid (**2’’**). The applied charge is shown for each data point as well as the corresponding qNMR yields of **1’’’**, **2’’**, **4** and **3**. * Quantitative NMR yields, analysed with ^{13}C Inverse Gated NMR spectroscopy. Integration versus the internal standard 1,3,5-trimethoxy-benzene.

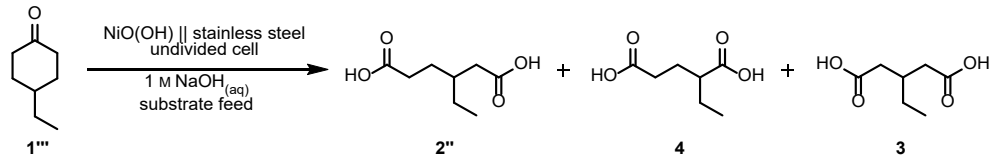

Sample no.	*Q* / *F*	*Y*(1’’’)* / %	*Y*(2’)* / %	*Y*(4)* / %	*Y*(3)* / %
1	0.5	10	4	0.0	0.0
2	1.0	6	12	0.0	0.4
3	1.5	4	15	0.8	0.3
4	2.0	9	25	1.5	1.0
5	3.0	5	31	2	1.3
6	4.0	7	30	0.4	0.2
7	5.0	0.6	46	3	2
8	6.0	3	46	3	3

5. Activation process

The nickel electrodes were used throughout the reported study. The activation protocol reported here reproducibly darkened the electrode surface, leading to nickel oxyhydroxide, NiO(OH) (Figure S6).

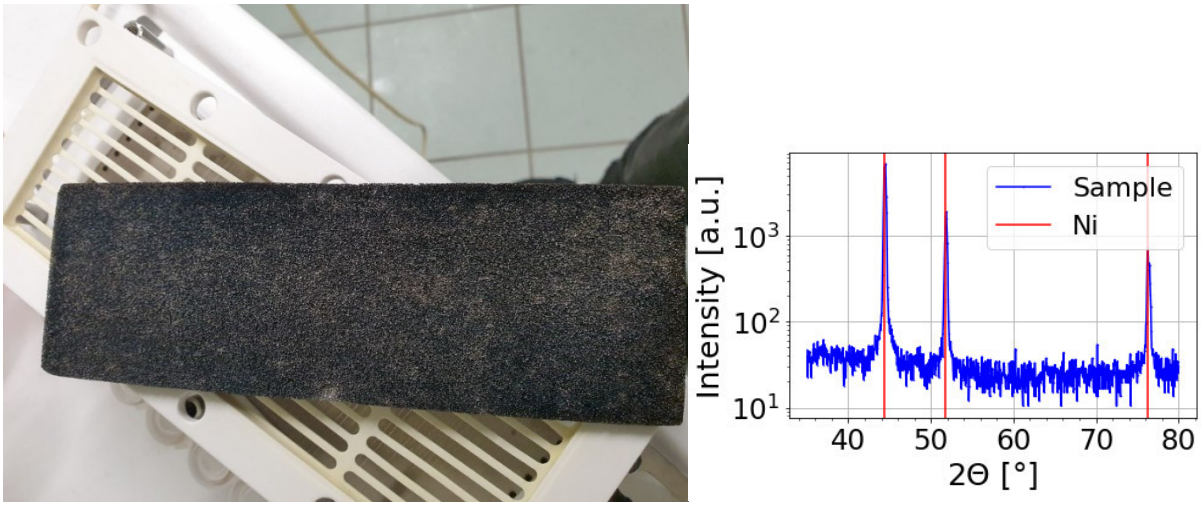

Figure S6. Left: Activated nickel foam anode. It is inserted in the underlying white half-open cage. Right: XRD measurement of the freshly activated nickel foam, showing the three known signals for nickel (111), (200) and (220). The nickel oxide hydroxide species do not appear as peaks, indicating that they are not crystalline.

In the course of the *DoE* parameter screening, the activation led to a deposition of nickel at the cathode, instead of hydrogen formation (Figure S7). After a few cleaning cycles of both electrodes, the cathode surface darkened increasingly, and more hydrogen formed. Thus, the depicted clean nickel surface after activation was only achieved for 6–8 activation cycles. Why the remarkable nickel deposition appeared and changed again, was not fully understood.

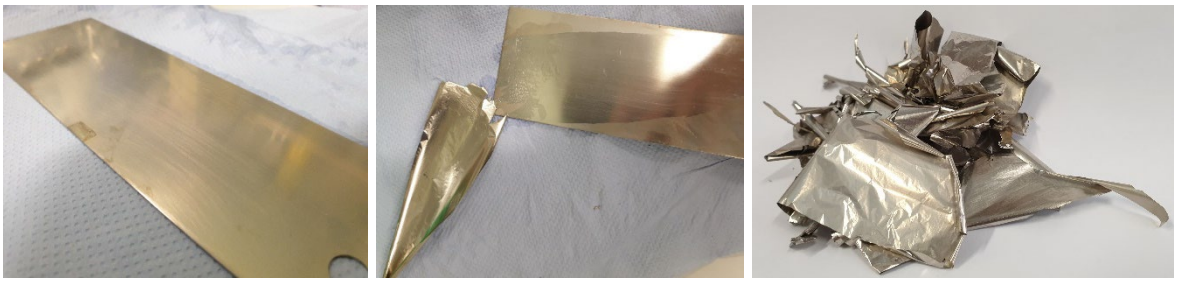

Figure S7. Left: During several consecutive activation runs in the cause of the screening, nickel was deposited on the stainless steel cathode. Middle: The nickel layer could be stripped of with a tweezer after the electrode was immersed in 4.5 M $H_2SO_{4(aq)}$ for a few seconds. Right: About 1.5 g of nickel were deposited in the course of these activation reactions.

After several cleaning cycles, the electrode darkened (Figure S8). The SEM images revealed that the pores could not fully be cleaned with the 4.5 M $H_2SO_{4(aq)}$. This is likely the main difference for the darkening of the electrode.

Figure S8. Image of pristine nickel foam electrode (left) and one after several uses and cleaning procedures (right).

6. Synthesis of 3-ethyladipic acid

3-Ethyladipic acid (2'')

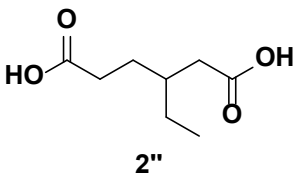

2''

2'' was electrochemically synthesized according to the described procedure above from 4-ethylcyclohexanol (6.41 g, 50 mmol, 0.2 M). The product **2''** was obtained by acid-base extraction, vacuum distillation, and recrystallization from *n*-heptane, obtained as a light yellow crystalline solid (3.31 g, 19 mmol, 38%, Figure S9).

Figure S9. Purified crystals of electrochemically synthesized 3-ethyladipic acid (**2'**).

^{1}H NMR (600 MHz, DMSO-d6): δ [ppm] = 12.04 (s, 2H), 2.18 (t, *J* = 7.9 Hz, 2H), 2.12 (d, *J* = 6.9 Hz, 2H), 1.68 (hept, *J* = 6.5 Hz, 1H), 1.57–1.42 (m, 2H), 1.33–1.21 (m, 2H), 0.81 (t, *J* = 7.5 Hz, 3H).

^{13}C NMR (151 MHz, DMSO-d6): δ [ppm] = 174.75, 174.29, 38.07, 35.41, 31.20, 28.17, 25.63, 10.69.

Melting point: (47.4–49.8) °C

HRMS (ESI+) *m/z*: calculated for $C_8H_{14}O_4$ + H^+ 175.0965 $[M+H^+]^+$, found 175.0965.

7. Spectra

3-Ethyladipic acid distillation residue (MALDI-ToF MS)

The vacuum distillation of the product mixture was done in an apparatus with the round bottom flask, containing the product mixture, a Vigreux column for superior separation, a distillation bridge, which can be tempered, and a Schlenk tube for product collection, getting freezed in liquid nitrogen. The pressure during distillation was 10^{-1} to 2 mbar. The oil bath temperature was stepwise increased up to 240 °C, where no main product evaporated any more. For the last distillation fraction between 220 and 240 °C, the Vigreux column was not used. MALDI-TOF MS analyses of the product mixture after electrolysis and of the black distillation residue

of a 3-ethyladipic acid synthesis was performed. The data reveals that the remaining molecules are of high molecular weight (Figure S10). Most of them have a weight of more than 2 kg mol^{-1}.

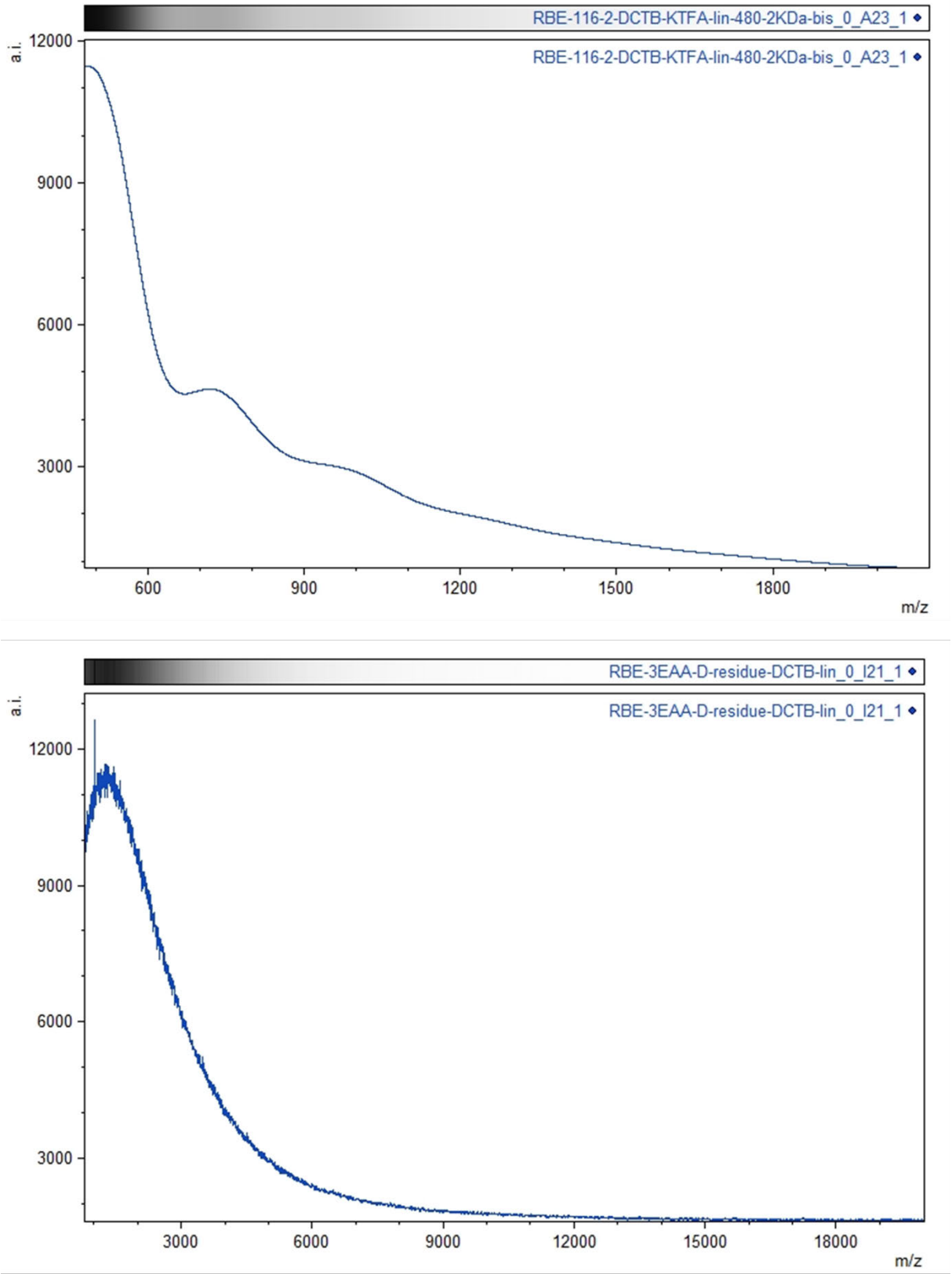

Figure S10. MALDI-TOF MS analysis of the product mixture after electrolysis (top) and distillation residue (bottom) from a 3-ethyladipic acid reaction. Measuring settings were linear mode and DCTB as a matrix.

3-Ethyladipic acid (^{1}H NMR spectrum)

The purified product **2''** was analyzed by ^{1}H (Figure S11) and ^{13}C Inverse Gated NMR spectroscopy (Figure S12).

Figure S11. ^{1}H NMR spectrum (600 MHz, DMSO-d6) of purified **2''**.

3-Ethyladipic acid (^{13}C Inverse Gated NMR spectrum)

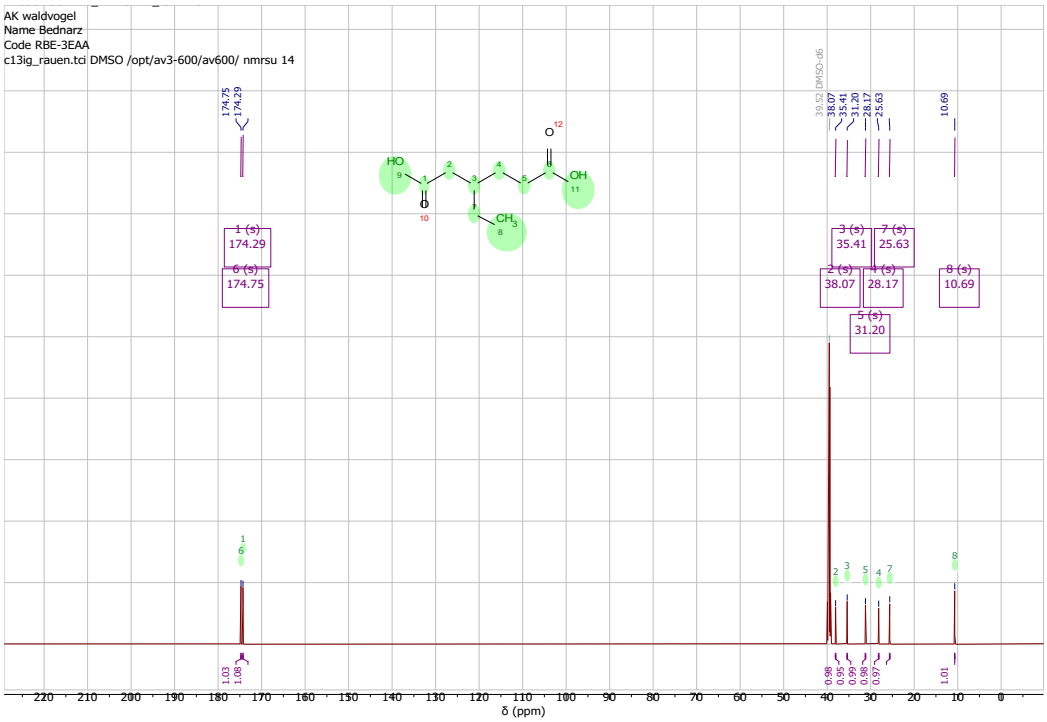

Figure S12. ^{13}C Inverse Gated NMR spectrum (151 MHz, DMSO-d6) of purified **2"**.

Product mixture of 3-ethyladipic acid, 3-ethyladipic acid-6-ethylester, 3-ethylglutaric acid, 2-ethylglutaric acid, ethylsuccinic acid and other unidentified products (^{1}H NMR spectrum)

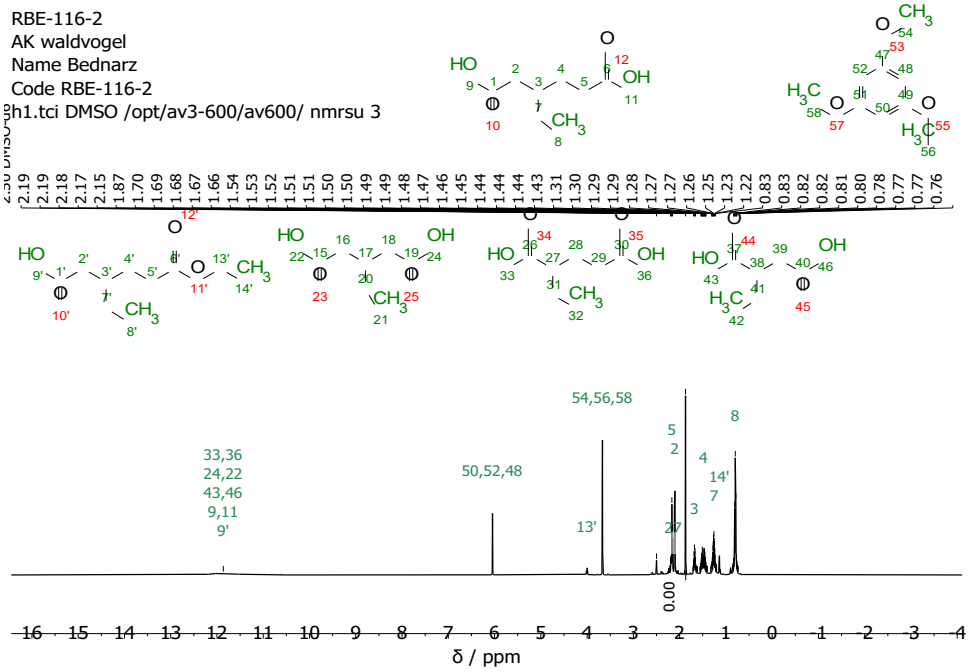

Figure S13. ^{1}H NMR spectrum (600 MHz, DMSO-d6) of crude product mixture of **2''**, the 3-ethyladipic acid ethylester **3**, **4**, **5** and unidentified side products.

Product mixture of 3-ethyladipic acid, 3-ethyladipic acid-6-ethylester, 3-ethylglutaric acid, 2-ethylglutaric acid, ethylsuccinic acid and other unidentified products (^{13}C Inverse Gated NMR spectrum)

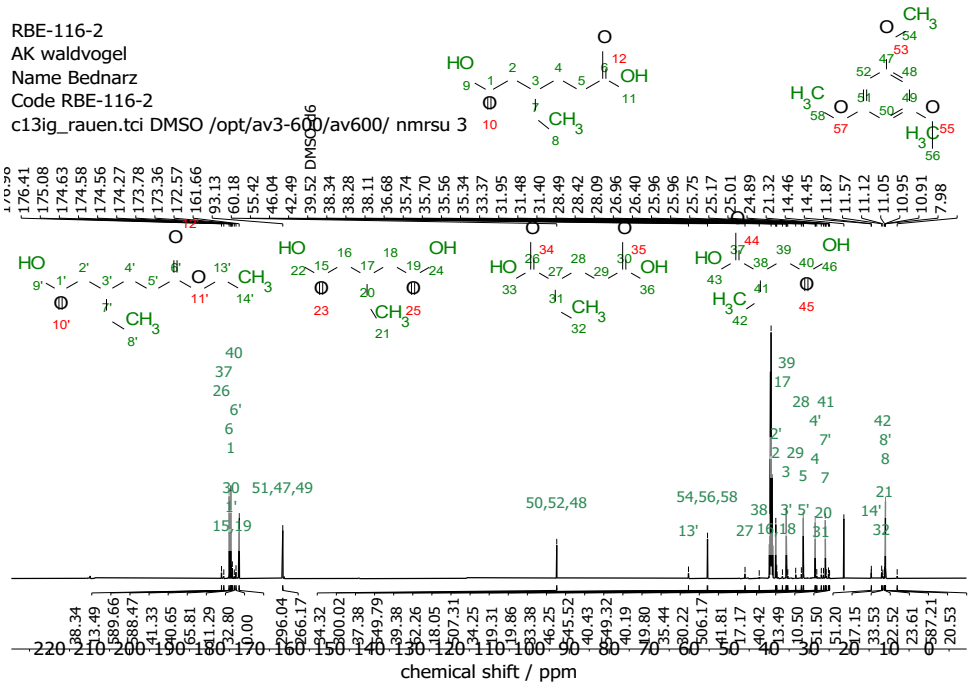

Figure S14. ^{13}C Inverse Gated NMR spectrum (151 MHz, DMSO-d6) of crude product mixture of **2''**, the 3-ethyladipic acid ethylester **3**, **4**, **5** and unidentified side products.

Product mixture of 3-ethyladipic acid, 3-ethyladipic acid-6-ethylester, 3-ethylglutaric acid, 2-ethylglutaric acid, ethylsuccinic acid and other unidentified products (^{1}H, ^{1}H COSY NMR spectrum)

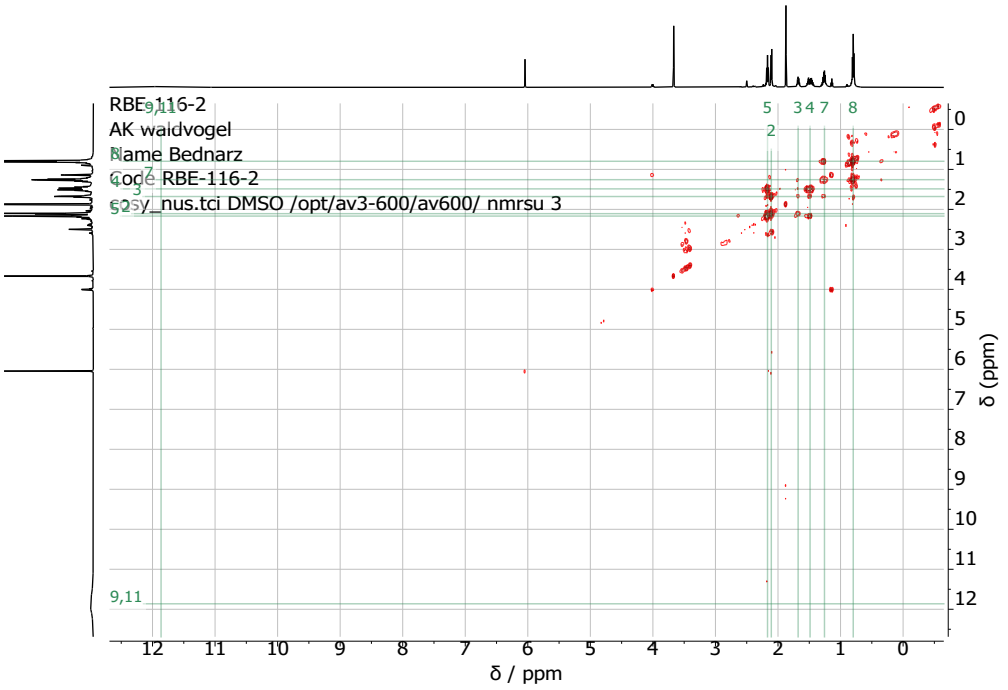

Figure S15. ^{1}H, ^{1}H COSY NMR spectrum (600 MHz, DMSO-d6) of crude product mixture of **2''**, the 3-ethyladipic acid ethylester **3**, **4**, **5** and unidentified side products.

Product mixture of 3-ethyladipic acid, 3-ethyladipic acid-6-ethylester, 3-ethylglutaric acid, 2-ethylglutaric acid, ethylsuccinic acid and other unidentified products (^{1}H, ^{13}C HSQC NMR spectrum)

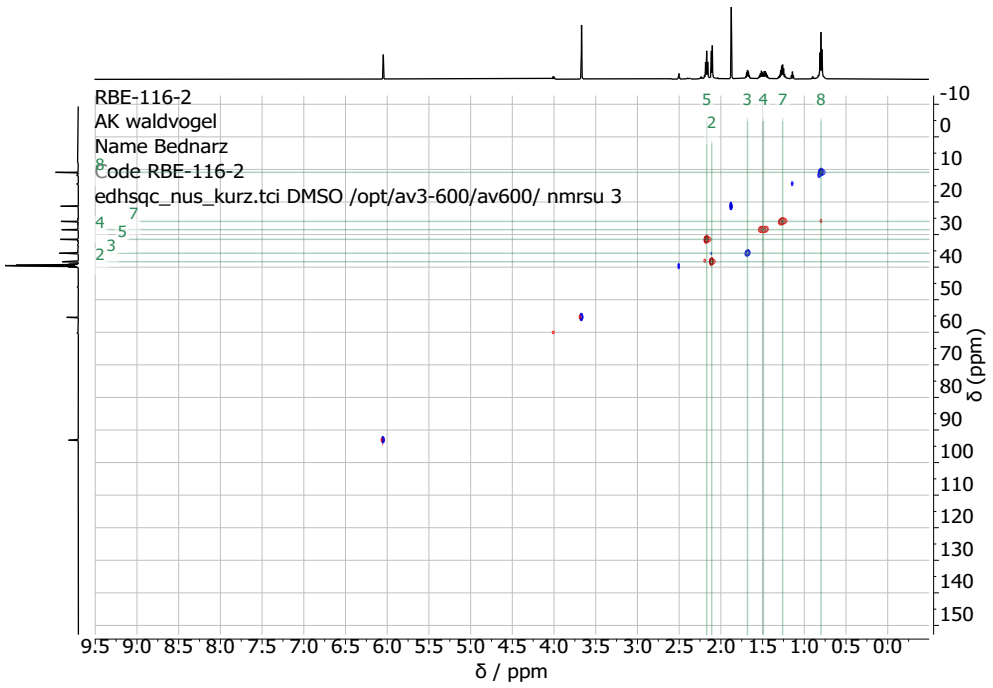

Figure S16. ^{1}H, ^{13}C HSQC NMR spectrum (600 MHz, DMSO-d6) of crude product mixture of **2''**, the 3-ethyladipic acid ethylester **3**, **4**, **5** and unidentified side products.

Product mixture of 3-ethyladipic acid, 3-ethyladipic acid-6-ethylester, 3-ethylglutaric acid, 2-ethylglutaric acid, ethylsuccinic acid and other unidentified products (^{1}H, ^{13}C HMBC NMR spectrum)

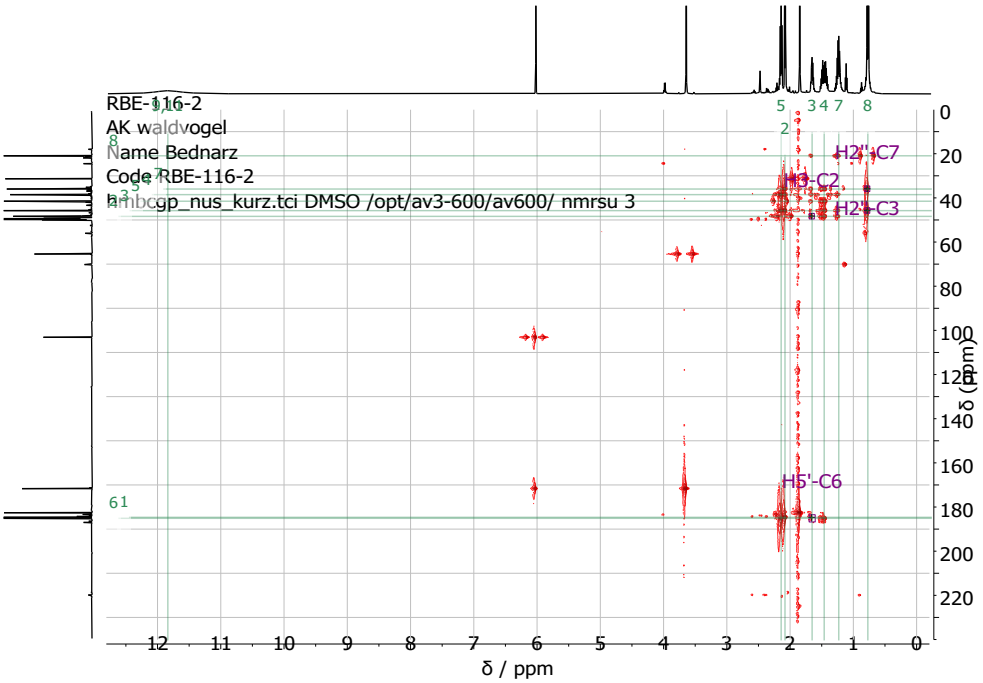

Figure S17. ^{1}H, ^{13}C HMBC NMR spectrum (600 MHz, DMSO-d6) of crude product mixture of **2''**, the 3-ethyladipic acid ethylester **3**, **4**, **5** and unidentified side products.

Product mixture of 3-ethyladipic acid, 3-ethyladipic acid-6-ethylester, 3-ethylglutaric acid, 2-ethylglutaric acid, ethylsuccinic acid and other unidentified products (^{1}H, ^{13}C HSQC-TOCSY NMR spectrum)

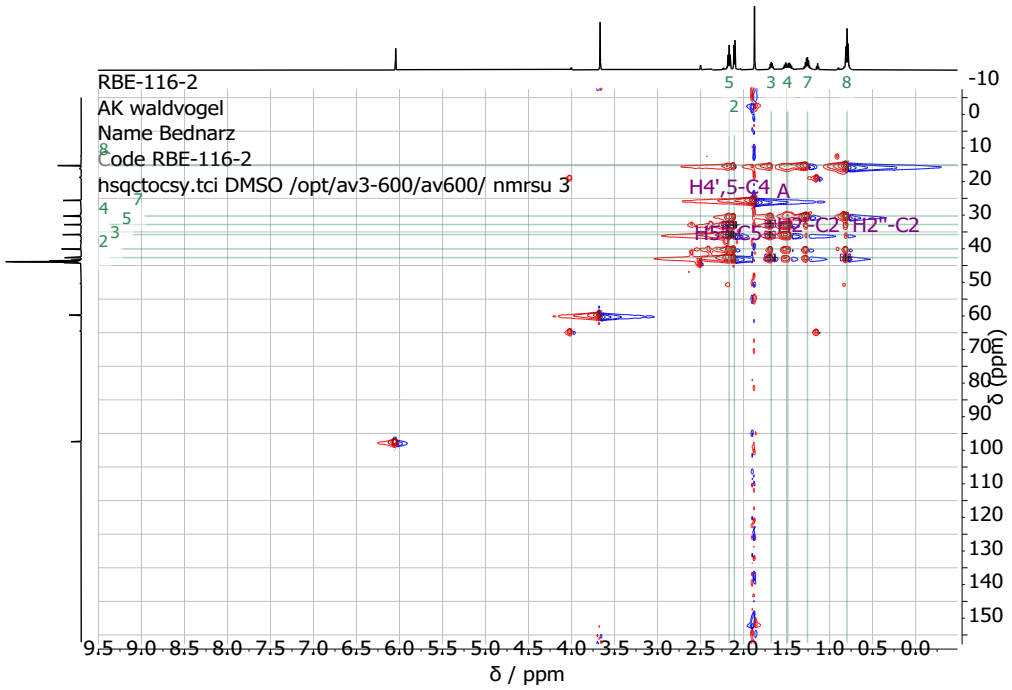

Figure S18. ^{1}H, ^{13}C HSQC TOCSY NMR spectrum (600 MHz, DMSO-d6) of crude product mixture of **2''**, the 3-ethyladipic acid ethylester **3**, **4**, **5** and unidentified side products.

8. References

[1] W. LF. Armarego, C. L. L. Chai, *Purification of Laboratory Chemicals*, Elsevier, Amsterdam, **2013**.
[2] R. J.-R. Bednarz, C. Brauer, S. R. Waldvogel, *GIT Laboratory Journal* **2021**, online, https://analyticalscience.wiley.com/do/10.1002/was.000600208/full/.

ChemCatChem

Supporting Information

Sustainably Scaled Electrochemical Synthesis of 3-Propyladipic Acid in Line with Fluctuating Grid Supply

Roland J.-R. Bednarz, Pilar Jiménez-Meneses, Annika S. Gold, Damián Monllor-Satoca, Andreas Stenglein, Roberto Gómez,* and Siegfried R. Waldvogel*

Table of Contents

1. General Information

All reagents were used in analytical or sufficiently pure grades. The solvents were purified by standard methods.[24]

Electrochemical reactions: For the reactions, ambient conditions are applied, unless stated different. All electrode materials are commercially available: Aqua Titan nickel foam (5 mm thickness), Recemat™ nickel foam RCM-Ni4753.05 and stainless-steel (alloy type EU norm 1.4571, ASTM: 316Ti). The Aqua Titan nickel foams were only used for the first DoE screening and replaced by the Recemat™ once for reasons of smaller porosity, longer lifetime, and eventually, significantly reduced short circuits. The electrodes were separated at the top with PTFE spacers (3 mm thickness) and all anodes as well as all cathodes were connected with flexible stainless-steel sheets, respectively. The university's workshop milled the electrodes and spacers such that they matched the desired length and width. An activation of the nickel foam was done in an electrode stack with an additional set of stainless-steel sheet electrodes. As DC power sources, a HMP4040 from Rhode&Schwarz was used for the small-scale screening reactions and a TDK Lambda Genesys 750 W/1500 W power supply for the scaled reactor. A FINK membrane pump was utilized for pumping the reaction mixture from the reservoir through the eductor and the pump into the reactor. The eductor piece was obtained from Zerodis Store. For feeding, a Masterflex EW-78018-14 peristaltic pump was used. The reservoir and reactor were tempered with a heating circuit, powered, and controlled by a Julabo MV-12 thermostat.

Melting point: The melting point of 3-propyladipic acid (**2**) was measured using a type M-565 device (Büchi, Essen, Germany). Uncorrected values are presented. The heating rate was 1 °C per minute.

NMR spectroscopy: A Bruker Avance III 600 (Bruker, probe head: 5 mm TCI-CryoProbe head with z gradient and ATM) NMR spectrometer was used to record ^{1}H (600 MHz) and ^{13}C (151 MHz) Inverse Gated spectra at 25 °C. Chemical shifts (δ) are reported in parts per million (ppm). The quantification was done by integrating the respective signals in the ^{13}C Inverse Gated spectrum against 1,3,5-trimethoxybenzene as internal standard (δ = (55.4±0.02) ppm). The DMSO-d_6 signal was chosen as a reference (δ = 39.52 ppm).

Liquid chromatography: A photodiode array analysis was performed by using a DUGA-20A3 device from Shimadzu, which was equipped with a C18 column from Knauer (Eurospher II, 100-5 C18, 150x4 mm). The column was conditioned to 25 °C and the flow rate was set to 1 mL min^{-1}. The aqueous eluent was buffered with formic acid (0.8 mL/2.5 L) and stabilized with Acetone (5 vol%). To prepare the samples, the carboxylic acid product mixture was extracted from the reaction mixture by acid-base extraction with ethyl acetate, dried over $MgSO_4$ and the solvent evaporated. The product was filtrated (VWR 13 mm syringe filters w/ 0.45 µm PTFE membrane), dissolved and diluted in acetonitrile (MS grade). This organic solution was analyzed by liquid chromatography.

High resolution mass spectra: The HRMS data was obtained using a G6545A Q-ToF (Agilent GmbH, Waldbronn, Germany) with dual AJS electrospray ion source (Dual AJS ESI). MS parameters were as follows: Mass rage: 80–3200 m/z, Scan rate: 1 spectrum s^{-1}, Nebulizer pressure: 25 psig, Capillary Voltage: 3500 V, Fragmentor: 50 V, Skimmer: 45 V, Dry gas temperature: 275 °C, Dry gas flow: 10 L min^{-1}, Sheath gas temperature: 350 °C, Sheath gas flow: 10 L min^{-1}. Mass calibration was performed on the day of measurement using an external standard. The mass accuracy of the measurement results is better than 5 ppm.

Chromatographic separation was carried out on a 1260 Infinity II HPLC system (Agilent GmbH, Waldbronn, Germany) with G7111B 1260 Quaternary Pump, G7129A 1260 Vial sampler, and G7116A 1260 Multicolumn Thermostat equipped with an Agilent EclipsePlus C18 RRHP (2.1 x 50 mm, 2.1 µm particle size) analytical column. Eluents were 98% H_2O with 2% ACN and 0.05% formic acid (Eluent A) and 2% H_2O with 98% ACN and 0.05% formic acid (Eluent B). The following gradient elution was applied for separation at flow rate of 200 µL min^{-1}: Starting at 10% B for 1 min, followed by a linear increase to 95% B at 10 min, maintaining 95% B until 30 min, before going back to 10% B at 33 min. The column was equilibrated at 10% B for 15 min before the next measurement. Injection volume was 2 µL. Data was recorded using Agilent MassHunter Workstation LC/MS software version 11.0 and data analysis was performed using Agilent MassHunter Workstation Qualitative Analysis software version 10.0.

MALDI ToF MS: The Autoflex MALDI TOF mass spectrometer by Bruker Daltonik GmbH (Fahrenheitstraße 4, 28359 Bremen, Germany) with a smartbeam ™II Nd:YAG laser (355 nm) was utilized. The image was measured in linear mode. 2-((2E)-3-(4-*tert*-butylphenyl)-2-methylprop-2-enylidene)malononitrile (DCTB) was used as a matrix.

2. Used Chemicals

Methanol [67-56-1] ROTISOLV®, ≥99%

Sulfuric acid [7664-93-9] Fisher Chemical, ≥95%

Nickel(II) sulfate heptahydrate [10101-98-1] Sigma-Aldrich, ≥99%

Sodium acetate [127-09-3] Acros Organics, >99%

Sodium hydroxide [1310-73-2] VWR, 98.8%

4-Propylcyclohexanone [40649-36-3] Sigma-Aldrich, ≥99.0%

Magnesium sulfate [7487-88-9] Thermo Scientific, 97%

3. General Procedures

3.1 Synthesis of 4-propylcyclohexanol from 4-propylcyclohexanone

An aqueous solution of $NaBH_4$ (0.826 mol, 2 H^- equivalents in 250 mL deionized water) was presented in a 1 L Erlenmeyer flask and rigorously stirred with a magnetic stirring cross (v_{mix} = 300 rpm, 30 mm stirring cross). 4-propylcyclohexanone (**1'**, 1,651 mol, 254 mL) was diluted in methanol (254:123, V:V, 4 M) and dropwise added to the aqueous solution (1 drop every 4 sec). After complete addition, the reaction mixture was stirred for another 20 h. The reaction progress was controlled via TLC (eluent was toluene, coloring agent: vanillin/sulfuric acid, R_f(**1'**) = 0.64, $R_f(B[OR]_4)$ = 0.28). Upon full conversion, the reaction mixture was acidified to pH 1–2 using diluted $H_2SO_{4(aq)}$. Afterwards, the mixture was alkalized again to pH 12 using 1 M $NaOH_{(aq)}$ to prevent boric acid from entering the organic phase during workup; instead tetrahydroxyborate forms and stays in the aqueous phase. Thereafter, a threefold liquid-liquid extraction using methyl *tert*-butyl ether was done, the organic fractions were combined, dried over $MgSO_4$ and the solvent was removed at reduced pressure. The product 4-propylcyclohexanol was isolated with a yield of 96%.

3.2 Procedure and results for batch-type electrolysis in first *DoE* screening

Assembly of the electrode stack: The electrode stack was assembled, first (Figure S1). Two PTFE hollow cylinders were initially pulled around two threaded rods, which are then both fixed on one side with one screw each, respectively. Next, a PTFE block is pulled above both PTFE rods as spacer to the screws and the first contacting plate was attached. Afterwards, a stainless-steel sheet, a contacting stripe to the next cathode on one rod and a PTFE spacer were subsequently added. Then, a nickel foam, its contacting stripe on the other rod and a spacer were stacked. Afterwards, the contacting stripe was pulled on the first rod, where a stainless-steel sheet was connected to. After that, the last contacting stripe was included, a spacer added, and the same procedure was repeated with the nickel foam. After the third cathode has been placed, one last spacer is added and the anode contacting stripe connected to its respective contacting plate. Lastly, another PTFE block is pulled above both PTFE rods and a screw ends the electrode stack from the other end.

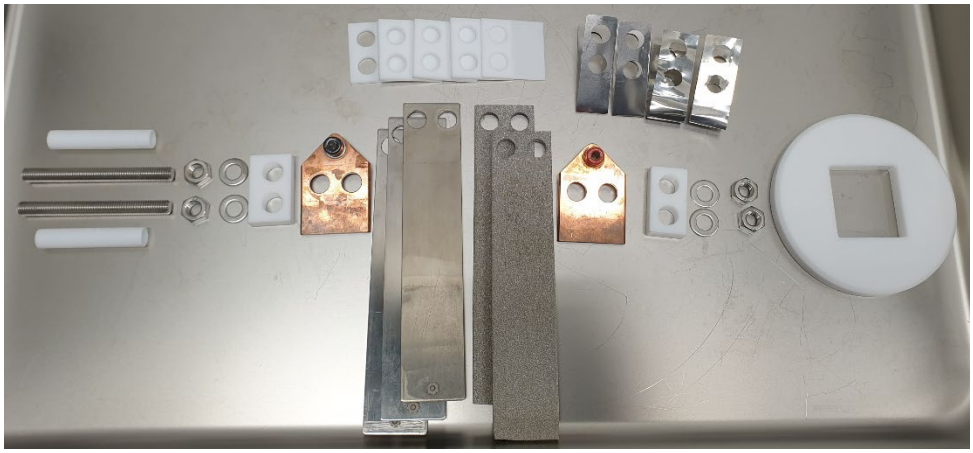

Figure S1. Photo of disassembled electrode stack. Top row: PTFE spacers and stainless-steel connections, main row (from left to right): threaded rod with PTFE hollow cylinder for isolation, nuts and shims, PTFE spacer for isolation, cathode side contact, three stainless-steel sheets (cathodes), two nickel foams (anodes), anode side contact, PTFE spacer, nuts and shims and electrode stack holder made of PTFE

Preparation of the activation solution: The activation solution was prepared in a bigger batch (e.g. 1 L), following a procedure known from literature[13,23], dissolving $NiSO_4 \cdot 7H_2O$ (100 mmol, 0.1 M) and $NaOAc \cdot 3H_2O$ (100 mmol, 0.1 M) in 1 L of deionized water. When NaOH (5 mmol, 5 mM) was dissolved, some flocculants were observed. Briggs et al. reported that those are $Ni(OH)_2$.[23] These flocculants do still enable a successful activation.

Activation process: The activation process follows a procedure developed in the Waldvogel group. 100 mL of the activation solution were presented in a beaker-type electrolysis cell by HWS with a magnetic stirring cross (stirring speed 300 rpm). The nickel foams in the electrode stack were first rinsed thoroughly with caustic soda (1 M). Once the caustic soda was not dripping any more, the electrode stack was connected to the power supply, inserted into the stirred activation solution and the activation process started with the tested parameter set. After the activation, the electrode stack was removed from the activation solution, disassembled and the anodes thoroughly rinsed with deionized water. The cathodes were additionally shortly immersed in diluted sulfuric acid (4.5 M), cleaned with deionized water again, dried and polished using sandpaper. Thereafter, the activated electrode set was reassembled, as described previously.

Reaction procedure: A cleaned and dried 100 mL beaker-type electrolysis cell by HWS was filled with the electrolyte caustic soda (1 M) and the substrate 4-propylcyclohexanol, according to the screening parameter. The mixing speed with a magnetic stirring cross as well as the heating circuit temperature were set, as stated in the respective reaction parameter set. Thereafter, the activated electrode stack was connected to the power supply and immersed in the reaction dispersion. After the respective charge was applied, the reaction mixture was collected and the setup, as well as electrode stack, thoroughly rinsed with caustic soda (1 M) and methyl *tert*-butyl ether (MTBE). All fractions were combined and extracted three times using MTBE (50 mL each) in a separating funnel. The organic fractions were combined, dried over $MgSO_4$ and the solvent evaporated and recovered. Meanwhile, the basic aqueous phase was acidified to pH 1–2 using sulfuric acid (4.5 M) and then extracted four times, using ethyl acetate (50 mL each). The organic fractions were combined, dried over $MgSO_4$ and the solvent evaporated. The remaining product mixture was weighed and analyzed via ^{13}C Inverse Gated NMR spectroscopy (600 MHz spectrometer) using 1,3,5-trimethoxybenzene (0.1 mmol) as internal standard and dimethoxysulfoxide-d_6 as deuterated solvent. For this screening, quantitative NMR yields were reported.

Results of first *DoE* screening: In the following table, the screening reactions are listed in rows, in the order they were performed. The screening parameters are listed in columns and the product yields given thereafter.

Table S1. Overview of reaction parameters for the first *DoE* screening. The experiments are listed in the run order with their seven tested parameters. In the last column, the quantitative ^{13}C Inverse Gated NMR yields of 3-propyladipic acid are displayed.

#reaction run order	c(1) / M	T / °C	v_{mix} / rpm	j_{rct} / mA cm^{-2}	Q_{rct} / F	j_{act} / mA cm^{-2}	Q_{act} / C cm^{-2}	Y(2) / %
1	0.5	40	200	8	7.5	6.5	0.5	5.1
2	0.5	40	200	8	7.5	6.5	0.5	6.3
3	0.5	40	200	6	7.5	3.5	10.5	5.0
4	0.5	40	200	6	7.5	3.5	10.5	8.3
5	0.3	40	500	6	7.5	6.5	10.5	14.2
6	0.5	40	500	6	6.5	6.5	0.5	31.6
7	0.3	40	500	8	7.5	3.5	0.5	8.5
8	0.3	40	500	6	7.5	6.5	10.5	10.4
9	0.5	40	500	6	6.5	6.5	0.5	23.4
10	0.4	50	350	7	7.0	5.0	5.5	14.7
11	0.4	50	350	7	7.0	5.0	5.5	16.8
12	0.3	60	200	8	7.5	3.5	10.5	14.7
13	0.3	60	200	6	7.5	6.5	0.5	18.7
14	0.3	60	200	8	7.5	3.5	10.5	8.5
15	0.5	60	500	6	7.5	3.5	0.5	34.8
16	0.3	60	500	8	6.5	6.5	0.5	29.2
17	0.5	60	200	6	6.5	6.5	10.5	19.8
18	0.3	60	500	6	6.5	3.5	10.5	26.4
19	0.5	60	500	8	7.5	6.5	10.5	9.0
20	0.5	60	200	6	6.5	6.5	10.5	16.9
21	0.3	40	200	8	6.5	6.5	10.5	5.4
22	0.3	40	200	8	6.5	6.5	10.5	5.9
23	0.3	40	200	6	6.5	3.5	0.5	5.7
24	0.3	40	200	6	6.5	3.5	0.5	6.1
25	0.5	40	500	8	6.5	3.5	10.5	20.9
26	0.5	40	500	8	6.5	3.5	10.5	20.5

27	0.5	60	200	8	6.5	3.5	0.5	7.3
28	0.5	60	200	8	6.5	3.5	0.5	11.0
29	0.3	60	200	6	7.5	6.5	0.5	9.1
30	0.3	40	500	8	7.5	3.5	0.5	6.9
31	0.3	60	500	6	6.5	3.5	10.5	22.6
32	0.5	60	500	8	7.5	6.5	10.5	20.1
33	0.5	60	500	6	7.5	3.5	0.5	14.2
34	0.3	60	500	8	6.5	6.5	0.5	8.2

3.3 Procedure and results for semi-flow electrolysis in second *DoE* screening

For this screening, the electrode stack preparation and activation were equal to the procedure described above.

Reaction procedure: One cleaned and dried 100 mL beaker-type electrolysis cell by HWS was connected with the tempering circuit and a 100 mL measuring cylinder was placed nearby, but lower than the reactor outlet. A Ritmo R033 dosing pump by *Fink Chem+Tec* was placed between the eductor outlet and the reactor inlet. The eductor sucked liquid from the reservoir via both inlet channels. From the reactor outlet, a tube connected it with the reservoir. The mixing speed with a magnetic stirring cross inside the electrolysis cell was set to 500 rpm.

Figure S2. Setup with semi-batch electrolysis cell, eductor, membrane pump and reservoir. Light yellow arrows indicate the flow direction of the reaction medium, while blue arrows show the direction of the heating circuit.

Results of second *DoE* screening: Below, the screening results are displayed in the run order of the reactions. The screening parameters and product yields are listed in columns.

Table S2. Overview of reaction parameters for the second *DoE* screening. The experiments are listed in the run order with their seven tested parameters. In the last column, the quantitative ^{13}C Inverse Gated NMR yields of 3-propyladipic acid (**2**) are displayed. *During the workup, ethyl acetate is hydrolyzed to acetic acid and ethanol, which formed ester species with the main product **2**. These ethyl ester yields (1–5% each) are incorporated in the given qNMR yield.

#reaction run order	*c*(1) / M	*Φ* / L h^{-1}	*Y*(2)* / %
1	0.4	2	27
2	0.7	30	29
3	0.7	2	22
4	0.55	16	35
5	0.4	30	33
6	0.55	16	17
7	0.4	30	30
8	0.7	5	29
9	0.7	30	17
10	0.4	2	12

Setting a significance level of α = 0,35, a R^2 value of only 34% resulted, with the Pareto chart listing the standardized effects in. This can be attributed to higher yield fluctuations within this DoE screening. Both, the substrate concentration, and the flow rate didn't have a statistically significant influence on the product yield, using the applied setup.

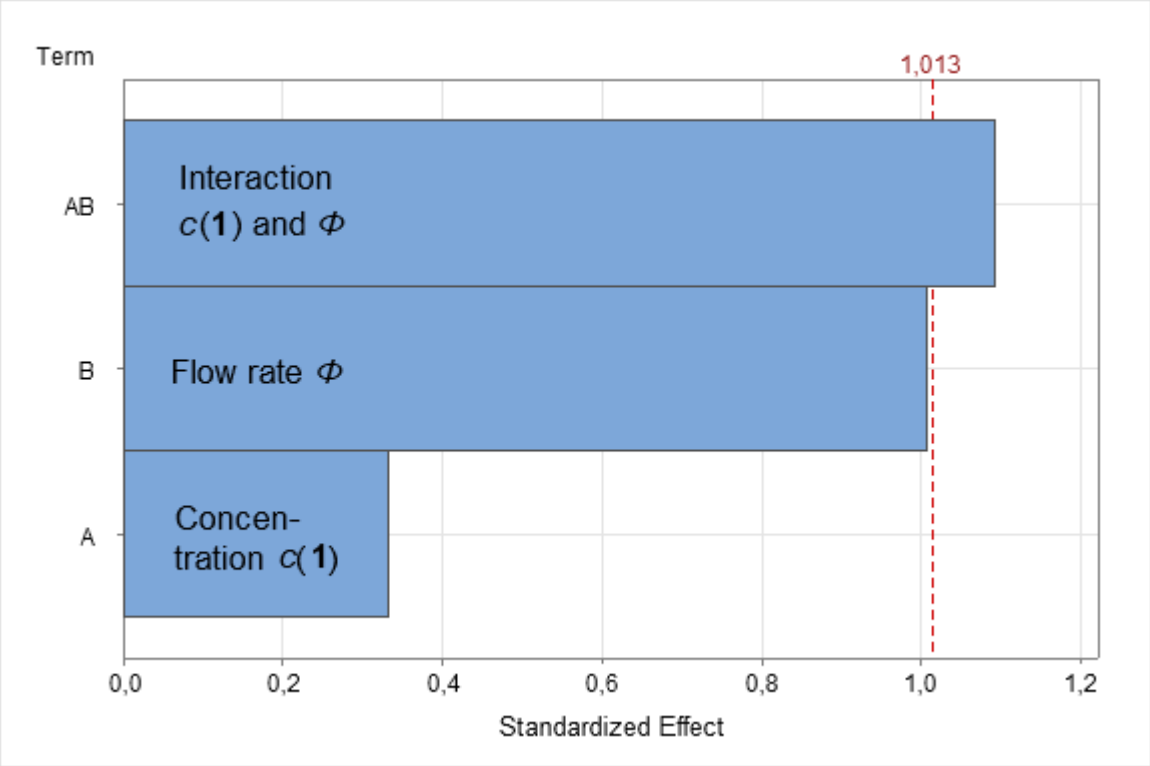

Figure S3. Pareto chart of the second *DoE* screening. The interaction of both tested parameters (flow rate *Φ* and concentration *c*(**1**)) is the only parameter above the significance level with a threshold for the significance level of α = 0.35.

3.4 Procedure of the reaction control experiments

Assembly and activation of the electrode stack: The large electrode stack, consisting of 5 nickel foams and 6 stainless-steel plates, was assembled in the same way as the small stack. The activation was performed in a 1.5 L batch-type cell.

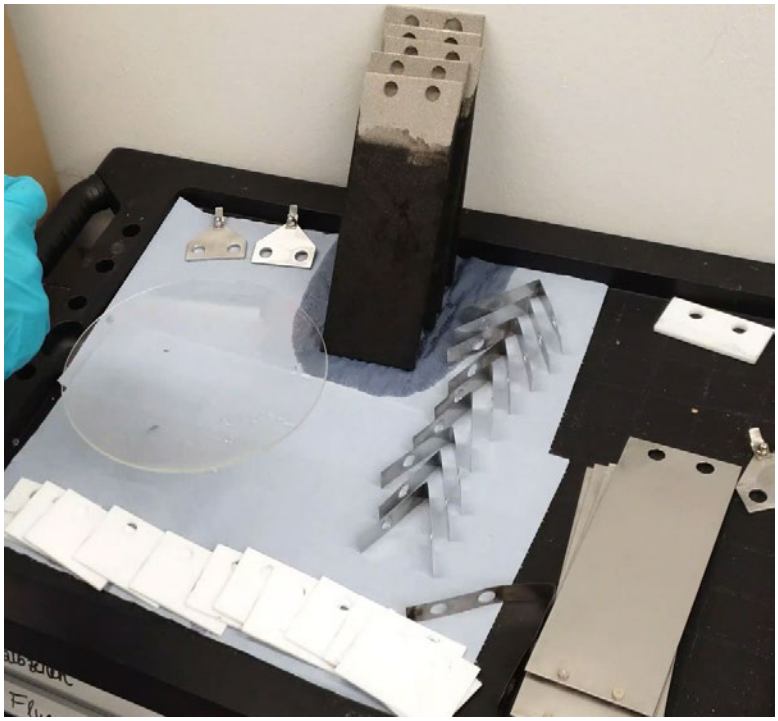

Figure S4. Photo of the large, disassembled electrode stack with activated nickel foam anodes (back), contacting pieces made of stainless-steel (center) and stainless-steel cathodes (right). In the foreground, the PTFE separators are strung. The contacting plates for the plus and minus pole are in in the background (left side). The threaded rod with PTFE hollow cylinder for isolation, nuts and shims are not displayed in the picture.

Reaction procedure: The general procedure was similar to the second *DoE*, apart from the approximately 15-times larger reactor cell, the multifold larger stirred reservoir with a heating jacket and the continuous substrate feeding, if applied. For feeding, a Masterflex EW-78018-14 peristaltic pump continuously fed equal amounts to the theoretically converted substrate into the reactor, keeping the concentration fairly stable. Since the first oxidation step from 4-propylcyclohexanol (**1**) is 4-propylcyclohexanone (**1'**), and for availability reasons, the kinetic investigations of its oxidation to 3-propyladipic acid were done with **1'** as the substrate.

Figure S5. Exemplary image of the electrolyte for a V_{tot} = 13 L reaction. 11.6 L caustic soda (1 M) and 1.4 L of **1'** are inserted into the reaction setup.

For the purpose of kinetic investigations, samples of (2.00±0.05) mL were retrieved from the reaction mixture at the outlet of the reactor using a syringe. The samples were acidified with 4.5 m $H_2SO_{4(aq)}$ to pH 1–2. Then, a liquid-liquid extraction with ethyl acetate (4 x 2 mL) was performed. The organic fractions were combined, dried over $MgSO_4$ and the solvent evaporated at reduced pressure. 1,3,5-Trimethoxybenzene as internal NMR standard was weighted into the product mixture and DMSO-d_6 was added as solvent. ^{13}C Inverse Gated NMR analysis was performed.

4. Synthesis of 3-propyladipic acid

3-Propyladipic acid (2)

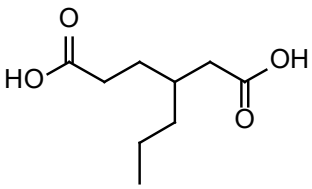

2

2 was electrochemically synthesized from 4-propylcyclohexanol using the procedure above. It was isolated after liquid-liquid extractions of i) the basic aqueous conditions using methyl *tert*-butyl ether and ii) the acidified aqueous medium using ethyl acetate including solvent removal; followed by vacuum distillation and recrystallization in *n*-heptane. **2** was obtained as colorless to light yellow crystals (Figure S6).

Figure S6. Isolated **2** in the form of colorless crystals.

^{1}H NMR (600 MHz, DMSO-d6): δ [ppm] = 12.05 (s, 0H), 2.19 (t, *J* = 7.9 Hz, 2H), 2.16 – 2.08 (m, 2H), 1.75 (hept, *J* = 6.5 Hz, 1H), 1.57 – 1.42 (m, 2H), 1.30 – 1.15 (m, 4H), 0.84 (t, *J* = 6.9 Hz, 3H).

^{13}C NMR (151 MHz, DMSO-d6): δ [ppm] = 174.64, 174.16, 38.41, 35.38, 33.63, 31.07, 28.50, 19.11, 14.23.

Melting point: (44.3–45.5) °C

HRMS (ESI+) m/z: calculated for $C_9H_{16}O_4$ - H^+ 187.0975 [*M*-H^+], found 187.0978

5. Spectra

<u>Distillation residue of 3-propyladipic acid product mixture (MALDI-ToF MS)</u>

The distillation setup with a Vigreux column for distillation with higher purity, a distillation bridge and a Schlenk tube as product receiving flask was installed. The Schlenk tube was frozen with liquid nitrogen to prevent product from releasing through the applied pressure of *P* = (10^{-2}–1.5) mbar. At an oil bath temperature of 190 °C, **2** was detected as the only compound, according to ^{1}H and ^{13}C NMR analyses. Above 220 °C, the Vigreux column was removed to distill remaining **2**, which didn't work quantitatively. In NMR analyses of the distillation residue, only **2** was visible, but the residue was a black, sticky solid. Therefore, a MALDI-ToF MS analysis (Figure S7) of the product mixture was performed, revealing molecular weights of more than 2000 g mol^{-1}.

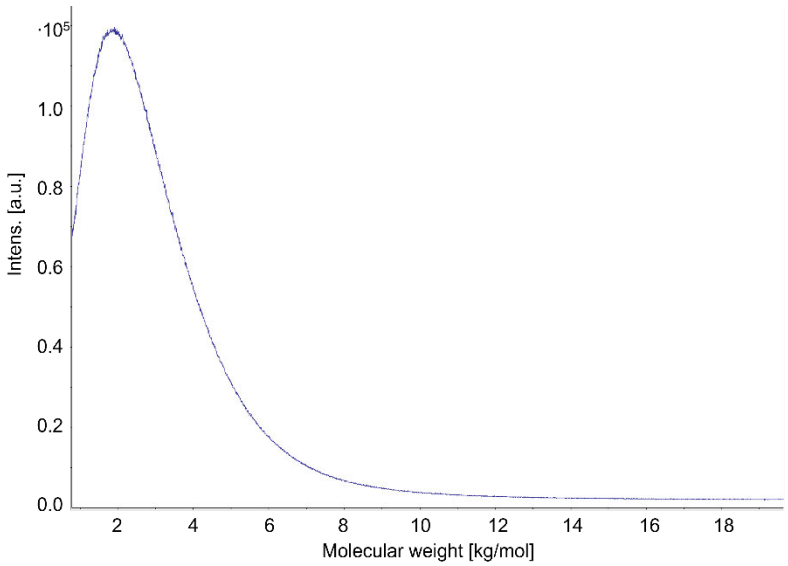

Figure S7. MALDI-ToF MS spectrum of the distillation residue after separating a product mixture including 3-propyladipic acid. Measuring settings: linear mode and DCTB as a matrix.

3-Propyladipic acid (^{1}H NMR spectrum)

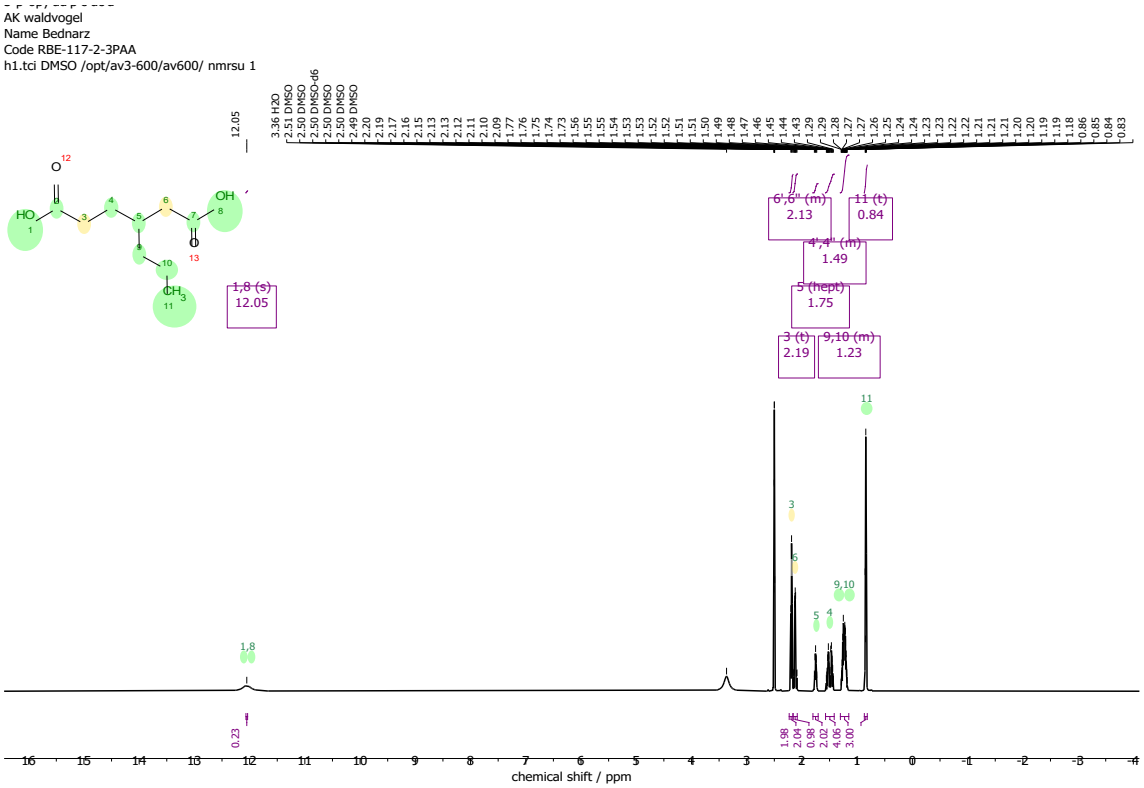

Figure S8. ^{1}H NMR spectrum (600 MHz, DMSO-d6) of purified **2**.

3-Propyladipic acid (^{13}C Inverse Gated NMR spectrum)

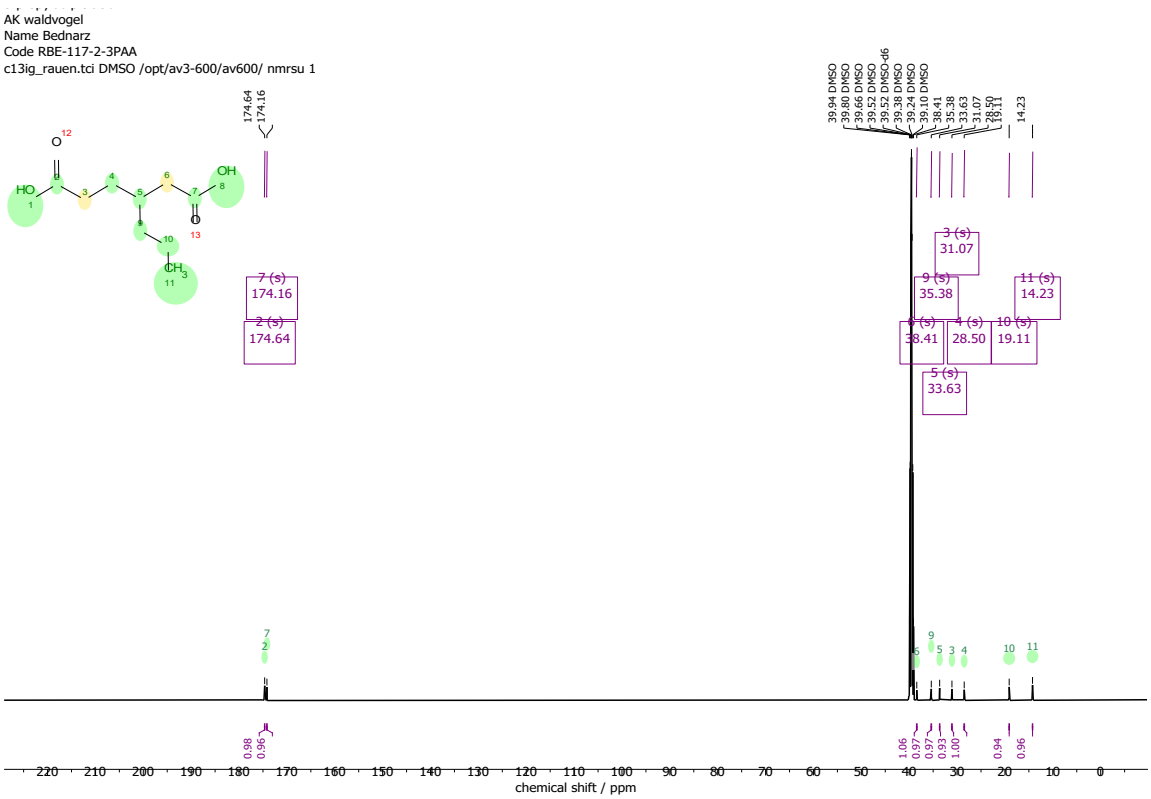

Figure S9. ^{13}C Inverse Gated NMR spectrum (151 MHz, DMSO-d6) of purified **2**.

3-Propyladipic acid (^{1}H, ^{1}H COSY NMR spectrum)

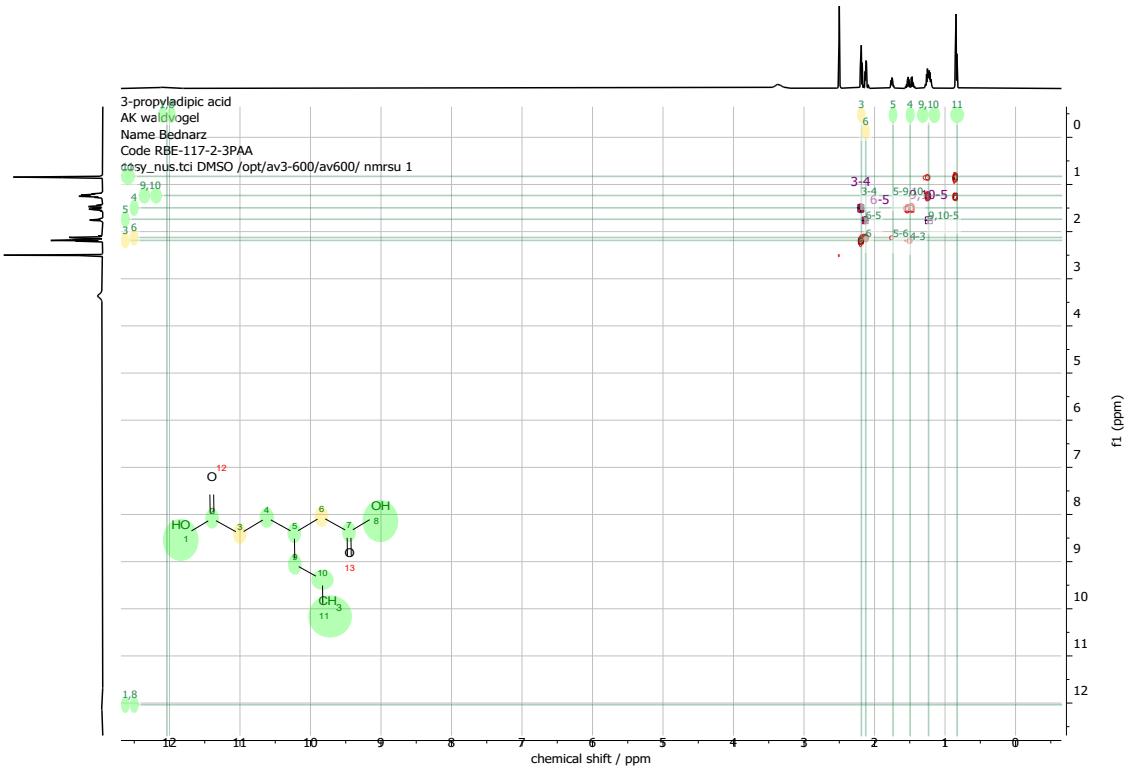

Figure S10. ^{1}H, ^{1}H COSY NMR spectrum (600 MHz, DMSO-d6) of purified **2**.

3-Propyladipic acid (^{1}H, ^{13}C HSQC NMR spectrum)

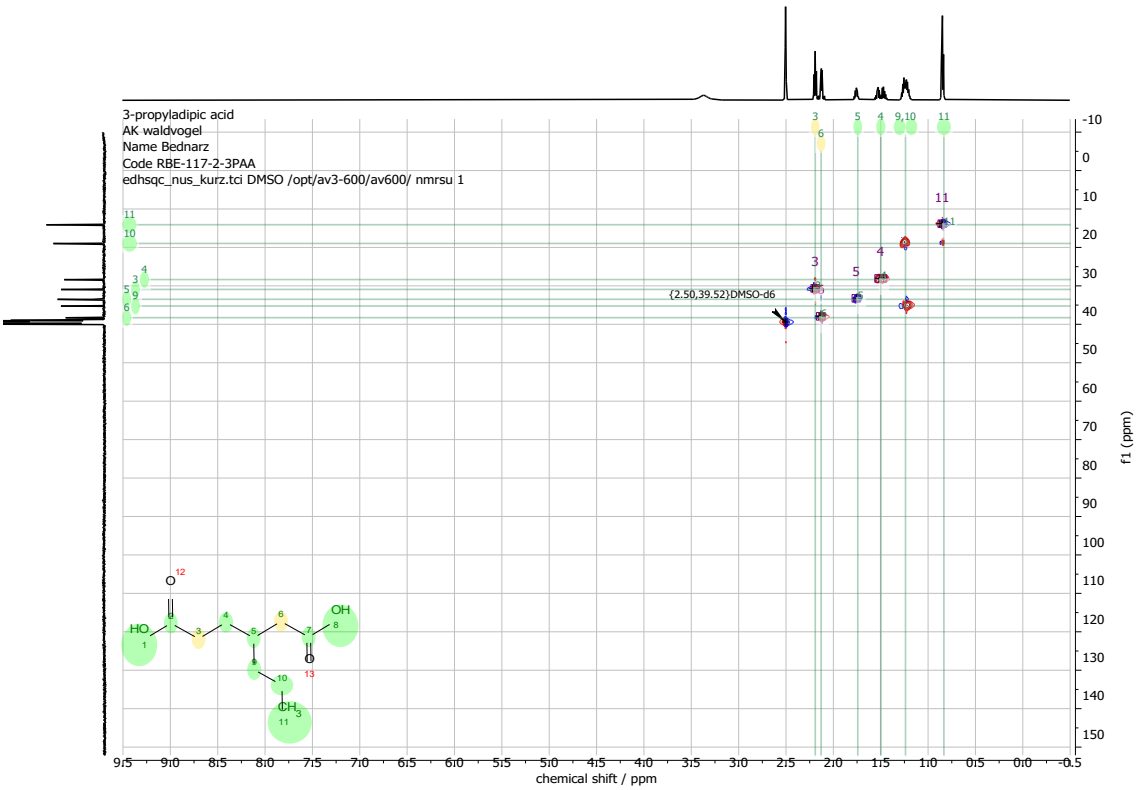

Figure S11. ^{1}H, ^{13}C HSQC NMR spectrum (600 MHz, DMSO-d6) of purified **2**.

3-Propyladipic acid (^{1}H, ^{13}C HMQC NMR spectrum)

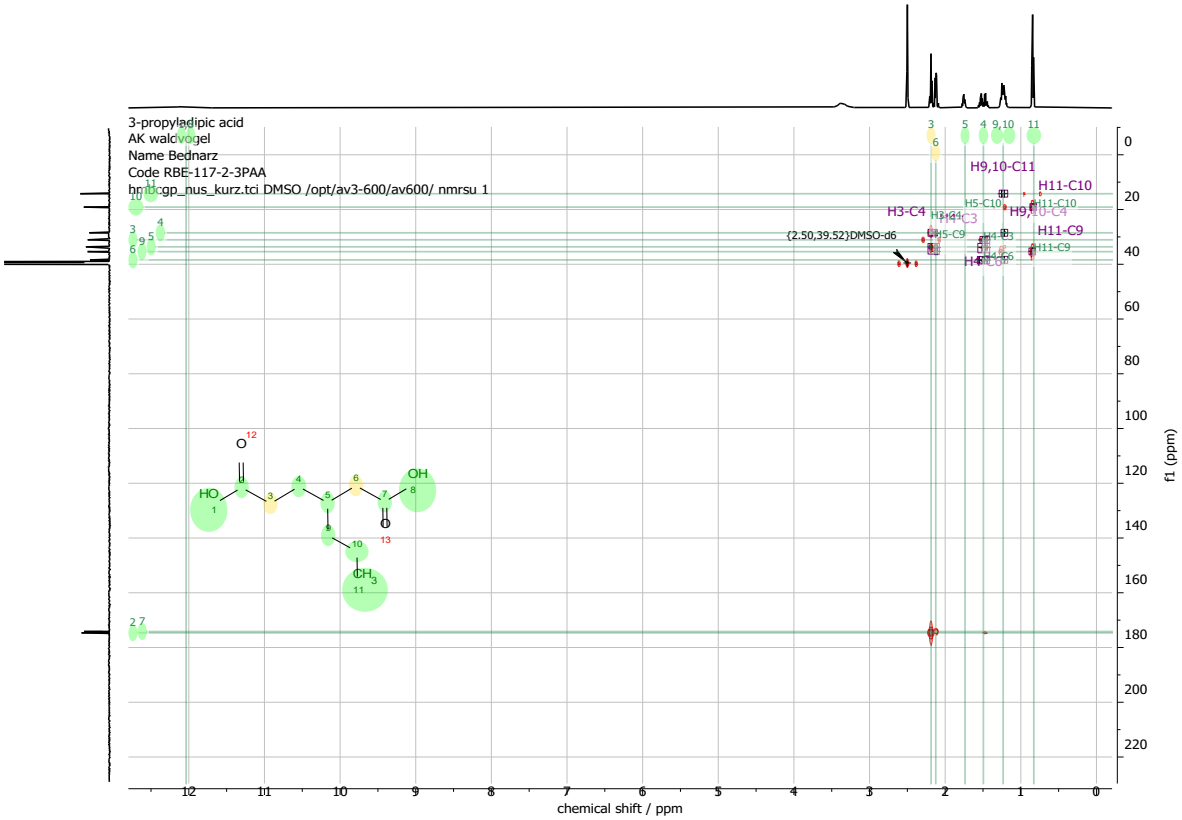

Figure S12. ^{1}H, ^{13}C HMQC NMR spectrum (600 MHz, DMSO-d6) of purified **2**.

Reaction control experiment for 3-propyladipic acid synthesis from 4-propylcyclohexanol (stack of ^{13}C Inverse Gated NMR spectra in the applied charge from 0 to 8.5 *F*)

In the following Figure S13, 30 ^{13}C Inverse Gated spectra taken during one electrochemical oxidation of 4-propylcyclohexanol were taken. The formation of several components, e.g. 4-propylcyclohexanone, was observed. Towards the end of the applied charge range, several products are detectable.

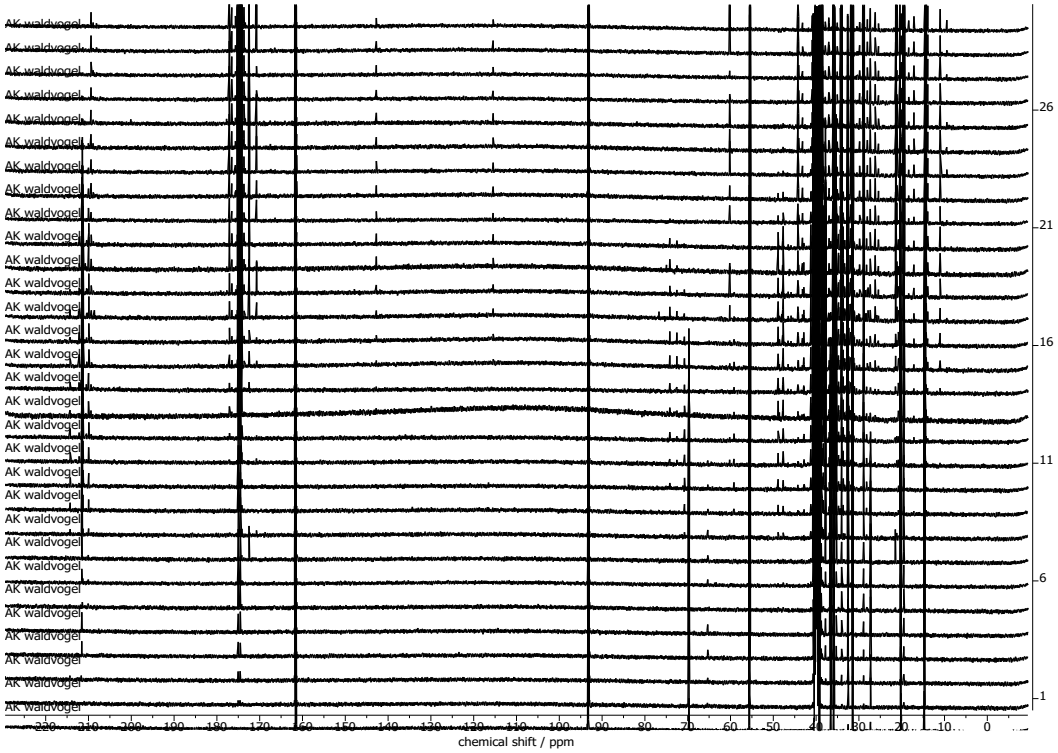

Figure S13. Stack of ^{13}C Inverse Gated spectra (151 MHz, DMSO-d6) of acidified and extracted reaction mixture samples with 1,3,5-trimethoxybenzene as internal standard.

6. References

[13] H.-J. Schäfer, J. Kaulen, *Tetrahedron* **1982**, *38*, 3299–3308.
[23] G. W. D. Briggs, E. Jones, W. F. K. Wynne-Jones, *Trans. Faraday Soc.* **1955**, *51*, 1433–1442.
[24] W. LF. Armarego, C. L. L. Chai, *Purification of Laboratory Chemicals*, Elsevier, Amsterdam, **2013**.

Supplementary data

Sun-powered electrosynthesis: assessing grid stabilization and the impact of direct coupling

Pilar Jiménez-Meneses[a]‡, Roland J.-R. Bednarz[b]‡, Vicente Montiel[a], Siegfried R. Waldvogel[b,c,]*, Roberto Gómez[a,]*

‡ These authors contributed equally to this work

[a]*Institut Universitari d'Electroquímica i Departament de Química Física - Universitat d'Alacant, Apartat 99, E-03080 Alicante (Spain). E-mail: roberto.gomez@ua.es*

[b]*Department of Chemistry – Johannes Gutenberg University, Duesbergweg 10–14, 55128 Mainz, Germany. E-mail: waldvogel@uni-mainz.de*

[c]*Institute of Biological and Chemical Systems – Functional Molecular Systems (IBCS-FMS) Hermann-von-Helmholtz-Platz 1, 76344 Eggenstein-Leopoldshafen, Germany*

*Corresponding authors. Emails: roberto.gomez@ua.es (R. Gómez); waldvogel@uni-mainz.de (S.R. Waldvogel)

Contents

1. Additional experimental details, materials, and methods

All reagents were used in analytical or sufficiently pure grades. Standard conditions were applied for all reactions, unless stated otherwise. All electrode materials are commercially available: Stainless steel (1.4571) plates and Recemat® nickel foam (RCM-Ni4753.05, average pore diameter: 0.4 mm). The electrodes were kept separate by PTFE spacers (3-mm thickness). Electrodes of equal polarity were connected by stainless-steel sheets. The workshop of the university of Mainz milled the electrodes and spacers in the desired size. As a galvanostat, an Origalys OGF500 with a maximum power output of 0.5 A and ±15 V was utilized for all reactions. The reaction mixture was pumped with a LabN6 Peristaltic Pump with a YZ1515x PPS pump head and using Norprene chemical tubing (ID 6.4 mm, OD 9.6 mm) from the tempered reservoir and the reactor. Zerodis Store was the supplier of the eductor piece. Both reservoir and reactor were kept hot with a heating circuit, powered by a thermostat, which was designed by the workshop of the University of Alicante. For the coupling experiments, a silicon polycrystalline solar panel was acquired from ATERSA (Solar panel 25W 12V –ESPMC25),

NMR spectroscopy: A Bruker AVANCE III HD (Bruker, probe head: PA BBO 500S2 BBF) NMR spectrometer was utilized for ^{13}C Inverse Gated (126 MHz) NMR measurements at 25 °C. All chemical shifts (δ) are reported in parts per million (ppm). The spectra (like **Fig. S1**) were analyzed, starting with automatic baseline and phase correction, using the software MestReNova. Next, the central signal for DMSO-d6 (δ = 39.52 ppm) was used as a solvent reference. Afterward, the aliphatic signal of the standard 1,3,5-trimethoxybenzene (δ = (55.4±0.02) ppm) was integrated and set to 300 (according to the carbons present in the molecule). Lastly, all peaks, known from literature (R. J.-R. Bednarz, Jiménez-Meneses et al., 2023), were integrated and set in relation to the weight of the standard (0.100 mmol).

2. Used chemicals

Nickel(II) sulfate hexahydrate [10101-97-0] Themo Scientific, purity

Sodium acetate [127-09-3] Acros Organics, >99%

Sodium hydroxide [1310-73-2] VWR, 99.1%

4-Propylcyclohexanol [52204-65-6] CM Fine-Chemicals, ≥98%

Sodium sulfate anhydrous [7757-82-6] VWR, 99%

Sulfuric acid [7664-93-9] Honeywell, 97%

3. Structure of some possible byproducts.

In previous NMR studies (R. J.-R. Bednarz, Gold et al., 2023; R. J.-R. Bednarz, Jiménez-Meneses et al., 2023), the following electrochemical byproducts were identified. They could also be shown in the NMR analyses for all reactions reported here.

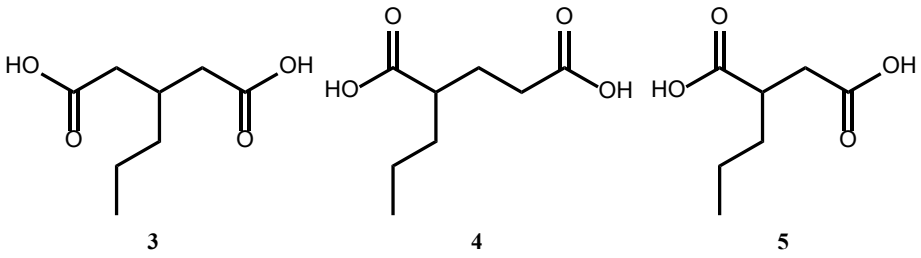

3 **4** **5**

Fig. S1. Literature-known byproducts 3-propylglutaric acid (3), 2-propylglutaric acid (4) and propylsuccinic acid (5).

4. qNMR yield for the main product and byproducts.

Table S1 shows the quantitative NMR yields of the known byproducts for this reaction.

Table S1. Overview of qNMR yield for the main product 2 and the byproducts 3–5.

Reaction	Y_{qNMR}(**2**) / %	Y_{qNMR}(**3**) / %	Y_{qNMR}(**4**) / %	Y_{qNMR}(**5**) / %
Conventional power supply	27	2	2	0.9
PV panel → continuous mode	11	2	1.1	1.0
PV panel → non-continuous mode	26	3	2	1.4

5. Synthesis, schematic workup for purification, and analysis of 3-propyladipic acid (**2**).

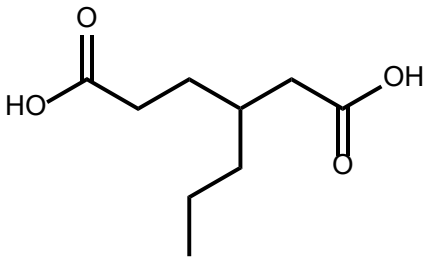

2

2 was synthesized in an electrochemical undivided semi-flow setup, as described above. It was coupled to either a power supply or a PV panel. The alkaline product mixture was subjected to liquid-liquid extraction using methyl *tert*-butyl ether to separate uncharged substances, e.g., the substrate or intermediate species. The acidified aqueous solution was extracted using ethyl acetate. After solvent removal, the product mixture was analyzed using ^{13}C Inverse Gated NMR spectroscopy.

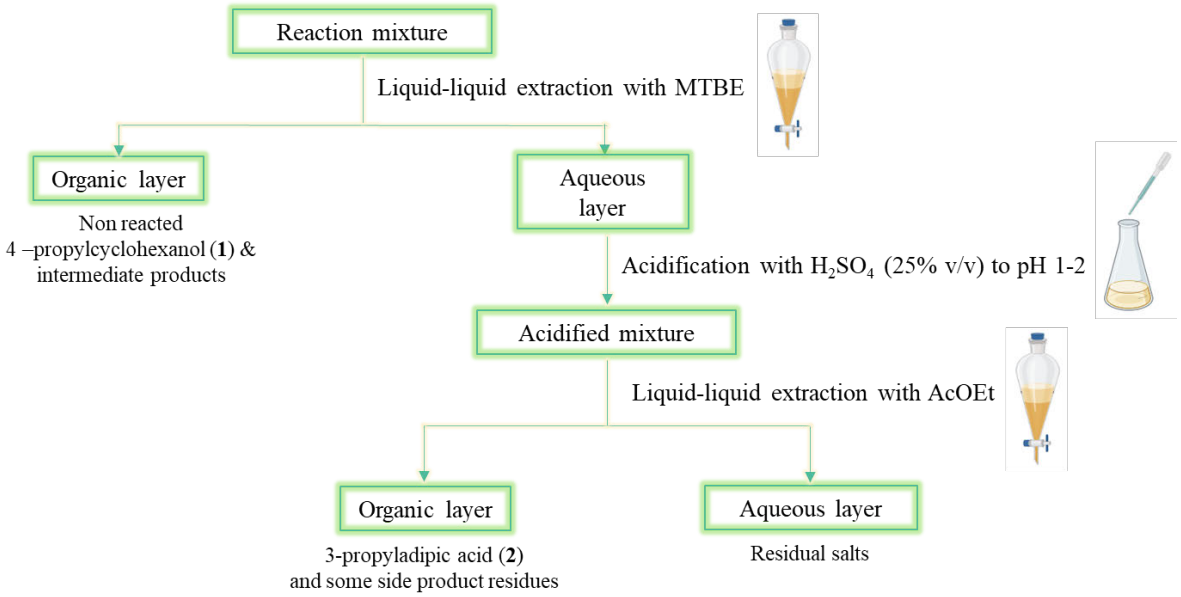

Fig. S2. Schematic workup for purification of the final product 3-propyladipic acid (**2**).

6. NMR spectra of 3-propyladipic acid (^{13}C Inverse Gated spectrum) in the product mixture when using a conventional power supply.

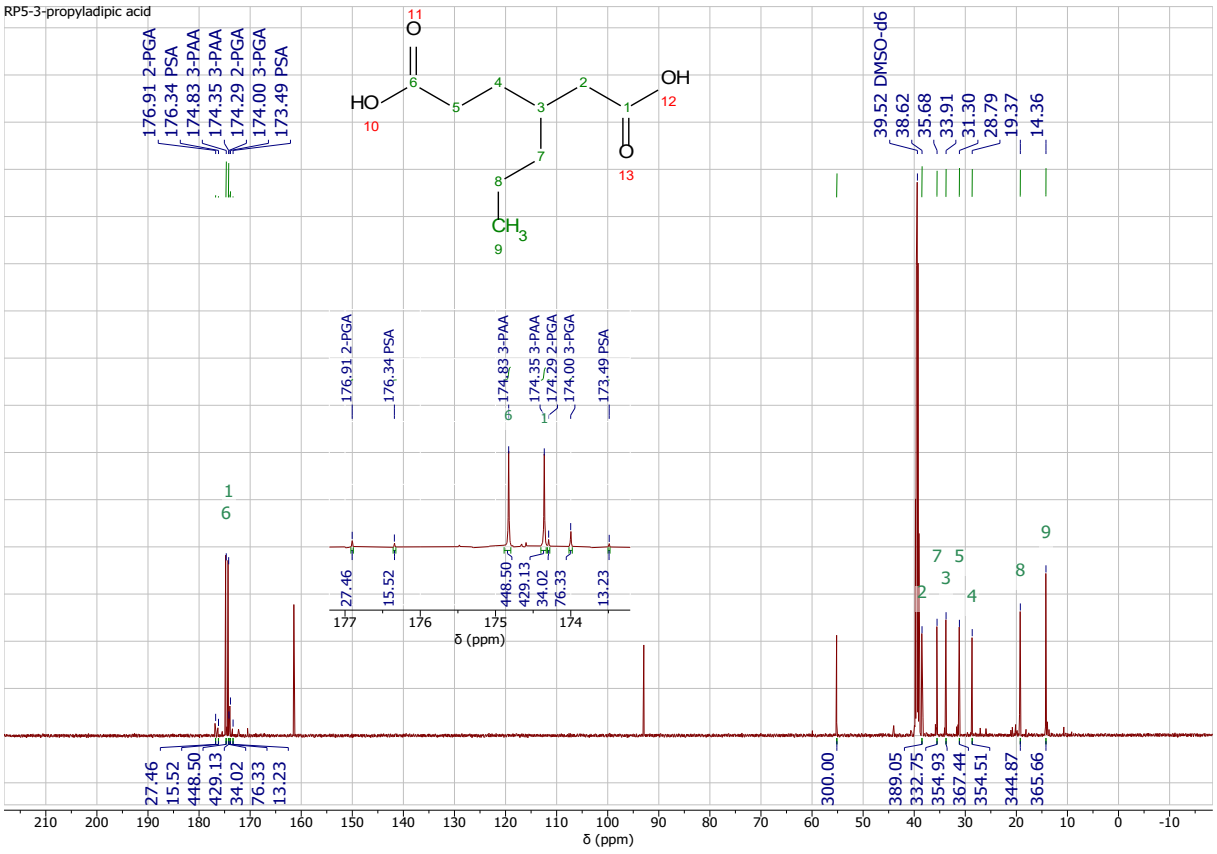

Fig. S3. ^{13}C Inverse Gated NMR spectrum (126 MHz, DMSO-d6) of **2** in the product mixture when using a conventional power supply.

Supporting Information

Robust and self-cleaning electrochemical production of periodate

Camila M. Kisukuri,[+[a]] Roland Jan-Reiner Bednarz,[+[a]] Christopher Kampf,[[a]] Sebastian Arndt,[[a]] and Siegfried R. Waldvogel*[[a]]

[a] Dr. C. M. Kisukuri, R. J.-R. Bednarz, Dr. C. Kampf, Dr. S. Arndt, and Prof. Dr. S. R. Waldvogel
Department of Chemistry
Johannes Gutenberg University Mainz
Duesbergweg 10-14, 55128, Mainz (Germany)
E-mail: waldvogel@uni-mainz.de

Table of Contents

1. General Information

All reagents were used in analytical or sufficiently pure grades. Solvents were purified by standard methods.[1]

Electrochemical reactions were carried out at boron-doped diamond (BDD) anodes. The BDD electrodes were obtained in DIACHEM© quality from CONDIAS GmbH, Itzehoe, Germany. The BDD had a 15 μm diamond layer on silicon support. Stainless steel of the type EN1.4401; AISI/ASTM was used as cathodes. Nafion™ from DuPont was used as membrane. A galvanostate HMP4040 from Rhode&Schwarz was used.

UV-*Vis* was performed on a Shimadzu UV-3600 Plus UV-VIS-NIR Spectrophotometer (Shimadzu, Japan) equipped with high performance R928 photomultiplier detector. A 1 cm quartz cuvette was used to make the measurements. The samples collected (2 mL) from the reaction were filtered (glass fritted disc Buchner filter funnel) and measured without additional procedures.

Gas chromatography was performed on a Shimadzu GC-2025 (Shimadzu, Japan) using a HP-5 column (Agilent Technologies, Santa Clara, California; length: 30 m, inner diameter: 0.25 mm, film: 0.25 µm, carrier gas: hydrogen). GC-MS measurements were carried out on a Shimadzu GC-2010 (Shimadzu, Japan) using a HP-1 column (Agilent Technologies, Santa Clara, California; length: 30 m, inner diameter: 0.25 mm, film: 0.25 µm, carrier gas: helium). The chromatograph was coupled to a mass spectrometer Shimadzu GC-MS-QP2010. To prepare the samples, two 2 mL of the solution were collected from the reaction, this was filtered and then neutralized using a solution of $NaHSO_4$ (5 M) to pH 6. Then an extraction with ethyl acetate (2 mL) was carried out. This organic solution was analysed by GC.

Liquid chromatography photodiode array analysis was performed by using a DUGA-20A3 device from Shimadzu, which was equipped with a C18 column from Knauer (Eurospher II, 100-5 C18, 150x4 mm). The column was conditioned to 25 °C and the flow rate was set to 1 mL/min. The aqueous eluent was buffered with formic acid (0.8 mL/2.5 L) and stabilized with Acetone (5 vol%). To prepare the samples, two 2 mL of the solution were collected from the reaction, this was filtered and then neutralized using a solution of $NaHSO_4$ (5 M) to pH 6. Then the solution was filtrated. This organic solution was analysed by liquid chromatography.

NMR spectra of ^{1}H (400 MHz) and $^{13}C\{1H\}$ (101 MHz) were recorded at 23 °C by Bruker Avance II 400 (400 MHz, 5 mm BBFO-SmartProbe with z gradient and ATM, SampleXPress

60 sample changer, Analytische Messtechnik, Karlsruhe, Germany). Chemical shifts (δ) are reported in parts per million (ppm) relative to traces of $CHCl_3$ (7.26 ppm in 1H, 77.16 ppm in $^{13}C\{1H\}$).[2]

High-resolution mass spectra were obtained using a G6545A Q-ToF (Agilent GmbH, Waldbronn, Germany) with dual AJS electrospray ion source (Dual AJS ESI). MS parameters were as follows: Mass rage: 80 – 3200 m/z, Scan rate: 1 spectrum s^{-1}, Nebulizer pressure: 25 psig, Capillary Voltage: 3500 V, Fragmentor: 50 V, Skimmer: 45 V, Dry gas temperature: 275°C, Dry gas flow: 10 L min^{-1}, Sheath gas temperature: 350°C, Sheath gas flow: 10 L min^{-1}. Mass calibration was performed on the day of measurement using an external standard. The mass accuracy of the measurement results is better than 5 ppm. Chromatographic separation was carried out on a 1260 Infinity II HPLC system (Agilent GmbH, Waldbronn, Germany) with G7111B 1260 Quaternary Pump, G7129A 1260 Vialsampler, and G7116A 1260 Multicolumn Thermostat equipped with an Agilent EclipsePlus C18 RRHP (2.1 x 50 mm, 2.1 µm particle size) analytical column. Eluents were 98% H_2O with 2% ACN and 0.05% formic acid (Eluent A) and 2% H_2O with 98% ACN and 0.05% formic acid (Eluent B). The following gradient elution was applied for separation at flow rate of 200 µL min^{-1}: Starting at 10% B for 1 min, followed by a linear increase to 95% B at 10 min, maintaining 95% B until 30 min, before going back to 10% B at 33 min. The column was equilibrated at 10% B for 15 min before the next measurement. Injection volume was 2 µL. Data was recorded using Agilent MassHunter Workstation LC/MS software version 11.0 and data analysis was performed using Agilent MassHunter Workstation Qualitative Analysis software version 10.0.

2. Used Chemicals

Sodium iodate [7681-55-2] Alfa Aesar, 99%
Sodium periodate [7790-28-5] Fisher Scientific, 99%
Sodium hydroxide [1310-73-2] Honeywell, Pellets, ≥98%
Sodium bisulfate monohydrate [10034-88-5] Acros Organics, 99%
Sudan I [842-07-9] Sigma-Aldrich, ≥95%
Diamine green [4335-09-5] Merck, 99%
Brilliant black [2519-30-4] Merck, ≥95%
Fluorescein [2321-07-5] Fluka Analytical, ≥98%
Methylene blue hydrate [122965-43-9] Acros Organics, 96%
Naphthol green [19381-50-1] Sigma-Aldrich, ≥97%
Rose Bengal [632-69-9] Sigma-Aldrich, 92%

Perylenetetracarboxylic dianhydride (PTCDA) [128-69-8] BASF (donation)
3,5-Diiodo-4-pyridone-1-acetic acid (diodrast) [101-29-1] Alfa Aesar, 99%
Diatrizoic acid (Diatrizoate) [117-96-4] TCI, ≥98%
5-[Acetyl(2,3-dihydroxypropyl)amino]-N,N'-bis(2,3-dihydroxypropyl)-2,4,6-triiodoisophthalamide (Iohexol) [66108-95-0] ABCR GmbH, 99%
5-Fluorouracil [51-21-8] Alfa Aesar, 99%
Diiodomethane [75-11-6] Sigma-Aldrich, 99%
Methyl 4-iodobenzoate [619-44-3] Sigma-Aldrich, 97%
2-Iodobenzoic acid [88-67-5] Acros Organics, 98%
3-Iodobenzoic acid [618-51-9] Acros Organics, 98%
2-Iodoaniline [615-43-0] Sigma-Aldrich, 98%
Dimethyl 5-iodoisophthalate [51839-15-7] prepared from own research laboratory
2,4,6-Triiodophenol [609-23-4] Sigma-Aldrich, ≥97%

3. Calibrations to analysis of *para*-periodate

The liquid chromatography photodiode array (LC-PDA) was used to verify the purity of the *para*-periodate produced. A similar method was previously demonstrated by our group.[2]

4. Procedure for flow electrolysis

A flow-electrolysis cell was divided through Nafion, tethered with 0.5 mm Teflon spacers, and connected with two Ritmo R033 pumps from Fink. BDD was used as anode and stainless steel (EN1.4401; AISI/ASTM) was used as cathode. Caustic soda (4 M, 200 mL) was circulated through the cathodic compartment, while NaI in caustic soda (0.21 M) was pumped through the anodic compartment. The anolyte was collected after electrolysis in test tubes, acidified with aqueous $NaHSO_4$ (5 M), diluted with water and was analyzed by LC-PDA. After all the experiments, no damage was observed in the membrane.

5. General setup

Electrolysis cells were manufactured in the workshop of the chemistry department of the Johannes Gutenberg University Mainz and are commercially available as parts of the IKA Screening System at IKA®-Werke GmbH&CO.KG, Staufen, Germany. The IKA company also sells the 4x12 cm^2 flow electrolysis cell as ElectraSyn Flow device. The stainless-steel flow electrolysis cell was purchased from CONDIAS GmbH, Itzehoe, Germany.

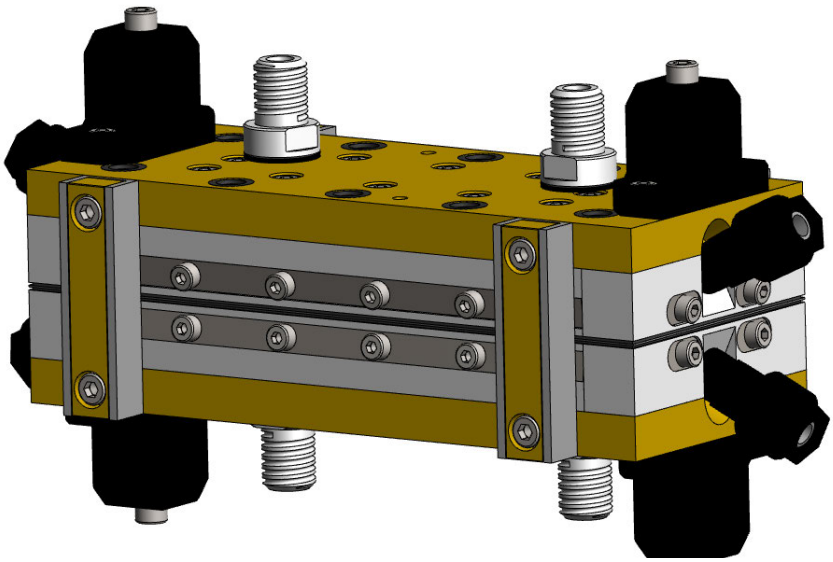

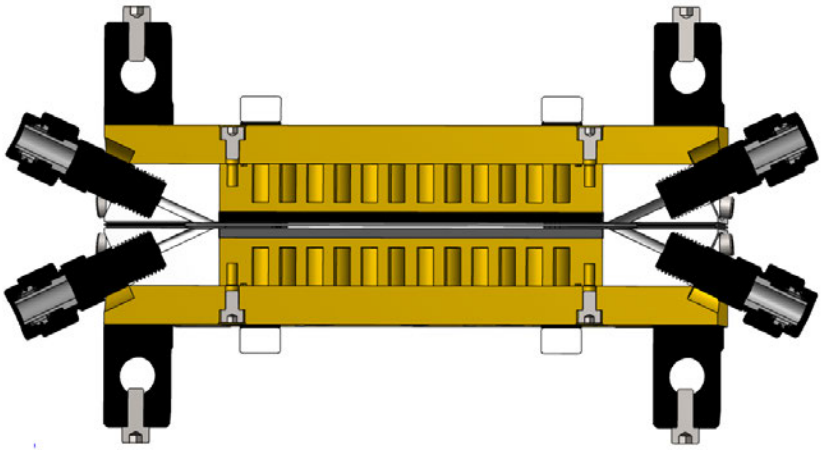

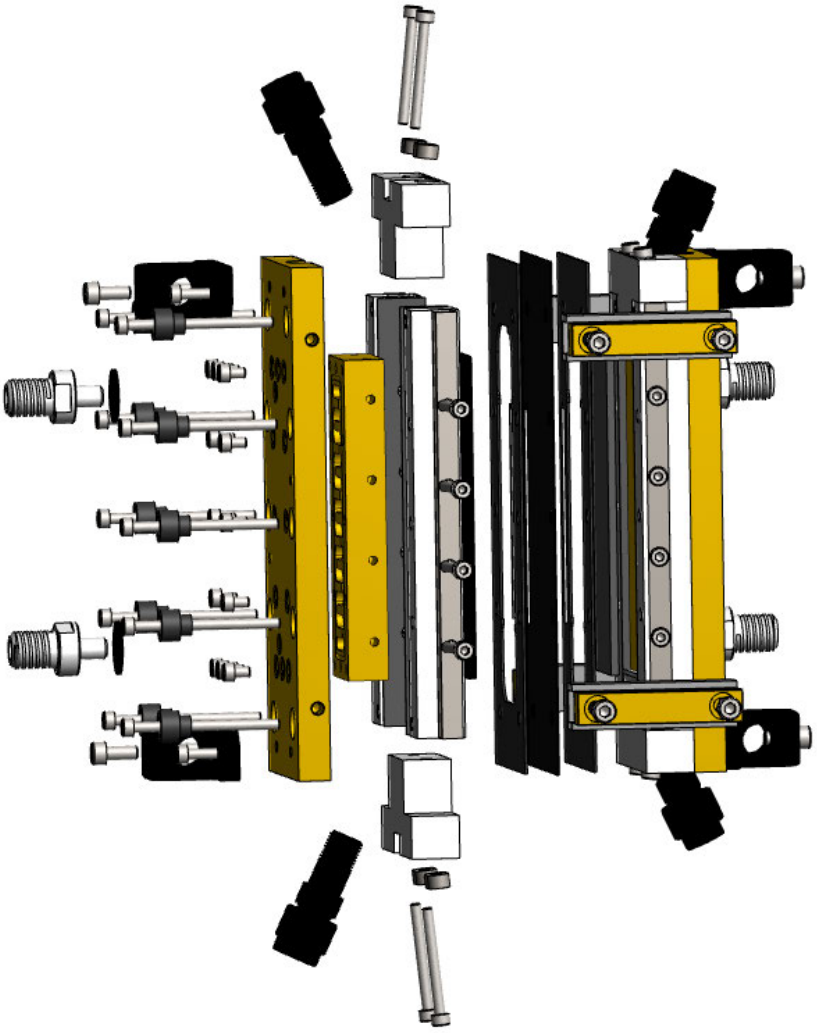

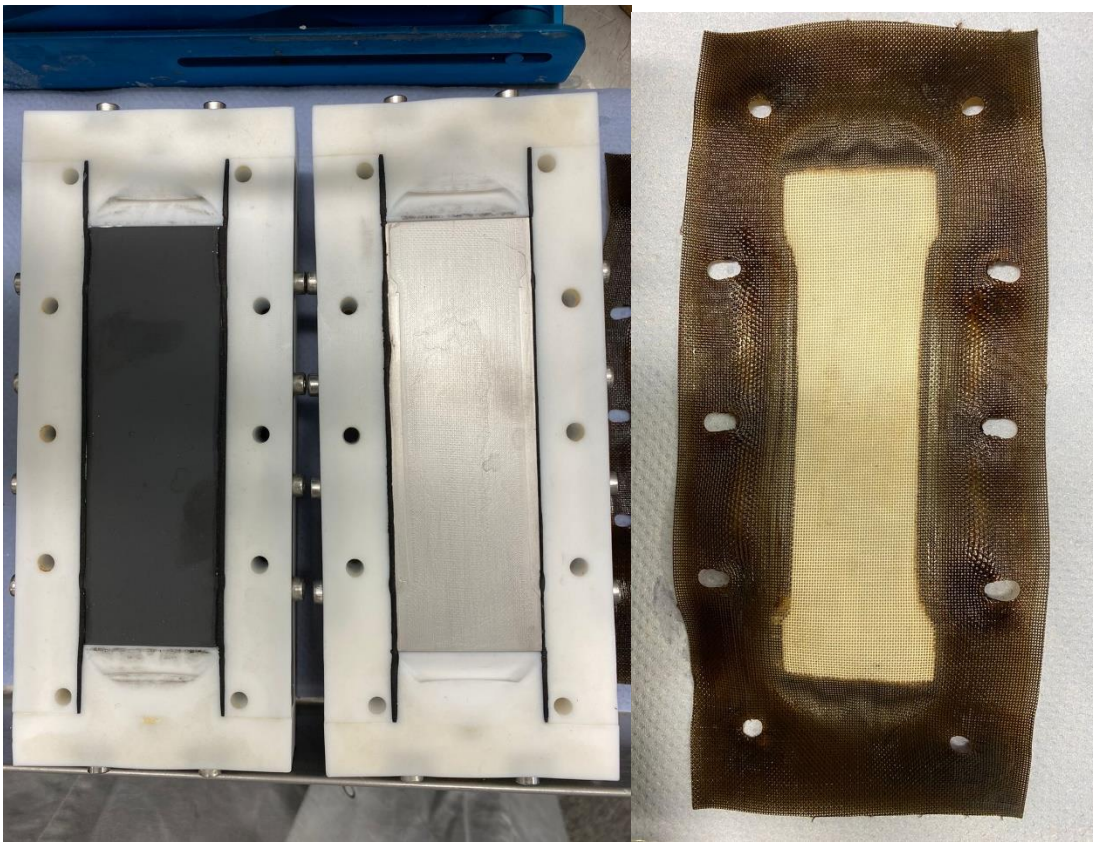

Figure S1. Divided flow cell with 4x12 cm^2 electrode surfaces.[3,4] Animations of assembled flow-electrolysis cell (top), intersection (middle), explosion diagram (middle) using the software SolidWorks, and picture of half-cells (bottom). Real photo of the dissembled cell and membrane used.

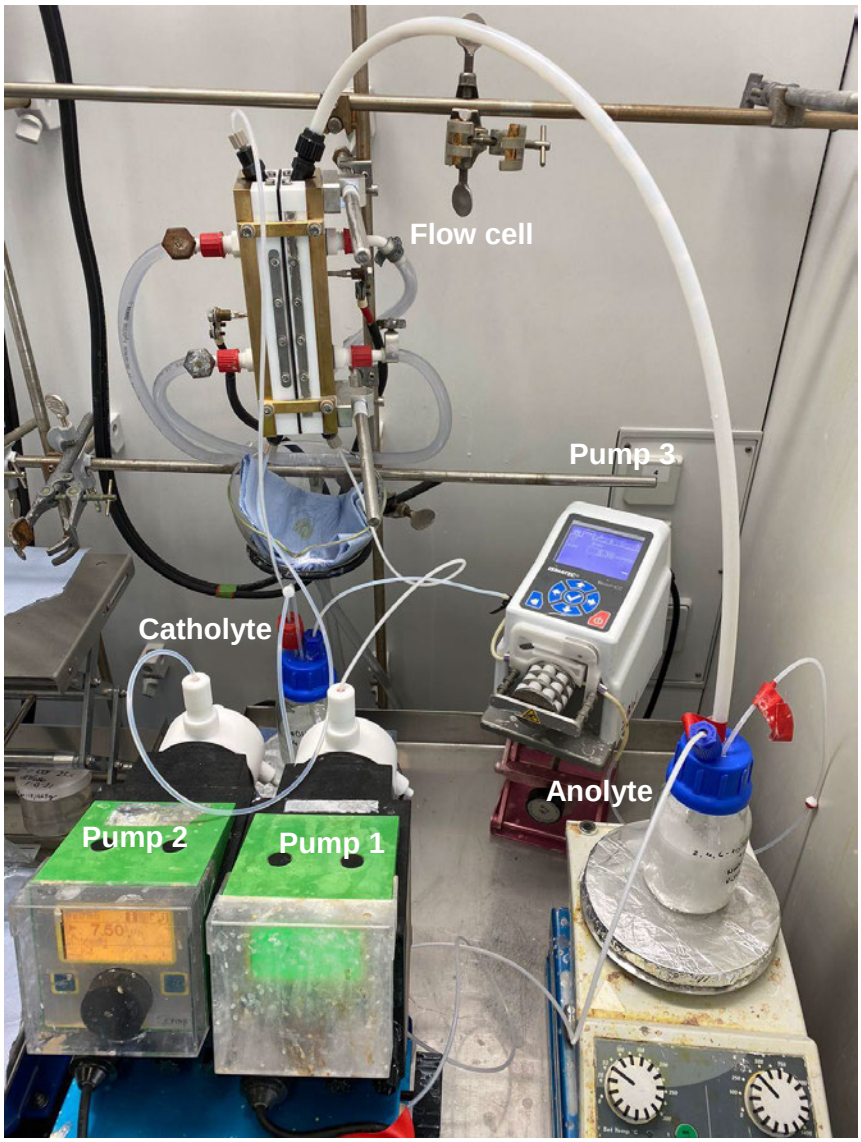

Figure S2. Image of periodate system production.

6. UV-*Vis* degradation analyses of dyes and photo of the samples

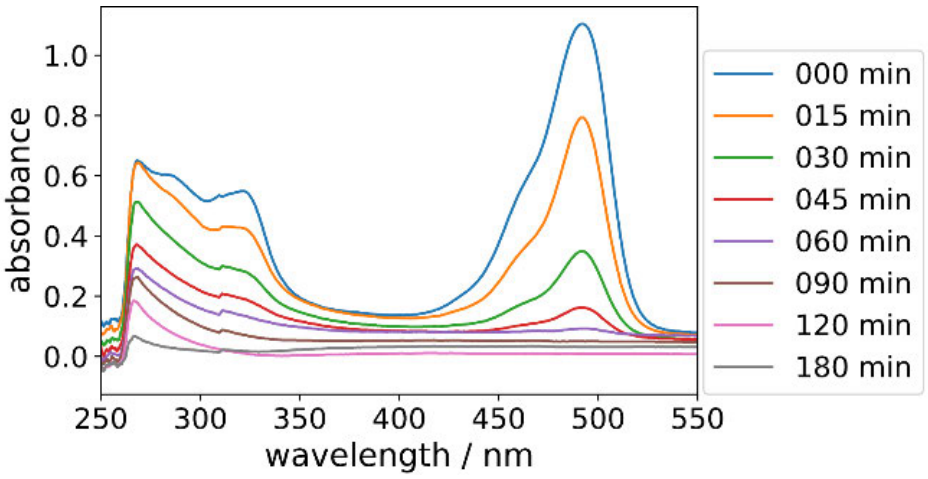

Figure S3. UV-*Vis* analysis of sudan I samples.

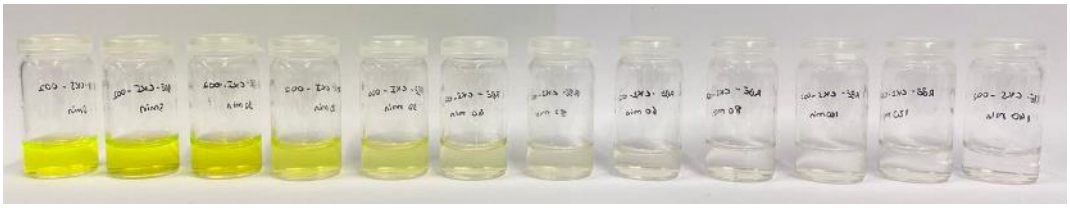

Figure S4. Photo of sudan I samples.

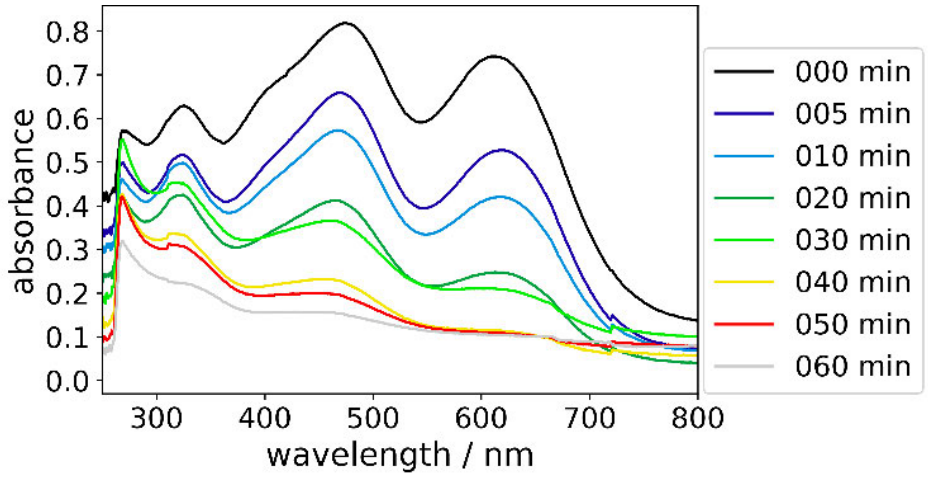

Figure S5. UV-*Vis* analysis of diamine green samples.

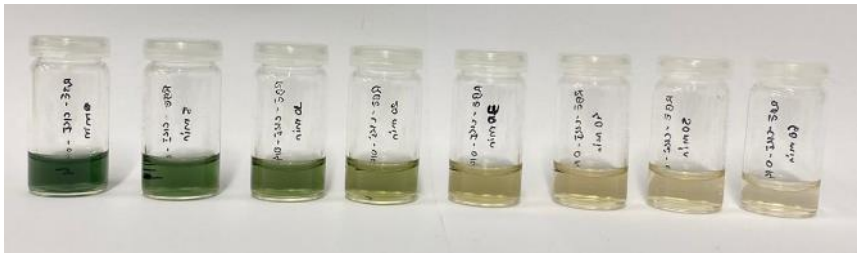

Figure S6. Photo of diamine green samples.

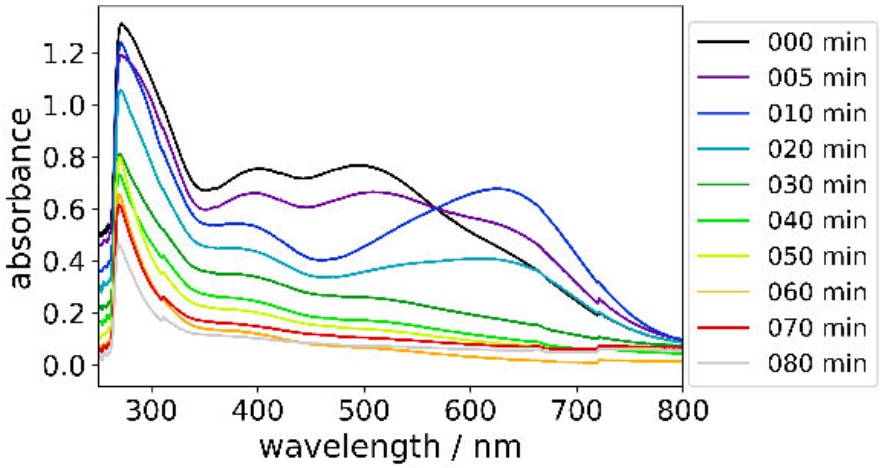

Figure S7. UV-*Vis* analysis of brilliant black samples.

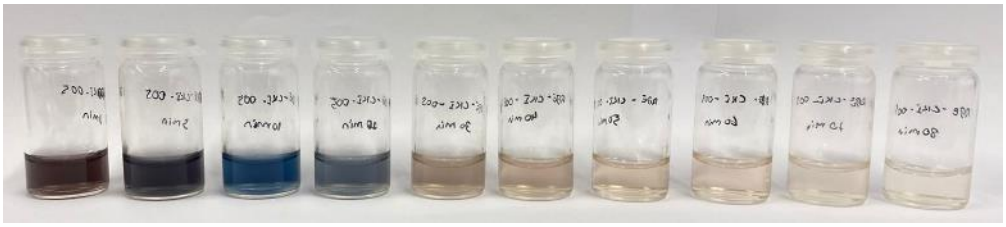

Figure S8. Photo of brilliant black samples.

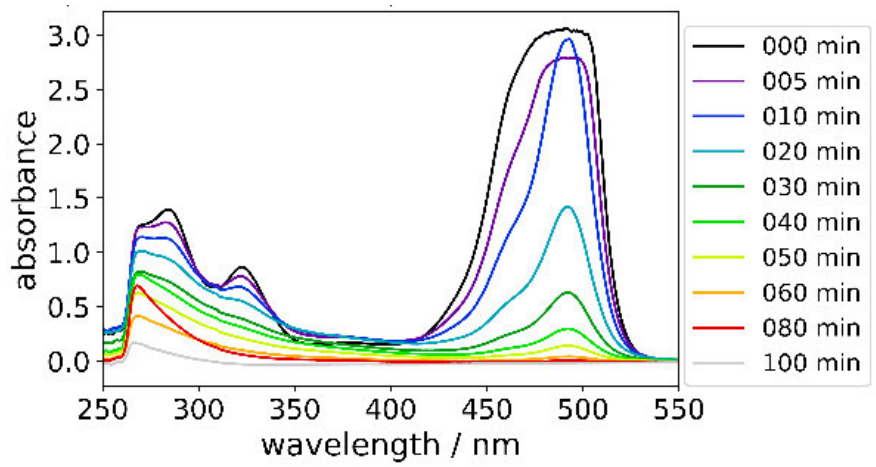

Figure S9. UV-*Vis* analysis of fluorescein samples.

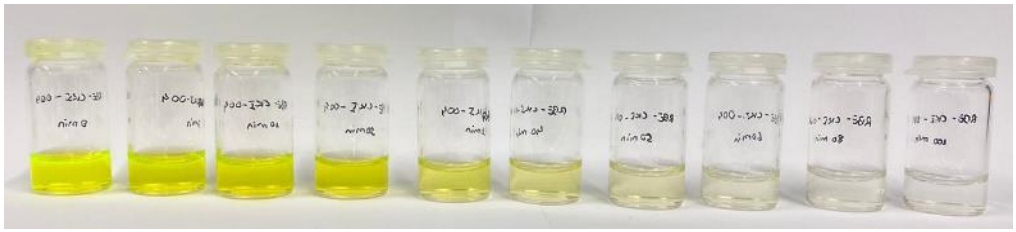

Figure S10. Photo of fluorescein samples.

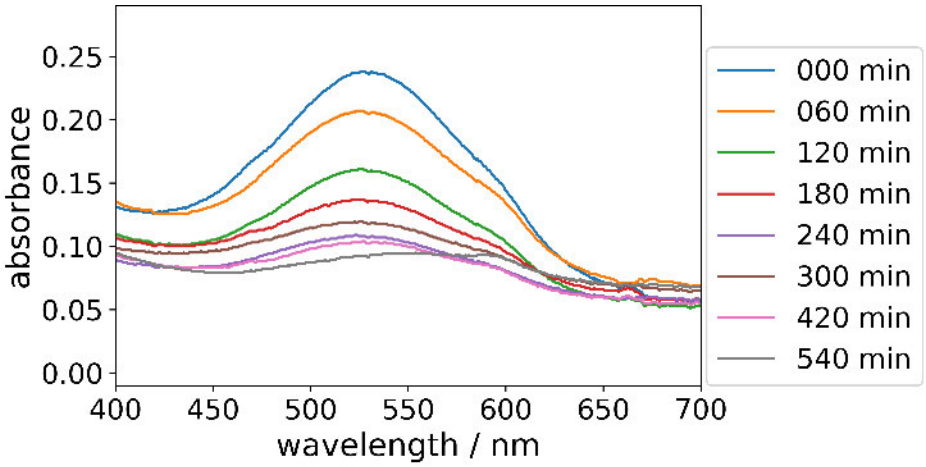

Figure S11. UV-*Vis* analysis of methylene blue samples.

Figure S12. Photo of methylene blue samples.

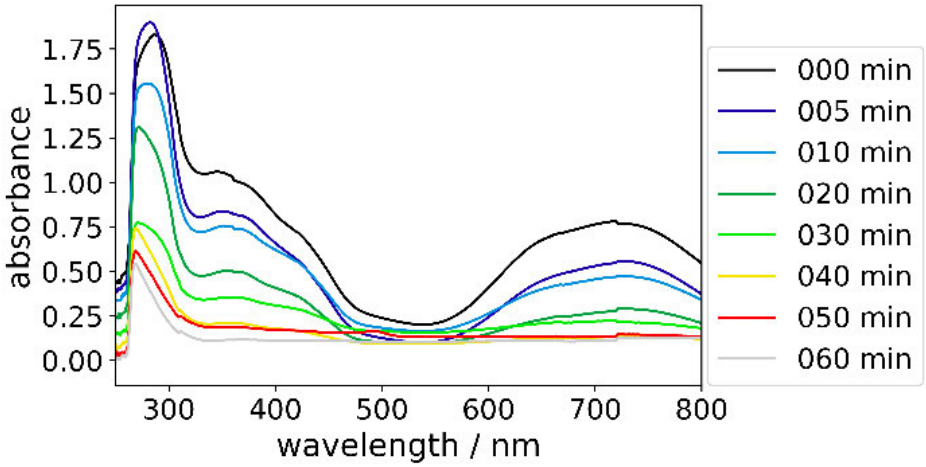

Figure S13. UV-*Vis* analysis of naphthol green samples.

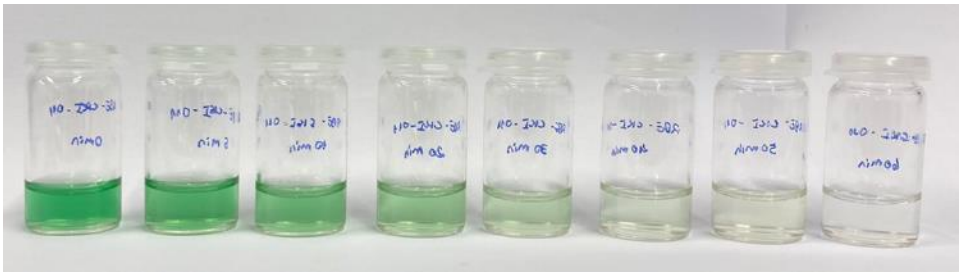

Figure S14. Photo of naphthol green samples.

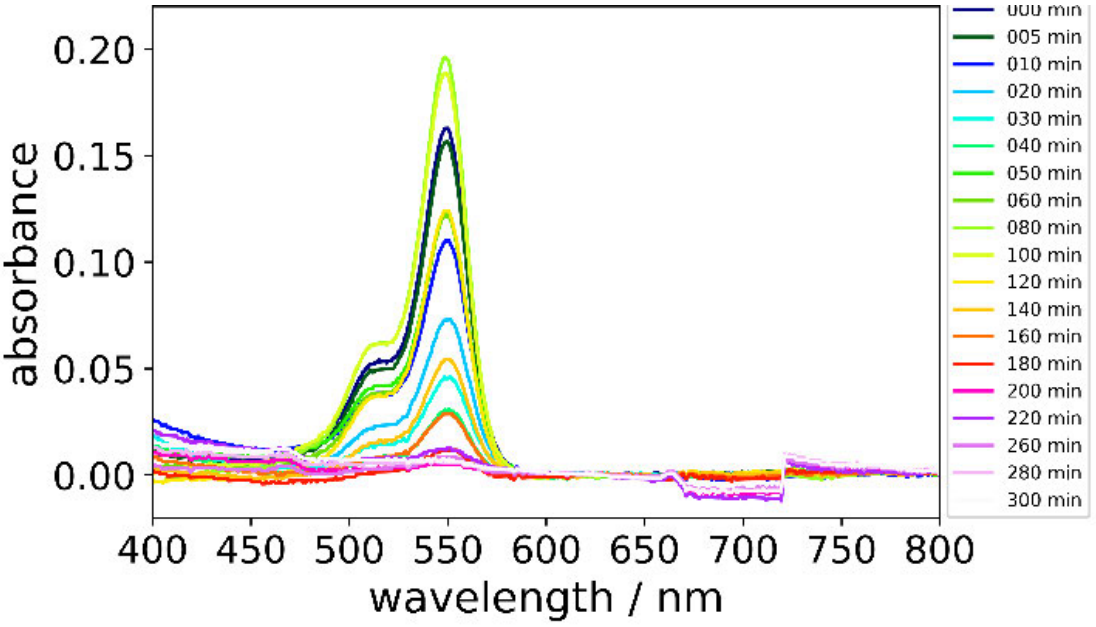

Figure S15. UV-*Vis* analysis of rose bengal samples.

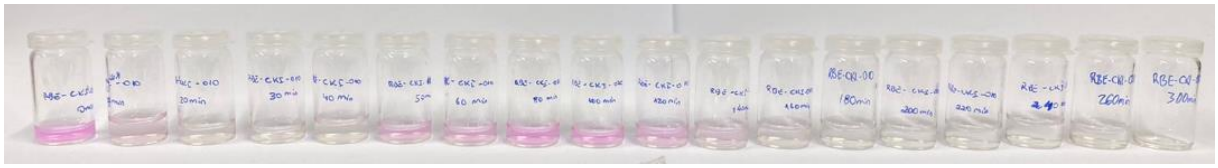

Figure S16. Photo of rose bengal samples.

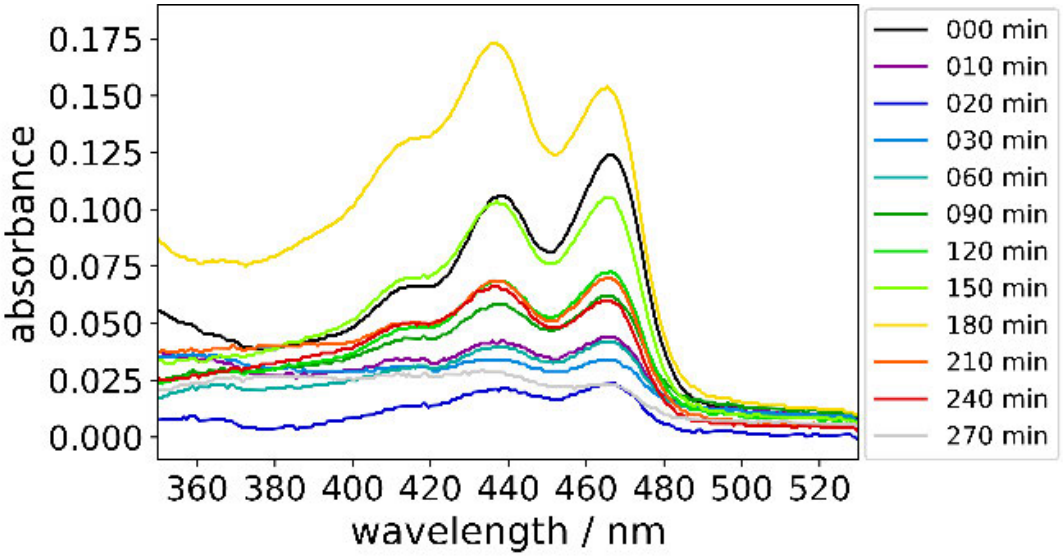

Figure S17. UV-*Vis* analysis of PTCDA samples.

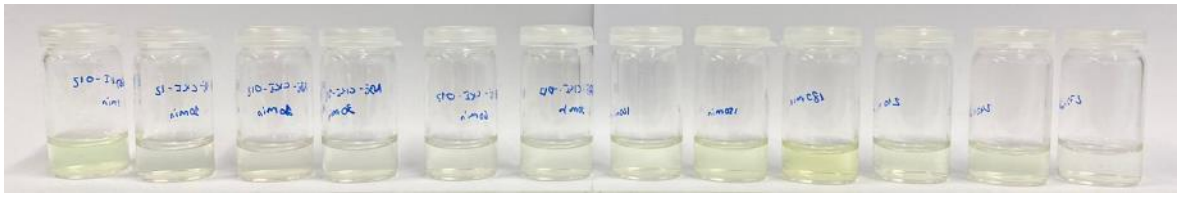

Figure S18. Photo of PTCDA samples.

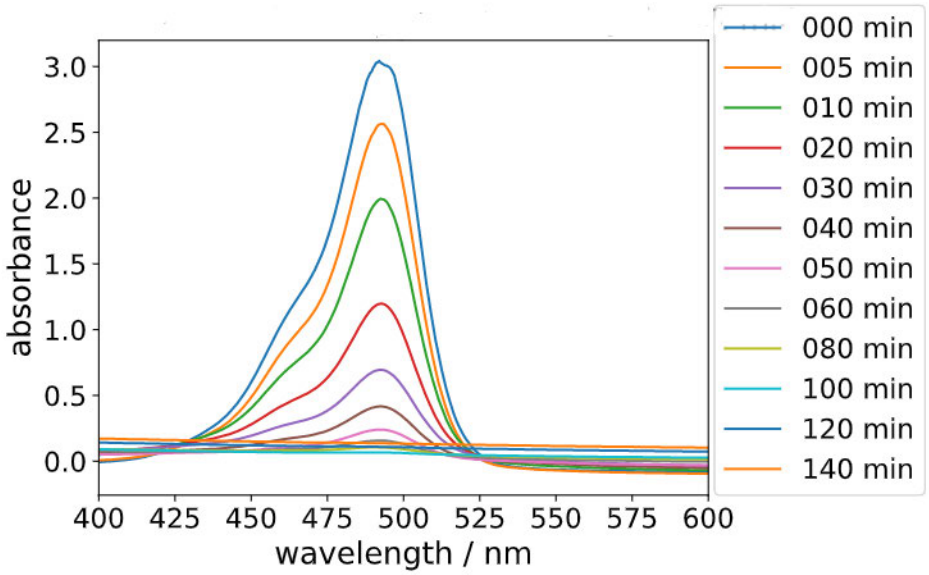

Figure S19. UV-*Vis* analysis of sudan I samples during the synthesis of *para*-periodate using NaI.

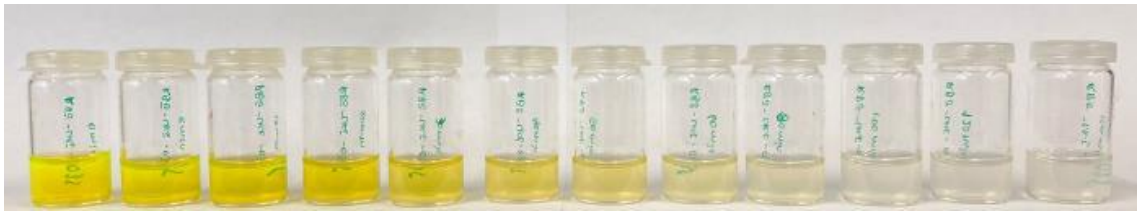

Figure S20. Photo of sudan I samples during the synthesis of *para*-periodate using NaI.

7. LC-PDA analyses for degradation of diodrast and diatrizoate

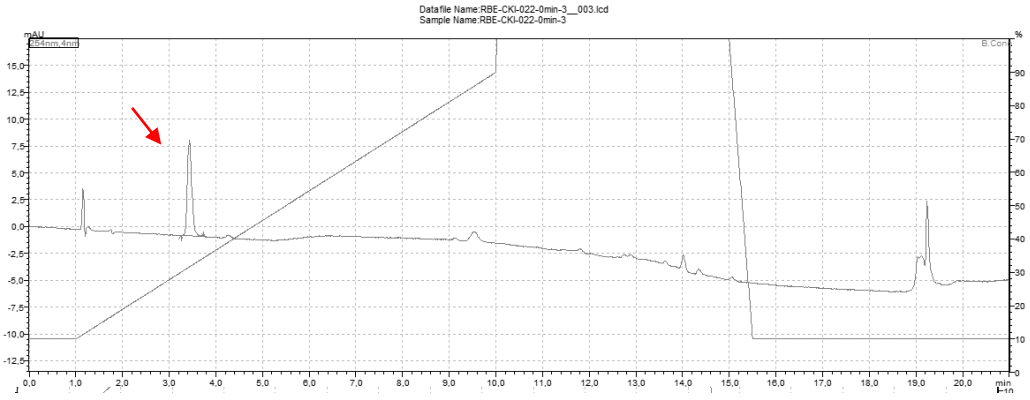

Figure S21. LC-PDA analysis of initial sample of diodrast.

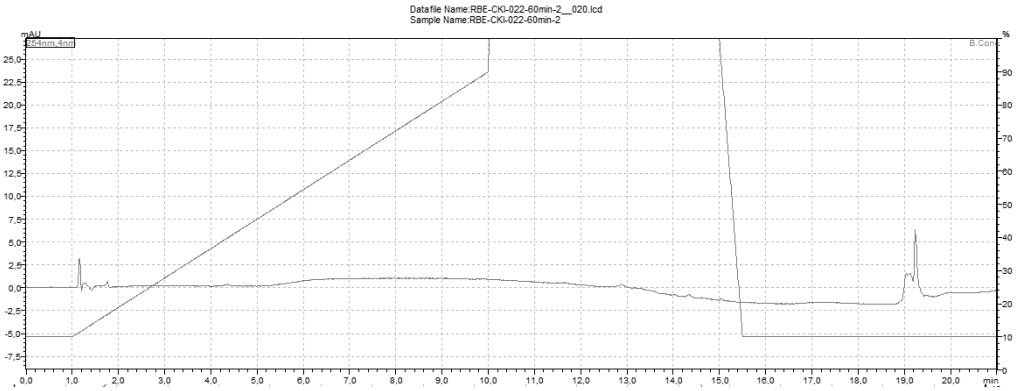

Figure S22. LC-PDA analysis of final sample of diodrast.

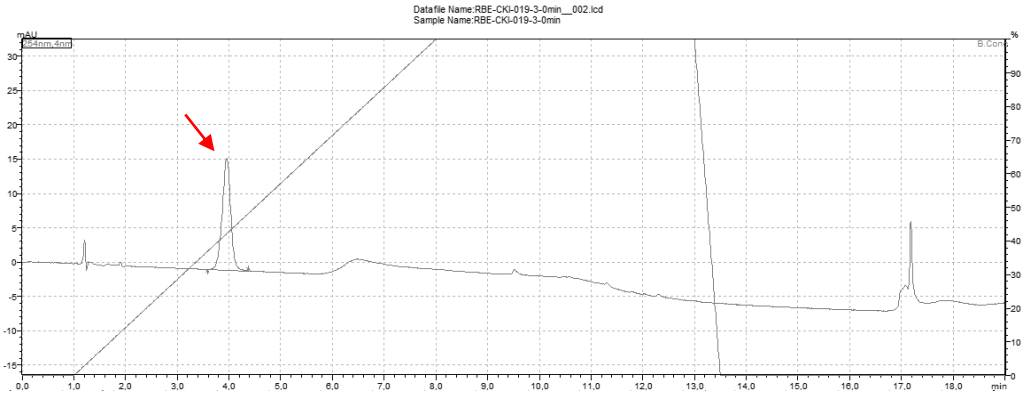

Figure S23. LC-PDA analysis of initial sample of diatrizoate.

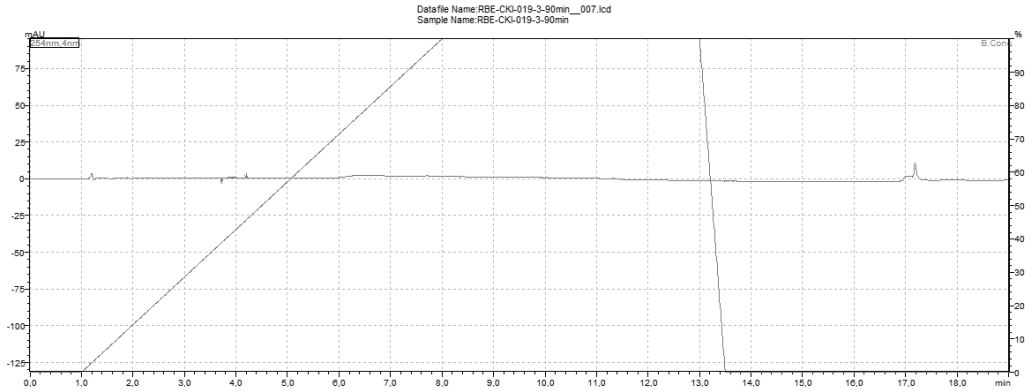

Figure S24. LC-PDA analysis of final sample of diatrizoate.

8. GC-MS analyses for degradation of 2-iodoaniline and 2,4,6-triiodophenol

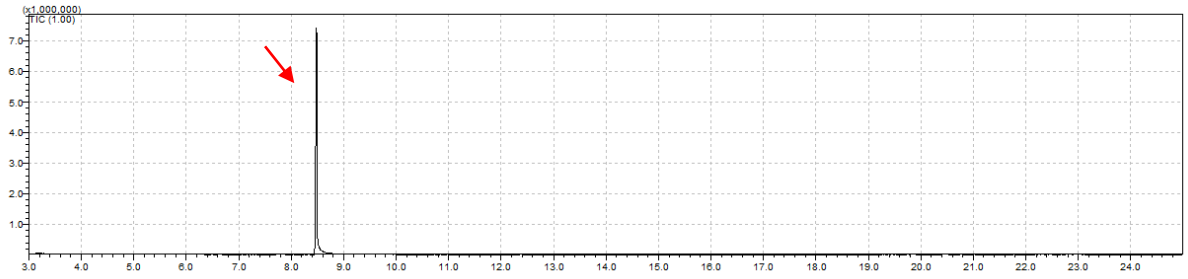

Figure S25. GC-MS chromatogram of initial sample of 2-iodoaniline.

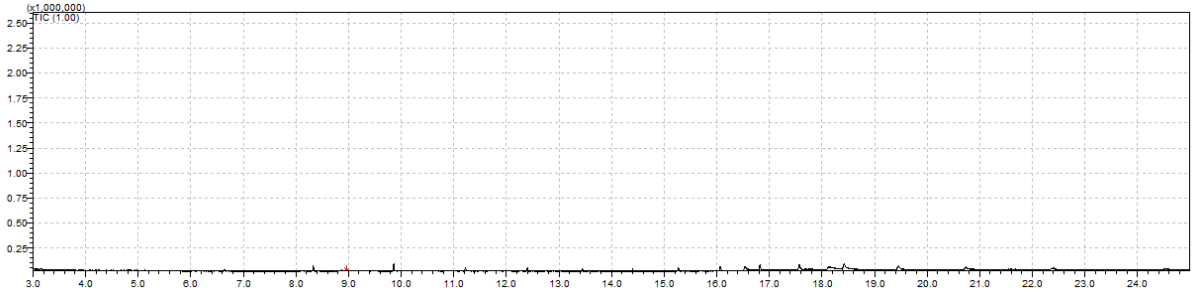

Figure S26. GC-MS chromatogram of final sample of 2-iodoaniline.

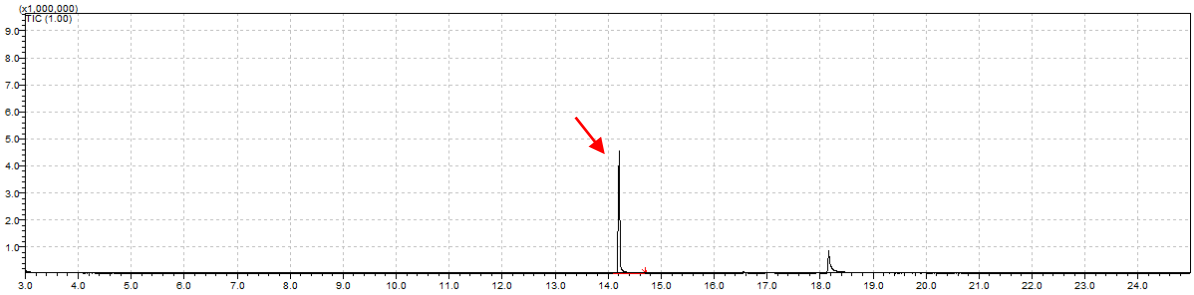

Figure S27. GC-MS chromatogram of initial sample of 2,4,6-triiodophenol.

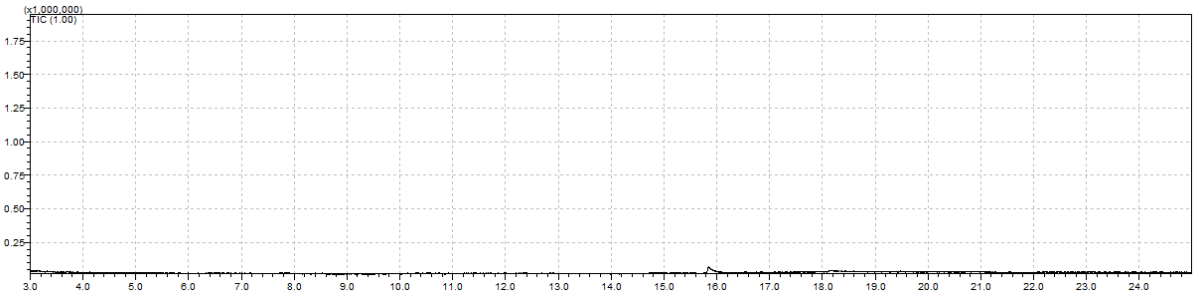

Figure S28. GC-MS analysis of final sample of 2,4,6-triiodophenol.

9. GC spectra for degradation of 2-iodobenzoic acid and dimethyl 5-iodoisophthalate

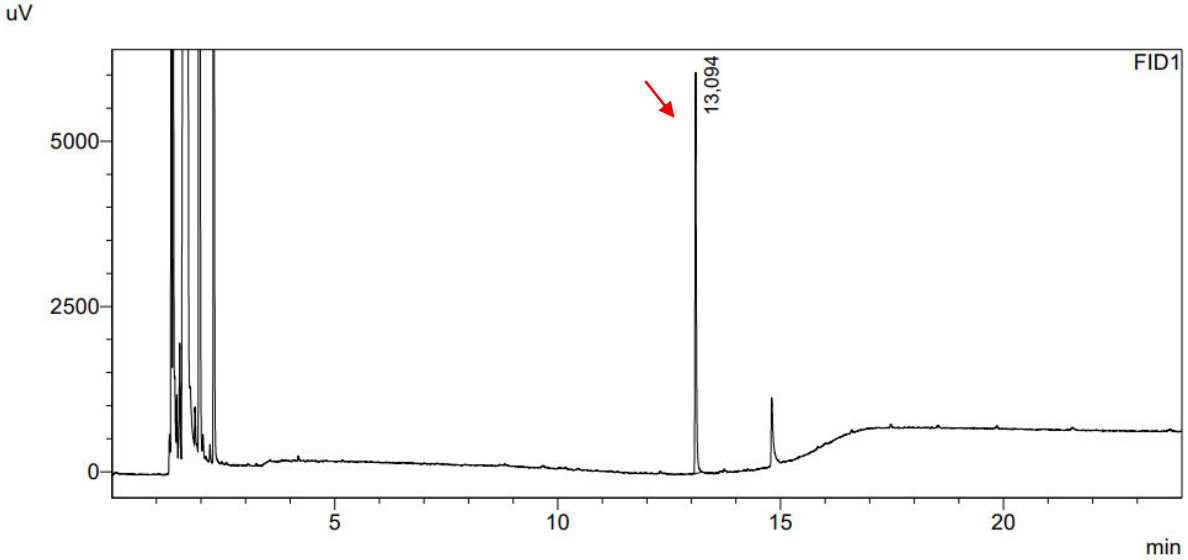

Figure S29. GC analysis of initial sample of Methyl 2-iodobenzoic acid.

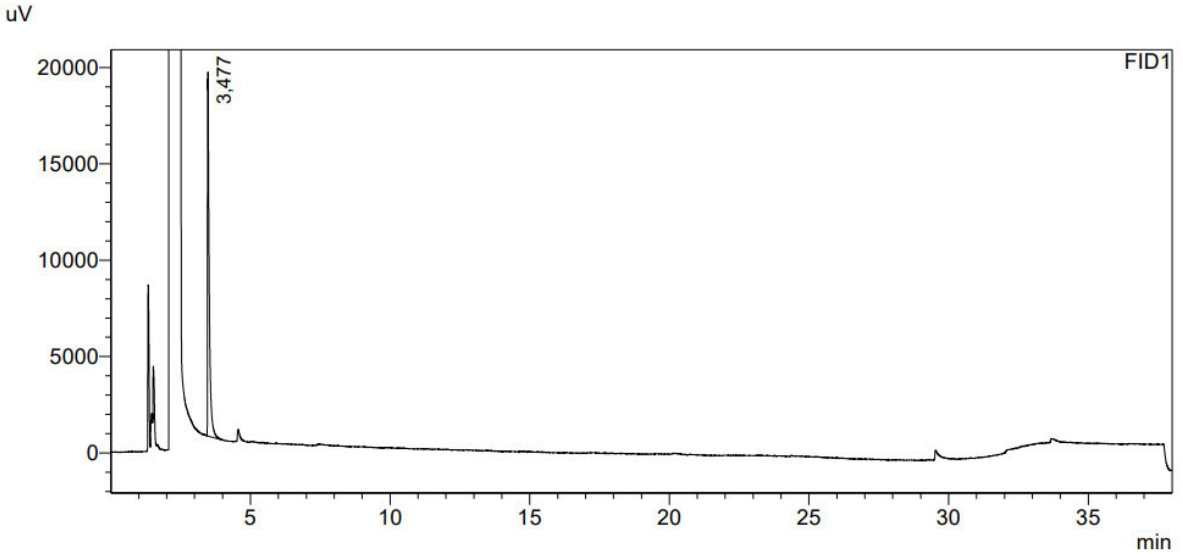

Figure S30. GC analysis of final sample of methyl 2-iodobenzoic acid.

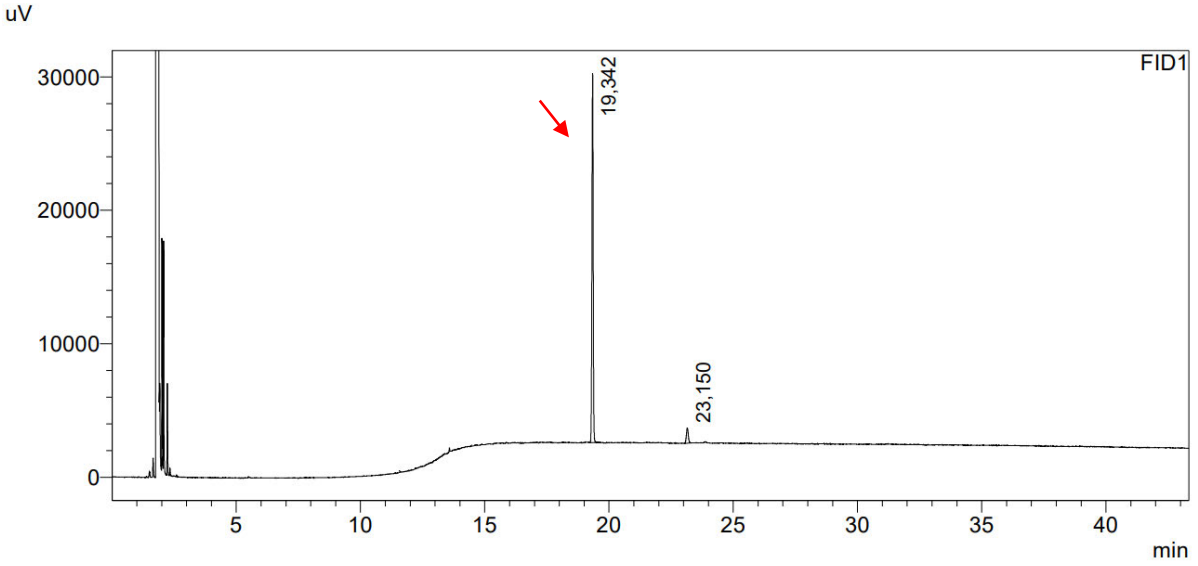

Figure S31. GC analysis of initial sample of dimethyl 5-iodoisophthalate.

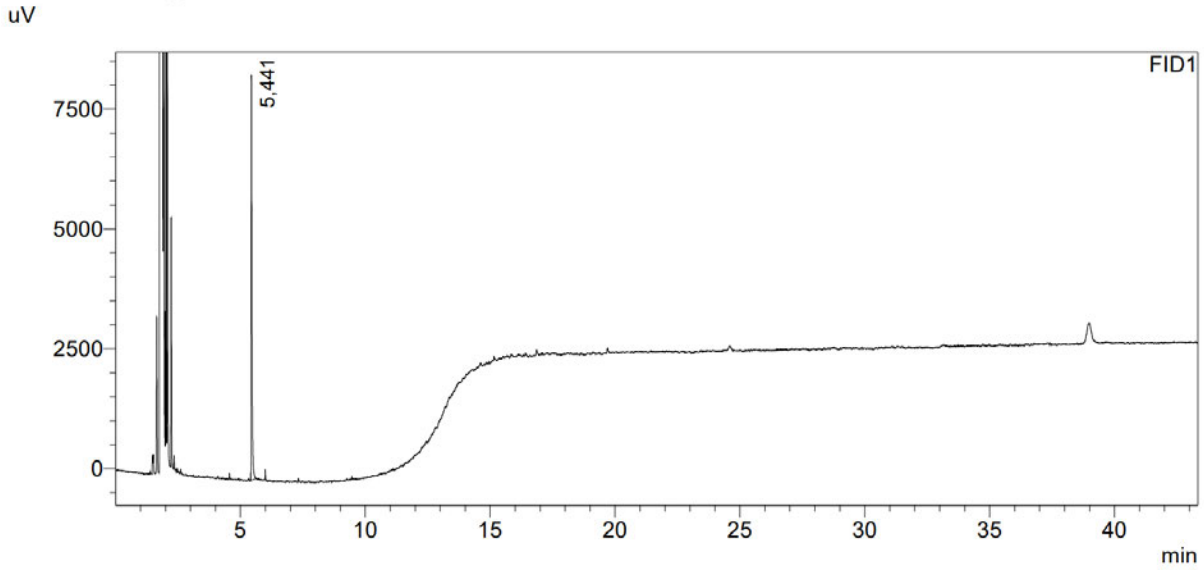

Figure S32. GC analysis of final sample of dimethyl 5-iodoisophthalate.

10. NMR analyses for degradation of 2-iodoaniline and 2,4,6-triiodophenol

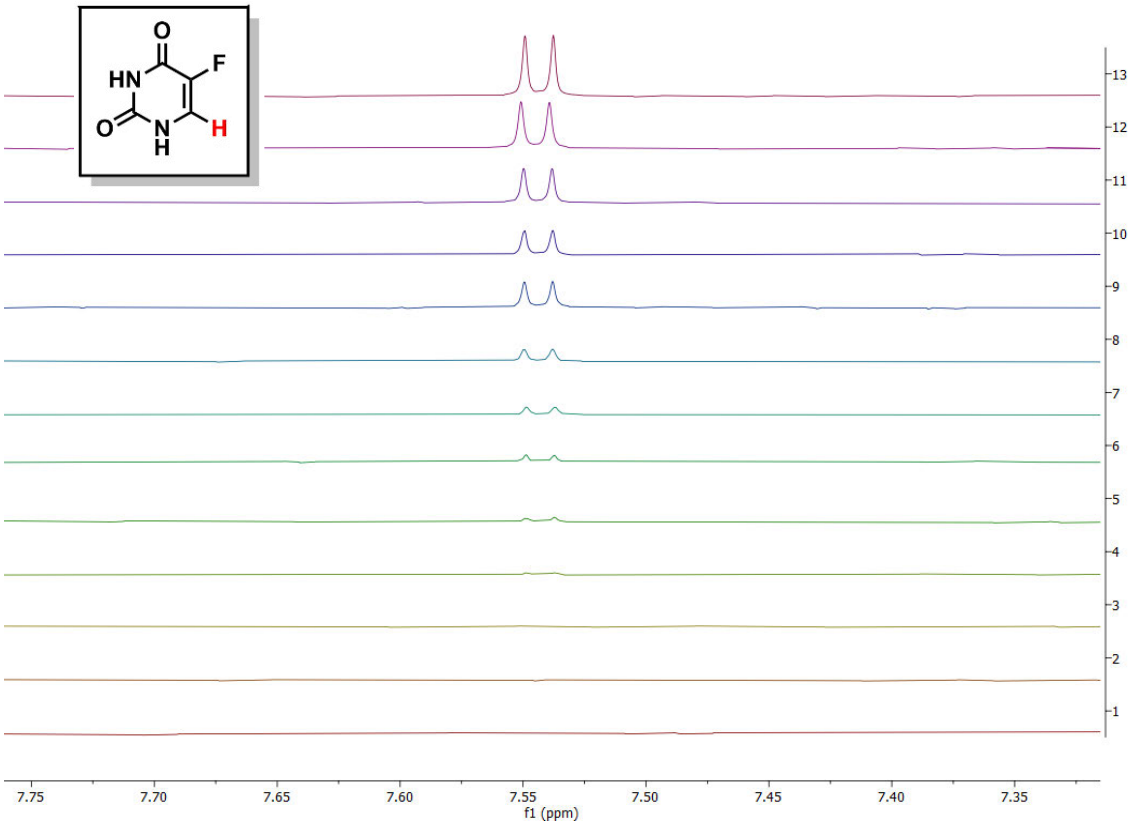

Figure S33a. ^{1}H NMR (H_2O/D_2O (8:2), 400 MHz) analysis for degradation of fluorouracil.

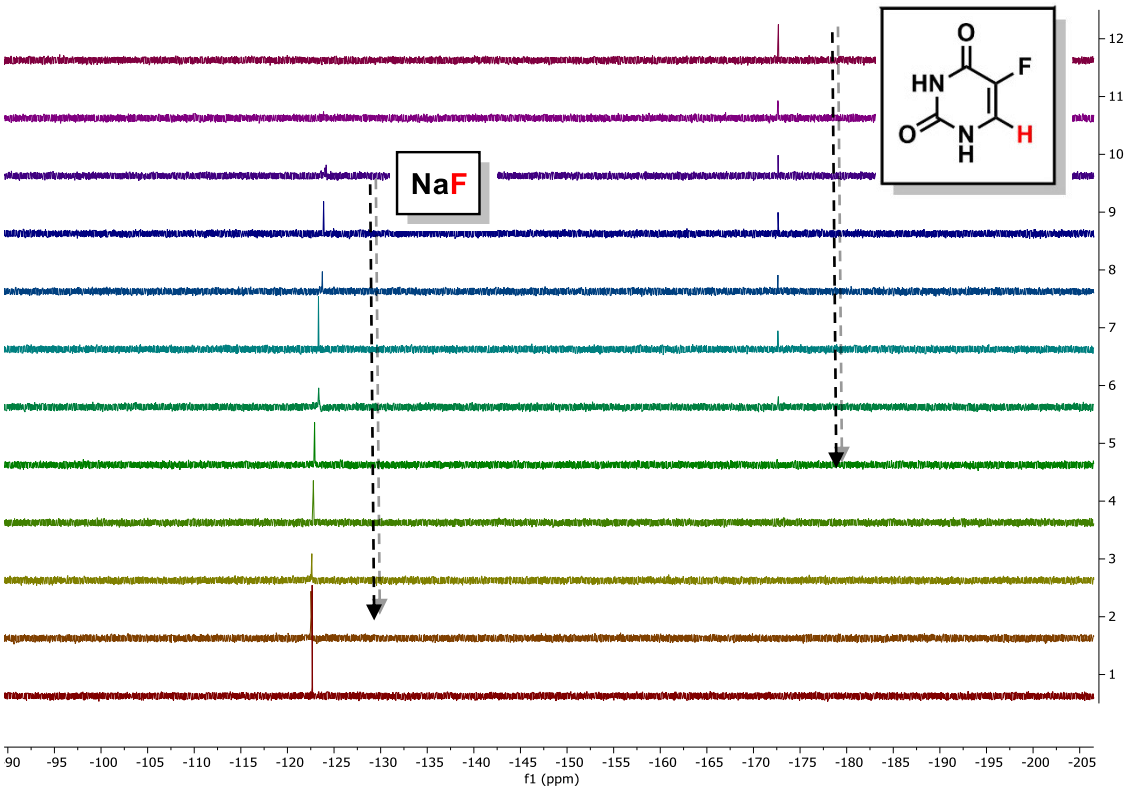

Figure S33b. ^{19}F NMR (H_2O/DMSO (7:3), 282 MHz) analysis for degradation of fluorouracil.

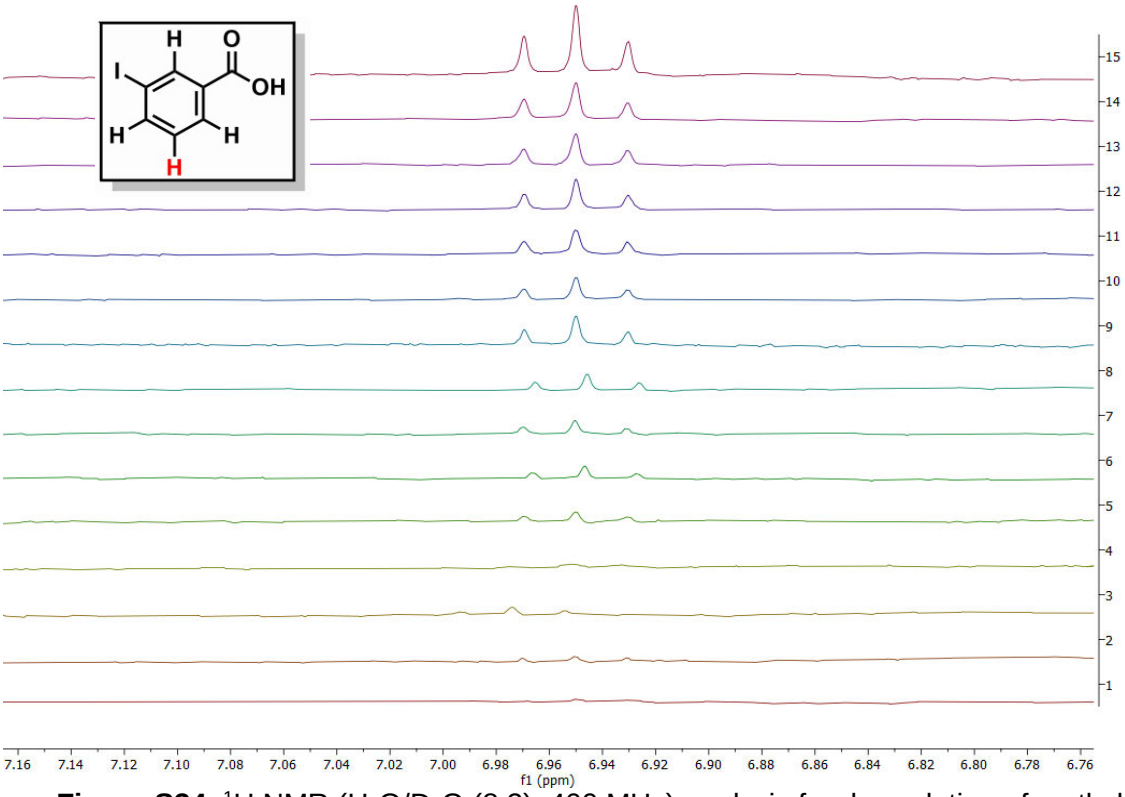

Figure S34. ^{1}H NMR (H_2O/D_2O (8:2), 400 MHz) analysis for degradation of methyl 3-iodobenzoic acid.

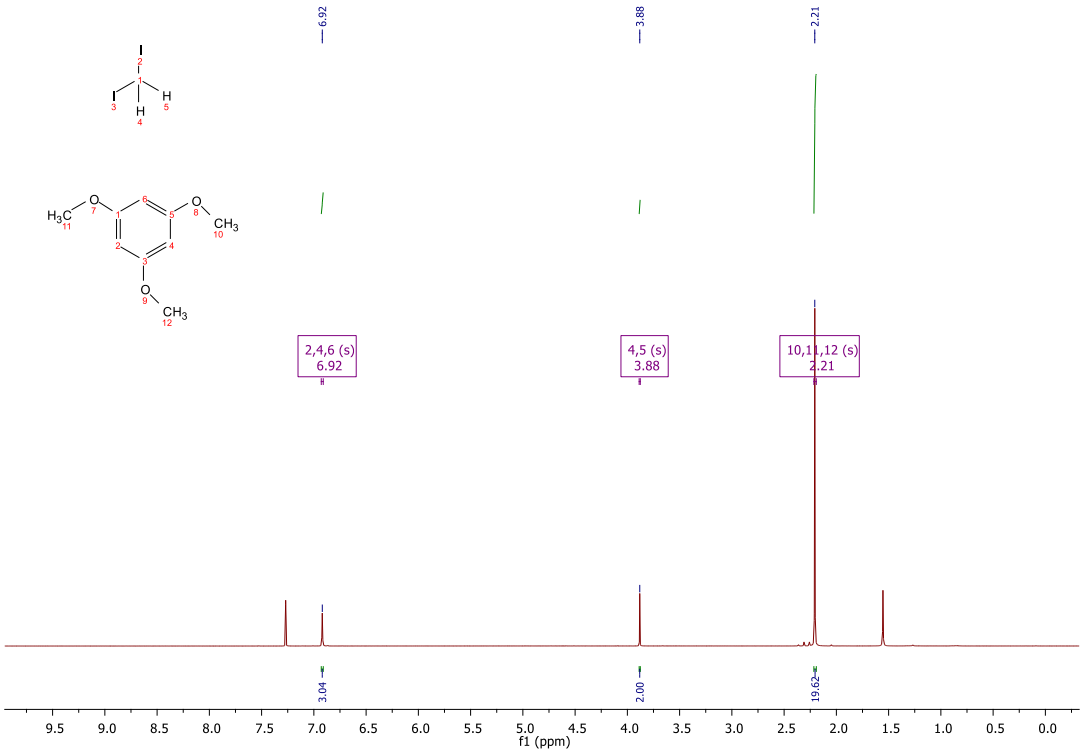

Figure S35. ^{1}H NMR ($CDCl_3$, 400 MHz) analysis of diiodomethane plus 1,3,5-Trimethoxybenzene as standard.

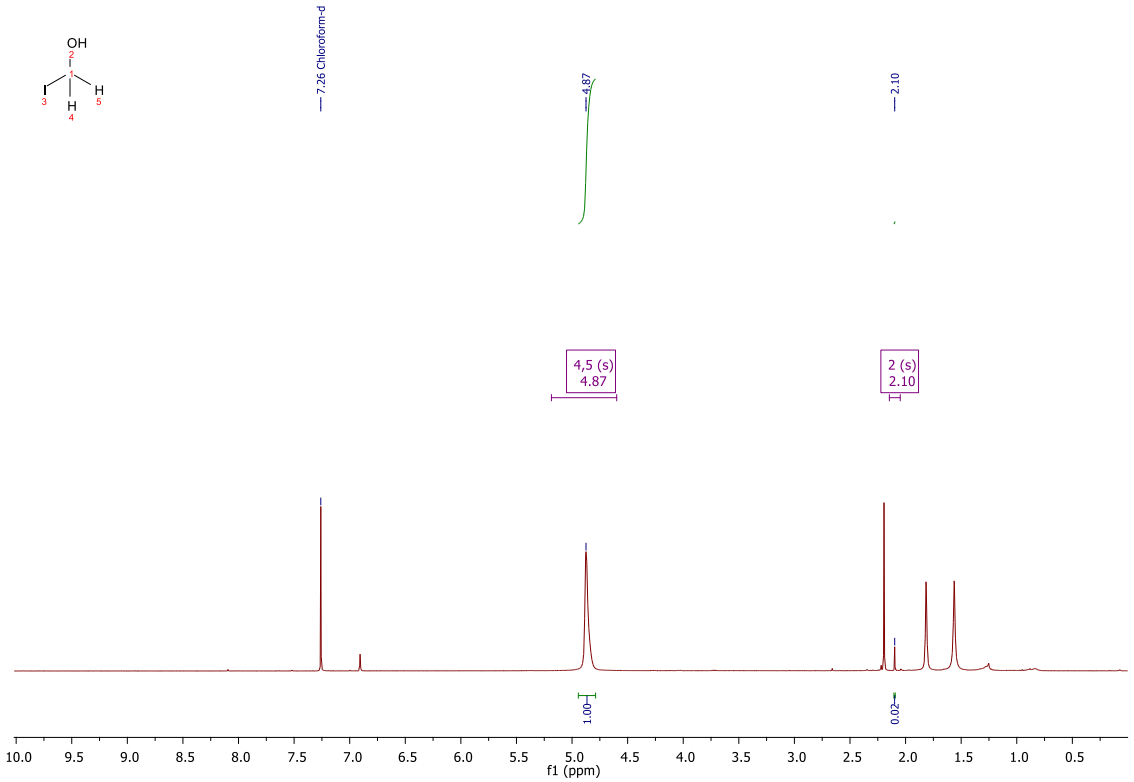

Figure S36. ^{1}H NMR ($CDCl_3$, 400 MHz) analysis of diiodomethane degradation

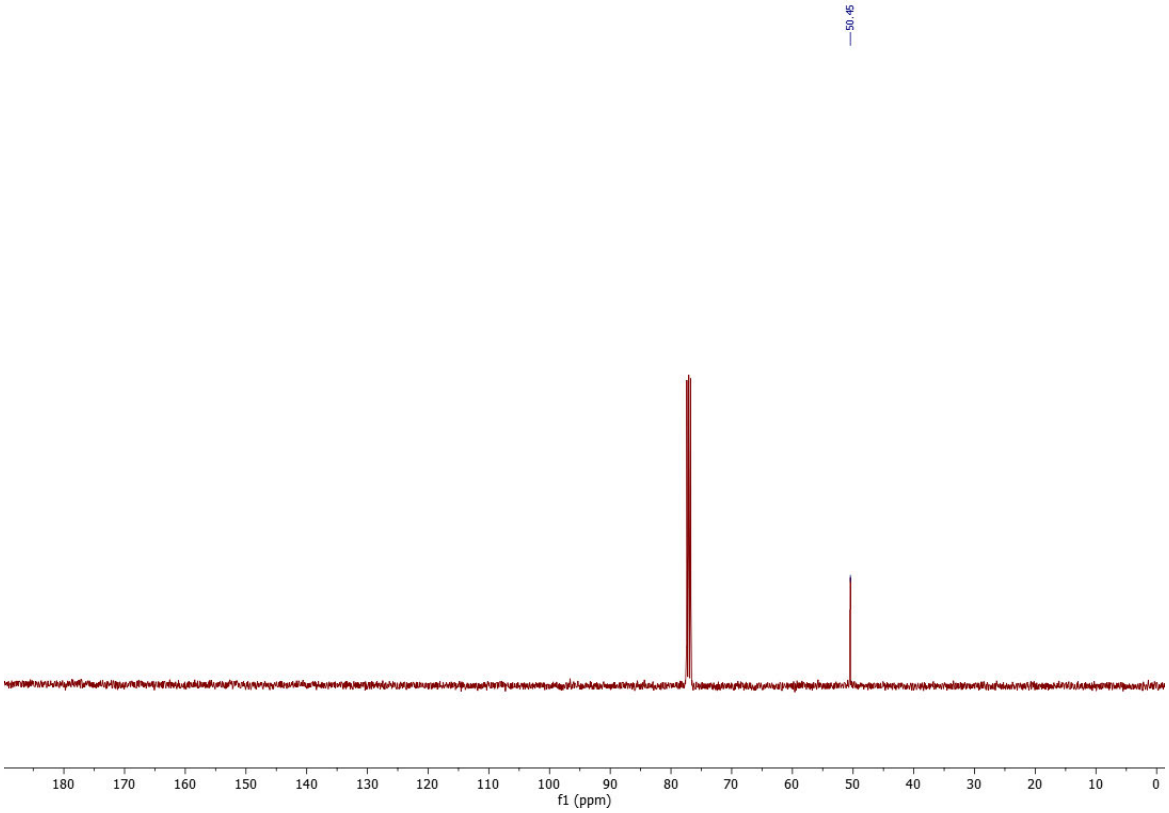

Figure S37. ^{13}C NMR ($CDCl_3$, 100 MHz) analysis of diiodomethane degradation

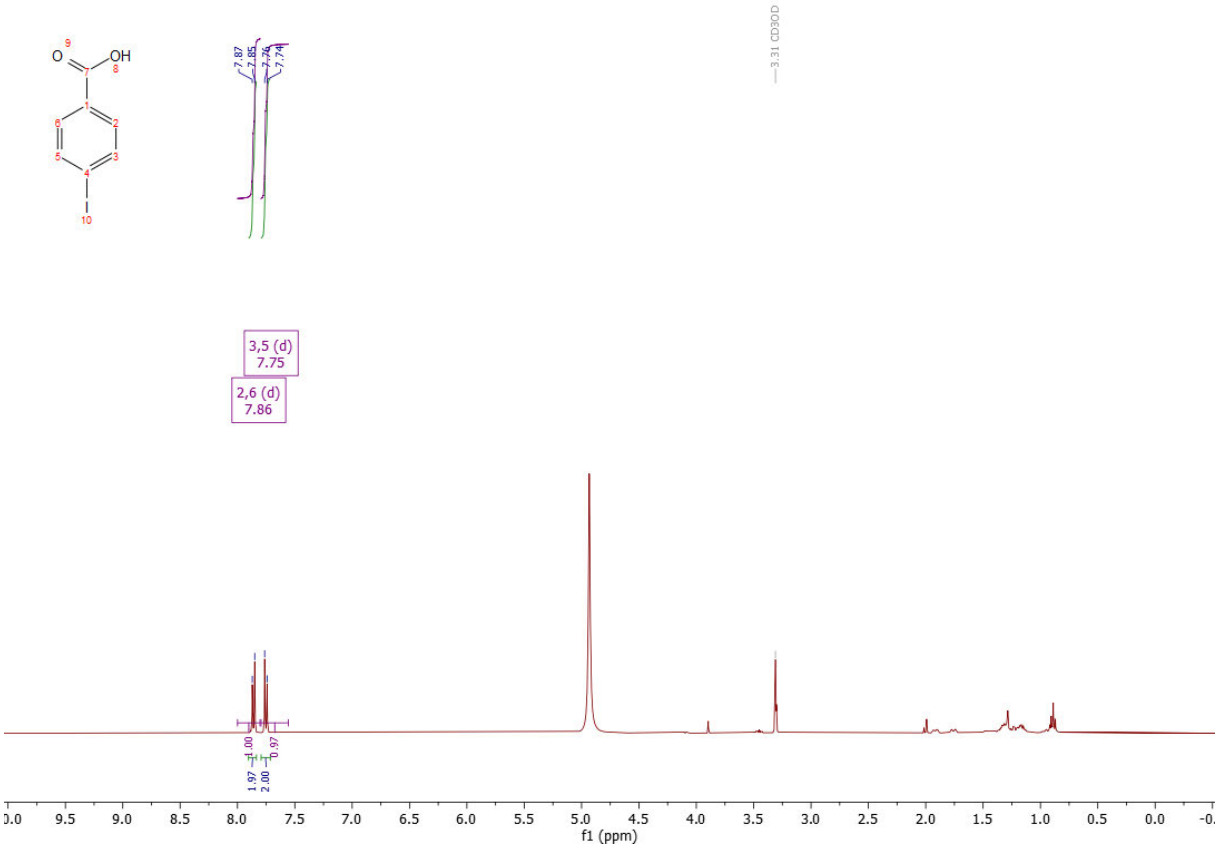

Figure S38. ^{1}H NMR(CD_3OD, 400 MHz) analysis of 4-iodobenzoic acid degradation.

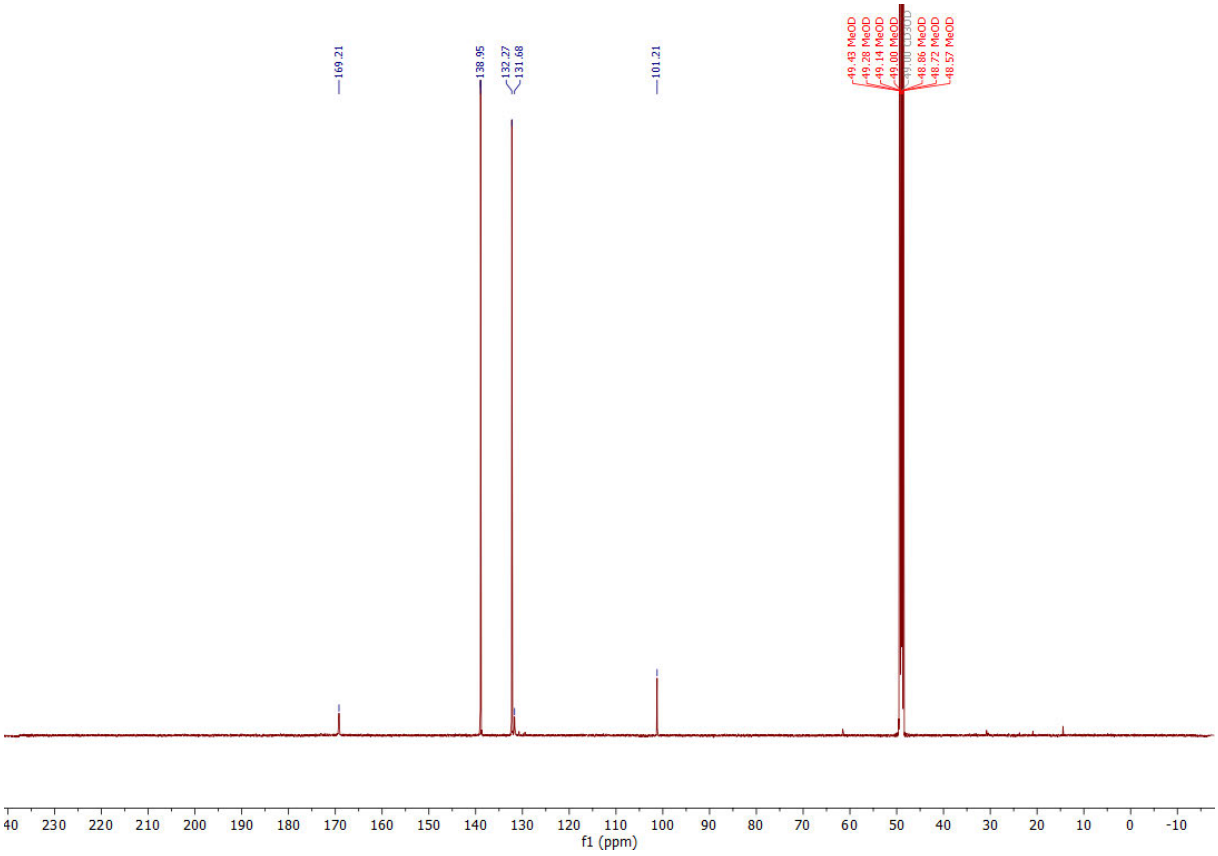

Figure S39. ^{13}C NMR (CD_3OD, 100 MHz) analysis of 4-iodobenzoic acid degradation.

11. Decay analyses of organic compound degradation using UV-*Vis*, GC, HPLC and ^{1}H and ^{19}F NMR

The data were plotted and fitted using python 3.9. For the fit, the fitting equation f(t) = exp(-a t) b and the python fitting command curve_fit were used. From the resulting optimized fitting parameters, the time for 90%, 95% and 99% degradation can be calculated.

To convert the time into the charge used for the respective degradation percentage, the Faraday's law of electrolysis $Q = n\ z\ F$ is applied. Hereby, Q is the charge, n the stoichiometry of the starting material, z the electrons used for the oxidation of one molecule and F the Faraday constant. With 10 Faraday being used for an optimal synthesis of periodate, the following equation holds: equivalents = $Q\ n^{-1}\ F^{-1}\ 10^{-1}$. Because of the relatively high numbers, the charge is given in kilo equivalents.

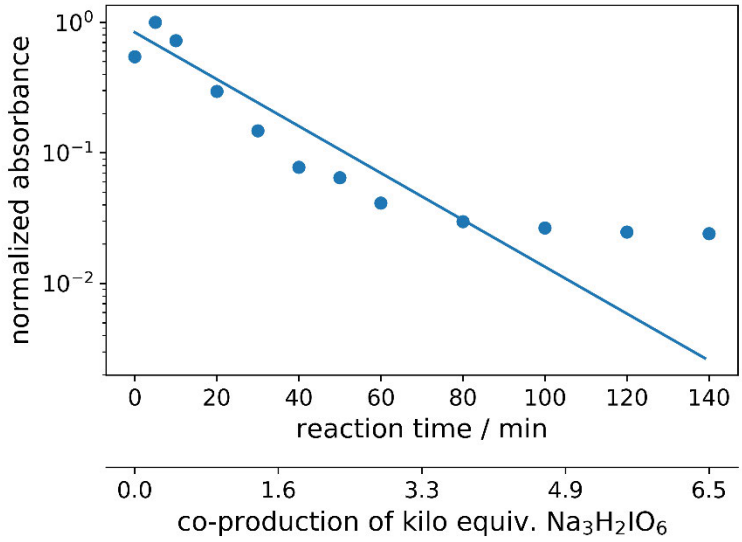

Figure S40. Degradation study of sudan I using UV/*Vis* analysis (band maximum at 436 nm). The curve fit equation is Abs=0.84*exp(-0.04*x) (x being kequiv. of $Na_3H_2IO_6$).

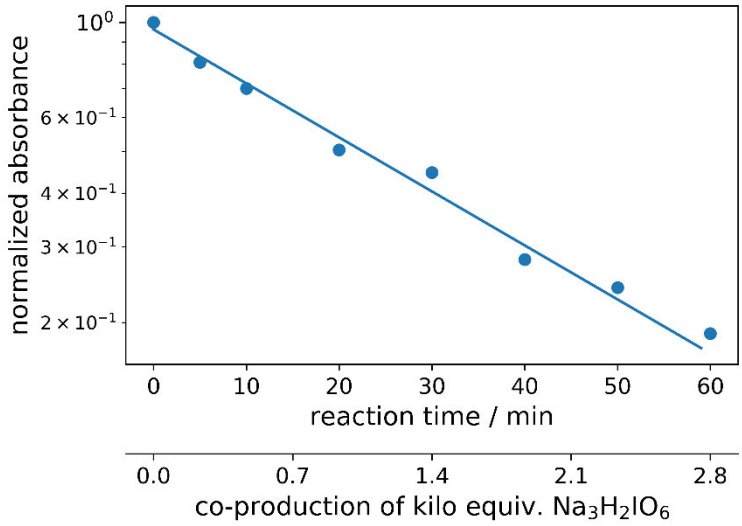

Figure S41. Degradation study of diamine green using UV/*Vis* analysis (band maximum at 469 nm). The curve fit equation is Abs=0.96*exp(-0.03*x) (x being kequiv. of $Na_3H_2IO_6$).

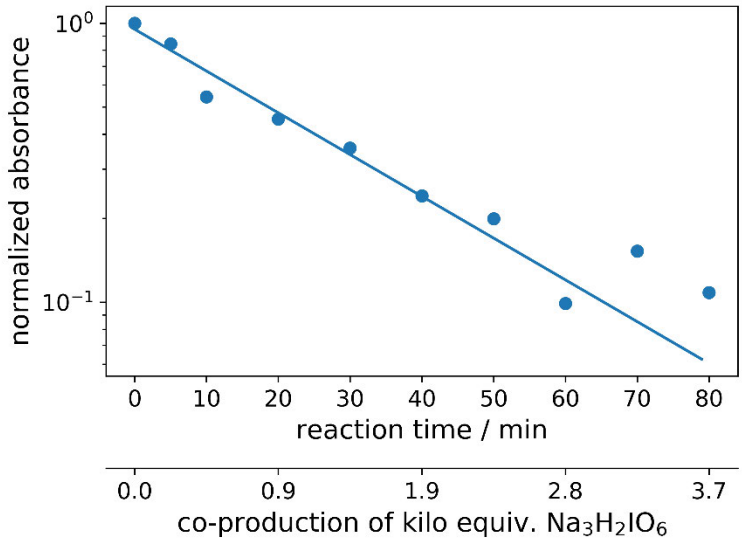

Figure S42. Degradation study of brilliant black using UV/*Vis* analysis (band maximum at 398 nm). The curve fit equation is Abs=0.95*exp(-0.03*x) (x being kequiv. of $Na_3H_2IO_6$).

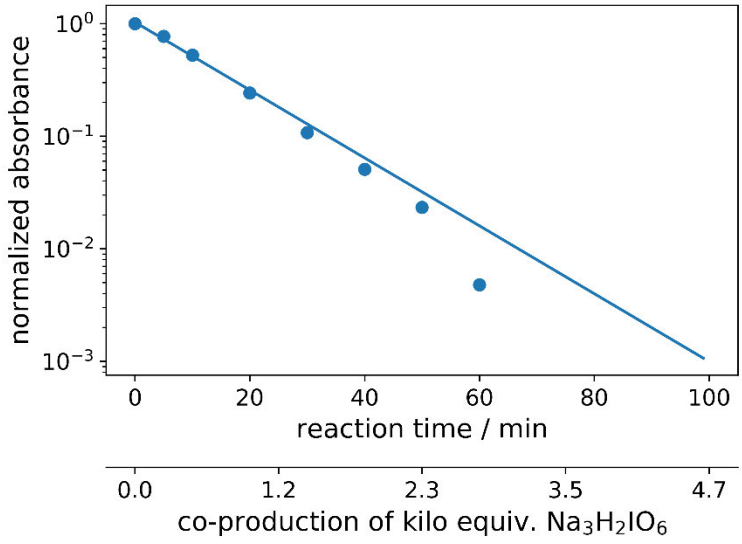

Figure S43. Degradation study of fluorescein using UV/*Vis* analysis (band maximum at 469 nm). The curve fit equation is Abs=1.03*exp(-0.07*x) (x being kequiv. of $Na_3H_2IO_6$).

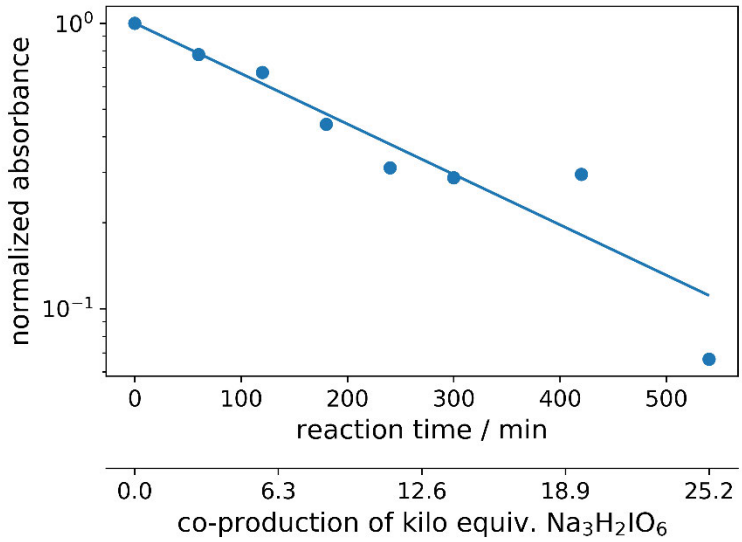

Figure S44. Degradation study of methylene blue using UV/*Vis* analysis (band maximum at 521 nm). The curve fit equation is Abs=1.00*exp(-0.004*x) (x being kequiv. of $Na_3H_2IO_6$).

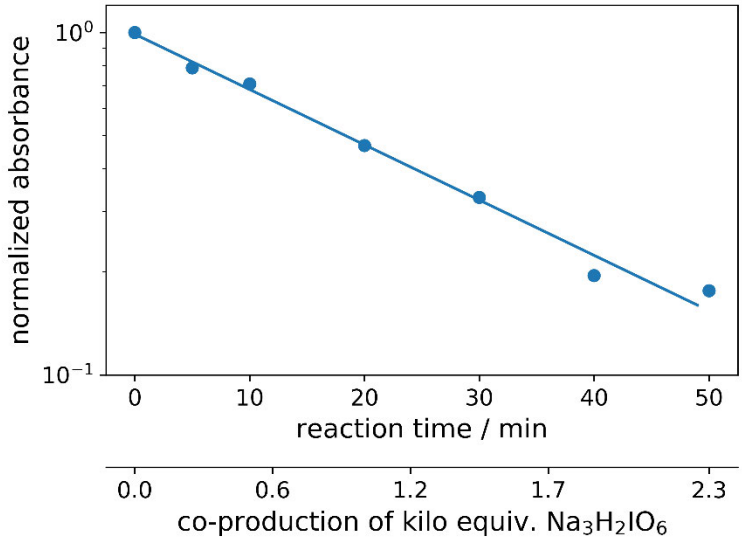

Figure S45. Degradation study of napthol green using UV/*Vis* analysis (band maximum at 345 nm). The curve fit equation is Abs=0.99*exp(-0.04*x) (x being kequiv. of $Na_3H_2IO_6$).

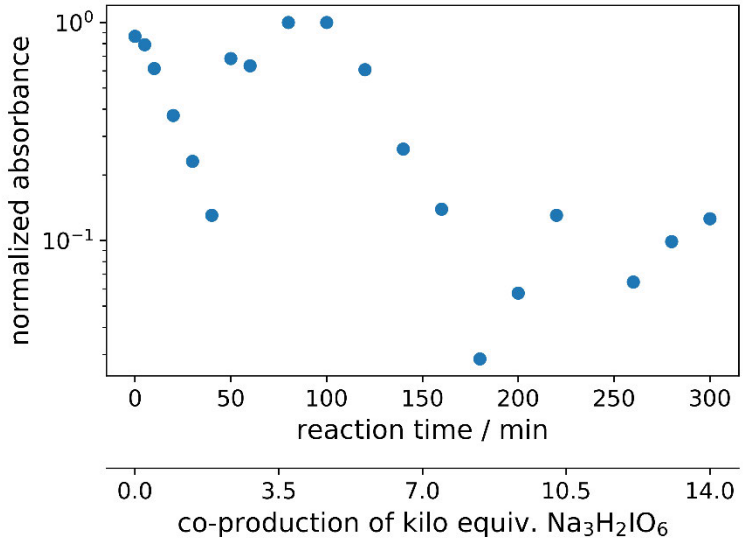

Figure S46. Degradation study of rose bengal using UV/*Vis* analysis (band maximum at 521 nm). The data were not fitted because of intermediate species.

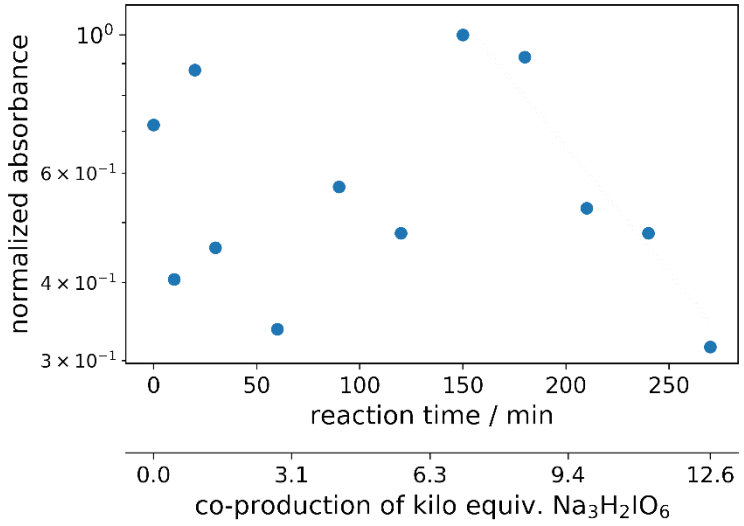

Figure S47. Degradation study of PTCDA using UV/*Vis* analysis (band maximum at 436 nm). The data were not fitted because of intermediate species.

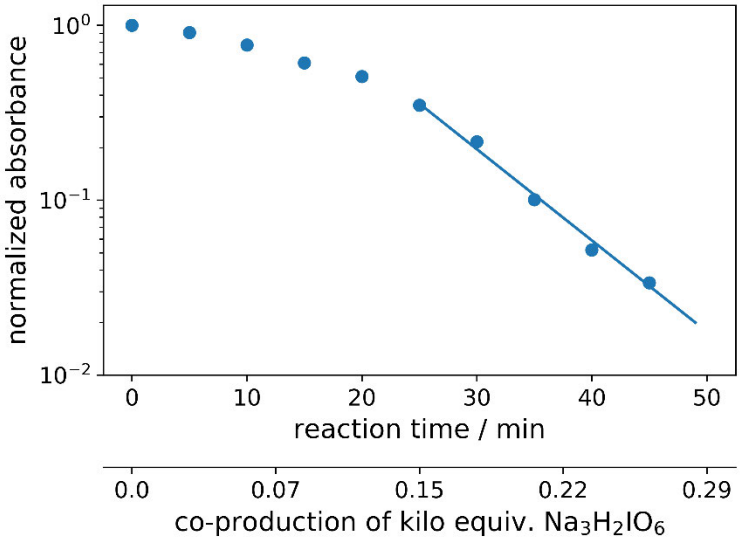

Figure S48. Degradation study of diodrast using LCMS. The curve fit equation is Abs=7.19*exp(-20.61*x) (for t>25 min, x being kg equiv. of $Na_3H_2IO_6$).

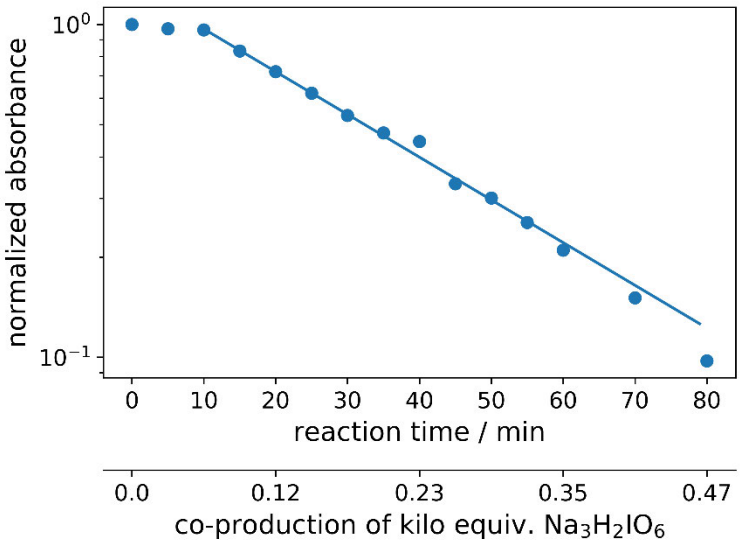

Figure S49. Degradation study of diatrizoate using LCMS. The curve fit equation is Abs=1.30*exp(-5.07*x) (for t>10 min, x being kg equiv. of $Na_3H_2IO_6$).

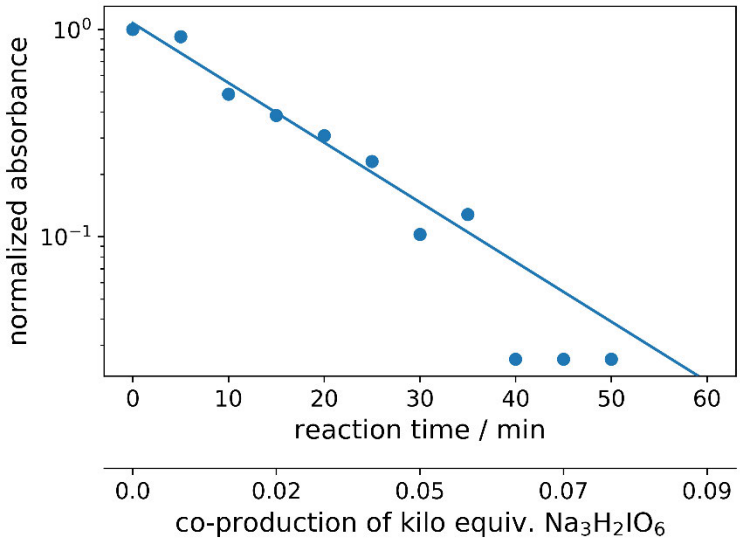

Figure S50. Degradation study of fluorouracil using ^{1}H NMR; compound integral related to initial compound integral via standard 1,3,5-methoxybenzene. The curve fit equation is Abs=1.07*exp(-42.66*x) (x being kg equiv. of $Na_3H_2IO_6$).

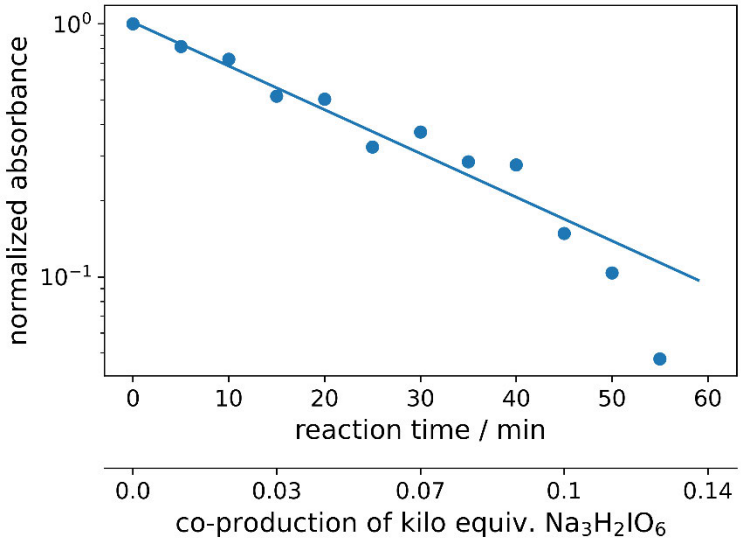

Figure S51. Figure 1 Degradation study of 2-iodobenzoic acid using ^{1}H NMR; compound integral related to initial compound integral via standard 1,3,5-methoxybenzene. The curve fit equation is Abs=1.01*exp(-17.06*x) (x being kg equiv. of $Na_3H_2IO_6$).

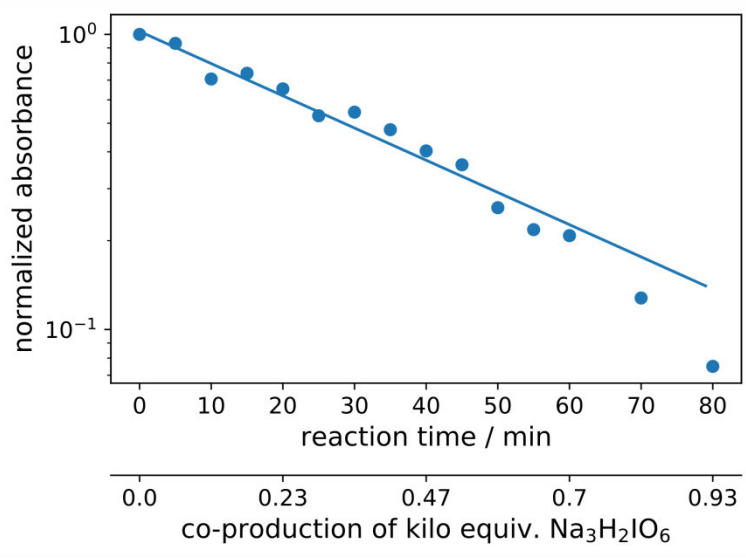

Figure S52. Figure 2 Degradation study of 3-iodobenzoic acid using ^{1}H NMR; compound integral related to initial compound integral via standard 1,3,5-methoxybenzene. The curve fit equation is Abs=2.31*exp(-48.32*x) (for t>10 min, x being kg equiv. of $Na_3H_2IO_6$).

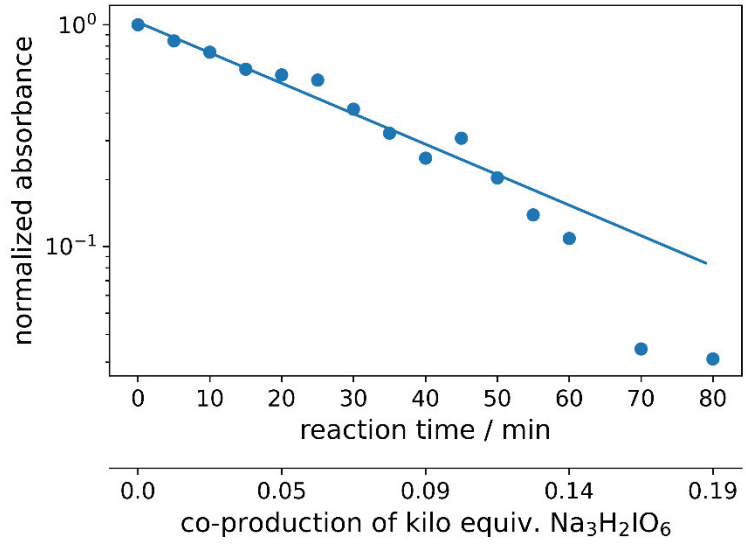

Figure S53. Degradation study of 2-iodoaniline using ^{1}H NMR; compound integral related to initial compound integral via standard 1,3,5-methoxybenzene. The curve fit equation is Abs=1.02*exp(-13.58*x) (x being kg equiv. of $Na_3H_2IO_6$).

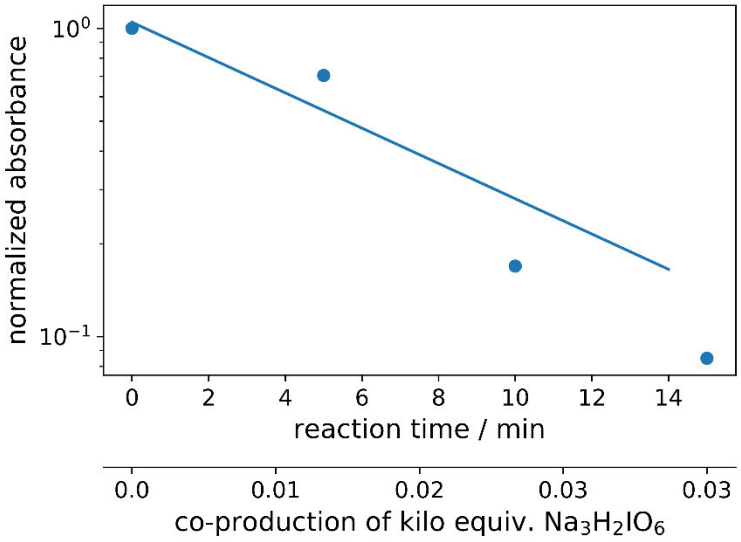

Figure S54. Degradation study of dimethyl-5-iodoisophthalate using GC. The curve fit equation is Abs=1.05*exp(-56.54*x) (x being kg equiv. of $Na_3H_2IO_6$).

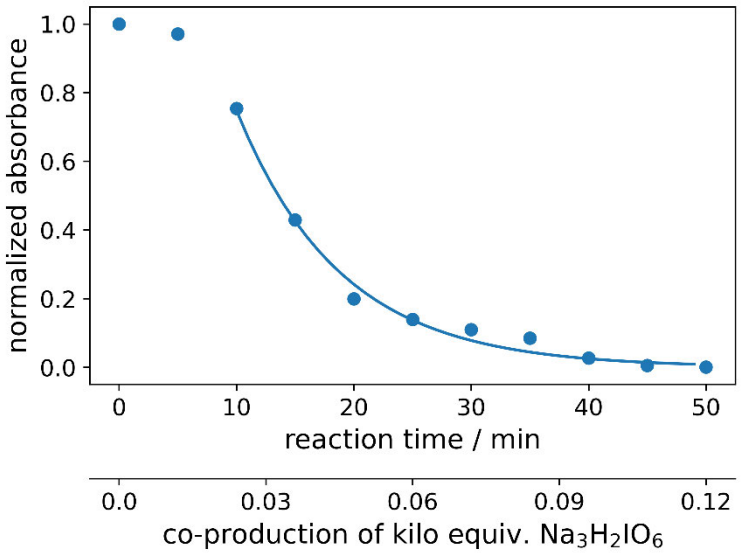

Figure S55. Figure 3 Degradation study of 2,4,6-Triiodophenol using ^{1}H NMR; compound integral related to initial compound integral via standard 1,3,5-methoxybenzene. The curve fit equation is Abs=2.31*exp(-48.32*x) (for t>10 min, x being kg equiv. of $Na_3H_2IO_6$).

12. LC-PDA analyses for degradation of periodate produced from NaI with contaminants

A buffered and diluted sample solution (c = 5.341 mM) was subjected to LC-PDA analysis using an injection volume of 3 μL. The separation was carried out isocratically. I^- , IO_3^- and IO_4^- were detected by the PDA detector at 1.23 min,1.61 min and 1.91 min at a wavelength of λ = 254 nm.

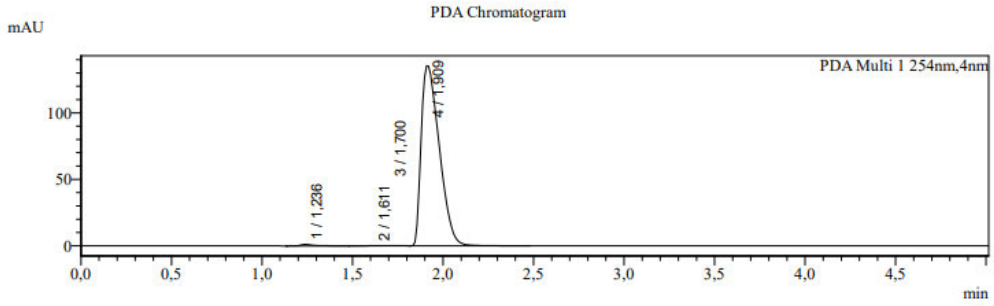

Figure S56. LC-PDA analysis of standard periodate.

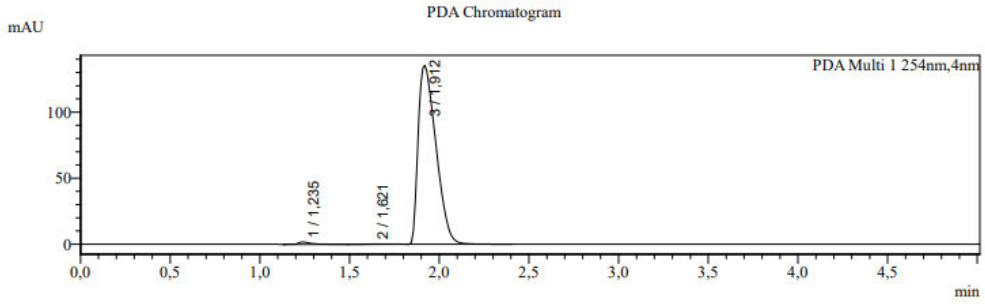

Figure S57. LC-PDA analysis of periodate produced during sudan I degradation.

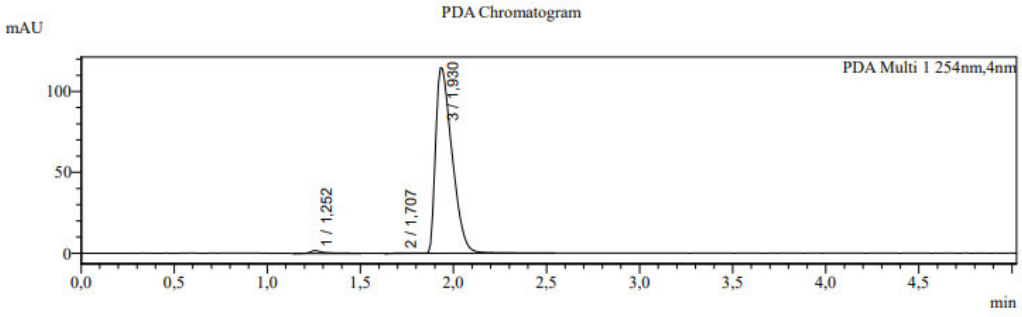

Figure S58. LC-PDA analysis of periodate produced during diodrast degradation.

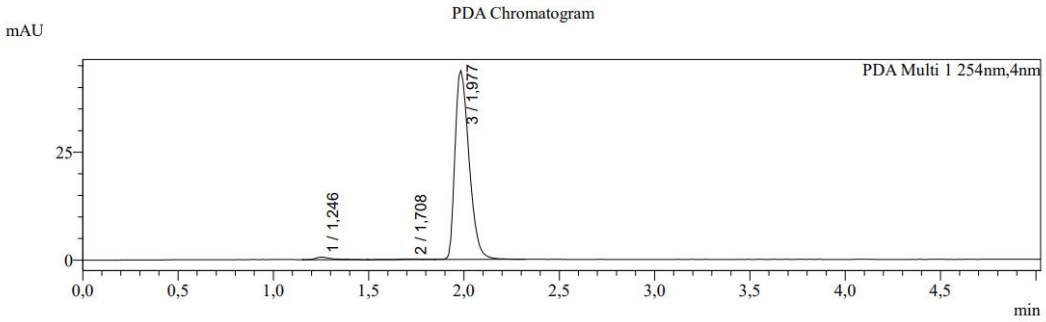

Figure S59. LC-PDA analysis of periodate produced during 2,4,6-triiodophenol degradation.

13. LC-PDA degradation analyses of Iohexol

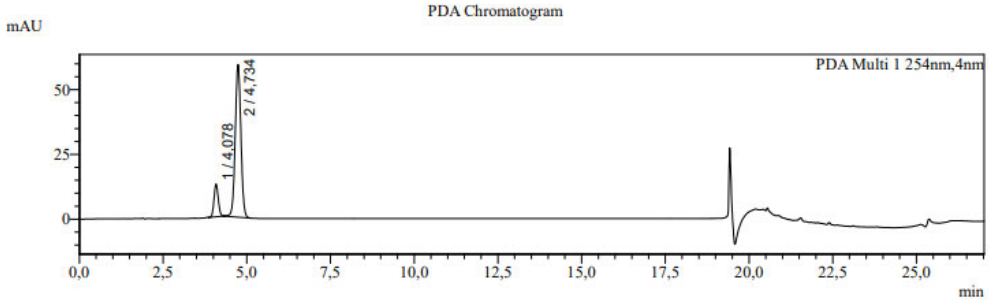

Figure S60. LC-PDA analysis of Iohexol (0.8 mM) in water.

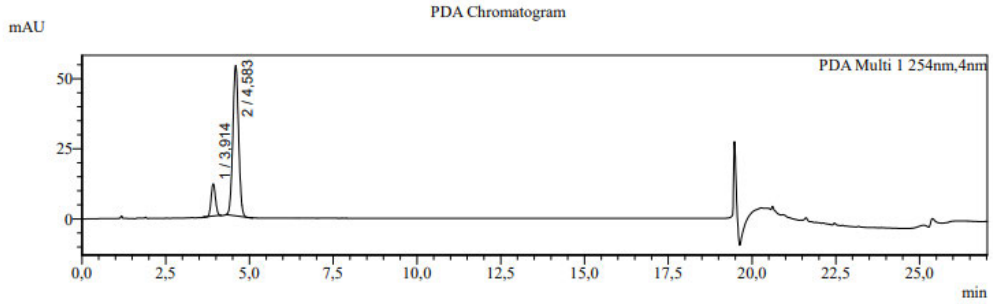

Figure S61. LC-PDA analysis of Iohexol (0.8 mM) in NaOH (4 M).

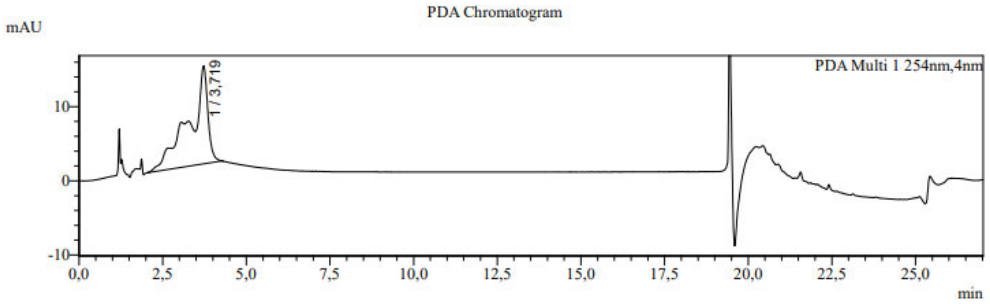

Figure S62. LC-PDA analysis of Iohexol (0.8 mM) in NaOH (4 M) and $Na_3H_2IO_6$ (0.21 M).

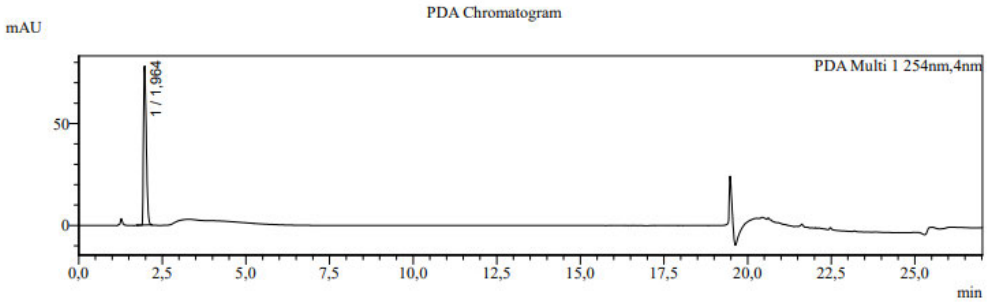

Figure S63. LC-PDA analysis of Iohexol (0.8 mM) in $Na_3H_2IO_6$ (0.21 M).

14. Examples of HRMS Analyses for degradation of fluorescein, rose Bengal and diodrast

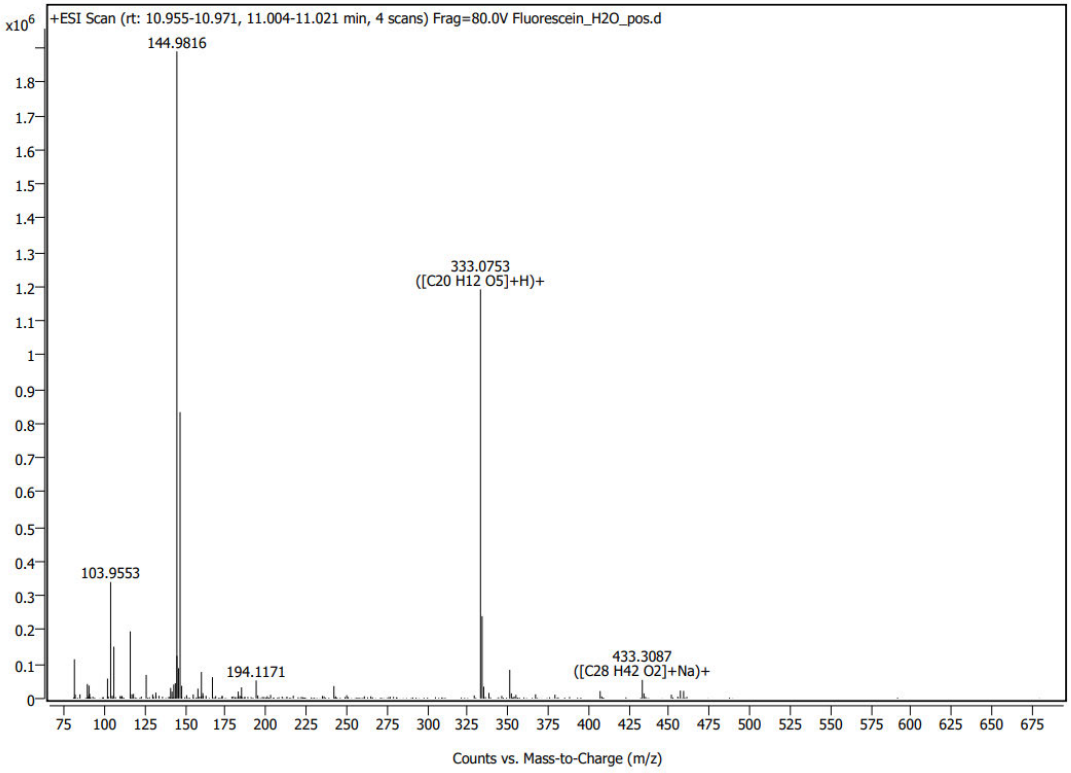

Figure S64. ESI MS Spectra of initial sample of fluorescein.

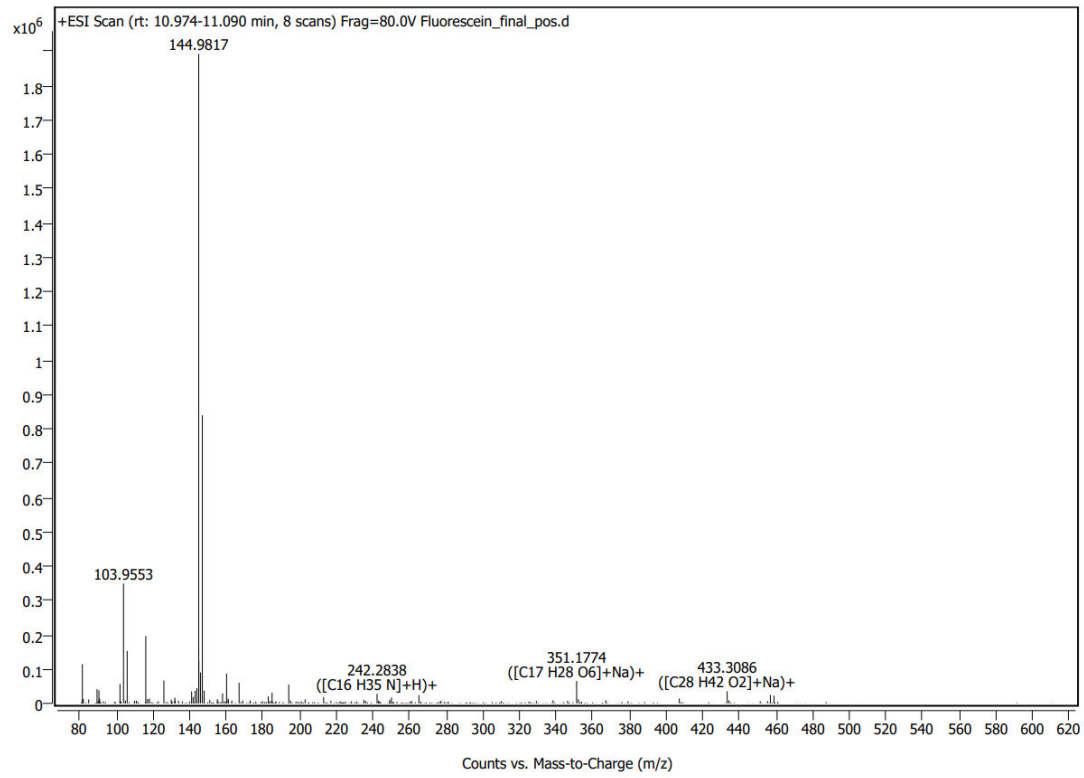

Figure S65. ESI MS Spectra of final sample of fluorescein.

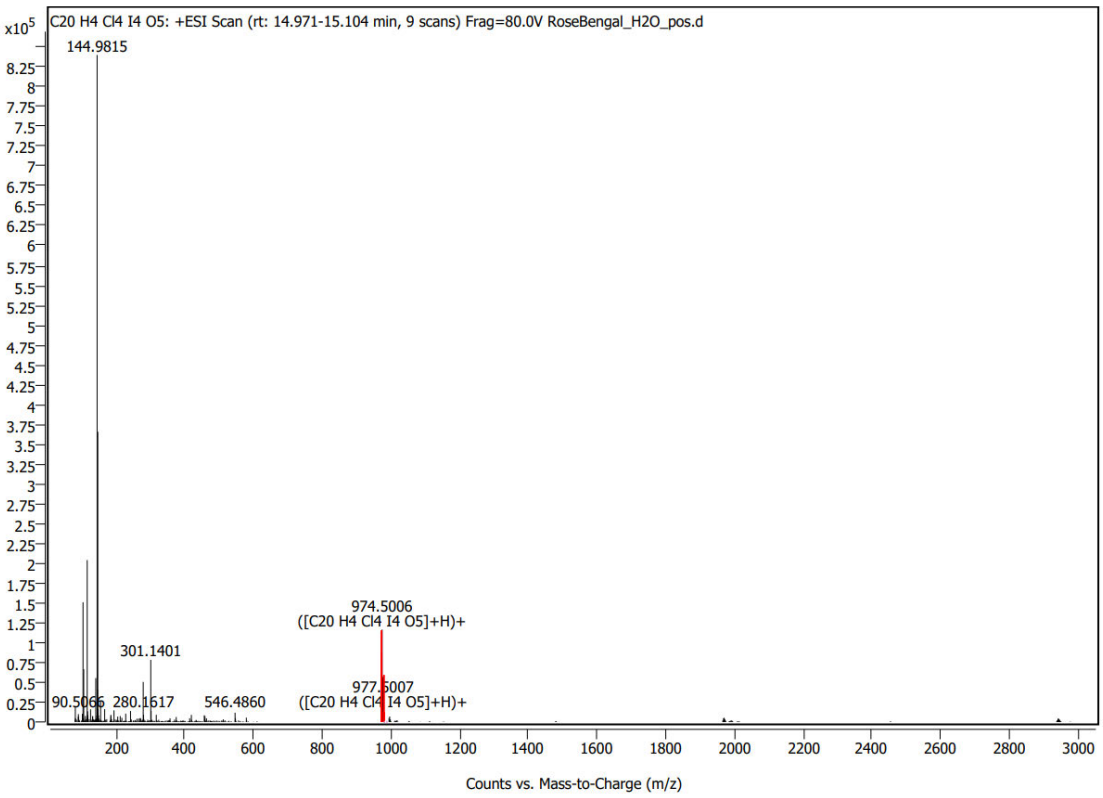

Figure S66. ESI MS Spectra of initial sample of rose bengal.

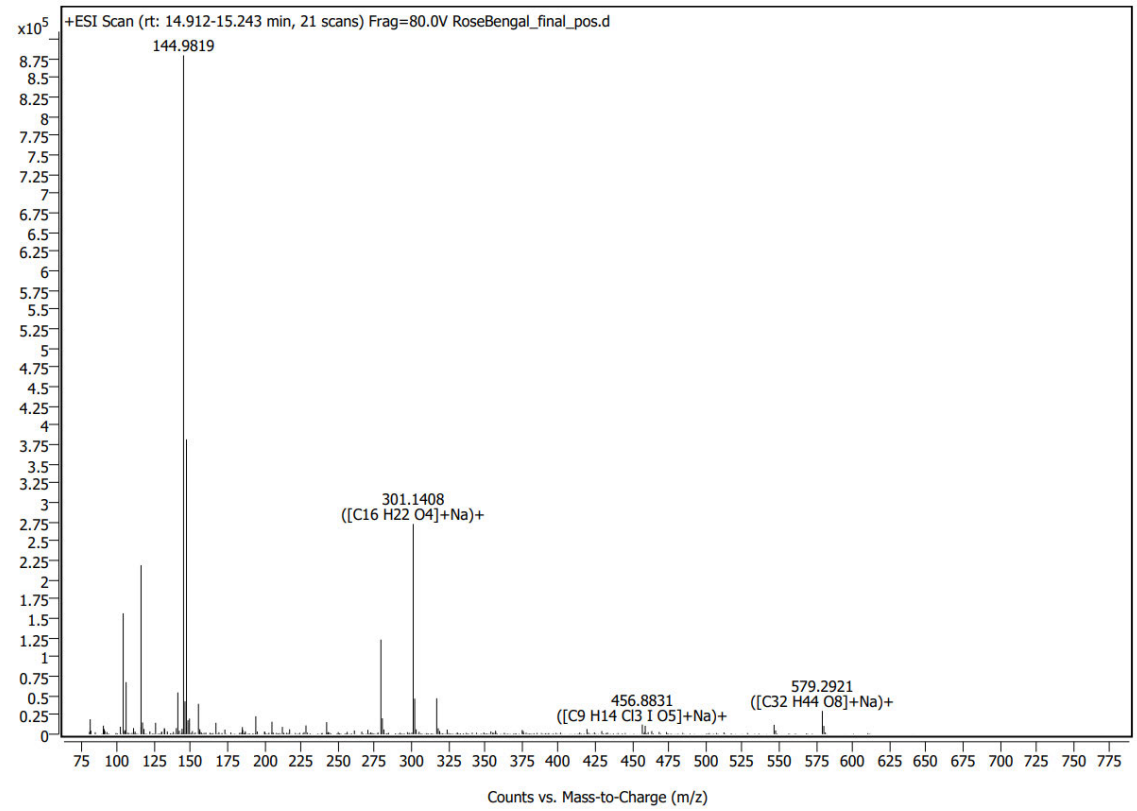

Figure S67. ESI MS Spectra of final sample of rose bengal.

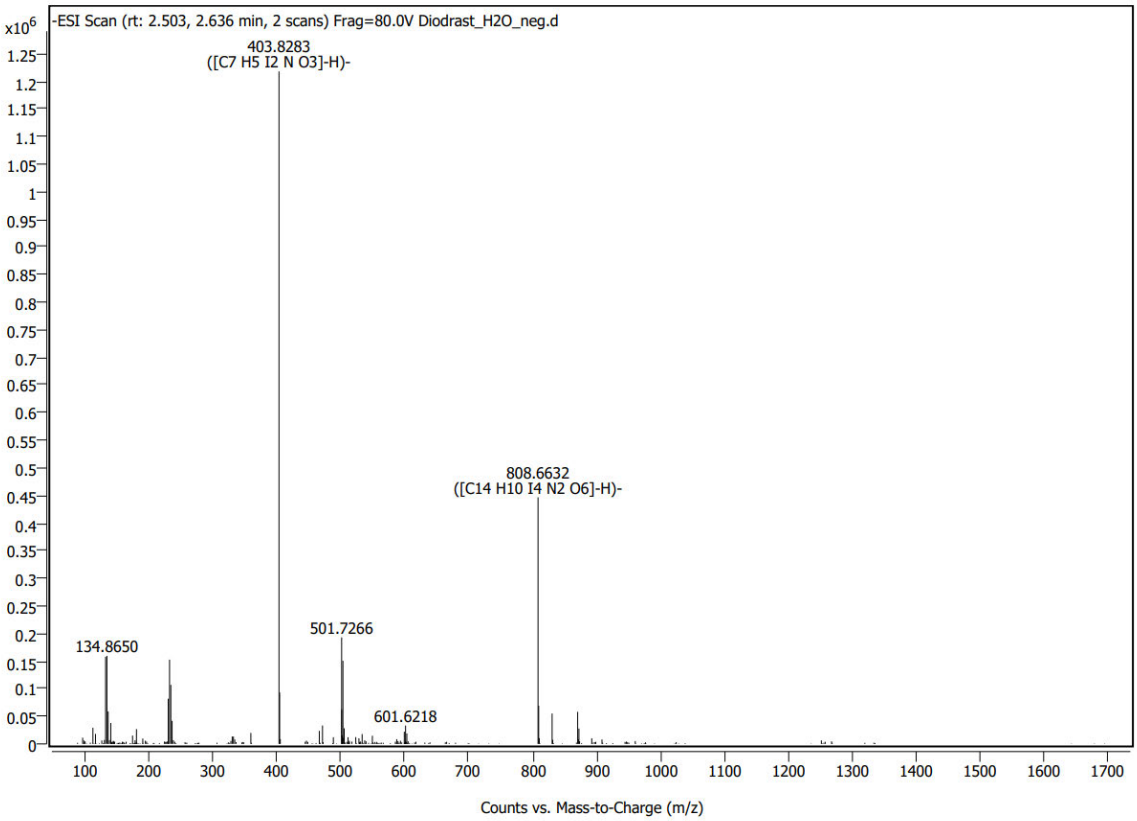

Figure S68. ESI MS Spectra of initial sample of diodrast.

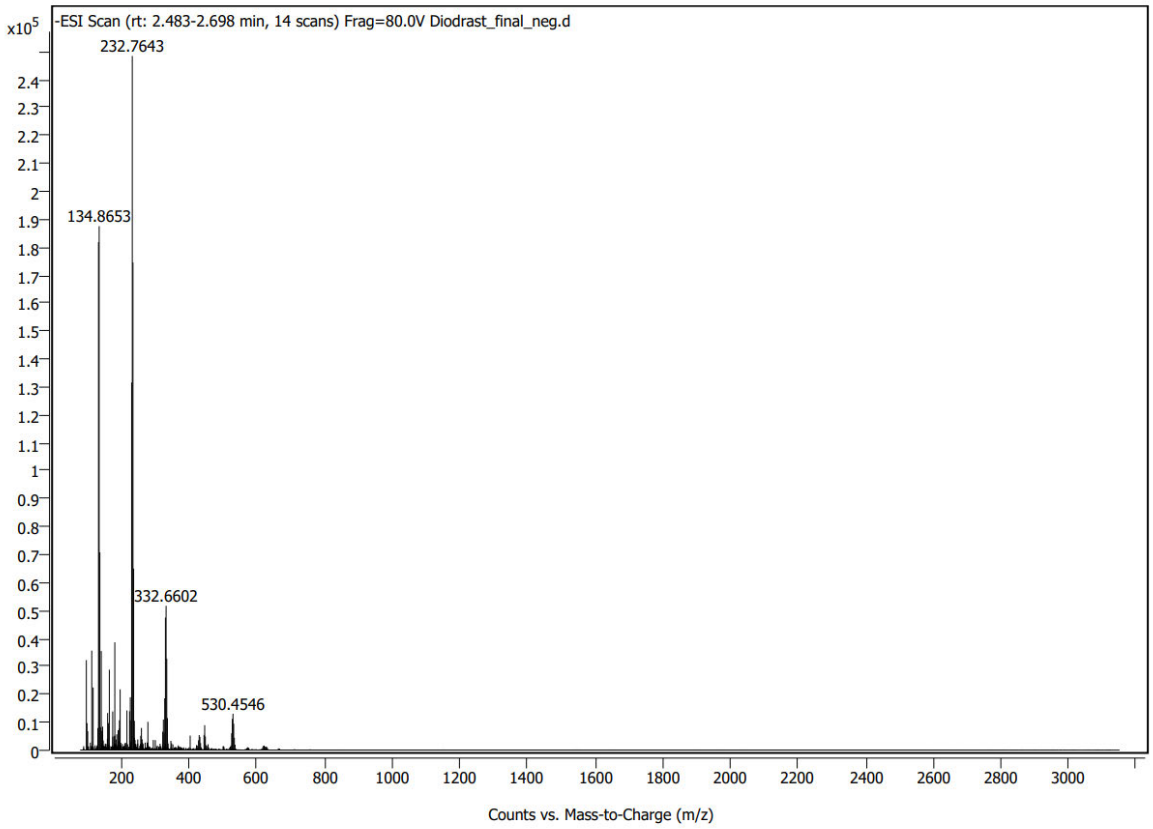

Figure S69. ESI MS Spectra of final sample of diodrast.

15. Cyclic voltammetry

The CV data were plotted using pyhton 3.9. First, a cyclic voltammogram was recorded with the reference potassium ferricyanide(III). The reference halfway potential was calculated to be 0.189 V. For all compound CV measurements, this halfway potential was substracted from the potential data. The cyclic voltammograms were recorded between -0.5 V and the first pronounced oxidation peak.

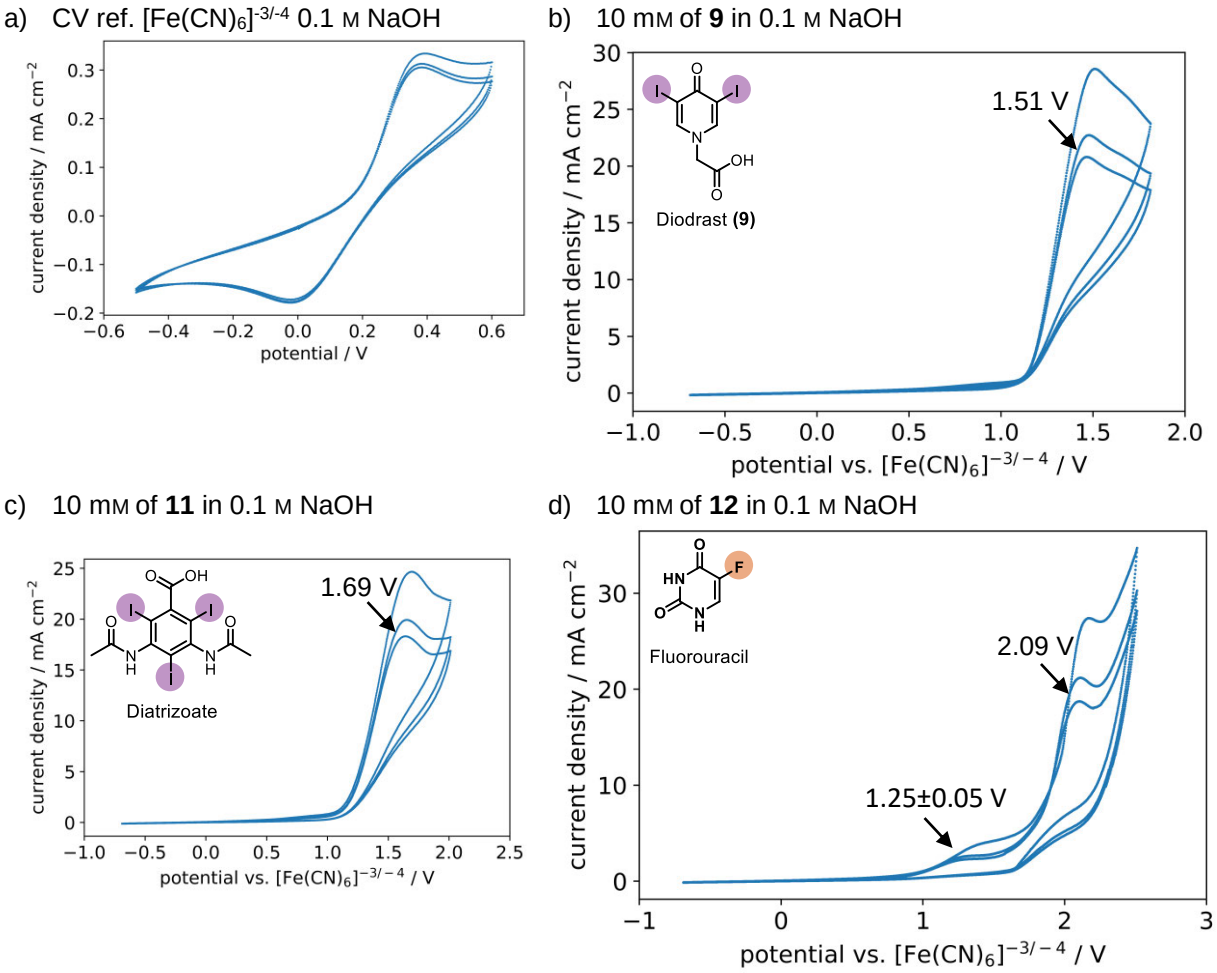

Figure S70. Cyclic voltammograms of diodrast (**9**), diatrizoate (**10**) and fluorouracil (**12**). 10 mM compound, 0.1 M NaOH in water. Working electrode: BDD, counter electrode: glassy carbon, reference electrode: Ag/AgCl in sat. KCl (3M). Scan rate: 0.1 mV/s, 3 scans. Potential referenced vs. $[Fe(CN)6]^{3-}/Fe(CN)6^{4-}$ in 0.1 M NaOH in water.

16. References

[1] W. L. F. Armarego, C. L. L. Chai, *Purification of Laboratory Chemicals*, Elsevier, Amsterdam, **2013**.

[2] S. Arndt, D. Weis, K. Donsbach, S. R. Waldvogel, *Angew. Chem. Int. Ed.* **2020**, *59*, 8036–8041; *Angew. Chem*. **2020**, *132*, 8112–8118.

[3] B. Gleede, M. Selt, C. Gütz, A. Stenglein, S. R. Waldvogel, *Org. Process Res. Dev.* **2020**, *24*, 1916–1926.

[4] Siegfried R. Waldvogel, Sebastian Arndt, Dominik Weis, Kai Donsbach, WO 2021110928 A1 20210610, **2020**.